Additively manufactured materials and structures: A state-of-the-art review on their mechanical characteristics and energy absorption

Yaozhong Wu[1], Jianguang Fang[2*], Chi Wu[3], Cunyi Li[2], Guangyong Sun[4], Qing Li[3]

[1]School of Automobile and Traffic Engineering, Wuhan University of Science and Technology, Wuhan 430081, China

[2]School of Civil and Environmental Engineering, University of Technology Sydney, Sydney, NSW 2007, Australia

[3]School of Aerospace, Mechanical and Mechatronic Engineering, The University of Sydney, Sydney, NSW 2006, Australia

[4]State Key Laboratory of Advanced Design and Manufacture for Vehicle Body, Hunan University, Changsha, 410082, China

Abstract

Lightweight materials and structures have been extensively studied for a wide range of applications in design and manufacturing of more environment-friendly and more sustainable products, such as less materials and lower energy consumption, while maintaining proper mechanical and energy absorption characteristics. Additive manufacturing (AM) or 3D printing techniques offer more freedom to realize some new designs of novel lightweight materials and structures in an efficient way. However, the rational design for desired mechanical properties of these materials and structures remains a demanding topic. This paper provides a comprehensive review on the recent advances in additively manufactured materials and structures as well as their mechanical properties with an emphasis on energy absorption applications. First, the additive manufacturing techniques used for fabricating various materials and structures are briefly reviewed. Then, a variety of lightweight AM materials and structures are discussed, together with their mechanical properties and energy-absorption characteristics.

*Corresponding Author

Jianguang.Fang@uts.edu.au; FangJG87@gmail.com

Next, the AM-induced defects, their impacts on mechanical properties and energy absorption, as well as the methods for minimizing the effects are discussed. After that, numerical modeling approaches for AM materials and structures are outlined. Furthermore, design optimization techniques are reviewed, including parametric optimization, topology optimization, and

30 nondeterministic optimization with fabrication-induced uncertainties. Notably, data-driven and machine learning-based techniques exhibit compelling potential in design for additive manufacturing, process-property relations, and in-situ monitoring. Finally, significant challenges and future directions in this area are highlighted. This review is anticipated to provide a deep understanding of the state-of-the-art additively manufactured materials and

35 structures, aiming to improve the future design for desired mechanical properties and energy absorption.

Keywords: Additive manufacturing; Mechanical properties; Energy absorption; Defects, Cellular and lattice structures, Optimization; Machine learning

Contents

List of Acronyms and Abbreviations

3D-CNN	three-dimensional convolutional neural networks
ABS	acrylonitrile butadiene styrene
ALD	atomic layer deposition
AM	additive manufacturing
AMGA	archive-based micro genetic algorithm
ANN	artificial neural network
BESO	bidirectional evolutionary structural optimization
BCC	body-center cubic
BEP	beetle elytron plate
BMS	bi-material structure
CA	cellular automaton
CAM	computer-aided manufacturing
CCF	continuous carbon fiber
CF	carbon fiber
CFD	computational fluid dynamics
CFRP	carbon fiber reinforced polymer
CFSFDP	clustering by fast search and find of density peaks
CLL	cuttlebone-like lattice
CNN	convolutional neural network
CT	computed tomography
D	Schwarz-Diamond
DAM	design for additive manufacturing
DCP	bi-directionally corrugated panel
DED	direct energy deposition
DL	diamond-like
DLF	directed light fabrication
DLP	digital light processing
DLW	direct laser writing
DMD	direct metal deposition
DNN	deep neural networks
DT	decision tree
EAE	energy absorption efficiency
EBAM	electron beam additive manufacturing
EBEP	end-trabecular beetle elytron plate
ECC	edge-center cube
ESL	equivalent static load
FCC	face-center cubic
FDM	fused deposition modeling

FE	finite element
FFF	fused filament fabrication
FIB	focused ion beam milling
FGS	functionally graded sheet structures
FRD	Schoen- F-graph-Rhombic dodecahedra graph
FGPB	functionally graded porous biomaterials
G	Schoen-Gyroid
GA	genetic algorithm
GBEPn	grid beetle elytron plates
GISSMO	generalized incremental stress state model
GP	gaussian processing
GTN	Gurson-Tvergaard-Needleman
HCA	hybrid cellular automaton
HDPE	high-density polyethylene
HOT	hollow octet truss
HSA	hollow sphere assembly
HTS	hybrid truss-sphere
IPC	interpenetrating phase composite
IWP	Schoen- I-graph-wrapped package graph
J-C	Johnson-Cook
KNN	K-nearest neighbors
LSF	laser solid forming
MJF	multi jet fusion
MJT	material jetting
ML	machine learning
MHH	multi-level hierarchical honeycomb
MMA	the method of moving asymptotes
MMC	moving morphable components
MMV	moving morphable voids
MWCNT	multi-wall carbon nanotube
NPR	negative Poisson's ratio
NSGA-II	non-dominated sorting genetic algorithm
OCT	octet truss lattice
P	Schwarz-Primitive
PA	polyamide
PBF	powder bed fusion
PC	polycarbonate
PCA	principal component analysis
PCU	polycarbonate urethane
PLA	polylactic acid
PPR	polypropylene random

PSF	pattern scale factor
PSO	particle swarm optimization
PμSL	projection micro-stereolithography
RD	rhombic dodecahedron
RF	random forest
RP	rapid prototyping
RSH	regular square honeycomb
SC	simple cubic
SCF	short carbon fiber
SCL	stretched cell lattice
SEA	specific energy absorption
SEBM	selective electron beam melting
SHH	square hierarchical honeycombs
SIMP	solid isotropic material with penalization
SLA	stereolithography
SLM	selective laser melting
SLS	selective laser sintering
SOM	self-organizing map
SOT	solid octet truss
SPPW	self-propagating photopolymer waveguide
SVM	support vector machine
TPL	two-photon lithography
TPMS	triply periodic minimal surfaces
TPU	thermoplastic polyurethane
UAV	unmanned aerial vehicle
UGAH	unidirectionally graded auxetic honeycomb
UV	ultraviolet
WAAM	wire + arc additive manufacturing

105

1 Introduction

Over the past decades, lightweight materials and structures have drawn growing attention in product design with more sustainable features, such as less material usage, less energy consumption, and less greenhouse gas emission, at the same time maintaining high mechanical performance in aerospace, automotive, civil, maritime, and nuclear engineering [1-3]. For this purpose, experimental, analytical, and numerical methods have been extensively used to predict what topological configuration or spatial distribution of materials is required at a nano to mesoscale to achieve anticipated mechanical performances at the macroscopic level [4-10]. Nevertheless, the sophisticated micro-scale topological configurations and/or complex spatial distribution of materials are restricted by traditional manufacturing technologies, somewhat hindering the improvement of mechanical performances [11-14].

Additive manufacturing (AM), also referred to as 3D printing or rapid prototyping (RP), is a relatively newer process of fabricating objects from 3D computer-aided design (CAD) models. The process can produce various structures by adding materials layer by layer to construct sophisticated 3D architectural configurations and reduce waste with satisfactory geometric accuracy [15, 16]. The AM provides more freedom to design novel structures which can better place the materials as needed to enhance and/or tailor their mechanical properties. Various AM technologies have been available to fabricate desired products used in aerospace, automotive, mechanical, civil, biomedical, and many other fields [17-19].

Energy absorption under large deformation is one of the most important mechanical characteristics of lightweight materials and structures for applications in automobile, railway, packaging etc. [20-22]. Essentially, materials and structures absorb substantial kinetic energy through plastic deformation and/or fracture to reduce risk of people's mortality/injury and damage of goods under impact loads [23-25]. Through AM techniques, various novel materials and structures, such as shell-lattices, bio-inspired design, and topology optimization-based structures that may not be fabricated by traditional manufacturing technologies, have been proposed and fabricated to improve their mechanical characteristics. These AM based materials

and structures have exhibited superior potentials in industrial applications [13, 26, 27]. However, there are also some associated issues for AM process such as AM-indued uncertainties and defects, and their effect on the mechanical characteristics, which should be investigated and understood systematically. The computational modeling of AM process and deformation behavior of the materials and structures represent an effective means to understand their associated mechanical properties.

Note that there is lack of systematic review to date on the mechanical behaviors of additively manufactured materials and structures subject to large deformation with a characteristic feature on energy absorption. This work aims to comprehensively review recent advances in AM materials and structures and their mechanical properties for energy absorption applications. **Figure 1** provides an overview on the framework and key aspects relating to the mechanical behaviors of AM materials and structures. The review first briefs the AM technologies commonly used to fabricate energy-absorbing structures in Section 2. Then, a range of geometrical configurations of energy-absorbers and their mechanical performances are discussed in detail in Section 3. Section 4 portrays various additive manufacturing defects and their effects on the mechanical performance of these structures. The numerical methods for simulating the mechanical performance and the fabrication process are reviewed in depth in Section 5. Section 6 provides an overview of design optimization methods for AM materials and structures. Section 7 discusses the data-driven and machine-learning research in additive manufacturing for enhancing the mechanical properties of fabricated materials and structures. Engineering applications for AM materials and structures are presented in Section 8. Section 9 concludes the existing advances and identifies some significant challenges confronting for future studies.
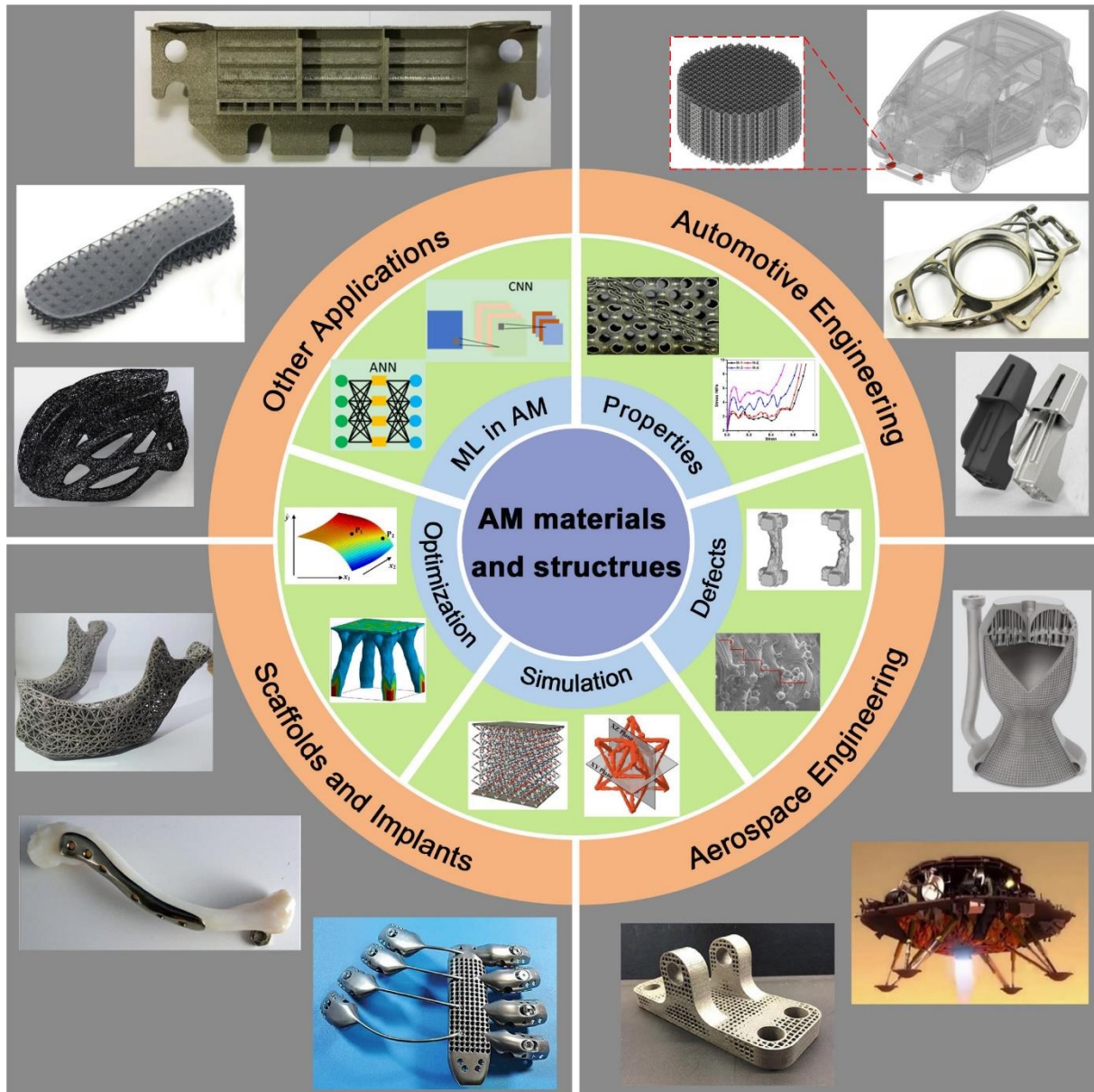
Figure 1. The framework of a state-of-the-art review for the additively manufactured materials and structures; properties [28, 29], defects [30, 31], simulation [32, 33], optimization [34], automotive engineering [35-37], aerospace engineering [38-40], scaffolds and implants [41-43], other applications [44-46].

160

2. Additive manufacturing technologies

Additive manufacturing (AM) has been widely employed in different applications to produce complex functional parts using a range of engineering materials [47]. Many reviews have been conducted on the AM techniques with specific information [15, 16, 48, 49]. Here,

we briefly outline the AM techniques that have been commonly used in fabricating a variety of energy-absorbing structures in the open literature.

2.1 Powder bed fusion (PBF)

Powder bed fusion (PBF) is an additive manufacturing process that forms parts from metallic or polymeric powder using an energy source, typically a laser beam or an electron beam [15, 16, 47]. More specifically, a PBF printer is typically composed of a roller, a powder supply platform, a fabrication platform, a powder bed, a laser source, and a scanner system, as shown in **Figure 2(a)**. In the PBF process, the roller is used to evenly spread a thin layer of powder onto the fabrication platform; then, the laser or an electron beam scans the powder layer following a well-designed moving trajectory of the cross-section of a designed 3D part [47, 50]. The fabrication platform moves down upon completion of the current layer, and subsequent layers of powders are rolled on top of the existing layers. The process is repeated until the whole 3D part is built, and finally, the unmelted powder should be removed to obtain the finished part.

Selective laser sintering (SLS), selective laser melting (SLM), and selective electron beam melting (SEBM) are the most reported PBF techniques in the literature for fabricating energy-absorbing structures. A wide range of materials has been available for the PBF techniques to produce various 3D parts. For example, maraging steel [28, 51], 316L stainless steel [52-56], aluminum alloy (AlSi10Mg) [57-59], thermoplastic polymer [60-62], and biocompatible materials such as titanium alloy (Ti6Al4V) [63-65], have been used to fabricate the advanced functional structures [66-68]. Note that different AM process factors, such as powder size, laser power, layer thickness, scan speed, scan strategy, etc., are crucial in determining the quality of the printed products. Some examples of 3D-printed energy-absorbing structures using different PBF techniques are shown in **Figure 2(b-d)**.

Multi Jet Fusion (MJF) is a recently developed PBF technique, which used an infrared lamp as the energy source [69-71]. MJF consists of two main components, a recoating carriage and printing/fusing carriage. The recoating carriage deposits the material powder and the printing/fusing carriage deposits the fusing/detailing agent, and the fusion agent covered areas

The main advantage of PBF techniques is that they do not have problems in removing supporting material which uses the powder bed as the support, and they possess considerable flexibility in material selection and processing environment at a room temperature. Moreover, the fine resolution and high quality make PBF suitable for printing complex functional structures with sufficient accuracy. However, the main drawbacks are low processing speed, high cost, and high porosity [72]. The surface quality and overall integrity of the printed parts also heavily rely on the quality and grain size of the used powders [15, 16].
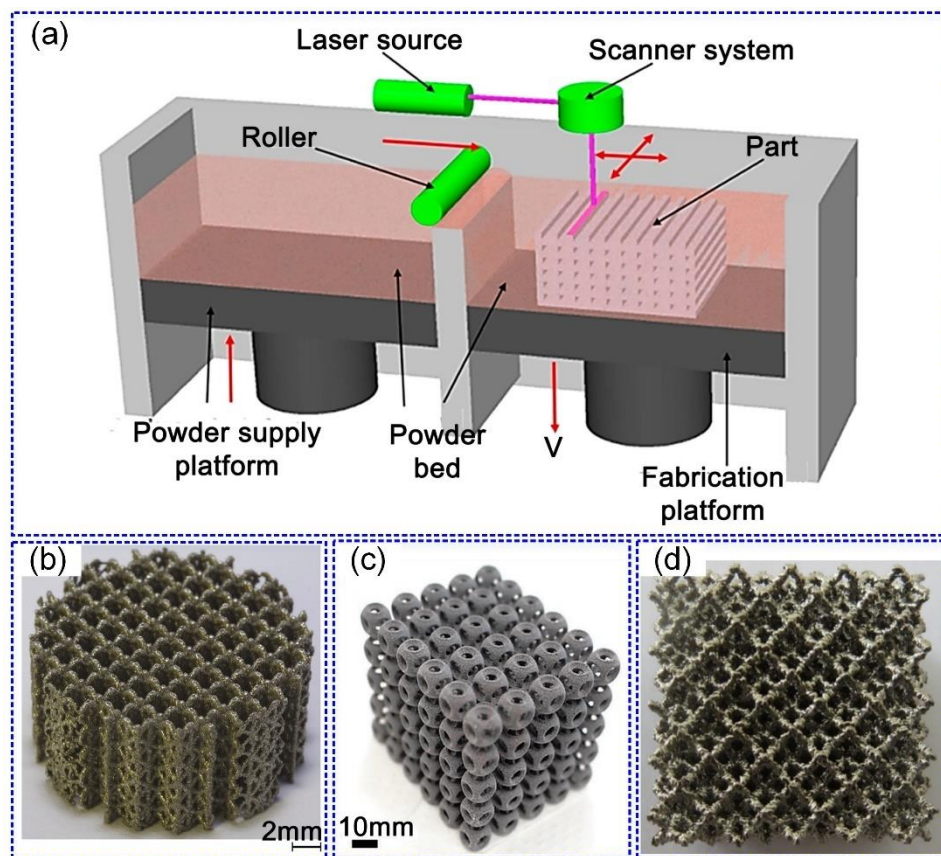
Figure 2. (a) Schematic for the PBF system [15]; examples of additively manufactured energy-absorbing structures by the PBF technique: (b) lattice-walled honeycomb fabricated by SLM with 316L stainless steel [55], (c) hollow spherical lattice fabricated by SLS with PA12 [73], (d) rhombic dodecahedron lattice fabricated by SBEM with Ti6Al4V [74].

2.2 Fused deposition modeling (FDM)

Fused deposition modeling (FDM), also known as fused filament fabrication (FFF), is the

most widely used AM technique, which was developed by Scott Crump at the end of the 1980s and commercialized in the 1990s by Stratasys [47, 49]. Typically, the FDM system consists of a fabrication platform, a print bed, a material spool, an extrusion nozzle, and a drive wheel, as

210   illustrated in **Figure 3(a)**. The thermoplastic filament is unrolled from the material spool to the heated extrusion nozzle, where it will be melted to a semi-liquid state. Then the semi-liquid state materials are extruded layer by layer on the platform or on the previously printed layers, where they are fused and then solidified. The process is repeated until the final parts are built. The nozzle can be moved in 3D space, horizontally on the X- and Y-axis and vertically on the

215   Z-axis, from a numerically controlled system, commanded by computer-aided manufacturing (CAM) software.

Polymeric materials with a low melting temperature, such as polycarbonate (PC), acrylonitrile butadiene styrene (ABS) [75], polyamide (PA), and polylactic acid (PLA) [76], are widely used as base materials for the FDM process. Recently, fiber-reinforced composites have

220   been fabricated by FDM to enhance their mechanical properties. Generally speaking, the quality of printed parts is affected by printing parameters, such as layer thickness, printing orientation, raster width, raster angle, and air gap [77]. Several examples of additively manufactured structures using the FDM technology are shown in **Figure 3(b-d).**

While FDM has the advantage of low cost and high speed [77], some common drawbacks

225   of FDM include weak mechanical properties of the printed parts, poor surface quality of final printed parts, and limited types of thermoplastic materials with suitable melt viscosity [78]. Also, this process could often have difficulties in complete removal of support structures [15]. For composite printing, the poor adhesion strength between the fiber and matrix, as well as the void formation are some main challenges in additively manufactured fiber-reinforced

230   composite parts [79].
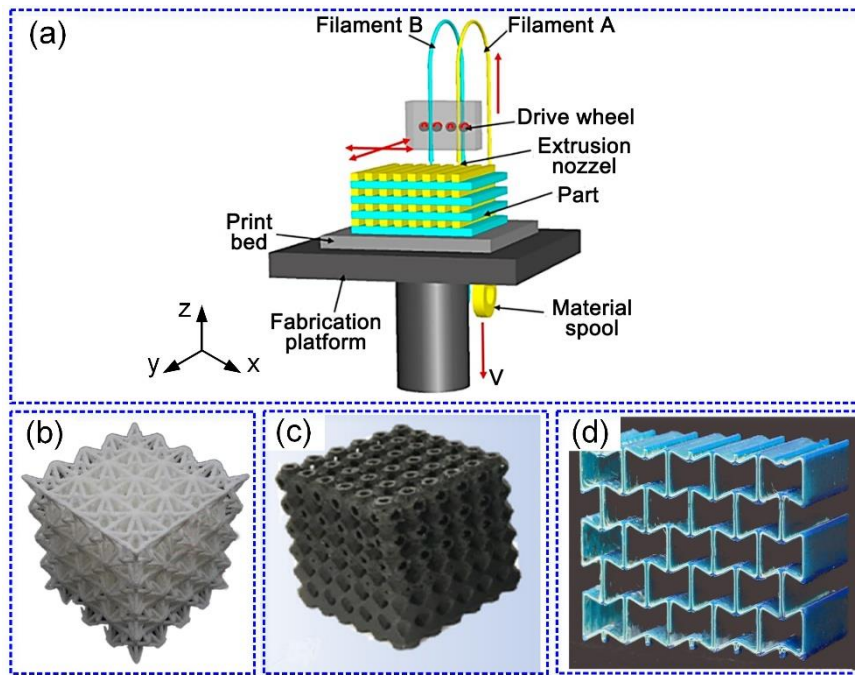
Figure 3. (a) Schematic of the FDM process [15]; examples of additively manufactured structures using FDM: (b) hybrid lattice structures with PLA [80], (c) lattice structures with short fiber-reinforced nylon [81], and (d) auxetic honeycomb with continuous fiber reinforced thermoplastic composite [82].

2.3 Vat photopolymerization

2.3.1 Stereolithography (SLA)

Stereolithography (SLA) is one of the earliest developed AM techniques introduced by Charles Hull in 1986 [47]. The SLA system typically consists of a resin tank, a building platform, an ultraviolet (UV) laser source, and an XY scanning mirror, as illustrated in **Figure 4(a)**. The photopolymer resin cured by UV laser is used as the SLA printing material. The UV laser beam generated from the laser source is manipulated using a digital XY scanning mirror and shot through the transparent bottom of the resin container to yield the desired pattern. The patterned 2D layer is polymerized using the laser, and the subsequent layers are cured on the bottom of the previous layer by raising the platform. The process is repeated until the whole 3D part is produced. Finally, the uncured resin should be removed after the completion of the layer-by-layer printing.

Photocurable resins, including acrylic and epoxy, are widely used as SLA materials. The quality of the final printed parts is affected by the curing reactions during polymerization, which can be controlled by the intensity of laser power, scan speed, and duration of exposure [15, 16, 83, 84]. Typically, the complex nanocomposites can be effectively produced by SLA with a fine resolution as low as 10 μm [16]. Some examples of lattice structures fabricated using the SLA technique are shown in **Figure 4(c-d)**.

The high resolution of the final printing parts is the main advantage of SLA [15]. However, SLA printing has some shortcomings, such as low speed, expensive and limited types of photocurable resins. Another concern is the possible cytotoxicity of residual photoinitiator and uncured resin [16].

2.3.2 Digital Light Processing (DLP)

DLP is similar to SLA except for the curing method. The DLP process employs a digital light projector to reflect a laser source, as illustrated in **Figure 4(b)**. The DLP process is faster than SLA as each layer is cured at a time by the digital light projector. The quality of the final parts depends considerably on the projector resolution [85]. An example of additively manufactured hierarchical lattice structures using the DLP technique is shown in **Figure 4(c)**.
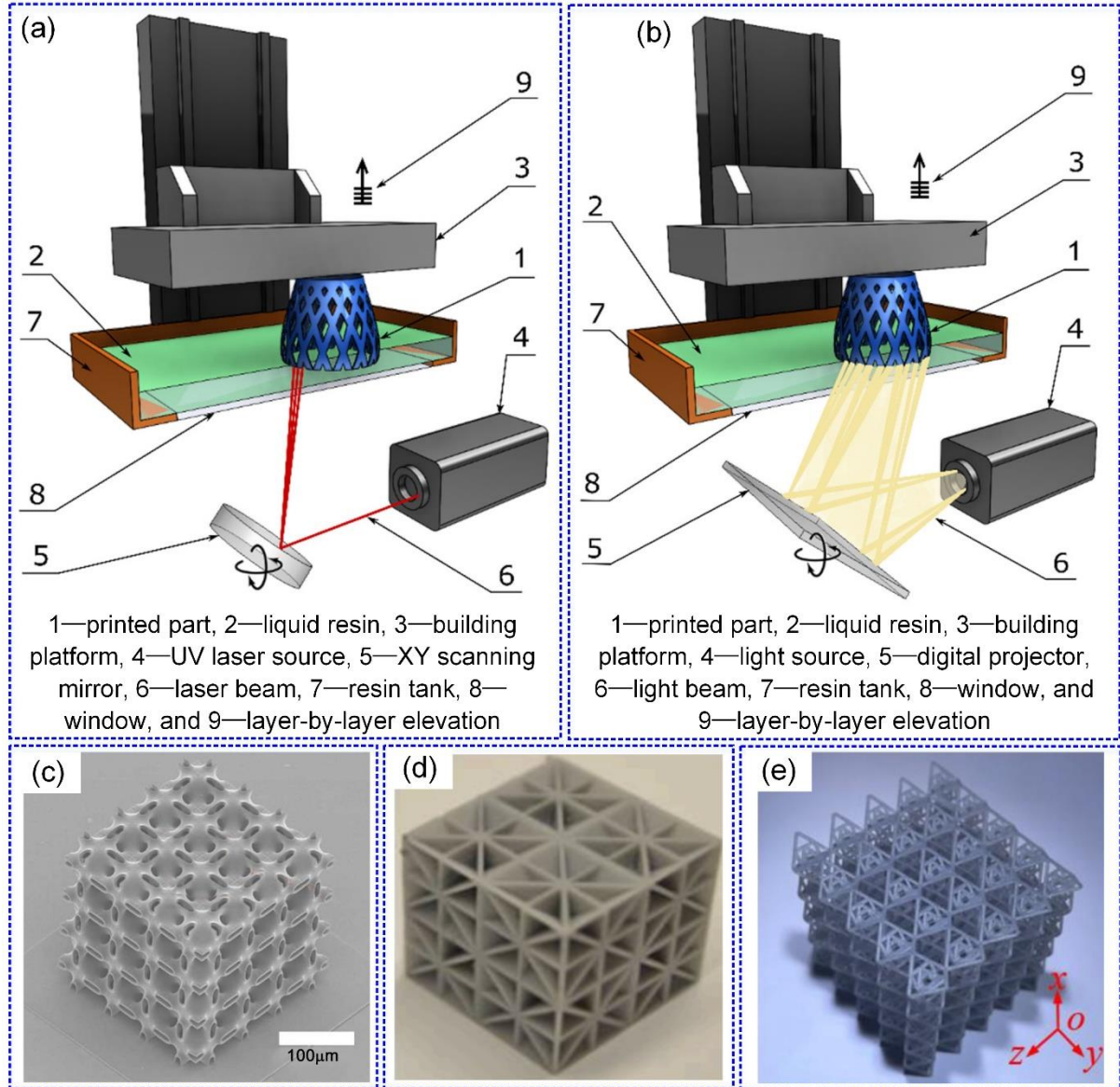
Figure 4. (a) Schematic of the SLA process [85], (b) schematic of the DLP process [85]; examples of additively manufactured materials and structures fabricated by SLA/DLP: (c) Neovius-micro-lattice fabricated by SLA with polymer [86], (d) SC-BCC hybrid lattices fabricated by SLA with PlasGRAY [87], (e) hierarchical lattice fabricated by DLP with urethane acrylate [88].

2.3.3 Micro-/Nanofabrication

2.3.3.1 Two-Photon Lithography (TPL)

Two-photon lithography (TPL) is a direct laser writing (DLW) technique that facilitates the fabrication of 3D complex polymeric micro/nano-scale structures [47, 89], as depicted in

Figure 5(a). The multiphoton absorption mechanism is used in TPL to cure photosensitive

275   materials. Typically, a femtosecond laser is required to provide a sufficiently high intensity of

light. A very high resolution down to 100 nm can be achieved using the TPL techniques to date

[89, 90]. Most conventional photocurable resins with fast curing speed, high viscosity, high

glass transition temperature post-curing, and resistance to shrinkage can be used in the TPL

process [91].

280   The highest precision is the main advantage of the TPL process, and the main drawback of

the TPL process is its scalability and efficiency [90]. Examples of additively manufactured

nano-/microstructures using the DLP technique are shown in **Figure 5(b)**.

2.3.3.2 Projection micro-stereolithography (PµSL)

PµSL is a layer-by-layer process used to fabricate 3D polymeric structures [89, 90], as

285   illustrated in **Figure 5(c)**. A 2D image slicing from a 3D model is projected onto the surface of

a liquid photomonomer bath by a UV light-emitting diode array [92]. The top surface of the

resin is polymerized with the projected image. The final object is eventually produced by

repeatedly lowering the cured layer into the liquid and polymerizing the top surface of the resin.

Typically, the quality of the final parts is controlled by the resolution of the bitmap image ($\approx$

290   1.3 µm) and the thickness of a single layer (10–100 µm) [89, 90]. A wide range of resins with

different stiffness [93] and viscosities [94] can be used as materials for the PµSL process.

The main advantage of PµSL is the high resolution and higher speed compared with other

AM techniques of its kind. An example of an additively manufactured structure using the PµSL

technique is shown in **Figure 5(d)**.

295   **2.3.3.3 Self-Propagating Photopolymer Waveguide (SPPW)**

SPPW process uses self-propagating photopolymer waveguides to fabricate polymeric

microscale structures [89, 90], as illustrated in **Figure 5(e)**. UV light is used to expose the

photosensitive liquid photomonomer. An array of self-propagating photopolymer waveguides

is formed through a lightproof mask with a patterned aperture; and the final polymeric structure

300   is obtained after removing the uncured monomer [95, 96]. The resolution of the SPPW can go

down to 10 µm [90].

The main advantages of SPPW are its high speed and scalability [89, 90]. An example of an additively manufactured structure fabricated using the SPPW technique is shown in **Figure 5(f)**.
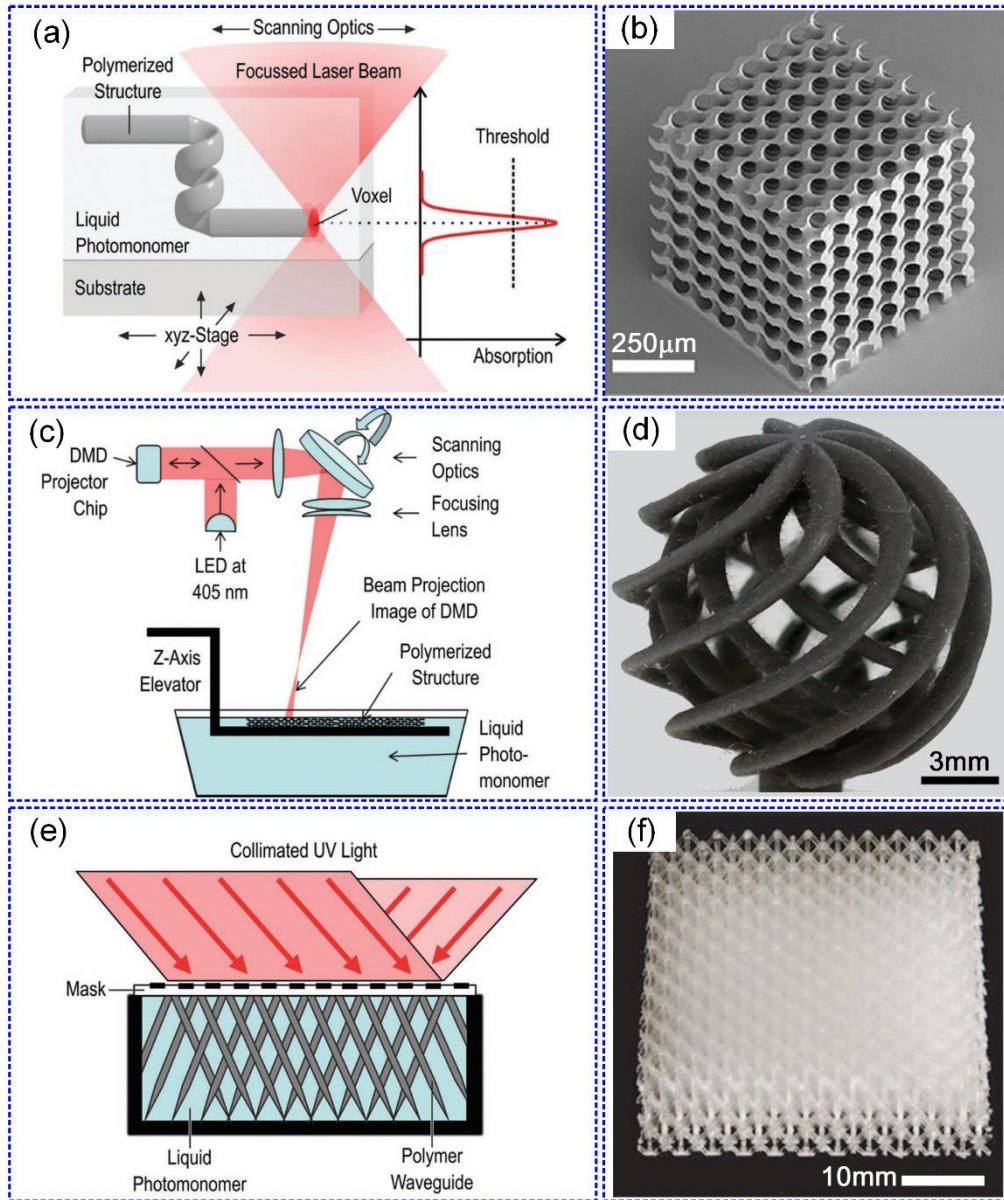
Figure 5. (a) Schematic of the TPL process [90], (b) a triply periodic minimal surface lattice fabricated by TPL with polymer [97], (c) schematic of the PμSL process [90], (d) structure fabricated by PμSL with carbon fiber reinforced polymer [98], (e) schematic of the SPPW process [90], (f) truss lattice fabricated by SPPW with polymer [95].

2.4 Material Jetting (MJT)

Material Jetting was patented by Objet Ltd. in 1999 under the name of PolyJet (which

merged with Stratasys in 2012). The PolyJet system consists of a resin tank, a platform, an extruder, and an ultraviolet light source, as shown in **Figure 6(a).** The process starts with heating the photo-sensitive polymer resin and using the inkjet heads to project hundreds of

315   micro-droplets, and then the photopolymer is cured through photopolymerization.

Fast speed, high-quality surface, and scalability are the main features of PolyJet [99-101]. Additionally, PolyJet can print multiple materials-based parts with the desired properties [84]. However, a main drawback of PolyJet is the difficulty of removing the support structures. In addition, the parts produced by Polyjet often have relatively lower mechanical properties than

320   those created by FDM/SLA [102]. Examples of additively manufactured structures fabricated by the material jetting technique are shown in **Figure 6(b-c)**.

2.5 Direct energy deposition (DED)

Direct energy deposition (DED), also known as laser-engineered net shaping [103], laser solid forming (LSF), directed light fabrication (DLF), direct metal deposition (DMD), electron

325   beam AM (EBAM), and wire + Arc AM (WAAM), is a class of additive manufacturing techniques which melt the feedstock material (powder or wire) using a source of energy (most commonly a laser, but could also be an electron beam or arc). The melted material is deposited to the desired spot and solidified, and the process is repeated until the whole part is constructed [15].

330   The main advantages of DED are its high printing speed and scalability, which can be used to produce parts larger than 6 meters in length [76]. However, the main drawbacks of DED are its lower accuracy and surface quality. In addition, only the parts with less complex topology can be produced by DED compared to SLS or SLM [104]. Examples of additively manufactured structures using the DED technique are shown in **Figure 6(d)**.
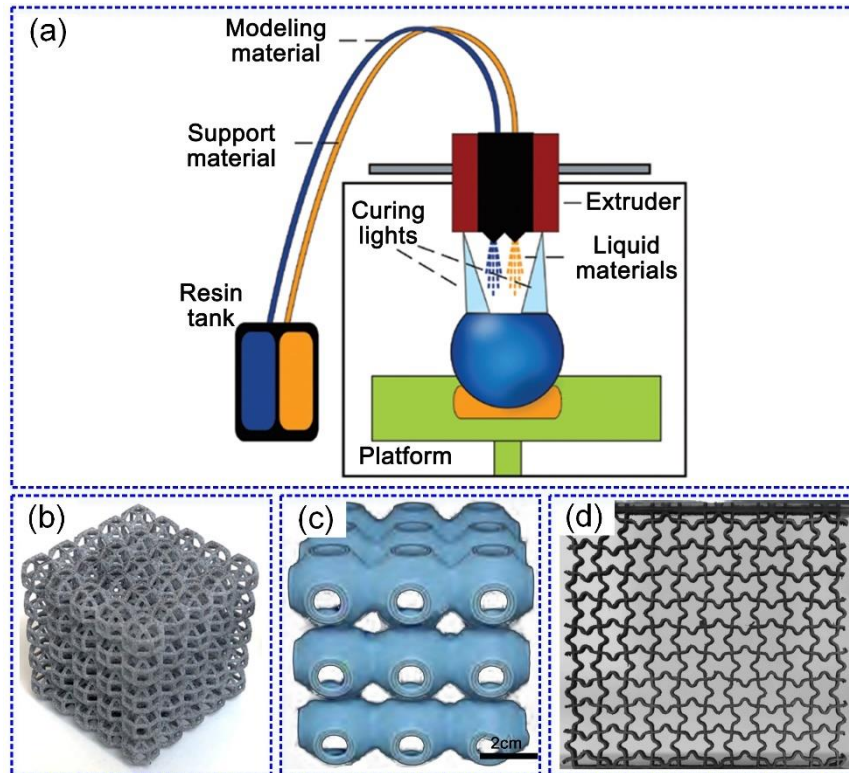
Figure 6. (a) Schematic of the PolyJet process [99], (b) Rhombicuboctahedron fabricated by MJF with PA12 [105], (c) triply periodic minimal surface (TPMS) lattice fabricated by PolyJet with VeroWhitePlus and Agilus [106], (d) auxetic lattice fabricated by DED with 316L stainless steel [107].

2.6 Hybrid Techniques

While the AM techniques exhibit numerous benefits, some unfavorable limitations exist, such as high production cost, relatively low building efficiency, and poor ability to produce larger parts [14]. Also, most reported micro-lattices are fabricated with polymeric materials [89]. To overcome such difficulties, hybrid techniques, which combine both advantages of AM process and traditional manufacturing technologies, have exhibited considerable potential.

2.6.1 AM assisted investment casting

Metallic AM parts often have severe metallurgical defects such as unmelted powder, porosity, distortion, and microstructural heterogeneity [108]. It is well known that the AM polymer parts possess high resolution and high surface quality [85], and the metal casting parts

have excellent microstructural and dimensional features [109, 110]. To fabricate the metallic structures with high quality and low cost, an indirect technology, additive manufacturing assisted investment casting, has been developed [111]. In this method, the AM method is firstly used to produce the polymer-based structure, and then the metallic parts are manufactured by investment casting and pressure infiltration technologies. It has been demonstrated that the proposed hybrid technology could avoid AM-induced defects and achieve an excellent microstructure with less anisotropy [112]. For instance, Xue et al. [110, 113, 114] fabricated the auxetic lattice structures by AM-assisted investment casting. Huang et al. [115] manufactured the pyramidal lattice structures by AM-assisted investment casting, which could be considered a variant of squeeze casting.

2.6.2 Combing AM with plating and coating

As mentioned above, most micro-lattices are fabricated by polymer-based techniques using polymer materials. Several post-processing techniques are developed to fabricate metal- or ceramic-based micro-lattices, including atomic layer deposition (ALD), sputtering deposition, electroless plating, electroplating, redox, and pyrolysis, as well as thermal treatments like sintering. A detailed description of these techniques can be found in the literature [89, 90].

A shellular low-density material was designed and fabricated by combining SPPW, electroless Ni-plating, polishing, and etching techniques [116]. For example, Zheng et al. [117] reported a class of mechanical metamaterials fabricated using projection micro-stereolithography, electroless nickel plating/ALD, and thermal decomposition to obtain the metallic/ceramic micro-lattices. Meza et al. [118] produced a polymeric scaffold using two-photon lithography direct laser writing, followed by postprocessing to obtain the ceramic nanolattices through ALD, focused ion beam milling (FIB), and etching techniques.

Table 1 summarizes the materials, benefits, and drawbacks of AM technologies.

.

Table 1. A summary of materials, benefits, and drawbacks of AM technologies

Methods	Materials used	Advantages	Disadvantages
PBF (SLM, SLS, SEBM)	Metals, alloys, polymers	-High resolution -High quality	-Low printing speed -Expensive
FDM	Thermoplastic polymers, fiber-reinforced polymers	-Low cost -High speed	-Weak mechanical properties -Limited materials
Vat photopolymerization (SLA, DLP, …)	Photo-active polymers	-High resolution -High quality	-Limited materials -Slow printing -Expensive
Material Jetting	Polymers	-Scalability -High speed	-Maintaining workability -Coarse resolution -Poor mechanical properties
DED	Metals, alloys	-High speed -Excellent mechanical properties -Controlled microstructure	-Low accuracy -Low surface quality
Hybrid techniques	Metals, ceramics	-Fine resolution -High quality	-Low printing speed -Expensive -Limited materials

3. Additively manufactured energy-absorbing materials and structures

Thanks to the advances in AM, numerous novel energy-absorbing materials and structures with sophisticated topologies have been fabricated by AM techniques using a variety of base materials such as polymers, metals, ceramics, and composites.

3.1 Lattice structures

3.1.1 Strut-based lattices

Due to their relatively simple spatial configuration, the most common lattice structures investigated in literature are strut-based frames composed of rigid joints and uniform or variable cross-section struts [12, 29, 119]. Among these strut-based lattices, the classical configurations which are proposed based on the crystal structures can be classified as simple cubic (SC), diamond-like (DL), body-center cubic (BCC), face-center cubic (FCC), edge center cube (ECC), and their combinations [29]. To enhance the mechanical characteristics of strut-based lattices, the additional reinforcing struts along with x, y, z, and diagonal directions have been proposed in a form of BCCz [120-123], BCCx [124], F2CCz [125, 126], FBCCxyz [127], and ECCz [128], etc.

Gümrük et al. [122] systematically investigated the mechanical behaviors of BCC, BCC BCCz, and F2BCC lattices fabricated by SLM with stainless steel 316L under compressive loading. All the BCC lattices exhibited deformation localization at the center of the lattice, as displayed in **Figure 7(a)**. Two diagonal shear band deformations were found on the BCCz lattices with a unit cell size of 2, 1.5, and 1.379 mm, one shear band was observed on the BCCz lattice with a unit cell size of 2.5 mm, and a deformation localization at the center of the lattice was seen on the BCCz lattice with a unit cell of 1.25 mm, as shown in **Figure 7(b)**. A diagonal shear band was observed on the F_2BCC lattices when the unit cell size was 2.5 mm, two shear bands were found on the F_2BCC lattices when the unit cell size was 2.5 mm, and a deformation localization at the center of the lattice was seen on the F_2BCC lattices when the unit cell size was 1.5 mm, as seen in **Figure 7(c)**. It can be concluded that the deformation modes of lattice

structures depend on both the unit cell size and topological configuration.
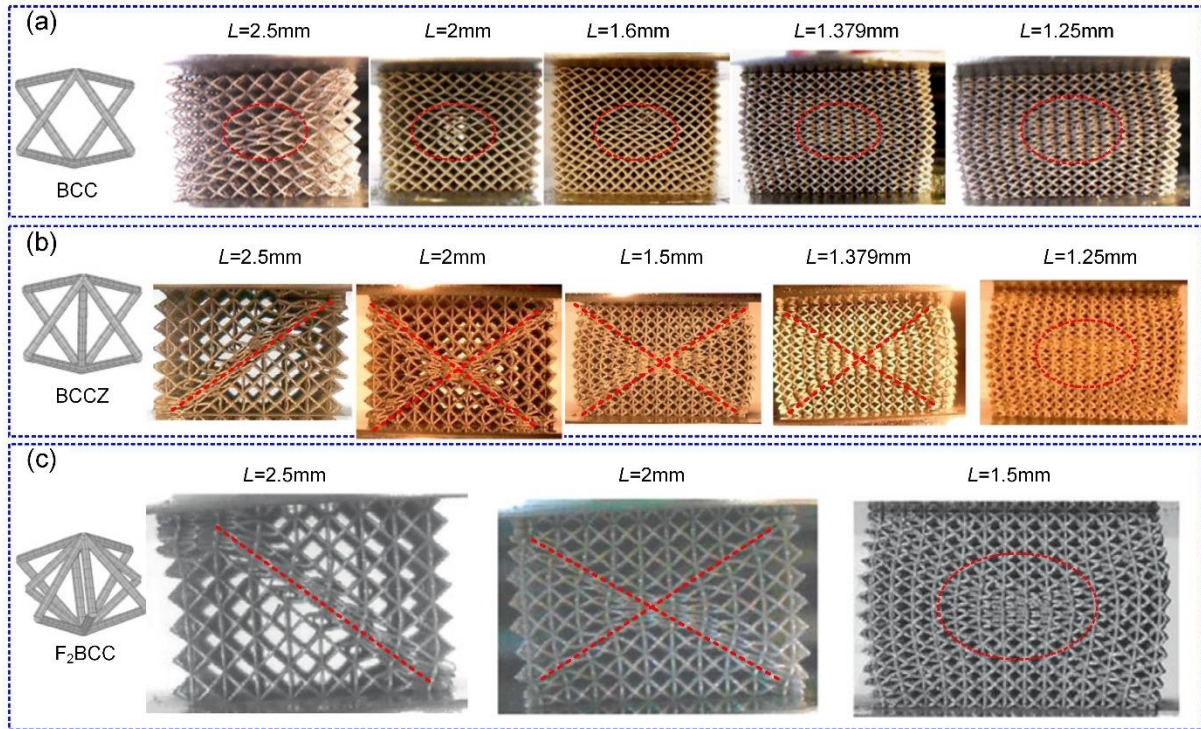
Figure 7. Comparison of the deformation modes of lattices with different topological configurations and unit cell sizes (*L*): (a) BCC, (b) BCCz, and (c) F2BCCz [122]. (ellipses: localization deformation mode, inclined lines: one diagonal shear band deformation mode, X shape: two diagonal shear band deformation mode)

As presented in **Figure 8**, the octet truss lattice (OCT) and its reinforced counterparts (HR_OCT: adding two horizontal struts, VHR_OCT: adding two horizontal struts and one vertical struct, BVHR_OCT: adding twelve boundary struts to BVHR_OCT), which belong to the FCC category, were studied to obtain their mechanical and energy absorption characteristics under compressive loading with the specimens fabricated by SLA with synthesized photosensitive resin [129]. For the OCT lattice, elastoplastic deformation and local buckling of the struts were presented, and the struts overlapped with each other due to the fracture of the struts. Similar deformation modes were observed for the HR_OCT lattices, but a remarkably higher yield and peak strength were identified. For the VHR_OCT lattice, as an additional vertical strut was placed parallel to loading directions, significant buckling of such additional vertical struts, a local buckling deformation, and fracture of inclined struts were observed as

the main deformation modes. A larger extent of deformability and higher load-bearing capacity was identified in the BVHR_OCT due to the additional vertical short struts in the boundary. Moreover, the mechanical behaviors and energy absorption characteristics of these AM-made octet-based lattices were compared with other cellular materials. It was found that the octet-based lattices possess a higher stiffness, higher strength, and higher energy-absorbing capacity than their counterparts.
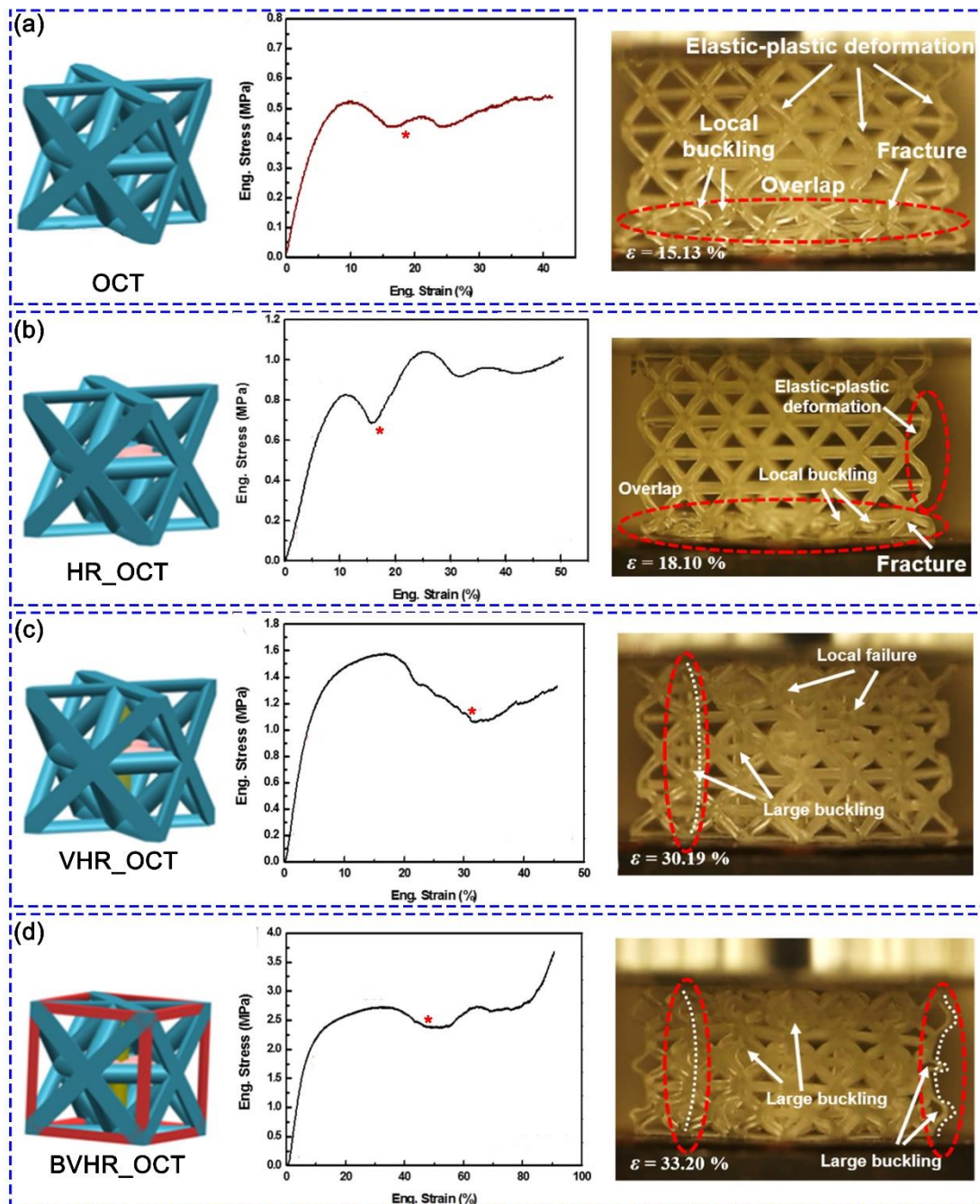
Figure 8. Topologies (left), engineering stress-strain responses (middle), and deformation

modes at a given strain (ε) indicated using a red asterisk at the engineering stress-strain

430   curves for (a) OCT, (b) HR_OCT, (c) VHR_OCT, and (d) BVHR_OCT lattices [129].

The lattice structures tend to collapse and/or rupture near the joints as a result of high-stress concentration under loading, which may suppress the load-bearing capacity of lattice structures [54, 119]. Recently, variable cross-section strut lattices with a smooth transition at the joints have been fabricated to enhance the local and overall mechanical properties. For

435   example, Tancogne-Dejean and Mohr [119] developed a BCC lattice with tapered beams and manufactured these BCC lattice samples by SLM with 316L stainless steel, as shown in **Figure 9(a)**. The results demonstrated that tapering the beam cross-sections can enhance the effective Young's modulus and specific energy absorption by 70% and 50%, respectively. Tancogne-Dejean et al. [130] presented an octet truss with tapered beams and fabricated the samples using

440   the SLM method with 316L stainless steel, as shown in **Figure 9(b)**. It was found that the octet lattices with the taper beams possess higher specific energy absorption than their uniform counterparts. Cao et al. proposed a modified rhombic dodecahedron (RD) lattice structure with a variable cross-section of the struts for quasi-static [131] and dynamic compression [54] tests, as shown in **Figure 9(c)**. It was found that the proposed lattice structures exhibit better

445   mechanical properties and energy absorption capacity.
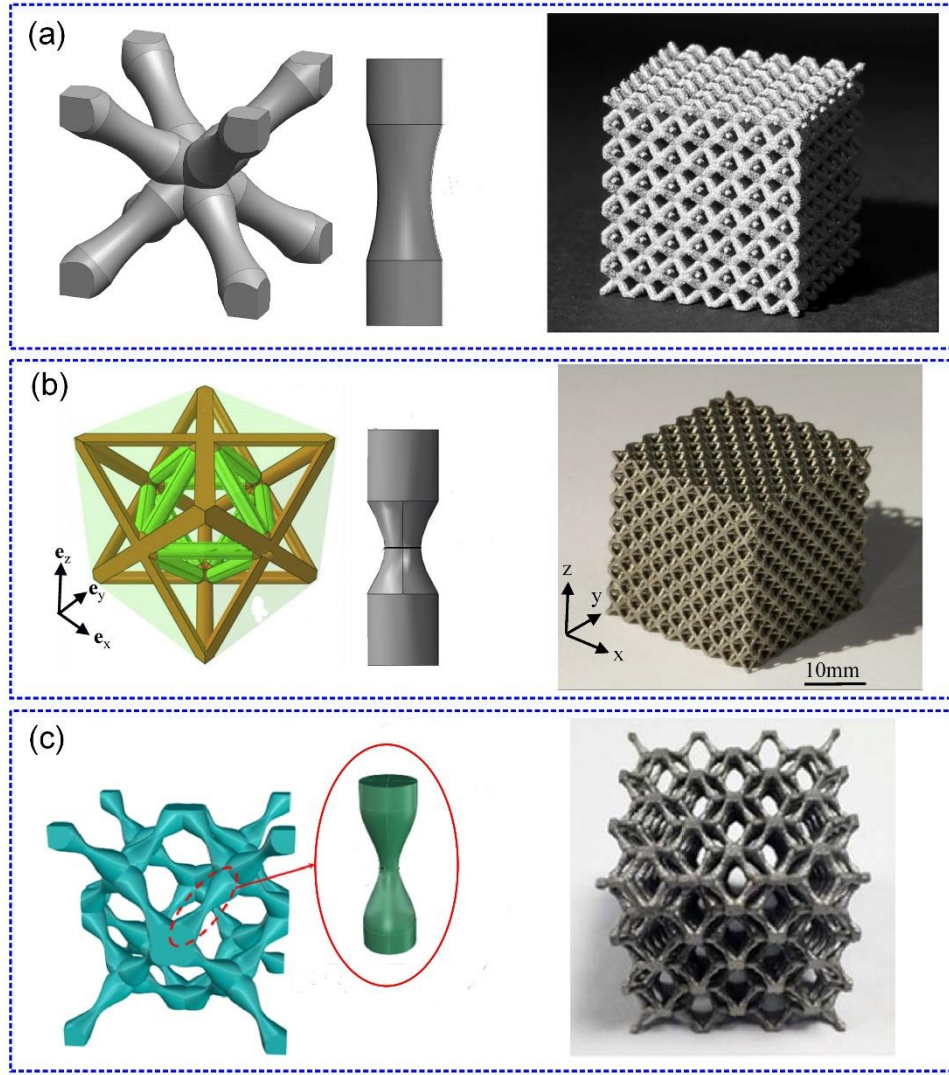
Figure 9. Topological configurations and printed samples for the lattices with taper struts. (a) BCC [119], (b) octet [130], (c) RD [131].

The variable cross-section struts design was also used to eliminate the shear band formation, thereby helping enhance energy absorption capacity. For example, the variable cross-section BCC lattices were designed by varying the diameter ratio (R_d) (a ratio of the strut end diameter (R_1) to strut center diameter (R_2)) [132], as shown in **Figure 10(a)**. It was found that the shear band formation could be controlled by adjusting the diameter ratio. Specifically, shear bands were found on the lattices with a high actual diameter ratio (R_d^{actual}) of 2.7 and 3.3, while no shear bands were observed with a low actual diameter ratios of (R_d^{actual}) of 1.1 and 2.0.

In literature, another approach to enhance the energy absorption capacity of a strut-based

lattice reported is to hybridize the octahedron and bending-dominated structures [80]. Two hybrid structures based on an octet lattice were fabricated by FDM with PLA material. The mechanical properties were obtained by the quasi-static compression tests. The results showed that hybrid structures display both a higher stiffness and a higher strength than the octet lattice counterparts. Moreover, the stress-strain responses of the proposed hybrid structures exhibit lower stress fluctuations in the post-yield phase compared with the octet lattice. The hybrid structures provide the highest specific energy absorption, meaning that the hybrid design can achieve more favorable energy absorption characteristics.

Furthermore, interpenetrating lattices (IPLs) were introduced by White et al. [133], which were constructed by interweaving two or more elementary lattices without connection. In their study, four $5 \times 5 \times 5$ RD+FCC interpenetrating lattices were fabricated by AM approaches with four different materials (i.e., 316L, VeroWhite, IP-S, and PA12). The compressive deformation modes and the stress-strain responses of these lattices are given in **Figure 10(b)**. It was found that the FCC and RD IPLs could present catastrophic failure caused by the shear banding, while the RD+FCC IPLs did not suffer a global failure. The stress-strain curves indicated that the energy absorbed by the IPLs is six times more than that by the individual RD or FCC lattices.
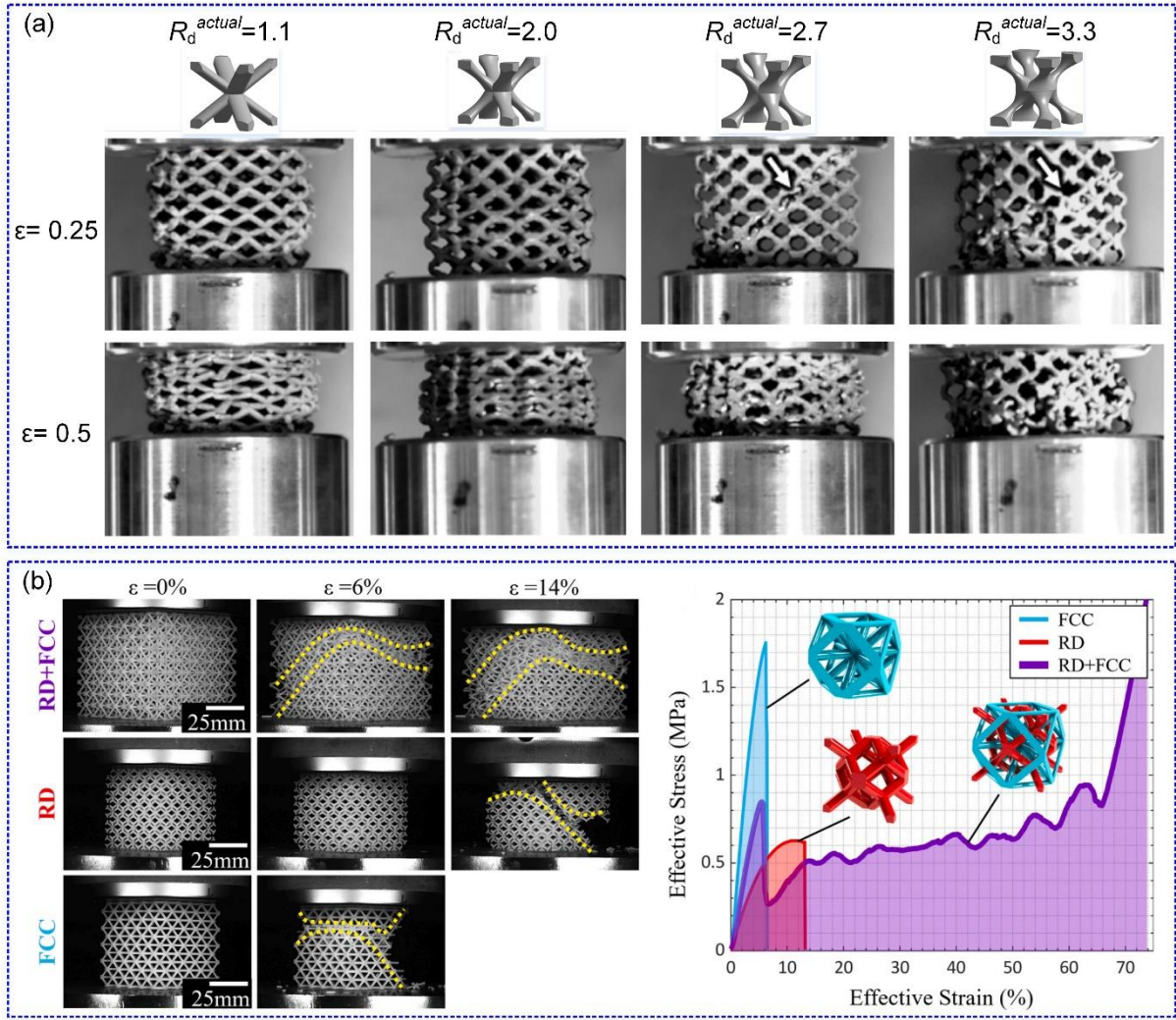
Figure 10. Methods for enhancing energy absorption of the lattices. (a) variable cross-section lattices: deformation modes at a given strain (ε) for additively manufactured BCC lattices with variable actual diameter ratios (R_d^{actual}): shear bands (marked as a red arrow) are observed on the lattices with actual diameter ratios of 2.7 and 3.3, no shear bands are observed with actual diameter ratios of 1.1 and 2.0 [132], (b) interpenetrating lattices: compressive responses of the RD, FCC, and RD+FCC IPLs with VeroWhite material, deformation modes(left), where catastrophic failure caused by the shear banding (yellow lines) is observed on RD and FCC while no global failure is observed on RD+FCC IPLs, stress-strain curves (right), where the energy absorbed by the IPLs is six times more than that by the individual RD or FCC lattices [133].

3.1.2 Hollow strut lattices and plate/shell lattices

Compared with solid strut counterparts, hollow strut lattices have higher second moments of area with the same mass, which can substantially increase the resistance to elastic or plastic buckling. Moreover, the relative density of cellular structures can be controlled by hollow strut design without changing the cell size or truss slenderness ratio [134]. Following this idea, the SC, BCC, FCC, and SC-FCC hollow strut lattices have been developed to obtain isotropic elastic properties; and experimental tests were carried out to validate the design on the SLA samples with glassy polymer [135]. By replacing the connecting joints of the lattices with the hollow sphere, Bonatti and Mohr [136] proposed hybrid truss-sphere (HTS), hollow sphere assembly (HSA), along with hollow octet truss (HOT), and solid octet truss (SOT) lattices. They studied their large deformation responses on the printed samples fabricated by SLM with 316L stainless steel. It was found that the HTS and HOT lattices exhibit the highest strength and energy absorption capacity at a 20% relative density; and the HTS lattices exhibit the highest relative Young's and bulk modulus.

Ultralight metallic micro-lattices were also developed and fabricated by SPPW, plating, and etching processes [95]. The resulting metallic micro-lattices exhibited a density $\rho <$ 10 mg/cm^3, and Young's module E scaled with the density as $E \propto \rho^2$. A diamond-structured hollow-tube lattice was designed and fabricated by SLA, plating, and high temperature calcination [137]. It was found that the density of the proposed lattice is $\rho \approx 20$ mg/cm^3, and the proposed lattices exhibit better mechanical performance than other cellular materials.

To achieve the Hashin-Shtrikman upper bounds on isotropic elastic stiffness [138, 139], a concept of plate lattices has been proposed in the literature [140]. Following this idea, a series of plate-shaped lattices was designed and experimentally investigated on the additively manufactured samples. For instance, Tancogne-Dejean and co-workers [141] designed an isotropic plate lattice by mixing the elementary structures (SC, BCC, FCC), as shown in **Figure 11(a)**. The proposed plate lattices were fabricated by TPL with glassy polymer, as shown in **Figure 11(b)**. It was found that the SC-BCC-FCC lattices possess an elastically isotropic property, and their elastic moduli are close to the upper limit of the Hashin-Shtriaman bound.

515   The high strain rate responses of the SC-BCC plate lattice were also investigated on the

SLM fabricated samples with 316L stainless steel, as shown in **Figure 11(c)** [142]. It was found

that the specific energy absorption (SEA) of the SC-BCC plate lattice is 34% higher than that

of the truss lattice. Andrew et al. [87] proposed plate lattices fabricated by DLP with

PlasGRAY^{TM} thermoplastic materials and studied their energy absorption properties under low-

520 velocity impact loading. It was found that the SC-BCC-FCC plate lattice exhibits a higher SEA

capacity compared to other plate lattices. Furthermore, the multi-wall carbon nanotube

(MWCNT) was incorporated into polypropylene random (PPR) copolymer and high-density

polyethylene (HDPE) using the FFF technique to enhance the energy absorption performance

[143]. It was found that the printed SC-BCC-FCC plate lattice exhibits a comparable energy

525 absorption performance with the conventional lattices.
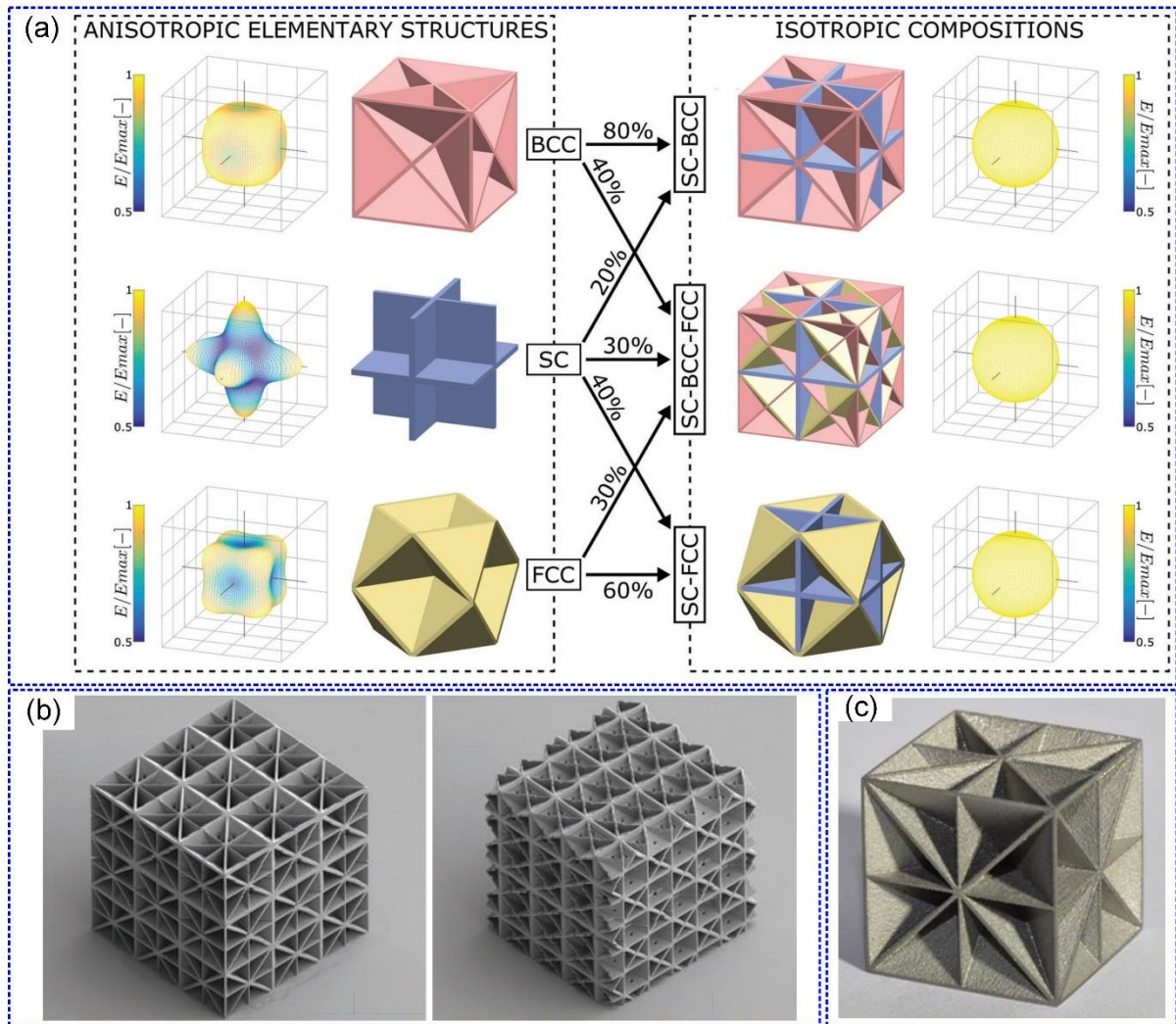
Figure 11. Illustration of the design for isotropic plate lattices and additively manufactured

samples: (a) Anisotropic elementary structures and isotropic plate-lattice compositions (SC-BCC, SC-BCC-FCC, SC-FCC) obtained by mixing the elementary structures [141], (b) 3D printed glassy polymer SC-BCC and SC-FCC samples [141], (c) 3D printed 316L stainless steel SC-BCC sample [142].

Similarly, Rui et al. [144] have proposed a series of dual-scale hybrid plate-lattices (namely $\{2FCC\}^3$, $\{2FCC\}^3|\{2SC\}^3$, $\{2FCC\}^3|\{SC\}<2\ 2\ 2>$, $\{2FCC\}^3|\{BCC\}<2\ 2\ 2>$, as shown in **Figure 12(a)**), which are structured in a $2\times2\times2$ array of unit-cells. The mechanical behavior and energy absorption characteristics of these proposed hybrid plate-lattices were studied by quasi-static compression tests using printed samples by SLS with nylon; the deformation modes are shown in **Figure 12(b)**. The experimental results indicated that the $\{2FCC\}^3|\{SC\}<2\ 2\ 2>$, $\{2FCC\}^3|\{BCC\}<2\ 2\ 2>$ lattices first bulked along the loading directions, and then overall bending deformation became dominant with increasing strain, in which no fracture failure was observed in the whole loading process. For the $\{2FCC\}^3$ and $\{2FCC\}^3|\{2SC\}^3$ lattices, some cracks were observed at the strain around 0.3 when the specimen was damaged severely. The results showed that the proposed hybrid plate-lattices are of higher specific strength, higher specific stiffness, and greater energy absorption capacity than the elementary plate-cell structures.
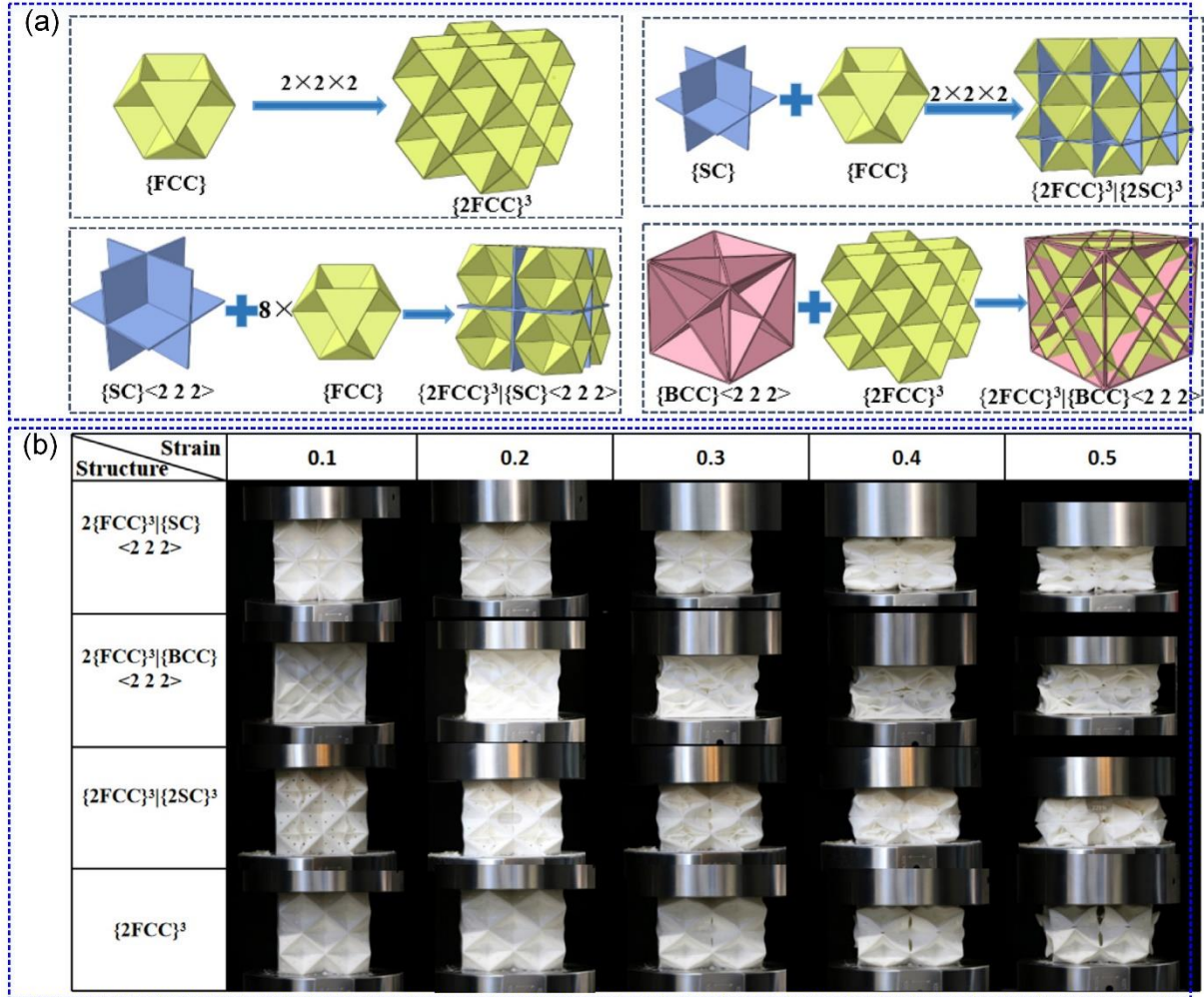
Figure 12. (a) From the elementary structures to the dual-scale hybrid plate-lattices, (b) compression deformation modes for the dual-scale hybrid plate-lattices fabricated by SLS with nylon [144].

Generally speaking, the plate-lattice structures with the closed-cell feature can be problematic for AM using vat photopolymerization or powder bed-based techniques since it is challenging to manufacture unsupported cell walls for the direct deposition techniques [145]. To this end, a family of half-open-cell plate lattices, by adding small holes on the plate to facilitate the vat photopolymerization or powder bed-based process, has been proposed by Duan et al. [145]. The mechanical performance and energy absorption of the proposed half-open-cell plate lattices were investigated on the samples fabricated by SLM with 316L stainless steel, as shown in **Figure 13(a).** It was found that the proposed half-open-cell plate lattices exhibit excellent elastic properties and remarkable energy absorption capacity.

Another attempt was made to design the semi-plate lattices by inserting a small hole in the plate structure [146]. The simple cubic semi-plate lattice and face center cubic semi-plate lattice were experimentally investigated using the samples fabricated by Ployjet, as shown in **Figure 13(b)**. It was found that the proposed semi-plate lattices are of higher elastic moduli and higher compressive strength than metallic foams with the same level of fracture toughness. Wang et al. [147] proposed a sandwich square tube constructed by filling a plate lattice into a square tube. Their axial and lateral crushing responses were investigated using the DLP fabricated samples, as shown in **Figure 13(c)**. It was found that the energy absorption capacity of the proposed sandwich square tube is improved by means of a stable and progressive collapse mode.
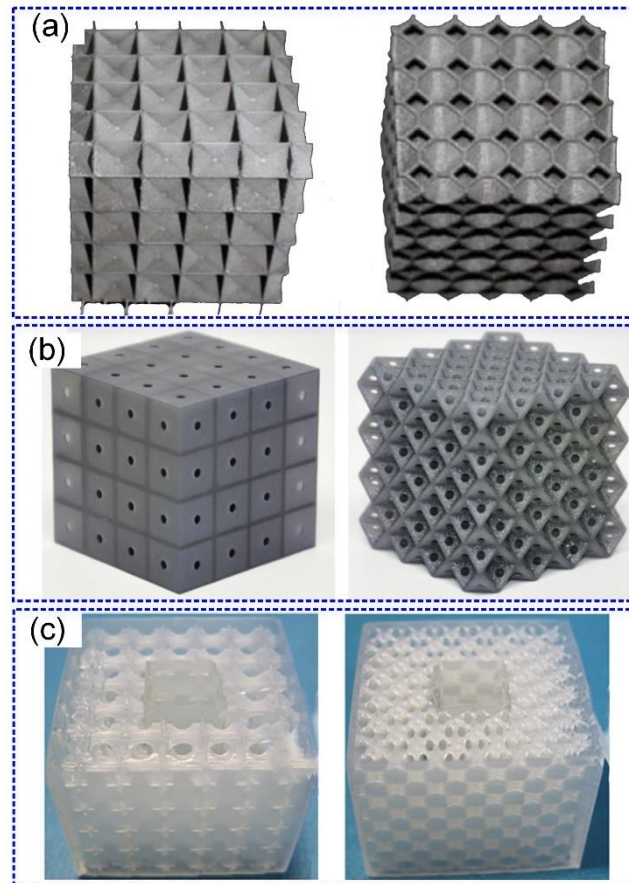
Figure 13. Examples of additively manufactured plate lattices: (a) ISO (left), and ANI plate lattices produced by SLM with 316L stainless steel [145], (b) semi-plate lattices produced by Ployjet with VisiJet M3 Black resin (left: semi-plate lattice with SC (SPL_SC), right: semi-plate lattice with FCC (SPL_FCC)) [146], (c) plate-lattice filled square sandwich tubes produced by DLP with PR48 resin (left: tubes filling with octet plate-lattice (TO), right: tubes

filling with cubic + octet plate-lattice (TCO)) [147].

Shell lattices comprising hollow spheres were proposed to produce desired mechanical properties. For instance, Dai et al. [148] presented a series of open-cell hollow-sphere structures (SC, BCC, and FCC) by connecting the hollow spheres with a hollow cylindrical tube to facilitate the 3D printing process, as shown in **Figure 14(a)**. The results showed that the mechanical properties of the proposed open-cell hollow-sphere structures are significantly influenced by wall thickness, connection radius, elastic modulus and yield strength of base materials. Chen et al. [149] proposed a stretching-dominated shell lattice and obtained its mechanical properties experimentally, as shown in **Figure 14(b)**. It was found that the proposed shell lattice exhibits ultra-stiff, ultra-strong, and high SEA characteristics. Huan et al. [150] proposed an architected polymer foam [139], which consists of perforated spherical shells and strut connectors, as shown in **Figure 14(c)**. It was found that the mechanical performances of APF can be controlled by the flat strut connectors, AM process parameters, and base material properties.

Furthermore, Bonatti and Mohr [151-153] proposed a novel family of smooth-shell structures and investigated the associated mechanical performances through the SLM fabricated samples with 316L stainless steel, as shown in **Figure 14(d)**. They found that the smooth shell lattices possess higher stiffness, strength, and energy absorption capacity due to their characteristics of geometric smoothness which reduces the stress concentrations at the joints or intersections. Interestingly, the triply periodic minimal surfaces (TPMS) like shell lattices are recovered in the study when the scalar parameter equals 1.

Bhat et al. [154] proposed tessellated lattice structures that constructed by tessellating the unit lattice cell in a metallic crystal manner (e.g., SC, BCC, FCC and HCP), where the spherical unit lattice cell was inspired by the sea urchin shell, as shown in **Figure 14(e)**. The proposed tessellated lattice structures were printed using MJF with PA12 and tested for their mechanical properties. The results showed that the proposed tessellated lattice structures possess superior mechanical and energy absorption abilities.
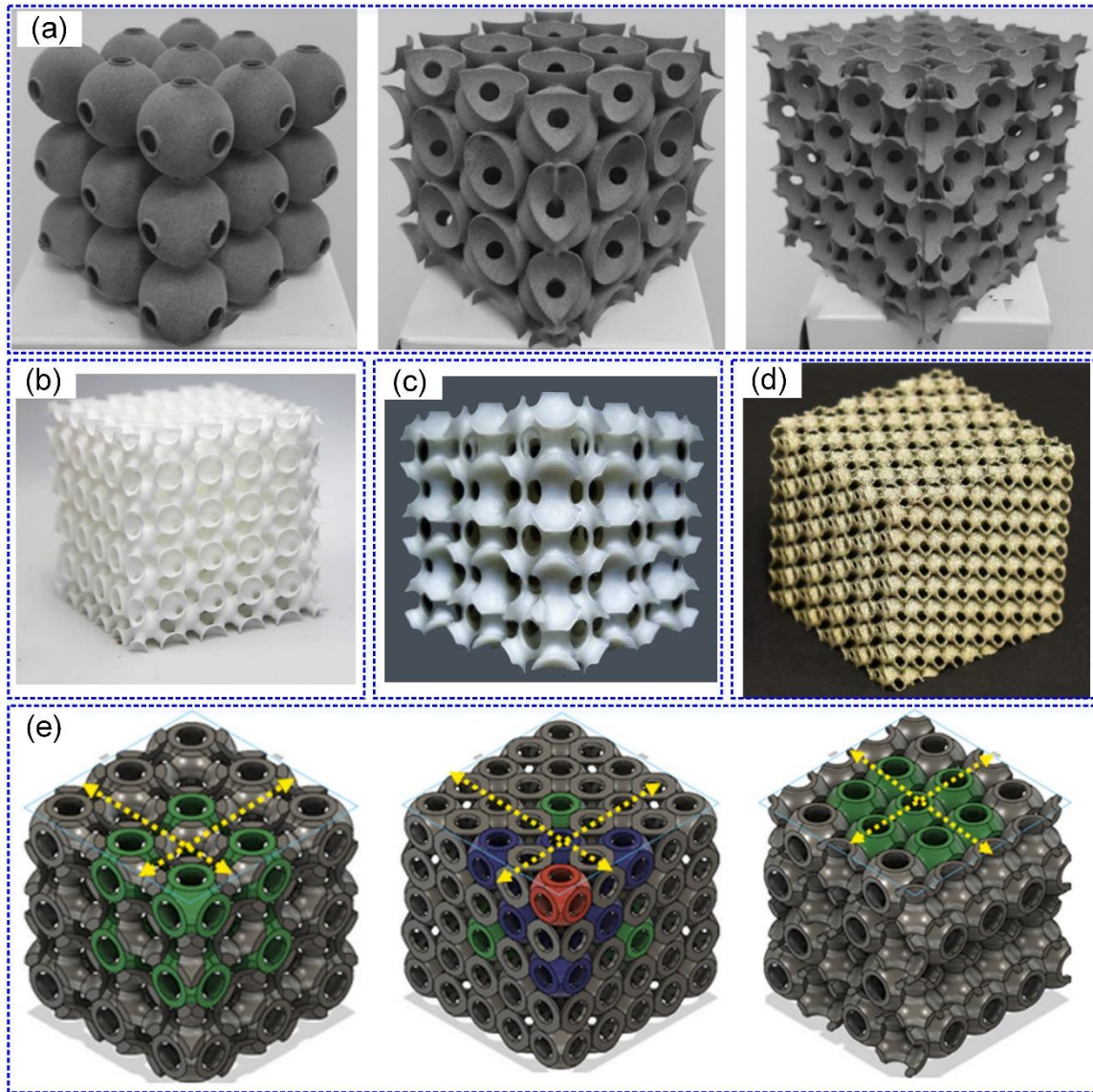
Figure 14. Examples of sphere-based shell lattices and smooth shell lattices: (a) Open-cell hollow-sphere structures produced by multi-jet melting with nylon PA12 [148], (b) stretching-dominated shell lattices produced by SLS with nylon PA2200 [149], (c) architected foams produced by Ployjet with polymer [150], (d) smooth shell lattices produced by SLM with 316L stainless steel [151] , (e) atomic tessellated lattice structures (BCC, FCC, and HCP)[154].

3.1.3 Triply periodic minimal surface (TPMS) lattices

Triply periodic minimal surfaces (TPMS) are a set of special surfaces in which the mean curvature is zero at any point on the surface. The TPMS is a smooth surface without sharp edges or joints, which has been found in nature, such as sea urchin skeletons [155], butterfly wings

[156], and soap films [157]. A comprehensive review of TPMS lattices can be found in [47].

The most used method to model TPMS is a level-set equation which can be defined in terms of the Fourier series [158],

$$\Psi(r) = \sum_{\mathbf{k}} F(\mathbf{k})\cos[2\pi\mathbf{k} \cdot r - \alpha(\mathbf{k})] \tag{1}$$

where $\mathbf{k}$ is the reciprocal lattice vector, $\alpha(\mathbf{k})$ is a phase shift, and the structure factor $F(\mathbf{k})$ is an amplitude associated with the given $\mathbf{k}$ vector.

Some examples of level-set equations for different TPMSs are provided as follows,

Schwarz-Primitive (P):

$$\phi_P \equiv \cos(x) + \cos(y) + \cos(z) = c \tag{2}$$

Schwarz-Diamond (D):

$$\phi_D \equiv \cos(x)\cos(y)\cos(z) - sin(x)sin(y)sin(z) = c \tag{3}$$

Schoen-Gyroid (G):

$$\phi_G \equiv \sin(x)\cos(y) + \sin(y)\cos(z) + \sin(z)\cos(x) = c \tag{4}$$

Schoen-IWP (IWP):

$$\phi_{IWP} \equiv 2\big(\cos(x)\cos(y) + \cos(y)\cos(z) + \cos(z)\cos(x)\big)$$
$$-(\cos(2x) + \cos(2y) + \cos(2z)) = c \tag{5}$$

Schoen-F-RD (FRD):

$$\phi_{FRD} \equiv 4(\cos(x)\cos(y)\cos(z))$$
$$-\big(\cos(2x)\cos(2y) + \cos(2y)\cos(2z) + \cos(2z)\cos(2x)\big) = c, \tag{6}$$

where $x = 2\pi x_L/L_x$, $y = 2\pi y_L/L_y$, $z = 2\pi z_L/L_z$, x_L, y_L, z_L, are the coordinates, and L_x, L_y, L_z are the unit cell sizes along X, Y, and Z directions, respectively.

Typically, two strategies can be used to construct the TPMS-lattice using the TPMS, namely (a) solid-network lattice and (b) sheet-network lattice. For the solid-network lattice, the volume is divided by the TPMS, and one of the subdomains possesses the solid material, whereas the other subdomain is void. The sheet-network lattice is modeled by thickening the TPMS with a given shell thickness, as shown in **Figure 15(a)**. Examples of some AM TPMS-lattices are shown in **Figure 15(b-e)**.

Over the last decade, researchers have carried out numerous studies on the TPMS lattices

to explore their mechanical and energy absorption characteristics in different loading scenarios using theoretical [57], numerical [28, 159], and experimental [160] methods. Various topologies of TPMS surfaces are used to construct the sheet-network or solid-network lattices; the typical TPMS lattices found in the open literature are summarized in **Figure 16**. It can be found that the most studied lattices were produced based on the P, G, D, and IWP surfaces.
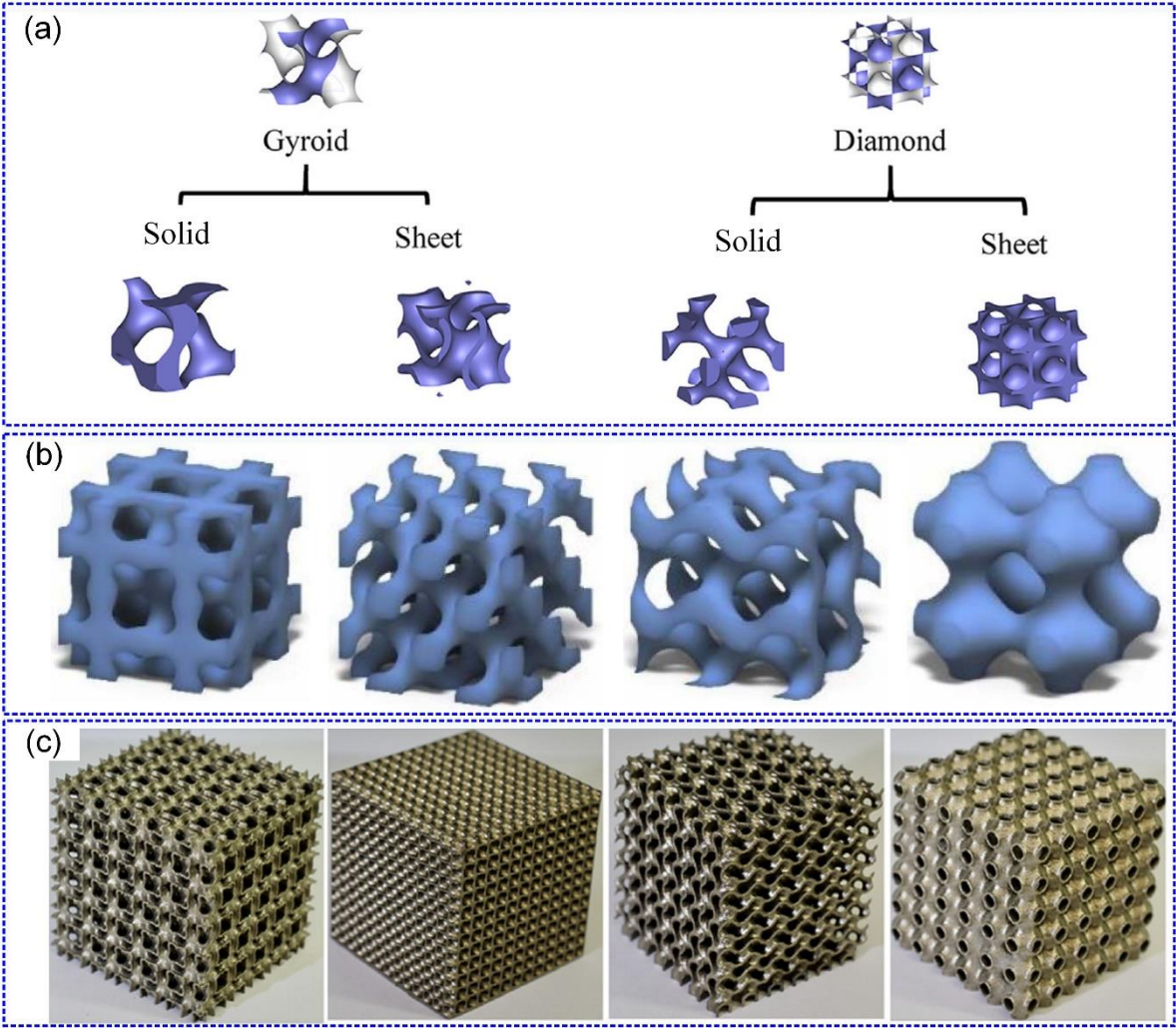
Figure 15. The modeling strategy for the TPMS lattices and their additively manufactured samples: (a) Illustration of the construction of solid-network and sheet-network lattices [97]; Examples of the 3D-printed TPMS-lattices: (b) solid-network lattice: IWP, D, G, P (from left to right) [161], (c) sheet-network lattice: IWP, D, G, P (from left to right) [28].
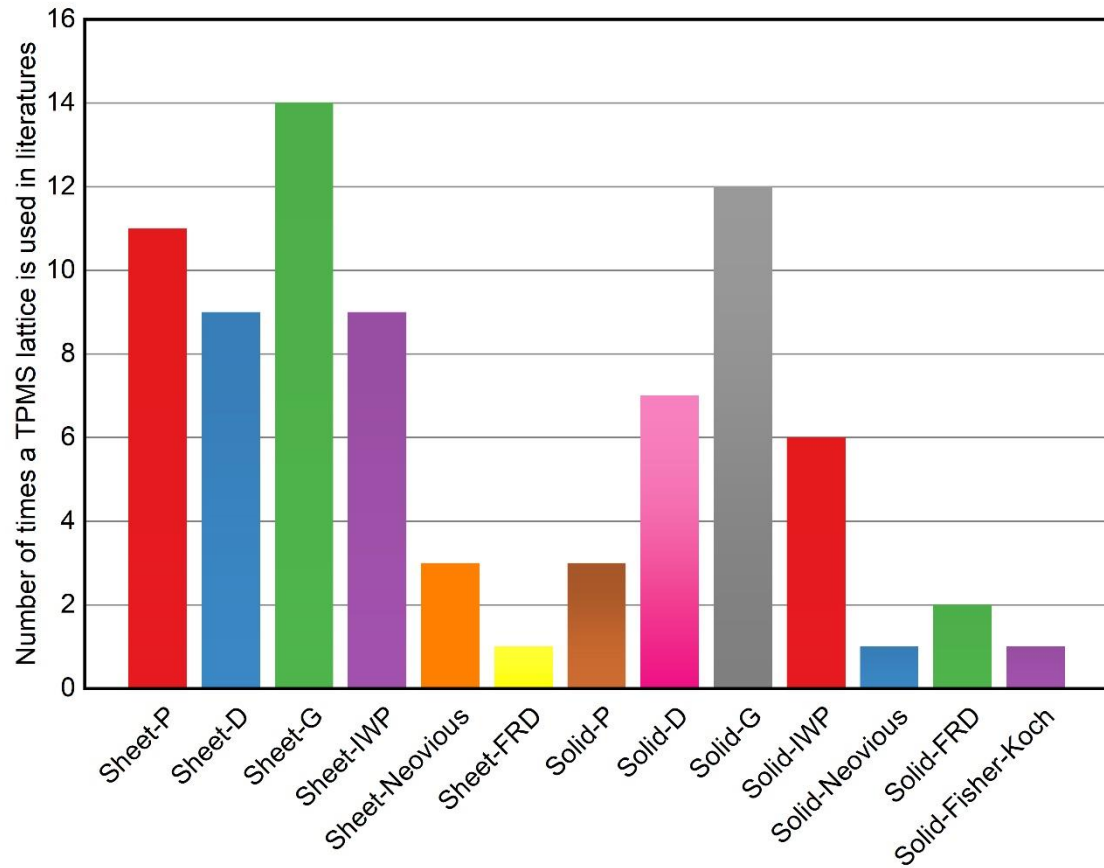
Figure 16. Various types of topologies of TPMS investigated in the analyzed literatures: Sheet-P [17, 28, 159, 162-169], Sheet-D [17, 28, 61, 97, 159, 165, 168, 170, 171], Sheet-G [17, 28, 61, 97, 159, 163, 165, 168-173], Sheet-IWP [17, 28, 61, 160, 163-165, 169, 174], Sheet-Neovious [86, 171, 175], Sheet-FRD [163], Solid-P [161, 176, 177], Solid-D [28, 65, 97, 161, 177-182], Solid-G [28, 65, 97, 161, 177-184], Solid-IWP [28, 160, 161, 178, 184, 185], Solid-Neovious [186], Solid-FRD [186, 187], Solid-Fisher-Koch [178].

In line with Gibson and Ashby's theory [1], the mechanical properties of lattices can be described by scaling laws, e.g., $\psi = C\rho^n$, where ρ is the relative density, ψ is the effective mechanical property of lattices, C and n are the fitting constants. In general, the ideal moduli of bending-dominated and stretch-dominated lattices have a scaling constant n of 2 and 1, respectively. The ideal strength of bending-dominated and stretch-dominated lattices has a scaling constant n of 1.5 and 1, respectively [188]. **Table 2** summarizes the experimentally obtained fitting constants for the mechanical properties and energy absorption characteristics of different TPMS-based lattices.

In general, it is anticipated that the solid-network lattices exhibit a bending-dominated performance while the sheet-network lattices exhibit a stretching-dominated performance [47]. In literature, most solid-network lattices exhibit a bending- or mix-mode of deformation [28, 61]. However, some solid-network lattices were found to deform in a stretching-dominated mode [160, 187]. Besides, the sheet-network lattices with the same topology may exhibit different deformation modes. For example, Al-Ketan et al. [28] and Abou-Ali et al. [61] obtained the stiffness scaling law with a constant of 1.42 and 1.08, while Zhang et al. [159] and Liang et al. [170] showed constants of 2.23 and 3.28 for the sheet-Gyroid lattices.

It was interesting to find that energy absorption per unit volume in literature was calculated through the area under the stress-strain curve up to different strains, e.g., 0.25 in [28, 160], 0.4 in [61, 170], 0.5 in [57, 185], 0.6 in [178], densification strain in [159, 172] and failure strain in [169].

Table 2. Experimental mechanical properties and energy absorption for different TPMS-based lattices

Sheet solid networks	Study	TPMS types	Materials	Unit cell length (mm)	Range of RD (%)	Young's modulus (GPa)		Maximum strength (MPa)		Yield strength (MPa)		Plateau strength (MPa)		Energy absorbed per unit volume (MJ/m^3)
						C	n	C	n	C	n	C	n	
Sheets	Al-Ketan et al. [28]	P	Maraging steel	7	10.3–20.6	19.6	1.31	1419	1.77			1667	1.94	5.07–19.44
		D			16.8–27.6	6.7	0.52	933	1.39	–		1112	1.53	18.15–38.78
		G			12.1–23.4	18.5	1.23	885	1.43			1402	1.76	8.52–27.20
		IWP			15.8–22.8	15.9	1.15	2354	2.13			1982	1.98	12.83–26.53
	Abou-Ali et al. [61]	D	PA1102	8	24.2–34.2	225.5	0.75			17.4	1.52	58.2	2.00	1.36–2.72
		IWP			16.5–25.0	232.8	0.93	–		17.4	1.57	62.0	2.27	0.42–1.07
		G			22.4–30.3	329.7	1.08			8.9	1.01	55.0	1.95	1.19–2.14
	Maskery et al. [57]	G	AlSi10Mg	3-9	22.0	81		–		330		–		16
	Li et al. [172]	G	316L stainless steel	4	31.4	–		–		253	1.25	851	1.67	49.19
	Zhang et al. [159]	P	316L stainless steel	4	10.4–18.2	106.4	1.89					1412	2.23	5.15–19.54
		D			17.8–31.4	81.7	1.42	–		–		973	1.76	31.31–77.53
		G			14.1–24.4	216.6	2.23					1449	2.1	12.31–47.55

41

	Shen et al. [169]	P	Ceramic	2-5	10–23	172.2	2.86	600	2.25					
		G			6.7–27.6	6.3	0.63	150	1.22	–		–		–
		IWP			14–33.6	21	1.32	750	1.94					
		s14			12.9–30.5	31.5	1.46	1450	2.14					
	Liang et al. [170]	P	316L stainless steel	2.5	22.5–34.4	114.9	1.34	–		–		1352	2.23	19.43–50.07
		G			26.0–36.7	772.3	3.28					4441	3.34	19.75–62.45
	Al-Ketan et al. [28]	IWP	Maraging steel	7	8.9–20.9	34.6	2.01	1531	2.17	–		1389	2.13	2.01–12.38
		D			12.3–26.1	62.5	2.22	4418	2.73			4566	3.28	1.18–13.90
		G			12.6–23.1	24.5	1.68	1189	1.86			1374	1.99	5.57–18.60
Solids	Abou-Ali et al. [61]	IWP	PA1102	8	7.4–28.1	1070.7	2.54	–		27.2	2.31	75.2	2.5	0.04–1.26
		G			6.5–27.1	1362.6	2.4			26.3	2.05	55.3	2.15	0.06–1.34
	Abou-Ali et al. [178]	D	PA1102	8	10.9–27.8	864	2.24	91.1	2.49	55.1	2.48	1753.2	4.48	0.05–3.40
		IWP			7.5–28.6	1296	2.71	67.1	2.53	39.3	2.56	181.6	3.15	0.03–2.11
		G			7.2–26.0	1257	2.36	62.3	2.26	27.3	2.10	101.1	2.55	0.07–1.95
		CY			10.7–24.6	1416	2.63	99.5	2.75	47.0	2.60	417.5	3.65	0.07–1.50
	Zhao et al. [185]	IWP	Ti6Al4V	4	0.1–0.3	21.6	1.80	–		1741.6	2.18	–		3.6–33.16

Al-Ketan et al. [160]	Primary IWP	Maraging steel	7	8.9–20.9	19.07	1.88	1531	2.17	1663	2.29	1531	2.17	2.01–12.81
	Secondary IWP			16.8–25.5	19.09	1.31	8575	2.94	2220	2.27	49385	4.58	3.5–23.63

670   Note: The energy absorbed per unit volume was calculated through summing the area under the stress-strain curve up to different strains 0.25 [28, 160], 0.4 [61, 170], 0.5 [57, 185], 0.6 [178], densification strain [159, 172] and failure strain [169].

It is generally known that the mechanical properties and energy absorption characteristics of the TPMS-based lattice structures are affected by the deformation modes, which largely depend on the topologies of lattices [75, 189-192]. For instance, Al-Ketan et al. [28] experimentally studied the compressive responses of the solid-TPMS (IWP, D, G) and sheet-TPMS (P, G, IWP, D) lattices fabricated by PBF with Maraging steel. The deformation modes of the solid-TPMS lattice and the sheet-TPMS lattice are compared in **Figure 17**. In general, three main deformation mechanisms were observed: (1) shear bands present in solid-D and IWP, and sheet-P, G, and D; (2) lattice collapses horizontally layer by layer in solid-D; (3) the lattice deforms uniformly in sheet-IWP. Interestingly, the deformation mode of the same topological lattice was independent of relative density.
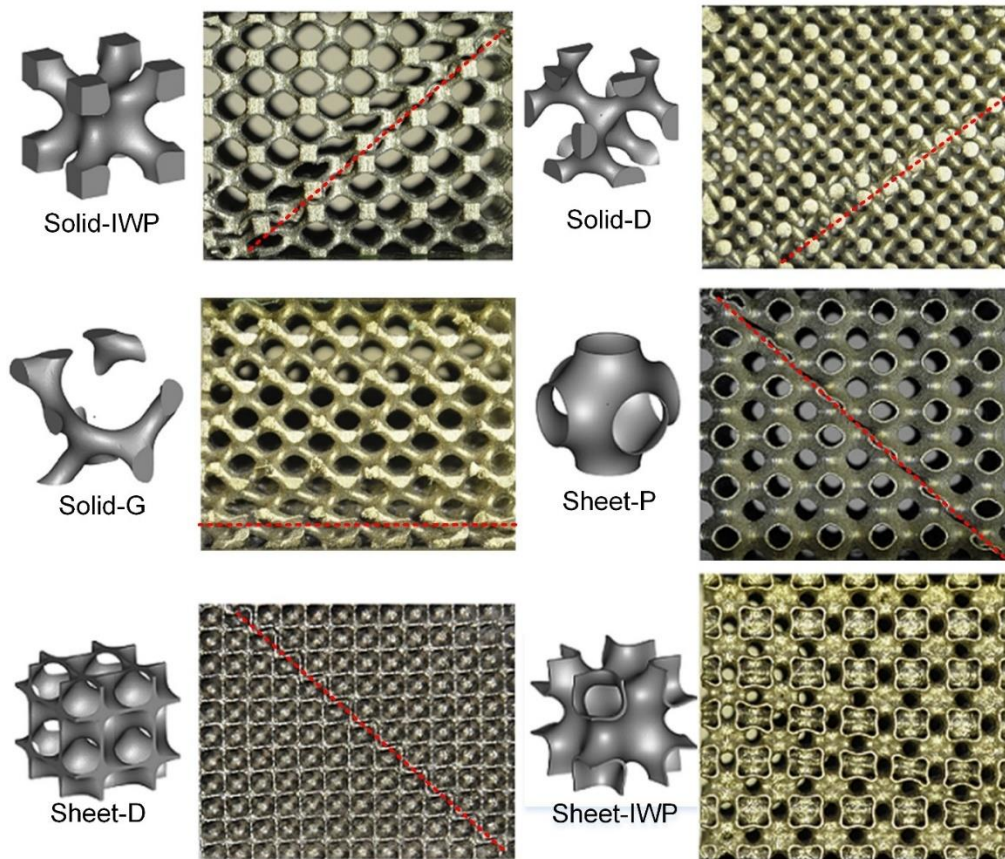
Figure 17. The deformation modes of TPMS lattices: shear bands in solid-D and IWP, and sheet-P and D, and layer-by-layer mode in solid-G, collective uniform compression mode in sheet-IWP [28].

44

Nevertheless, the same topology of TPMS lattices could present different deformation modes in different studies. For example, sheet-P exhibited single shear band deformation mode in [28] but dual shear bands mode in [163] and [159], as shown in **Figure 18(a)**. A shear band mode was presented in [28] for sheet-G but a collective deformation mode in [159, 163], as shown in **Figure 18(b)**. Sheet-IWP exhibited a collective deformation mode in [28] but a layer-by-layer mode in [163], as shown in **Figure 18(c)**. For sheet-D, a single shear band mode was observed in [28] but a collective deformation mode in [159], as shown in **Figure 18(d)**. These phenomena may be due to variations in the additive manufacturing parameters and base material properties [163, 178].
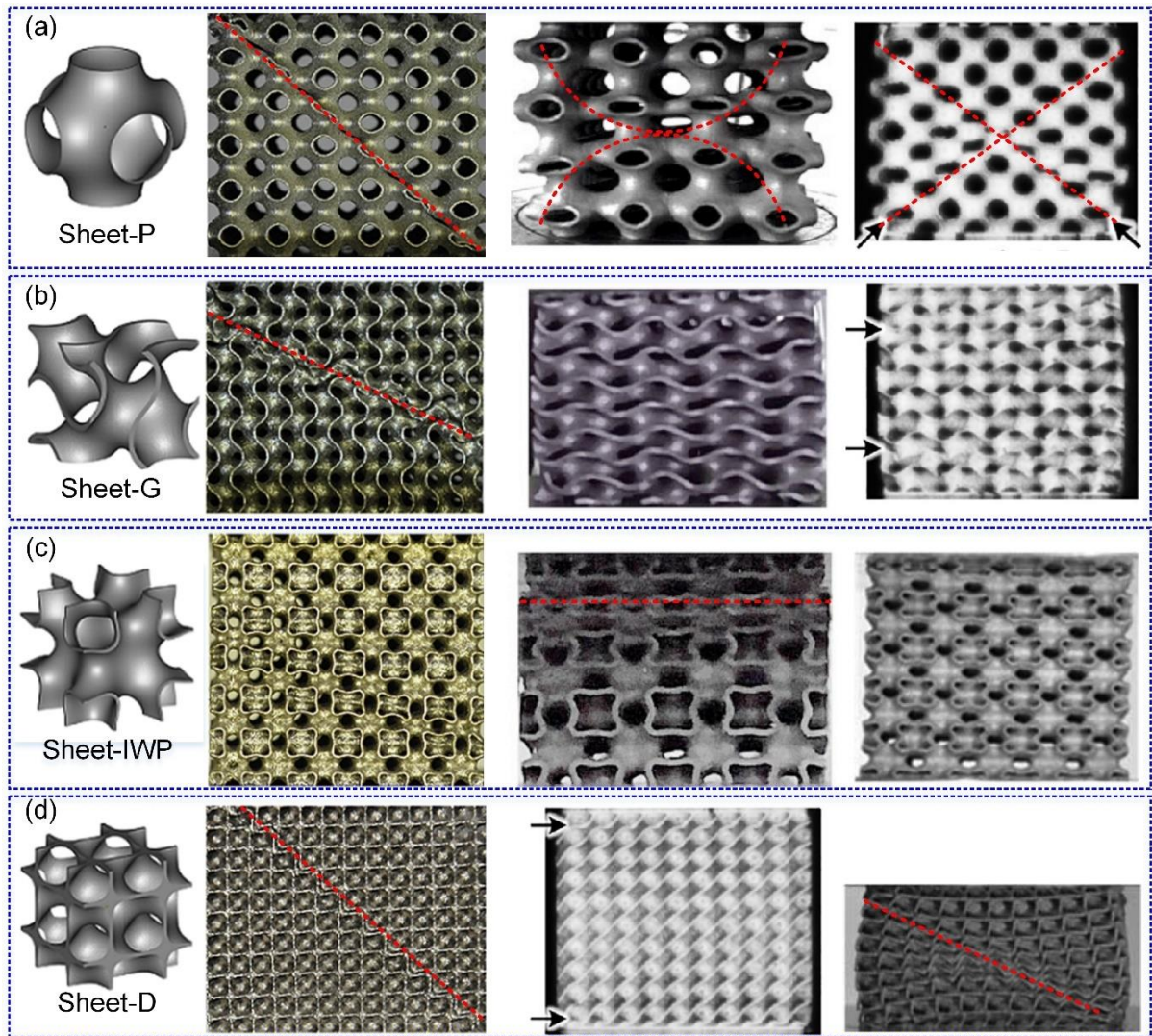
Figure 18. Comparison of the deformation modes of the TPMS lattices in different studies: (a) Sheet-P: single diagonal shear band in [28] (left), dual diagonal shear bands in [159, 163] (middle and right); (b) Sheet-G: one diagonal shear band in [28] (left), collective compression mode in [159, 163] (middle, right); (c) Collective mode in [28, 61] (left and right), layer by layer mode in [163] (middle); (d) Sheet-D: one diagonal shear band in [28, 61] (left and right), collective compression mode in [159] (middle).

Moreover, the studies also found that the unit cell size of lattice structures may influence the deformation modes of the TPMS lattices. For example, Maskery et al. [57] investigated the compressive responses of the double gyroid (sheet-G) lattice fabricated by the SLM method with AlSi10Mg material. It was found that three main failure modes depend on the cell size of the structures as shown in **Figure 19**: i.e., (1) a successive collapse failure for those composed of 4.5 mm unit cells (**Figure 19(a)**); (2) cracking or cracking propagation through the lattices for those composed of larger cells, 6 mm and 9 mm (**Figure 19(b)**); and (3) diagonal shear failure for the DG lattices with the 3 mm cells (**Figure 19(c)**).
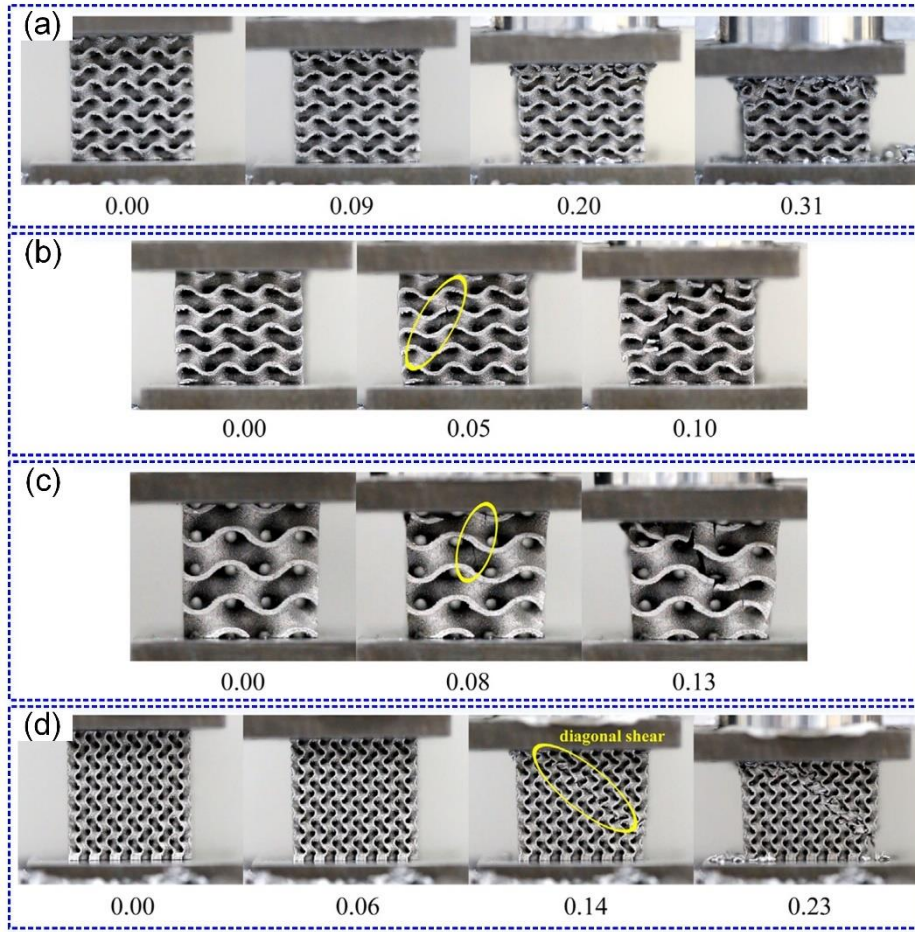
Figure 19. The deformation process and failure modes of sheet-G lattices with different unit cell sizes: (a) 4.5mm, (b) 6mm, (c) 9mm, and (d) 3mm [57].

As discussed in Section 3.1.1, shear bands in the compressive deformation modes may significantly reduce the energy absorption capacity. Studies have been conducted to suppress shear bands in literature. For example, the sheet-P lattice was modified to enhance energy absorption based on stress and strain distribution where the higher stress or higher strain areas were thickened; and their compressive deformation modes were experimentally investigated by the samples fabricated using the SLS method with nylon PA2200 material [162]. The results are shown in **Figure 20(a)**, which indicates that the normal sheet-P lattice exhibit a shear band mode while the enhanced sheet-P lattices deform in a layer-by-layer mode, which is considered more beneficial for the energy absorption of the lattice structure.

Another attempt to suppress the shear bands in the deformation process is to use the heat
treatment method [57]. The printed parts are post-processed through a one-hour solution
treatment at $520°C$ and a six-hour water quench and artificial aging at $160°C$. The
deformation mode of heat-treated samples is shown in **Figure 20(b)**. Interestingly, it is
observed that the deformation led to bulging or barreling without shear bands compared to the
shear band mode for the 3 mm unit cell size (**Figure 19(d)**).
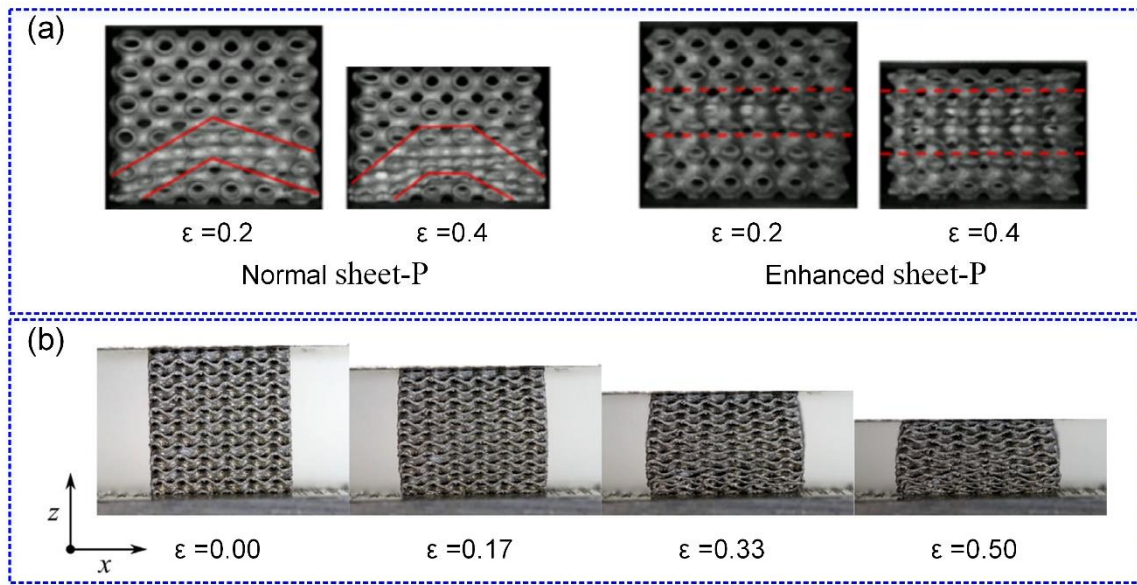
Figure 20. (a) Experimental deformation modes of normal and enhanced P-TPMS lattices
[162], (b) Compressive deformation modes of the heat-treated sheet-G lattices with 3 mm
unit cells [57].

3.2 Bio-inspired structures

Over millions of years of evolution, biological systems such as plants and animals in nature
have optimized their structures to adapt its growth and survival in various extreme
environments [193]. Researchers have attempted to learn from and imitate these biological
systems to devise novel structures with remarkable energy absorption capacity [194-198].
Various bio-inspired structures have been used as energy absorbers, and readers can refer to the
comprehensive review articles in the literature [48, 199, 200]. Additive manufacturing is an
effective method for fabricating various sophisticated bio-inspired structures. This review is

focused on the AM-based experimental investigation into the mechanical properties and energy absorption characteristics of such bio-inspired structures.

The brick-and-mortar composite structures inspired by nacre in nature have been proposed to mimic the stiff tiles and compliant organic glue to improve the overall mechanical behaviors [201]. Typical nacre-like composites consist of a stiff platelet phase and a soft matrix phase, as shown in **Figure 21(a)**. In nature, beetle elytron has evolved a remarkable structure that can protect the body and contributes to flight. The bioinspired sandwich structure with a trabecular-honeycomb core mimicked to beetle elytron has exhibited considerable potential for achieving lightweight and high energy absorption performance, as shown in **Figure 21(b)** [202].

A bone may be regarded as a sandwich structure composed of a dense outer shell and a soft core, and its anatomic morphology is shaped in response to the loads applied to it. In this regard, Ghazlan et al. [203] presented a bio-inspired thin-walled structure by mimicking femoral bone, as shown in **Figure 21(c)**. Zhang et al. [204] proposed a novel porous architecture based on the diamond lattice. Song et al. [205] fabricated hierarchical and porous hydroxyapatite structures by combining freeze casting and AM. Arjunan et al. [206] investigated the mechanical performance and permeability of 3D printed bone scaffolds using theoretical, experimental and numerical methods.

The deep-sea hexactinellid sponges were extensively studied to construct bio-inspired structures for energy absorption. For example, Fernandes et al. [207] proposed a robust lattice inspired by Euplectella aspergillum. The robust lattice has a chequerboard-like pattern constructed by adding a double set of diagonal bracings on a square-grid-like architecture, as shown in **Figure 21(d)**.

Cuttlebone has been recognized as one of the extraordinary lightweight and stiff materials in marine species [208], which offers a unique layer-based structure with excellent mechanical properties and energy absorption capacity [209-214], as shown in **Figure 21(e)**.

Table 3 summarizes the additively manufactured bio-inspired structures and their mechanical characteristics.
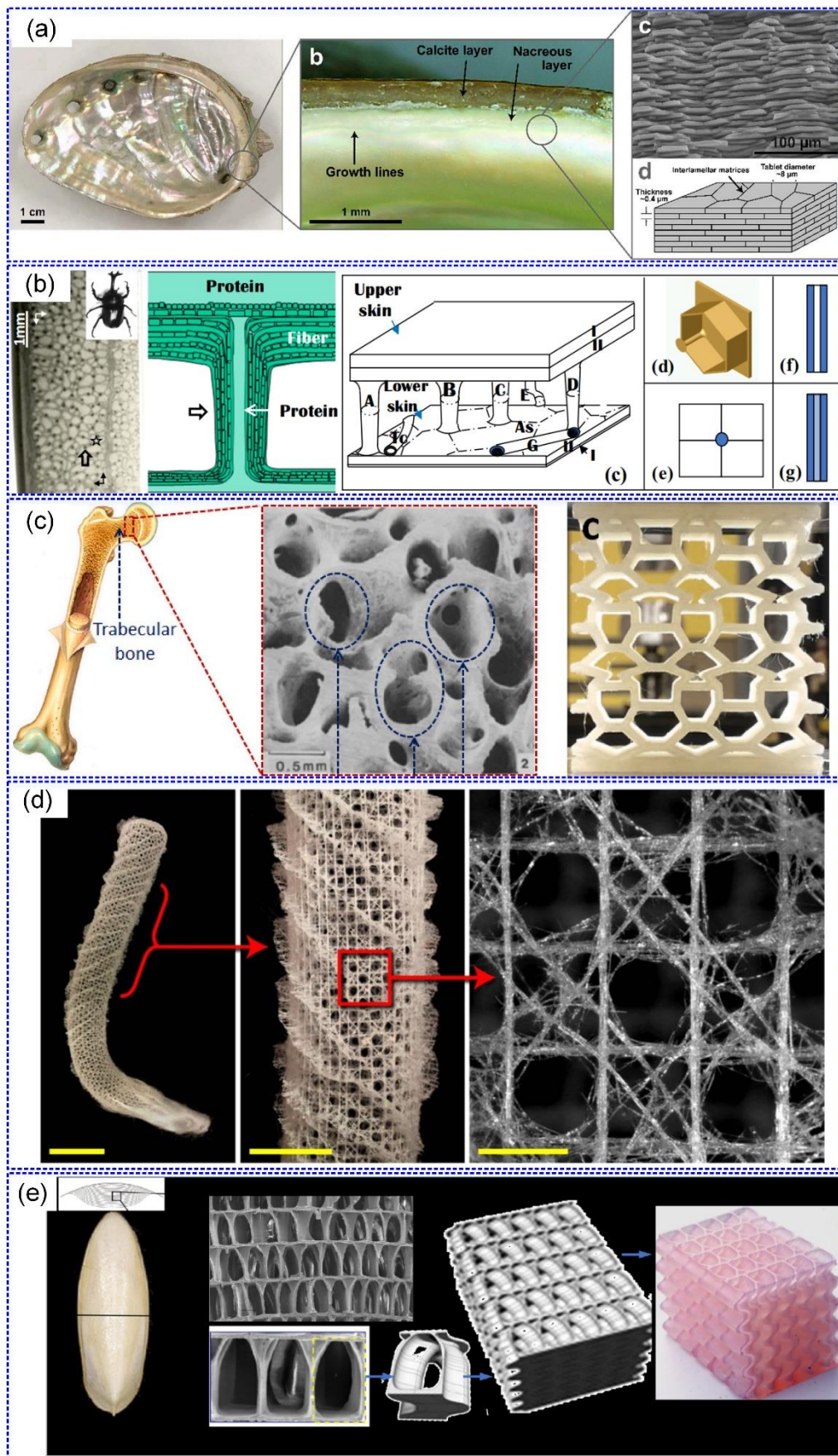
770   **Figure 21.** (a) Nacre-like composites [201], (b) sandwich structure biopsied from a beetle

elytron [202], (c) thin-walled structures inspired by femoral bone [203], (d) robust lattice

inspired from Euplectella aspergillum [207]; (e) cuttle-bone inspired layered structure [208,

209].

Table 3. A summary of additively manufactured bio-inspired materials and structures

Bionic method	Structures	AM methods	Materials used	Loading methods	Characteristics	Refs.
Nacre	Brick-and-mortar/Composite	Polyjet	Veromagenta, Tangoblackplus	Low-velocity impact	-The Nacre-like design can prevent the perforation of the projectile upon impact.	[201]
	Composite	FDM	PLA, Thermoplastic polyurethane (TPU)	Three-point bending	-The composite has highly enhanced ductility with reduced strength under three-point bending.	[215]
	Voronoi-based composite	FDM	ABS, PLA, TPU	Blast-induced impulsive loading	-The impacting energy can be mitigated and absorbed by the cohesive and adhesive bonds between two materials.	[216]
	Voronoi-based composite	Polyjet	Verowhite, TangoPlus	Pendulum impact test	-The gradient design can significantly improve the energy absorption capacity for the brick-mud structure. -The stiff material stores strain energy twice more as the soft material in the gradient structure.	[217]
Beetle elytron	Lattice	SLM	AlSi10Mg	Compressive test	-The lattice structure produced with laser power at 375W exhibited excellent energy absorption of 3.45 J.	[218]
	Sandwich	SLA	ABS	Compressive test	-The grid beetle elytron plates (GBEPn) possessed a higher compressive strength and energy absorption capacity than the end-trabecular elytron plate (EBEP).	[202]
	Beetle elytron plate (BEP)	SLM	stainless steel PH1	Compressive test	-Main peak force of BEP crash boxes was almost the same as that of the conventional crash box, but the SEA and load uniformity values are about three times and between 1/3 and 1/4, respectively.	[219, 220]

Bone	Plate-like thin-walled cellular structure	FFF	Nylon	Compressive test	-The bioinspired structures exhibited superior energy absorption compared to the re-entrant and hexagonal structures.	[203]
	Hierarchical and porous hydroxyapatite (HAP) structures	Combining freeze casting and FDM	Hydroxyapatite	Compressive test	-The 3D-printed scaffold exhibited superior compressive strength and biocompatibility.	[205]
	Lattice	SLM	Ti6Al4V	Compressive test	-The novel porous structures can be redesigned to imitate the mechanical properties of natural bones.	[204]
Muscle tissues	Tube	FDM	TPU	Compressive test	-Structural hierarchical design can improve force resistance and energy absorption characteristics under the same applied displacement.	[221]
Luffa sponge	Sandwich	FDM	TPU	Compression test	-The cushion performance of the bionic structure inspired by the luffa sponge was close to that of the luffa sponge.	[222]
Mantis shrimp	Corrugated panel	SLM	AlSi10Mg	Compressive test	-The load-bearing capacity of the bi-directionally corrugated panel (DCP) structure can be improved by increasing the wavenumber. -Three deformation modes (full-folded, transitional, and global buckling) are identified in the compressing process of the DCP structure with different wavenumbers.	[58]
Glass sponges	Lattice	Ployjet	FLX9795-DM	Compressive test	-The sponge's diagonal reinforcement strategy achieves the highest buckling resistance.	[207]
Cuttlebone	A cuttlebone-like lattice (CLL)	SLM	Inconel 718	Compressive test	-The CLL lattice exhibited a higher energy absorption performance than the BCC lattice.	[213]

775

53

3.3 Auxetic structures

Auxetic materials and structures exhibit a deformation mode of contraction in the lateral direction under longitudinal compression or expansion under axial tension, which are often termed to be the negative Poisson's ratio (NPR) phenomenon. Auxetic materials and structures present some extraordinary mechanical properties over conventional materials, such as significant energy absorption capability [223-226], remarkable fracture toughness [227], excellent in-plane indentation resistance [228, 229], and high shear stiffness [230, 231]. Numerous geometric configurations of auxetic materials and structures were proposed with 2D and 3D patterns, and their mechanical properties and energy absorption characteristics have been exhaustively investigated through analytical, numerical, and experimental methods [107, 226, 232-236]. For further details on the classification of general auxetic patterns, the reader is recommended to the comprehensive review in [237-240]. This section is focused on the AM-based experimental investigation into mechanical properties and energy absorption of the auxetic materials and structures.

Re-entrant honeycombs are a class of commonly used 2D auxetic configurations in the literature. For example, the chiral structures are fabricated by SLM, and their elastic and failure characteristics were studied in [241], as shown in **Figure 22(a)**. A novel series of chiral structures was proposed by integrating various polynomial curves and fabricated by FDM with carbon fiber (CF) reinforced PLA composites, as shown in **Figure 22(b)** [242]. It was found that the CF-reinforced design can enhance the tensile modulus, fracture strength, and energy absorption properties of the chiral samples. As displayed in **Figure 22(c)**, the arrowhead auxetic structures were developed and additively manufactured by FDM with PLA and TPU materials [243]. The arrowhead auxetic material can effectively reduce the shocking and/or impacting loading. Hybrid types of auxetic materials were proposed by combining the star and triangular structures [244], as shown in **Figure 22(d)**. Interestingly, the results indicated that the energy absorption performance of the star-triangular honeycomb in the two orthogonal

directions is much higher than that in the mono direction. A new octagonal auxetic material

was also proposed and fabricated using the TPU material [245], as shown in **Figure 22(e)**. The

auxetic behavior of the octagonal structures can be controlled by adding triangles and squares

805   to the vertices.
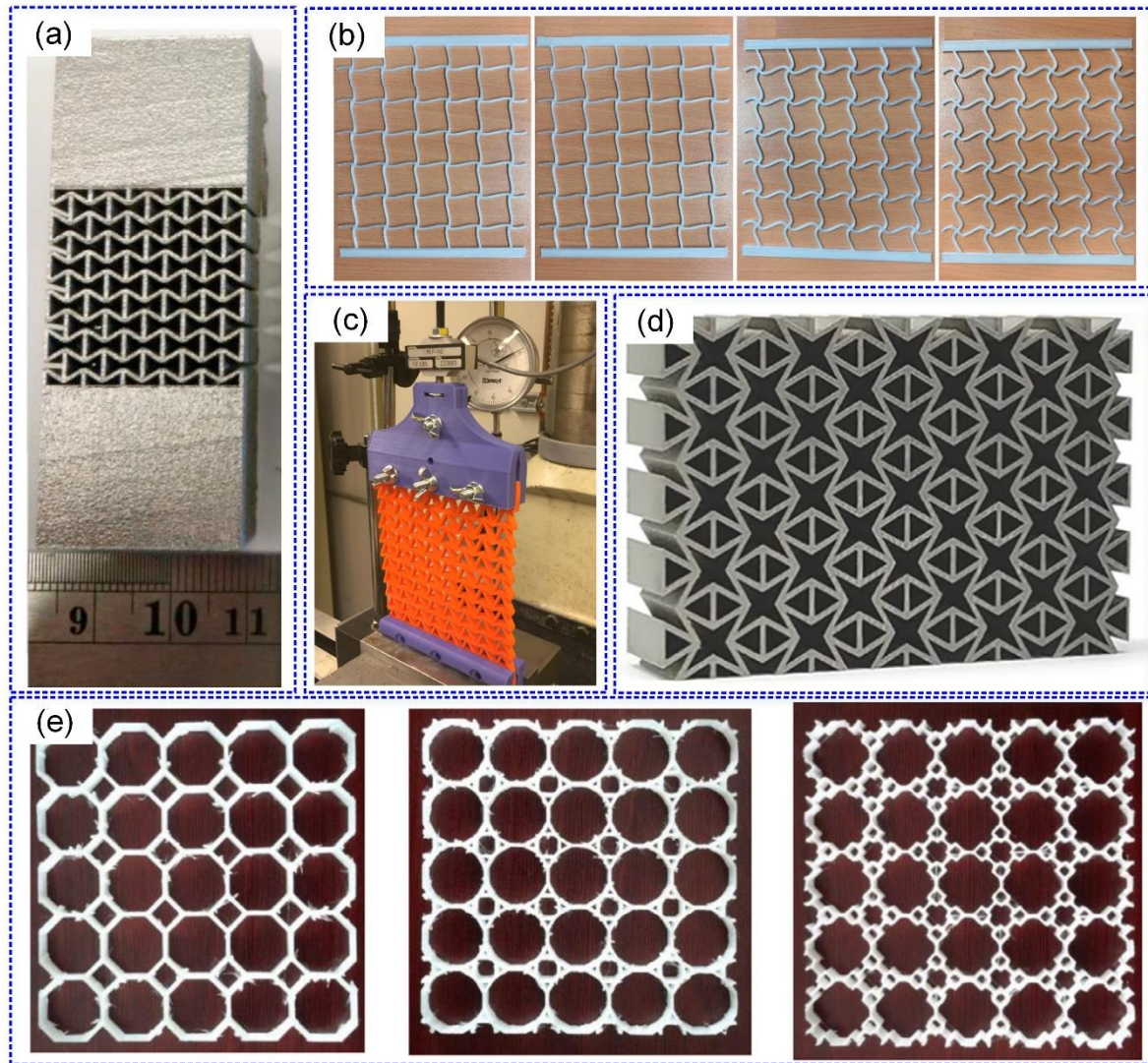
Figure 22. Examples of the 2D patterned auxetic structures: (a) Chiral structures produced by

the SLM method with the Ti6Al4V material [241], (b) chiral structures with various

polynomial curves produced by the FDM method with carbon fiber (CF) reinforced polylactic

810   acid (PLA) composites [242], (c) arrowhead auxetic structures produced by the FDM method

with the PLA and TPU materials [243], (d) star-triangular honeycomb produced using the

316L stainless steel material [244], (e) octagonal auxetic material produced with the TPU material [245].

For 3D auxetic patterns, Logakannan et al. [235] proposed a spatial re-entrant structure and fabricated it by the MJF method with the nylon PA12 material, as shown in **Figure 23(a)**. The dynamic characteristics of this structure were studied, and the results showed that the 3D re-entrant structure provides a large design space for energy absorption applications. The 3D chiral structures were also designed and fabricated through the SEBM technique with the Ti6Al4V material [246], as shown in **Figure 23(b)**. The crushing responses were obtained through the compression tests, and it was found that the unit cell size is the most prominent parameter affecting the maximum displacement and specific energy absorption (SEA). A novel 3D double-U hierarchical structure was devised and fabricated through SLM with the 316L stainless steel [223], as shown in **Figure 23(c)**. It was found that the smooth geometry of the proposed 3D double-U hierarchical structures can reduce the AM-induced defects and stress concentration within the elastic regime. Additionally, these structures exhibit improved mechanical properties such as enhanced auxetic behavior, excellent toughness, and high stiffness, indicating that they are suitable for various energy absorption applications.

A new 3D zero Poisson's ratio lattice structure was proposed by combining auxetic configuration and non-auxetic hexagonal configuration [247]. The mechanical behaviors of such structures were studied through a series of uniaxial compression tests using the samples fabricated by MJF with the nylon PA12 material, as shown in **Figure 23(d)**. The results showed that these lattice structures could improve energy absorption efficiency.

Moreover, tubular structures consisting of auxetic material as a core were proposed and fabricated by MJF with the TPU material [248], as shown in **Figure 23(e)**. Compressive tests and numerical simulations were carried out to investigate the deformation modes and mechanical properties of the proposed structures; the results revealed that the Poisson's ratio depends on the pattern scale factor (PSF) and the layer number of unit cells.
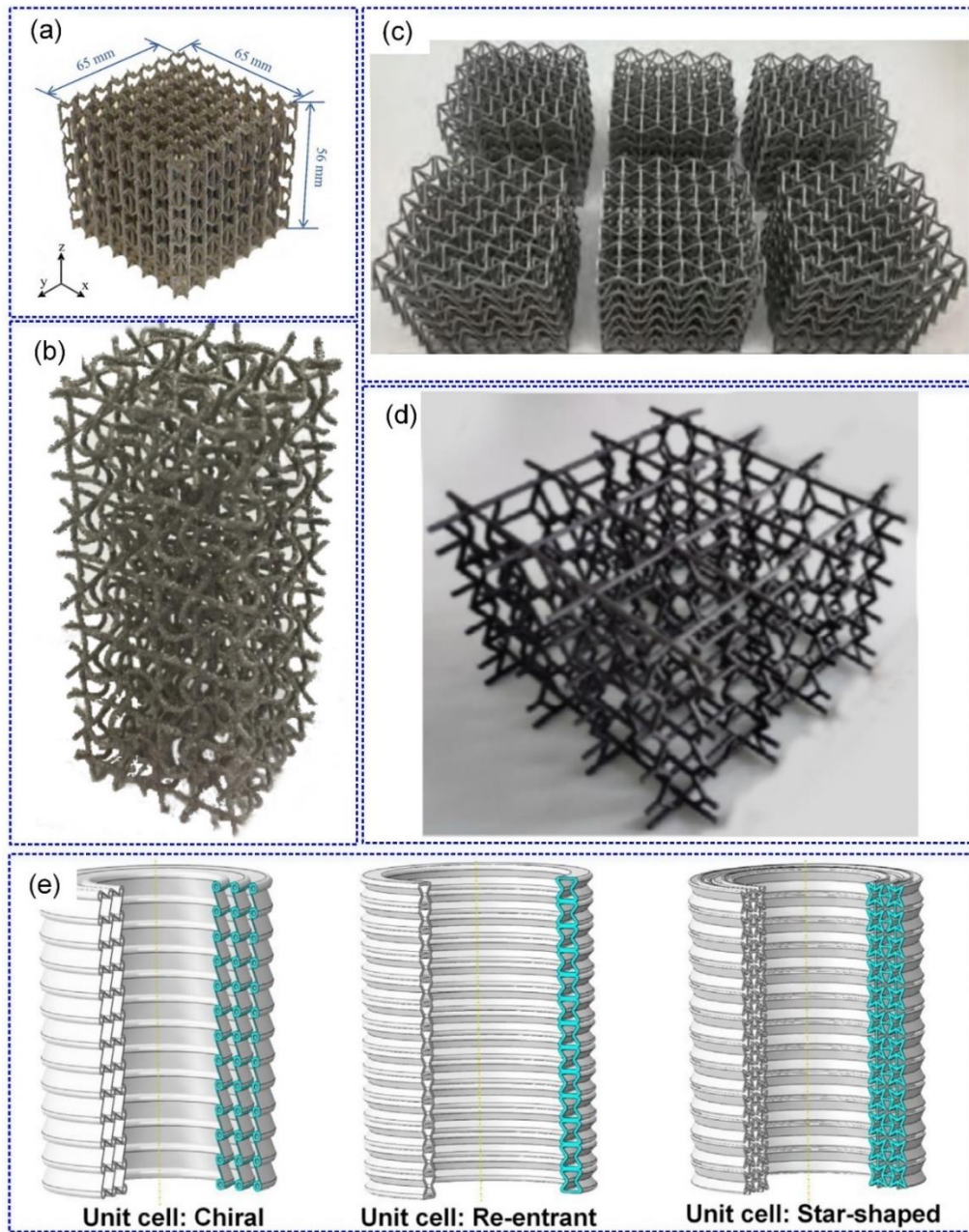
Figure 23. Examples of the 3D pattern auxetic structures: (a) 3D Re-entrant structure produced by the MJF method with nylon PA12 [235], (b) 3D chiral auxetic material produced by the SEBM method with the Ti6Al4V material [246], (c) 3D double-U auxetic structures produced by the SLM method with the 316L material [223], (d) 3D zero Poisson's ratio lattice structures produced by the MJF method with nylon PA12 [247], (e) tubular structure with auxeticity produced using TPU material [248].

3.4 Honeycomb and foam structures

2D honeycombs and 3D foams are the most studied cellular structures in the literature [2, 249-251]. Some honeycombs and foams were proposed through additive manufacturing technologies to improve their mechanical and energy absorption performances. For instance, a lightweight (~90 mg/cm^3) and super-strong (16.6 MPa compressive Young's modulus) honeycomb structure was designed and fabricated by FFF with all-cellulose ink [252], as shown in **Figure 24(a)**. The proposed honeycomb structures can support over 15,800 times their weight, meaning that they possess superb mechanical performance. The conventional honeycombs were fabricated using the Laser Engineered Net Shaping with Ti6Al4V material, as shown in **Figure 24(b)** [253].

3D Voronoi foams were designed and additively manufactured using the FDM method with various materials [254-257], as shown in **Figure 24(c)**. The deformation behavior and mechanical characteristics have been investigated through quasi-static compression tests. Interestingly the results divulged that the PLA foams with random meso-structures possess higher specific energy absorption, low-stress fluctuation, and stable deformation process than those with regular meso-structures [258]. Two types of open-cell foam structures using uniform and dual-size base cell configurations were constructed and manufactured by AM-assisted lost-wax casting, as shown in **Figure 24(d)**. The stiffness and energy absorption of these structures were characterized through compressive tests, and the results demonstrated that the dual-size structures exhibit higher efficiency compared to the uniform structures [259].
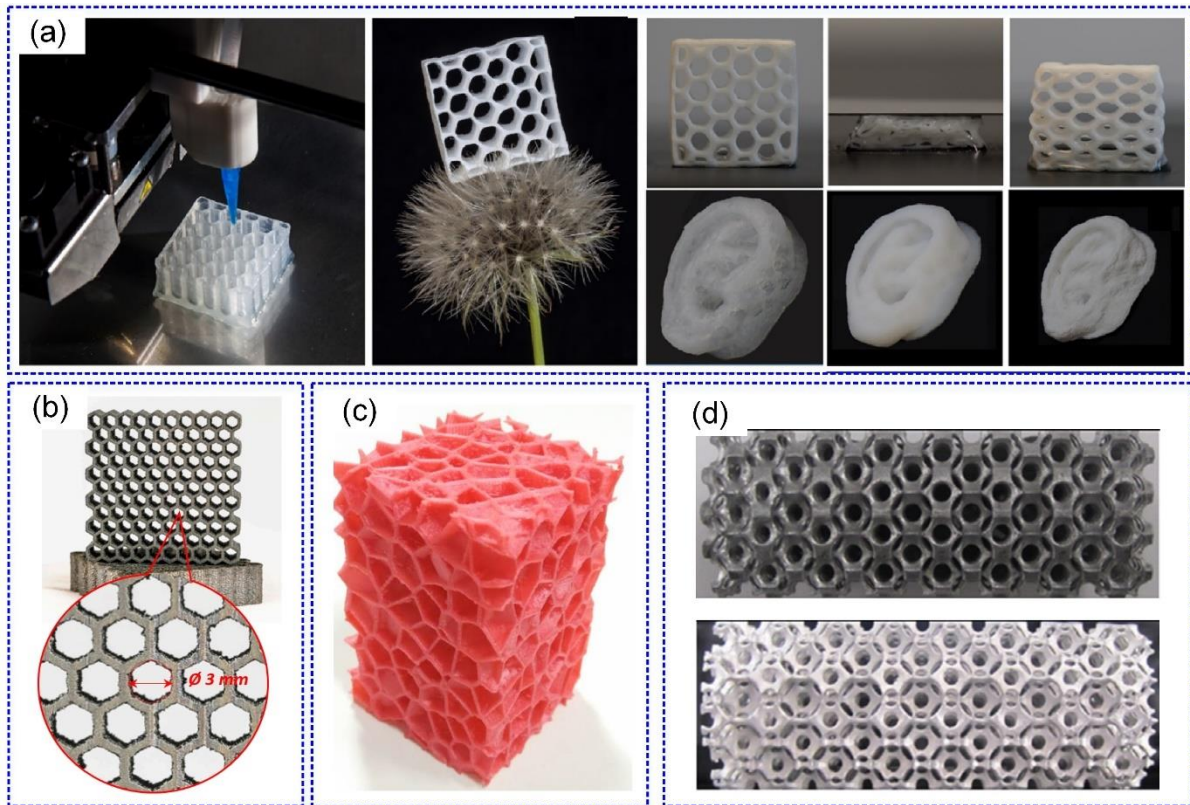
Figure 24. (a) Lightweight, strong cellular structural materials produced by FFF with all-cellulose ink [252], (b) honeycombs produced by the Laser Engineered Net Shaping with Ti6Al4V material [253], (c) 3D Voronoi closed-cell foams produced by the FDM method with the ABS material [258], (d) open-cell foam structures produced by AM assisted lost-wax casting [259].

3.5 Fiber-reinforced materials

The polymeric base materials often have relatively poor mechanical properties compared with metals and ceramics, which prevents the pure polymeric materials and structures from being used for load-bearing parts. On the other hand, carbon fiber offers significant advantages that characterize lightweight with high strength, high stiffness, and excellent resistance to corrosion and fatigue. To improve the mechanical performance of the polymeric structures, fiber was introduced to the polymeric materials to construct the fiber-reinforced composites. These fiber-reinforced composites can be fabricated by AM techniques nowadays [79].

Generally speaking, the AM technologies for fiber-reinforced composites can be
categorized into short and continuous fiber-reinforced composites. The short fiber-reinforced
structures can be printed through various AM approaches, such as vat photopolymerization,
FFF, and SLS using the polymeric materials mixed with short fibers [260]; whilst most
continuous fiber-reinforced structures are fabricated by FFF [261]. For instance, carbon fiber-
reinforced polymeric micro-lattices were fabricated through a PμSL system [98], as shown in
Figure 25(a). The results indicated that these carbon fiber-reinforced polymeric micro-lattices
exhibit a comparable specific stiffness to commercial carbon fiber-reinforced polymers (CFRPs)
while being dissipative like elastomers.

Short carbon fiber-reinforced perforated structures were fabricated by FFF [262], as shown
in **Figure 25(b)**. The results indicated that a well-designed auxetic composite structure exhibits
higher specific energy absorption and higher relative Young's modulus compared to re-entrant
honeycombs and elliptical perforations.

A continuous fiber-reinforced composite auxetic honeycomb was also devised and
fabricated through an FDM system [82], as shown in **Figure 25(c)**. It was found that the
continuous fiber-reinforced composite increases the stiffness and energy absorption by 86.3%
and 100%, respectively, while only increasing the total mass by 6%. Continuous fiber-
reinforced composite honeycomb structures were proposed and manufactured through the FFF
technology [263], as shown in **Figure 25(d)**. The out-of-plane/in-plane compression tests
revealed that the designed structures exhibit excellent compressive strength and specific energy
absorption compared to other cellular materials.

Table 4 summarizes the investigation of the additively-manufactured fiber-reinforced
materials and structures and their characteristics.
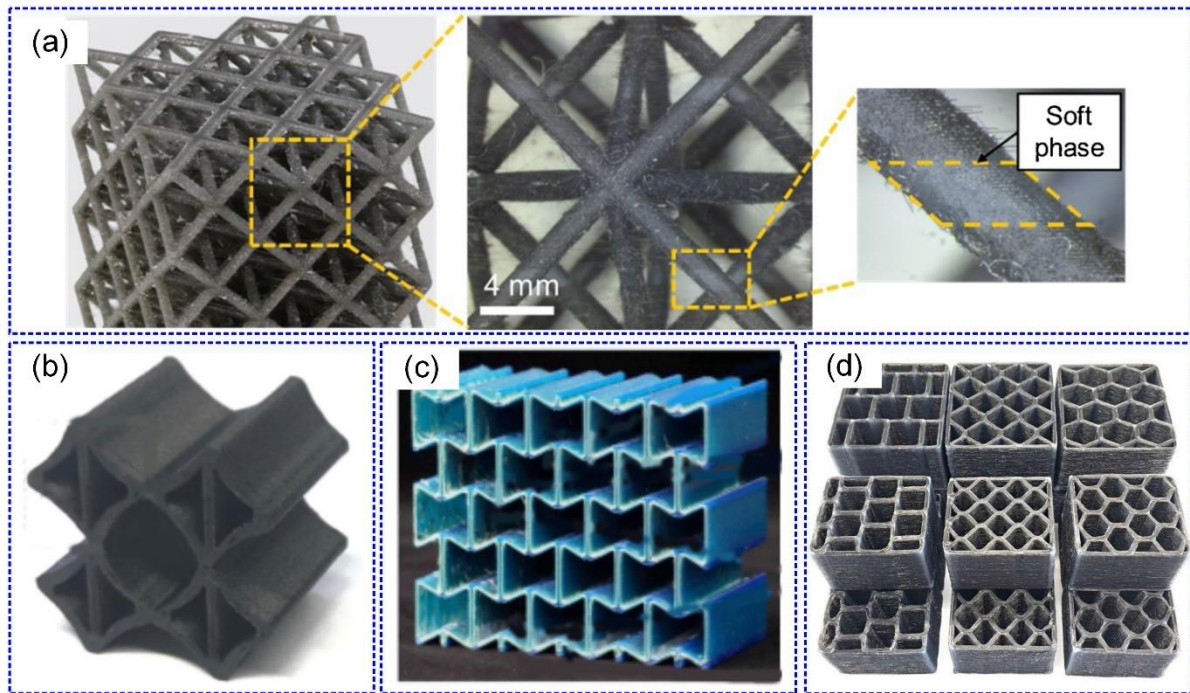
Figure 25. AM fiber-reinforced composites: (a) Lightweight and strong cellular structural materials produced by using 3D printing of all-cellulose ink [98], (b) honeycombs produced by the Laser Engineered Net Shaping with Ti6Al4V material [262], (c) 3D Voronoi closed-cell foams produced by the FDM method with ABS material [82], (d) open-cell foam structures produced by AM assisted lost-wax casting [263].

Table 4 A summary of the studies on the additively manufactured fiber-reinforced materials and structures

Categories	AM methods	Materials used	Highlighted results	Refs.
Short fiber-reinforced material	Microstereolithography (PµSL)	CFRP	-The proposed micro-lattices exhibit a high specific stiffness and damping coefficient.	[98]
	FDM	CF reinforced polyacrylonitrile	-The CF-reinforced polyacrylonitrile structures exhibit higher tensile strength, modulus, and energy absorption capacity.	[242]
	FFF	Nylon polymer, short carbon fiber-reinforced nylon polymer	-The proposed auxetic structures possess a higher SEA and higher relative Young's modulus.	[262]
Continuous fiber-reinforced material	FDM	PLA, Kevlar R fiber	-The continuous fiber-reinforced composite increases stiffness and energy absorption by 86.3% and 100%, respectively; while only increasing the total mass by 6%.	[82]
	FDM	Onyx, a binder-infused continuous fiber feedstock	-There are different failure modes of the proposed structures under impact loading.	[264]

	FFF	PLA, T300B–3000–40B carbon fiber	-The proposed structures exhibit excellent compressive strength and specific energy absorption. -3D printed carbon fiber reinforced structures have the highest shape recovery ratio.	[263]
	FFF	Continuous carbon fiber reinforced polyamide (CCF/PA), short carbon fiber reinforced polyamide (SCF/PA)	-The CCF/PA parts possess better mechanical performance than the SCF/PA parts. -The matrix damage is a predominant failure for the proposed 3D-printed CF/PA composites.	[265]

910

3.6 Sandwich cores

Typically, the sandwich structures consist of two thin and stiff skins and a low-density and crushable core [1]. The tensile and compressive loading is distributed by the skin structures, and most of the impact energy is expected to be absorbed by skins/core and their interaction [196, 266-270]. Therefore, four typical factors affecting the energy-absorption capability of sandwich panels can be classified as (a) geometry, (b) mass, (c) material properties of the core and skins, and (d) core cell topological structures [237]. With growing applications of additive manufacturing technologies for fabricating sandwich structures [271-277], this section will review the recent and related experimental studies, thereby understanding their mechanical performances and energy absorption characteristics under quasi-static and impact loading.

3.6.1 Quasi-static loading

Compression. During the out-of-plane compressive loading, the responses of sandwich panels are dominated by the responses of the core structures, which are affected by the base material properties, cellular core topology, and geometry [237, 246, 278]. Interestingly, the failure mode with the in-plane compression tests was mainly caused by buckling of the core structure and plastic yielding of skin sheets [278].

Bending. The damage failure and energy absorption performances of sandwich structures are affected by the cellular core topology, geometry, and base material properties under transverse bending [279-289]. The studies were carried out on the AM Ti6Al4V BCC core sandwich samples; and it was found that the energy absorption of the samples with heat treatment is improved compared to the as-built counterparts [290].

3.6.2 Dynamic loading

Drop-weight impact. The dynamic responses of the additively manufactured sandwich panels under drop-weight impact loading were extensively studied in the literature [271, 273, 291-294]. For example, Beharic et al. [273] investigated the drop-weight impact characteristics

of sandwich panels fabricated by SLS with the nylon 12 material. It was found that the auxetic cellular structures provide the highest total energy absorption, the best pre-strike energy absorption abilities, and the highest structural performance efficiency for such applications.

Blast impact. The dynamic properties of a sandwich structure subjected to blast loading were investigated using the 3D-printed samples [55, 295, 296]. For example, Novak et al. [246] explored the blast responses of the additively manufactured sandwich panels using SEBM with Ti6Al4V. It has proven that the auxetic core offers a higher SEA than the core with a positive Poisson's ratio with the same porosity and the same mass.

Table 5 summarizes the investigation of the additively manufactured sandwich structures.

Table 5 A summary of the investigation on the additively manufactured sandwich structures

Refs	AM methods	Materials used	Core topology	Loading conditions	Result highlights
[291]	SLM	316L stainless steel and Ti6Al4V	BCC	-Static Compression -Drop weight impact	-The Ti6Al4V BCC micro lattice structures exhibit a comparable impact performance with aluminum honeycomb.
[297]	FDM	PLA	Lattice	-Static Compression	-The 3D-printed lattice structure has a superior energy absorption capacity and specific strength.
[290]	SLM	Ti6Al4V	BCC	-Static Compression -Tension -Four-point-bending	-The 3D-printed cellular structures with heat treatment can improve their energy absorption and ductility.
[273]	SLS	Nylon 12	Re-entrant, BCC, Octet	-Drop weight impact -Static Compression	-The auxetic cellular design exhibits an optimal overall energy absorption performance.
[246]	SEBM	Ti6Al4V	Chiral	-Static Compression -Dynamic Compression -Blast loading	-The sandwich panels with auxetic cellular cores have great potential for blast protection structures.
[279]	FDM	Continuous fiber-	Honeycomb, rectangle,	-Three-point-bending	- The mechanical properties of CFRTP sandwich structures can be designed freely based on the

		reinforced thermoplastics (CFRTP)	circle		continuous carbon fiber 3D printing technology.
[298]	SLA	Aluminum GPPlus	B, T, Q, K-grid FCC, BCC	-Three-point-bending	-The sandwich panel with a 3D lattice core had a high energy absorption efficiency.
[278]	SLM	AlSi10Mg	Pyramidal	-Static Compression -Shear	-Multi-layered pyramidal lattice truss cores show outstanding load support capability.
[299]	Ployjet	VeroWhite	Truss Honeycomb Re-entrant	-Static Compression -Three-point-bending	-The re-entrant honeycomb sandwich structures exhibit a higher energy absorption capacity than truss and honeycomb counterparts.
[33]	SLM	AlSi10Mg	BCC, BCCz	-Static Compression	-The compressive modulus of lattice core sandwich panels was decreased with the increasing number of layers.
[281]	FDM	ABS	TPMS-P, Neovious, IWP	-Three-point-bending	-The sandwich structures with Neovius core exhibit a higher bending strength and energy absorption capacity, and the shear failure mode of core is the dominant failure mechanism.

[300]	SPPW-Coat	Ni-P	Micro-lattice	-Static Compression	-The sandwich panel exhibits superior strength and stiffness for a greater wall thickness design.
[301]	FFF	CFRP	Corrugated	-Static Compression	-The strength and energy absorption properties were increased by increasing core thickness.
[282]	SLM	304 stainless steel	BCC	-Static Compression -Drop weight impact	-The metallic Kagome lattice sandwich panels possess a higher strength-to-weight ratio.
[302]	FFF	high‐density polyethylene (HDPE)	Foam	-Three-point-bending	-The 3D-printed syntactic foam core sandwiches exhibited higher specific mechanical properties.
[303]	FFF	PLA/PHA	Honeycomb, diamond, corrugated	-Static Compression -Tension -Three-point-bending -Drop weight impact	-The diamond core sandwich panel possessed the highest compression and three-point bending strength, and the corrugated core sandwich panel exhibited superior tensile strength.
[292]	FDM	PLA	Auxetic, rectangular, hexagonal	-Drop weight impact	-The auxetic sandwich panel exhibited a higher energy absorption capacity.
[304]	FDM	PLA	BC, BCZ,	-Three-point-bending	-The mechanical performances and energy absorption

			BFCZ, FCZ, PS, HEX		capability of the sandwich panels were affected by the core topologies.
[305]	FDM	ABS/PC	Honeycomb	-Three-point-bending -Tension	-The failure modes of sandwich panels were explored.
[281]	FDM	ABS	TPMS	-Three-point-bending	-The mechanical performances and energy absorption capability of the sandwich panels were affected by the relative density and geometrical parameters of core materials/structures.
[306]	SLM	AlSi10Mg	Pyramidal lattice	-Static Compression	-Five failure modes were considered for the sandwich panel under in-plane compression.
[279]	FDM	PLA	Cubic, octet, Isomax, auxetic	-Three-point-bending -Drop weight impact	-The failure mechanism and energy absorption of the sandwich structures were affected by the topology and geometrical parameters of the core.
[307]	SLM	Ti6Al4V	Corrugated channel core	-Four-point-bending	-Four failure modes were identified for the sandwich panels.
[308]	FDM	Hemp/PLA	Honeycomb	-Static Compression -Four-point-bending	-The small-scaled prototypes were tested for the car fog light and UAV frame.
[309]	DLP	Ceramic	strut-based	-Static Compression	-The star structure has maximum strength under

		resin	topologies	-Tension	bending loading.
				-Three-point-bending	
[310]	FDM	PLA	BCC, BCCZ, F2CC, F2CCZ	-Three-point-bending -Drop weight impact	-The F2CCZ lattice core sandwich panel provided better energy absorption capacity under impact loading.
[311]	FDM	TPU 95A	BCC, ECC	-Drop weight impact	-The ECC core sandwich structures exhibited better absorption capability.
[312]	FDM	CFRP	Trapezoidal corrugated	-Three-point-bending	The additively manufactured sandwich panel presented excellent shape memory capability.
[313]	FDM	PLA	Honeycomb	-Three-point-bending	-The horizontal core sandwich panels have higher fracture strength and better energy absorption.
[314]	SLS	PA12	Honeycomb, re-entrant honeycomb, TPMS	-Three-point-bending	-The gyroid core sandwich panel possesses the highest strength, modulus, and stiffness-to-weight ratio.
[271]	FDM	ABSplus-P430	BCC, BCCAV, BCCZ	-Drop weight impact	-The energy absorption capability can be improved by introducing vertical support struts.

| [294] | FDM | ABS | Honeycomb, re-entrant honeycomb | -Drop weight impact | -The sandwich panels with in-plane re-entrant core had better impact strength and energy absorption capacity. |
| [293] | FDM | PLA | Cubic, octet, Isomax, auxetic | -Drop weight impact | -The sandwich panels with Isomax core provided the highest energy absorption capability. |

3.7 Functionally graded structures

By introducing morphological gradients to materials and structures, the corresponding mechanical properties and energy absorption performance can be improved and/or tailored for a specific purpose [47, 315-317]. Generally speaking, a functionally graded design can be achieved by varying: (1) relative density (RD), (2) characteristic size, and (3) structural topology [47].

RD: The most widely used functionally graded design is to tailor relative density, which can be achieved by varying thickness or strut size in one or more directions [75, 318-324]. For instance, Fan's study [325] showed that the structures with a graded direction along with the loading direction deformed in a layer-by-layer mode while the uniform structures exhibited a shear band deformation mode; thus, the former can more effectively enhance the mechanical properties and energy absorption, as shown in **Figure 26(a)**.

Geometry: Another type of graded design is gradually varying the size of the unit cell [022, 028, 146, 156]. The size-graded lattice structures were proposed based on the BCC, TPMS-P, and TPMS-G and fabricated by FDM with short carbon fiber-reinforced nylon [81], which however divulged that the graded unit cell size may not affect energy absorption significantly. Similar findings were reported in [326], in which the grading pattern does not greatly affect the mechanical properties of the TPMS lattices.

Topology: Multi-morphologically graded structures can be constructed by hybridizing two or more structural topologies [38, 327]. For instance, the multi-morphology Gyroid-Diamond sheet network lattice was designed and fabricated by SLM with stainless steel [326], in which the deformation modes are shown in **Figure 26(b)**. A layer-by-layer deformation mode was found in the structure with a topological gradient parallel to the loading direction. In contrast, a shear band deformation mode was found in the structure with a topological gradient perpendicular to the loading direction. Multi-tessellated functional architected materials consisting of multiple layers of tessellated lattices were proposed and printed by MJF with PA

975   12 [328]. The results showed that the multi-tessellated lattices can achieve multi-material like properties without interface issues founded in the multi-material lattice structures.

Table 6 summarizes the additive manufacturing methods used for fabricating the functionally graded structures.
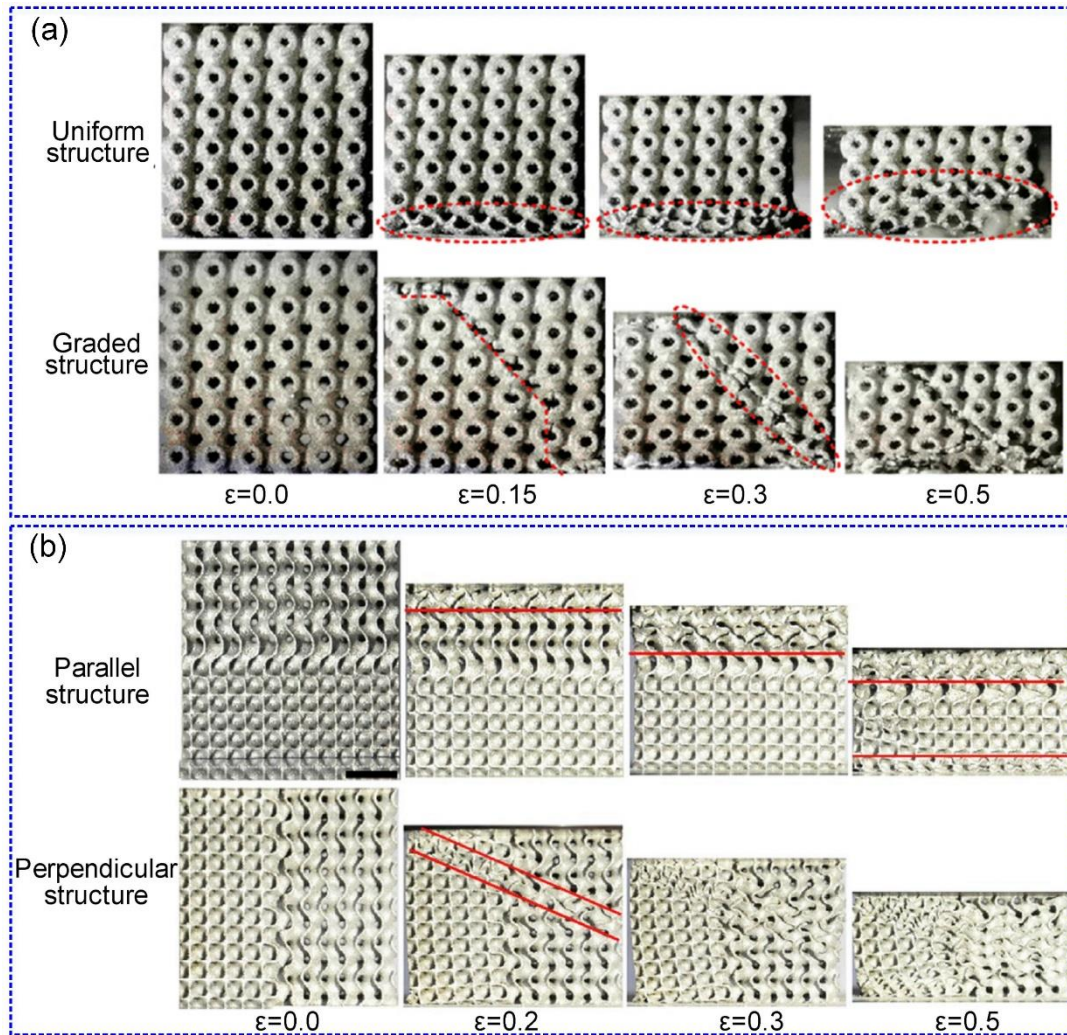
980   **Figure 26.** Comparison of the deformation modes for the AM-based functionally-graded structures: (a) functionally RD graded structures, a layer-by-layer deformation mode was observed on the uniform structure (top) whereas a shear band deformation mode was observed on the graded structure (bottom) [325], (b) multi-morphology structures, a layer-by-layer deformation mode was observed on parallel structure (top) and a shear band

985   deformation mode was observed on perpendicular structure (bottom) [326].

Table 6 A summary of the additively manufactured functionally graded structures.

Refs	AM methods	Materials used	Functionally graded methods	Loading conditions	Highlighted results
[322]	SLM	Stainless steel 316L	RD	-Quasi-static Compression	-The elastic-plastic mechanical properties of the lattice structure were optimized by the cell geometry and relative density.
[81]	FDM	short carbon fiber-reinforced nylon	RD, Geometry	-Quasi-static Compression	-The density-graded lattice exhibited a better energy absorption capacity, while the lattices with a unit cell size gradient showed the same absorption capacity.
[326]	SLM	Maraging steel	RD, Geometry, Topology	-Quasi-static Compression	-Sheet-network multi-morphology lattices exhibited higher elastic properties.
[329]	SLM	AlSi10Mg	RD	-Quasi-static Compression	-The dissipation energy of the unidirectionally-graded auxetic honeycomb (UGAH) was lower than that of the bidirectionally-graded auxetic honeycomb.
[330]	SLM	Stainless steel 316L	Topology	-Quasi-static Compression	-The multi-morphological lattices exhibited a higher energy absorption performance.

[331]	SLA	ABS	RD	-Three-point bending	-The bending behavior and energy absorption capacity of honeycomb-filled thin-walled structures can be improved by a graded design.
[332]	SLM	TC4	RD	-Quasi-static Compression	-The functionally graded sheet-G lattice showed higher energy absorption performance.
[333]	SLM	Ti6Al4V	RD	-Quasi-static Compression	-A layer-by-layer failure mode was found in the functionally graded sheet structures (FGS) lattice structures. -The energy absorption of the FGS samples was higher than its uniform structure counterparts by approximately 60%.
[62]	SLS	PA2200	RD	-Quasi-static Compression	-The functionally graded lattice structures exhibited a superior energy absorption ability compared with other structures.
[334]	Ployjet	VeroWhitePlus, TangoPlus	RD	-Quasi-static Compression	-The geometrically tailored honeycomb design can enhance the energy absorption capacity.
[335]	Ployjet	VeroWhite	Geometry	-Quasi-static Compression	-The cell-wall angle-graded auxetic metamaterials exhibited a higher energy absorption performance.
[336]	SLS	PA2200	RD	-Quasi-static Compression	-The graded structures can absorb more energy compared to their non-graded counterparts.

[337]	SLM/FDM	Ti6Al4V/ABS-M30	RD	-Quasi-static Compression	-The functionally graded Kagome structures absorbed more energy than the uniform counterparts.
[338]	SLM	Stainless Steel 316L	Geometry	-Quasi-static Compression -Dynamic compression	- Specific mechanical properties of the lattice can be tailored by the topology gradually design.
[324]	FDM	short carbon fiber-reinforced nylon	RD	-Quasi-static Compression	-Ungraded and slightly graded BCC lattices absorbed more energy for a given strain than their SP counterparts.
[339]	SLA	-	RD	-Quasi-static Compression	-The desirable mechanical properties could be achieved in each layer by functionally graded design.
[175]	FDM	ABS	RD	-Quasi-static Compression	-A positive density gradient can enhance energy absorption for cylindrical shell-based lattices. -For cylindrical shell-based lattice sandwich, density gradient can efficiently reduce the peak crushing force but have little effect on the energy absorption.

[340]	SLM	Ti6Al4V	RD Topology	-Quasi-static Compression	-Both Gyroid and Diamond structures presented superior strength and comparable elastic modulus with the natural cortical bone.
[341]	SLM	Ti6Al4V	RD	-Quasi-static Compression	-The functionally graded porous biomaterials (FGPB) exhibited a combination of low density, moderate Young's modulus, high yield strength, high peak stress, and favorable ductility.
[342]	Ployjet	VeroGray	RD	-Quasi-static Compression	-The stretching-dominated structures showed better mechanical properties and higher efficiency under mechanical loads.
[343]	SLM	Ti6Al4V	RD	-Quasi-static Compression	-The graded lattice structures exhibited higher specific strength and higher specific energy absorption than the uniform counterparts.
[325]	SLM	Ti6Al4V	RD	-Quasi-static Compression	-The graded-thickness structures were of better mechanical properties than the uniform counterpart.

| [344] | FDM | TPC, PA12 | Geometry | -Quasi-static Compression | -The structures with a gradual change in topologies exhibited higher energy absorption and better mechanical performance than the uniform structures.
-Dual-material lattice structures provided higher energy absorption than the corresponding single material counterparts. |

3.8 Hierarchical materials and structures

It has been demonstrated that hierarchical materials and structures can often lead to superior mechanical properties, higher energy absorption, and tailorable material characteristics [193, 345-348]. The overall mechanical properties and energy absorption performance of these structures can be enhanced by increasing levels of structural hierarchy [193]. However, high-level hierarchical structures cannot be easily fabricated using conventional manufacturing techniques. The development of various additive manufacturing techniques paves a feasible way to produce such sophisticated hierarchical structures [349-356].

For instance, Tao et al. [357] designed square hierarchical honeycombs (SHHs) and fabricated these structures employing the Ployjet method with VeroWhitePlus, as shown in **Figure 27(a)**. It was found that the SHHs are of superior compressive strength, specific energy absorption, and crush force efficiency compared with the regular square honeycomb (RSH) of equal mass. Zhang et al. [59] proposed a self-similar hierarchical honeycomb and fabricated these structures using the SLM method with AlSi10Mg, as shown in **Figure 27(b)**. It was concluded that the in-plane failure of hierarchical honeycombs is dominated by bending, axial compression, and shear deformation. Tan et al. [35] proposed an auxetic hierarchical honeycomb as a crash box filler and made this honeycomb using the Ployjet method with VeroWhitePlus, as shown in **Figure 27(c)**. It was found that the auxetic hierarchical crash box structure possesses a higher energy dissipation capacity than its counterparts.

Inspired by skeletal muscles, Tsang et al. [221] proposed a hierarchical tubular structure to study in-plane compressive characteristics using the specimens fabricated by FDM with TPU, as shown in **Figure 27(d)**. The force resistance and energy absorption of these hierarchical tubular structures were enhanced by increasing the hierarchical order. Hierarchical nanolattices were also proposed and fabricated using the TPL-DLW and ALD technologies, as shown in **Figure 27 (e)**. It was found that the proposed hierarchical nanolattices exhibit a unique combination of properties: ultralightweight, recoverability, and a near-linear scaling of stiffness

and strength with density [358]. **Table 7** provides a summary of some additively manufactured
hierarchical materials and structures.
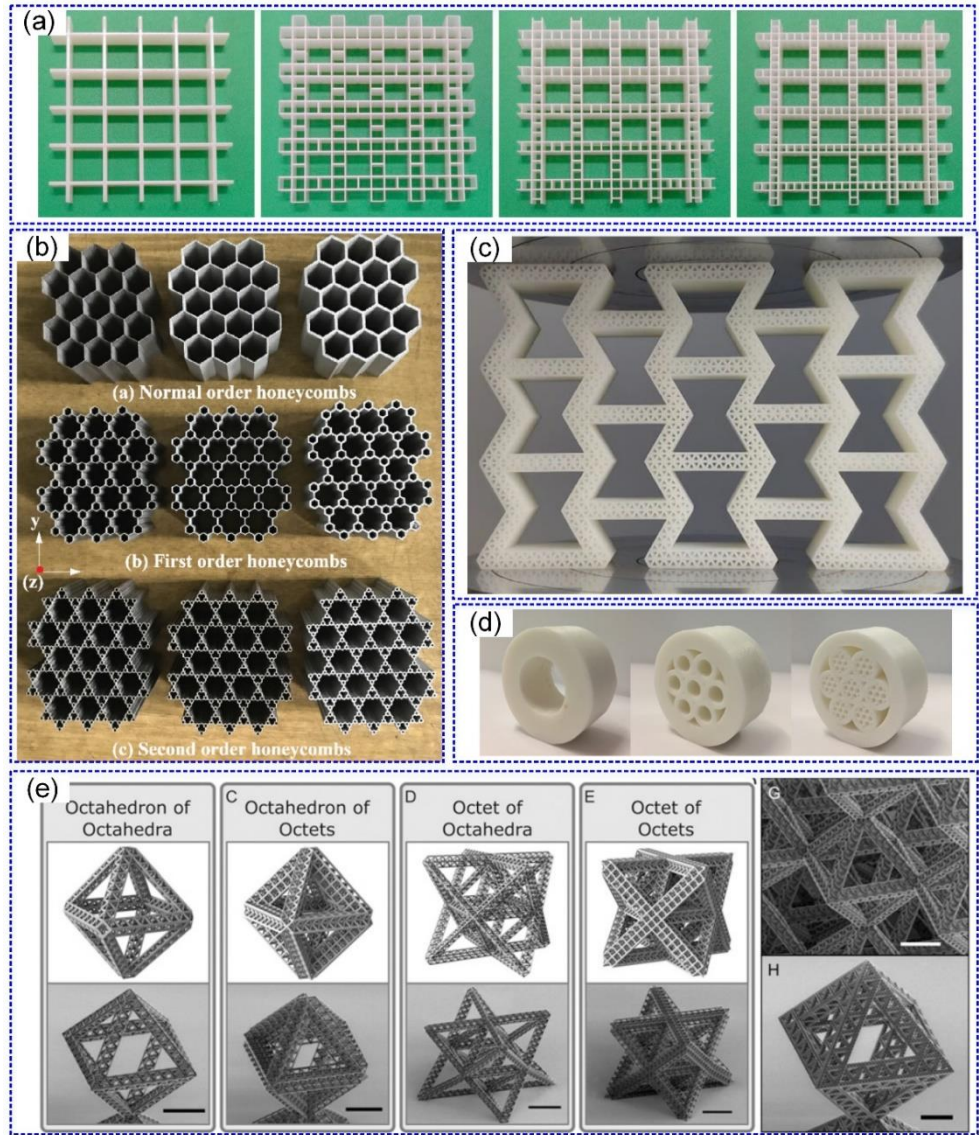
Figure 27. Additively manufactured hierarchical structures: (a) Square hierarchical honeycombs produced by the Ployjet method with VeroWhitePlus [357], (b) hierarchical honeycombs fabricated using the SLM method with AlSi10Mg [59], (c) auxetic hierarchical honeycomb produced using the Ployjet method with VeroWhitePlus [35], (d) hierarchical tubular structure produced using the FDM method with TPU [221], (e) hierarchical nanolattices are proposed and fabricated using the TPL-DLW and ALD methods [358].

Table 7 A summary of some additively manufactured hierarchical materials and structures

Refs	AM methods	Materials used	Topology	Loading conditions	Highlighted results
[359]	FDM	PLA	honeycomb	Static Compression	-The hierarchical honeycombs exhibited better energy absorption capabilities.
[358]	TPL-DLW	Ceramic, polymer	hierarchical nanolattice	Static Compression	- Resilient 3D hierarchical metamaterials showed ultralight weight, recoverability, and nearly-linear scaling of stiffness and strength with density.
[59]	SLM	AlSi10Mg	honeycomb	In-plane compression	-The in-plane failure of hierarchical honeycombs was dominated by the bending, axial compression, and shear deformation of original unit cell walls.
[360]	PμSL	polymer	honeycomb	In Situ Micro-Compression, Dynamic experiment	-Multi-level hierarchical honeycomb (MHH) exhibited a higher collapse strength and better energy absorption properties than single-level hierarchical honeycomb (SHH).
[357]	PolyJet	VeroWhitePlus	square hierarchical honeycombs	In-plane compressive test	-The square hierarchical honeycombs showed better mechanical properties and energy absorption performance than traditional cellular materials.

[221]	FDM	TPU	hierarchical tubular	Quasi-static compression	-The muscle-inspired hierarchical structures exhibited better loading resistance and energy absorption.
[361]	FDM	PLA	hierarchical honeycomb	In-plane compressive	-Hierarchical honeycombs possess favorable characteristics such as a more stable post-yield stress plateau and higher mean crushing stress which can be used to design efficient energy absorbers.
[35]	-	VeroWhitePlus	Auxetic hierarchical crash box	Static compression	-The auxetic hierarchical crash box presented the highest energy absorption capacity.

1025

3.9 Multi-material structures

Multi-material structures signify a class of composite materials made of two or more phases of base materials to obtain the best effective (overall) mechanical properties [362]. Through additive manufacturing techniques, multi-material structures can be fabricated using various materials with different mechanical properties [60, 73, 363, 364].

For instance, co-continuous composites, also called interpenetrating phase composites (IPCs), were proposed to achieve enhanced mechanical characteristics [365]. Al-Ketan et al. [365-367] proposed the TPMS-based IPCs and fabricated these IPCs by using the Ployjet technique with hard VeroWhite and soft TangoGray materials, as shown in **Figure 28(a)**. The results indicated that the bulk mechanical properties of these IPCs can be adjusted by varying the composition of the IPCs. Another type of multi-material structure inspired by the nacre presents an architecture similar to brick-and-mortar [215]. These nacre-like composites were fabricated by FDM with PLA and TPU materials, as shown in **Figure 28(b)**. It was found that the nacre-like design can enhance the stiffness, strength, and toughness of the multi-material structure systems [201, 215]. Prajapati et al. [368, 369] presented tessellated lattice structures filled with foam materials. The lattice structures were fabricated by FFF with TPU and then the PU foams were injected by a syringe dispenser system. The results showed that the foam filled lattice structures exhibit higher specific damping capacity which cannot be achieved by varying the shell thickness of empty lattices.

Table 8 summarizes some additively manufactured multi-material structures and their characteristic features.
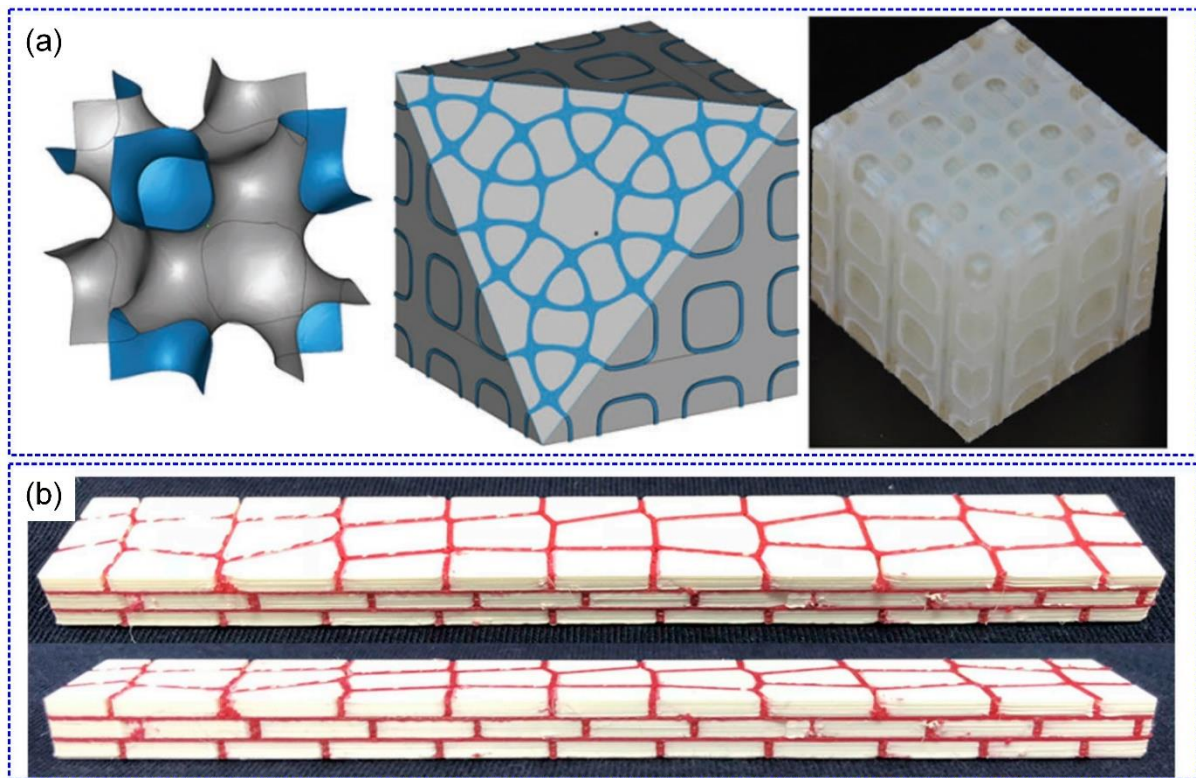
Figure 28. Additively manufactured multi-material structures: (a) Co-continuous composites produced by the Ployjet method with VeroWhite and TangoGray [365], (b) bio-inspired bi-material composites produced by the FDM method with PLA and TPU [215].

Table 8 A summary of the additive manufacturing methods used in some multi-material structures

Refs	AM methods	Materials used	Topology	Loading conditions	Highlighted results
[370]	Ployjet	Vero White and Tango Plus	Honeycomb	Static and dynamic compression	-The five-layered sandwich multi-material honeycomb structure has better energy-absorbing capability.
[371]	Binder jetting	Plaster, Silicone	Beams	Four-point-bending	-The plaster phase of the bi-material structure (BMS) dominates the stiffness and strength against bending, while the elastomer phase enhances the toughness.
[215]	FDM	PLA, TPU	Nacre-like laminated composites	Three-point-bending	-Multi-material composites with natural hierarchical patterns can enhance ductility.
[372]	SLM	316L stainless steel, acrylic	Hybrid composite	Static and dynamic (SHPB) compression	-The proposed stretched cell lattice (SCL) exhibited a higher SEA and higher energy absorption efficiency (EAE) than OTL by 26% and 17%, respectively. -The yield strength of the proposed SCL was 80% higher than that of OTL. -The hybrid composite showed a 47% higher specific

					strength than the bare stainless steel structure.
[366]	Polyjet	VeroWhite, TangoGray	TPMS	Static compression	-The shell-core cellular composites were found suitable for energy absorption applications.
[365]	Polyjet	VeroWhite, TangoGray	TPMS	Static compression	-The sheet-network interpenetrating phase composites exhibited superior mechanical properties.
[367]	Polyjet	VeroWhite, TangoGray	TPMS	Static compression	-The secondary IWP is of the highest yield strength and the highest Young's modulus. -The IPCs can be applied for energy-absorbing and damage-tolerance applications.
[368]	FFF	TPU, PU foam	Closed cell lattice structure	Static compression	-The foam filled closed cell lattice structures exhibit higher stiffness and energy absorption
[201]	Polyjet	Veromagenta, Tangoblackplus	Nacre-like composite	Drop tower impact	-The Nacre-like design was of a better performance in impact resistance.

1055

3.10 Origami-inspired materials

The word origami refers to the ancient art of paper folding, and it contains two Japanese roots: ori and kami, meaning 'folded' and 'paper', respectively [373]. Introducing initial folds into an energy absorber can control the deformation modes to obtain the desired force-displacement curves. Meanwhile, the peak force during the crushing process can also be adjusted by the initial folds. Further details of the classification of origami-inspired materials and structures can be referred to a more comprehensive topical review in [374]. This section focused on the experimental investigation into mechanical properties and energy absorption characteristics of the origami-inspired materials and structures fabricated by AM.

The circular tubes with two different origami patterns were experimentally investigated using 3D printing technology [375]. It was found that the circular tubes with pre-folded origami patterns exhibit a higher specific energy absorption and a lower initial peak force compared to conventional circular tubes. The Ron Resch origami absorber was proposed and experimentally studied by using the SLS method with nylon material [376]. The results showed that the proposed origami absorber displays a new collapse mode with a lower peak force and longer effective stroke. The dynamic responses of the metallic stacked origami-based cellular materials were experimentally investigated by the SLM method with 316L stainless steel [295]. It was found that the thin-walled configurations exhibit a higher normalized efficiency compared with thick-walled configurations.

Table 9 summarizes the additive manufacturing methods used for fabricating some origami-inspired structures and their characteristic features.

Table 9 A summary of the additive manufacturing method used in the origami-inspired structures.

Refs	AM methods	Materials used	Topology	Loading conditions	Highlighted results
[375]	-	Brass	Yoshimura origami planar pattern	-Axial quasi-static compression	-Tubes with pre-folded origami patterns can significantly reduce the initial peak force and increase the SEA.
[376]	SLS	Nylon	Ron Resch Pattern	-Axial quasi-static compression	-The energy-absorbing structure with Ron Resch origami pattern exhibited a new collapse mode, which helped reduce the peak force and improve the effective stroke.
[295]	SLM	316L stainless steel	Stacked Miura-origami	-Dynamic compression	-The thin-walled configurations exhibited a higher normalized energy absorption efficiency than thick-walled configurations.
[377]	FFF	TPU	Square origami honeycomb	-Compression (100mm/min)	-The energy absorption profile of square honeycombs structured with origami folds can be adjusted by the fold parameters.
[378]	SLA	-Godart 8228	origami-inspired	-Drop-weight impact	-The origami-inspired honeycomb sandwich structure possesses an excellent energy absorption capability.

| [379] | FDM | PLA | honeycomb origami-inspired tessellated pattern | -Drop-weight impact
-Quasi-static compression | -The rectangular origami-inspired tessellated meta-materials are more effective at absorbing impact loads. |

1080

4. Defects of the additively manufactured materials and structures

4.1 Additive manufacturing defects and their effects on mechanical properties and energy absorption

Due to the inherent process characteristics such as the staircase effect, residual stresses, and entrapped gases induced defects in the additively manufactured structure cannot be completely avoided by adjusting the printing parameters [12, 380, 381]. These imperfections in the printed materials/structures can to a certain extent affect the mechanical properties and energy absorption characteristics [31, 73, 127, 382-387]. The defects induced by AM were reviewed more generally in the literature [12, 77, 380, 388]. Here, we focus on the quantitative characterization of the defects and their effect on mechanical properties and energy absorption of AM materials and structures. As shown in **Fig. 29**, the AM defects are classified into three main categories, i.e., geometric imperfections, surface quality, and porosity.
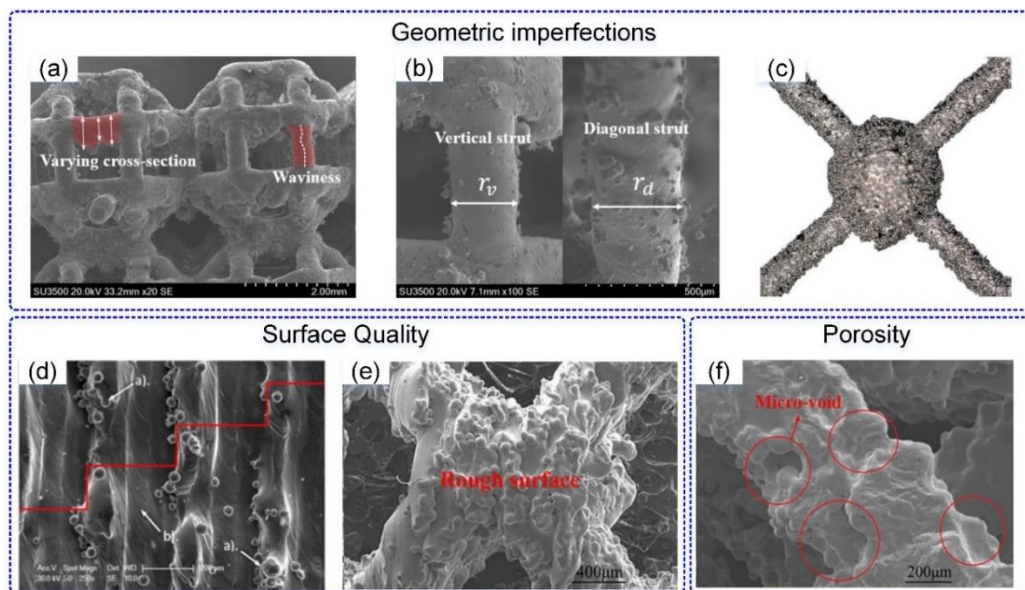

Figure 29. Geometric imperfection caused by additive manufacturing processes. Geometric imperfections: (a) waviness and varying cross-section [32], (b) strut oversizing or undersizing [32], (c) node diameter [31]; surface quality: (d) stair-step profile [31], (e) bonded particle [389]; Porosity: (f) micro-voids [389].

Concerning the geometric imperfections, Liu et al. [32] summarized the geometric imperfections of some SLM lattices through X-ray computed tomography (CT) scan in three categories: (a) strut waviness, (b) strut thickness variation, and (c) strut oversizing or undersizing. The geometric imperfections could be depicted by the probability distributions that are normalized by the nominal values of the as-designed models. They found that the compressive strength and stiffness of the lattices are decreased by geometric imperfections. Specifically, the compressive strength and stiffness of lattices deteriorated with the increase of strut thickness variation or struct waviness. They also found that the different distributions of oversizing or undersizing on horizontal/vertical struts and diagonal struts have a significant influence on the mechanical performance and failure mode of the lattices.

Moreover, Dallago et al. [390, 391] identified five types of defects in the printed lattices (1) variable equivalent radius of strut cross-section, (2) offset of the cross-section centers from the axis connecting two junction centers, (3) eccentricity of strut cross-section, (4) missing/interrupted struts, and (5) junction center position. They found that the elastic modulus of structures could be increased by increasing the mean cross-section, while the elastic modulus decreased with the increase in the strut waviness and misalignment of the junction centers.

Li et al. [382] investigated the effect of strut waviness and strut thickness variation on the energy absorption performances of the AM lattices. It was found that the SEA of the lattice is more significantly affected by the variation in strut thickness than strut waviness. The thickness variation in the diagonal strut may increase the SEA of the lattice, but the thickness variation in the vertical strut may decrease the SEA of the lattice.

For surface-based structures, the deviations of shell thickness or geometry dimension are amongst the most common geometric imperfections in the AM parts. For instance, Cao et al. [167] studied mechanical and energy absorption properties of the AM P-TPMS cylinder structure considering the hole dimensions and thickness deviations induced by the AM technology.. They found that the mechanical performance and energy absorption of the AM P-TPMS cylinder structure could be deteriorated by imperfections in thickness compared to the

1125 ideal model. Zhang et al. [159] found that the mechanical and energy absorption characteristics of the AM TPMS lattices may be worsened due to the existence of AM defects. Thus, the shell thickness used in the finite element model was reduced to reproduce the response in the experiments correctly.

Due to stair-step phenomenon and melt pool instabilities, the stair-case-shaped profile and
1130 bonded particles may be formed on the printed parts [184]. Profile roughness parameters (Ra), as defined by ISO 4287 [392], were used to describe the deviation of the surface quantitatively. In this regard, Wen et al. [65, 182] quantified the Ra for the printed parts ranging from 6 to 52.8 μm.

Pores were typically referred to as enclosed voids beneath the part's surface [380]. Based
1135 on the measurements, internal porosity values could be formed within a range of 1.98–3.32% [393]. Jiang et al. [394] investigated the effects of porosity on the mechanical properties of the AM lattices numerically. It was found that the AM lattices with porosity defects degraded their elastic modulus compared with their defect-free counterparts, and the elastic responses of these AM lattices was affected by the fraction of porosity and the space distribution of the defects.
1140 Sombatmai et al. [395] investigated the influence of AM induced defects on mechanical behavior of AM lattices using the FE models. They found that the internal voids negligibly affect the elastic modulus and initial yielding stress, partly because of their low volume fraction (less than 1%).

4.2 Methods for minimizing defects in additive manufacturing

1145 **4.2.1 Design constraints**

While additive manufacturing technologies make it possible to fabricate sophisticated materials and structures, some manufacturability constraints still need to be considered to ensure the fabrication quality of the printed parts [380, 396, 397]. Taking the SLM method as an example, overhanging surfaces cannot be printed when the inclination angle is smaller than
1150 the minimum allowable level. In general, this minimum inclination angle can be affected by

the processing parameters, material types, and powder characteristics and it is often simplified as being 45° [12].

The SLM process cannot print the parts when the feature size is smaller than the minimum feature size. For example, Pattanayak [398] pointed out that the fabrication of wall thicknesses below 300μm was infeasible for Ti metal powder. In contrast, Zhang et al. [159] fabricated a lattice with a minimum thickness of 200μm with 316L stainless steel.

Melancon et al. [399] presented an admissible design space by exploring a range of pore sizes, maximum volume fraction, and minimum strut diameter. Following these design constraints, a density-based topology optimization method was proposed to optimize the additively manufactured lattice materials [400].

4.2.2 Processing parameters

AM process parameters can considerably affect the formation of defects and the quality of fabricated parts [401-406]. Taking PBF as an example, two types of processing parameters, i.e., laser power P and scan speed v, are often used to control the part quality. For example, Großmann et al. [125] investigated the influence of processing parameters on the quality of the printed lattices. It was found that suitable lattice surface qualities could be achieved when the laser power P and energy inputs satisfied $2\,J/mm^2 < E_{input} < 8\,J/mm^2$ and $170\,W < P < 350\,W$, respectively. The effects of processing parameters on relative density of the printed parts were investigated by Du et al. [218]. It was found that the greatest relative density of 99.93% can be obtained when the laser power is $450\,W$, and the scanning speed is $3500\,mm/s$, while the lowest relative density of 97.47% can be achieved with the combined process parameters of P ($400\,W$) and v ($2750\,mm/s$).

Three scan strategies, i.e., contour, points, and pulsing, were explored to divulge their influence on strut thickness [407]. It was found that the contour strategy was able to produce the samples with the highest strength-stiffness and strength-weight ratios. Effects of power and exposure time on the relative porosity of the printed parts were investigated by Egan et al. [408].

It was demonstrated that the power and exposure time can significantly influence the relative porosity and mechanical properties of the additively manufactured structures.

4.2.3 Post-processing

Post-processing is the last chance to mitigate the effects of defects and to improve the mechanical properties and energy absorption characteristics. A comprehensive review of post-treatments for AM parts can be found in [57, 381]. Here we briefly highlight the post-processes used in the additively manufactured lightweight materials and structures.

Chemical etching methods have been widely used to reduce the surface roughness of the AM energy-absorbing structures. For instance, de Formanoir et al. [409] used the hydrofluoric acid and nitric acid solution to post-process the AM octet-truss lattice structures. It was found that the chemical etching process can efficiently reduce the bonded particles on the lattice surfaces. In addition, Yan et al. [179] used a sandblast method to remove the bonded metal particles and improve the surface quality of the struts. It was found that nearly all the bonded particles were removed, and the quality of strut surfaces was considerably improved compared to the original surfaces obtained from AM.

Heat treatment is another efficient way to improve the mechanical properties and energy absorption of the AM materials and structures. For example, Brenne et al. [290] examined the mechanical behaviors of the as-built and heat-treated AM cellular structures. It was found that heat treatment can improve the ductility and energy absorption of the AM cellular structures. Jin et al. [410] investigated the effect of different heat treatments on the mechanical properties of the BCC and FCC lattices fabricated by SLM. The results showed that the rational heat treatment temperature could considerably improve the mechanical properties of the AM BCC and FCC lattices. Gorny et al. [411] found the energy absorption of a heat-treated structure is higher that of an as-built counterpart. Wauthle et al. [412] demonstrated that a proper selection of the heat treatment is important for the AM lattices in different applications. Yan et al. [413] found that the total energy absorption of the heat-treated lattices is higher than that of the as-

built counterparts.

The heat treatment of the AM materials and structures can lead to a more favorable deformation mode and stress-strain responses thereby improving their energy absorption. For example, Suzuki et al. [414] provided an examples that a heat treatment lattice presents an evident plateau region while the as-built lattice exhibits fracture failure without a plateau region. Maskery et al. [57] conducted a post-manufacturing heat treatment to modify the microstructures of printed structures; and they found that the heat treatment can prevent the formation of a shear band in the deformation mode, which leads to a flatter stress plateau.

5. Modeling of additively manufactured energy-absorbing structures

Numerical modeling techniques provide an effective and insightful way to evaluate the mechanical properties and energy absorption characteristics of additively manufactured parts. Numerous finite element (FE) models have been developed to simulate the mechanical responses of various printed parts [33, 415-424]. In literature, there are two main types of FE modeling methods: (a) defects-free modeling, which is performed based on the ideal CAD models [136, 153, 425]; and (b) modeling with defects, which takes into account the defects induced from the additive manufacturing process [29, 32, 390]. Another important area of study on numerical modeling is to simulate specific AM process for characterizing the as-manufactured materials/structures [426-428].

5.1 Defect-free modeling

In literature, different types of material constitutive models, finite elements, boundary conditions, and failure criteria have been considered in the defects-free modeling process, enabling to evaluate specific mechanical properties and energy absorption characteristics.

5.1.1 Material models

The most widely used material model for predicting the elastic and yield properties of the

energy-absorbing structures could be simple elastic–perfectly plastic constitutive models. For example, Al-Ketan et al. [97] used such a model for a polymer to simulate the mechanical responses of the TPMS micro-lattices. In another study, Al-Ketan et al. [160] used this model for maraging steel to characterize the mechanical properties of cellular structures. Chen et al. [149] also used this model for nylon PA 2200 to simulate the mechanical characteristics of the shell lattices.

Other models are also employed to investigate the large deformation behavior of printed parts. For example, Li et al. [29] adopted a plasticity model with isotropic hardening to capture the large deformation behavior of cellular structures . Tancogne-Dejean et al. [130] used a rate-independent J2-plasticity model with isotropic hardening for stainless steel 316L to obtain the static and dynamic responses of the metallic micro-lattice materials. To consider the effects of isotropic strengthening, kinematic strengthening, temperature variation and the associated variation in yield strength, the Johnson-Cook model has been widely used to evaluate the deformation responses and the mechanical performances of energy-absorbing structures. For example, Yang et al. [429] adopted this model for Ti6Al4V material to simulate the mechanical response of the solid-G structures. Abueidda et al. [164, 430] explored some more sophisticated and accurate finite deformation constitutive models (namely, elastic-viscoplastic Arruda-Boyce model (AB) model and hyperelastic-viscoplastic flow evolution network (FEN) model) to study the mechanical properties of printed parts. They found that the FEN model exhibited a better predictive accuracy compared with the AB model.

5.1.2 Failure criteria

One of the most critical aspects of numerical modeling is how to simulate the failure and fracture of energy-absorbing materials and structures [386, 431-434]. The failure would greatly influence the deformation modes and mechanical properties, and thus its modeling can be critical to the analysis and design of additively manufactured structures and materials.

5.1.2.1 Brittle fracture

A brittle fracture occurs when a crack is initiated at a mesoscale level with negligible inelastic deformations [435]. **Figure 30 (a)** schematically describes the brittle cracking model. Suppose that the elastic modulus of undamaged materials is E. After reaching a critical load σ_{cr}, the stress starts declining due to damage, softening the mechanical behavior. If the material experiences an unloading process, the elastic modulus will reduce to $(1-d)E$.
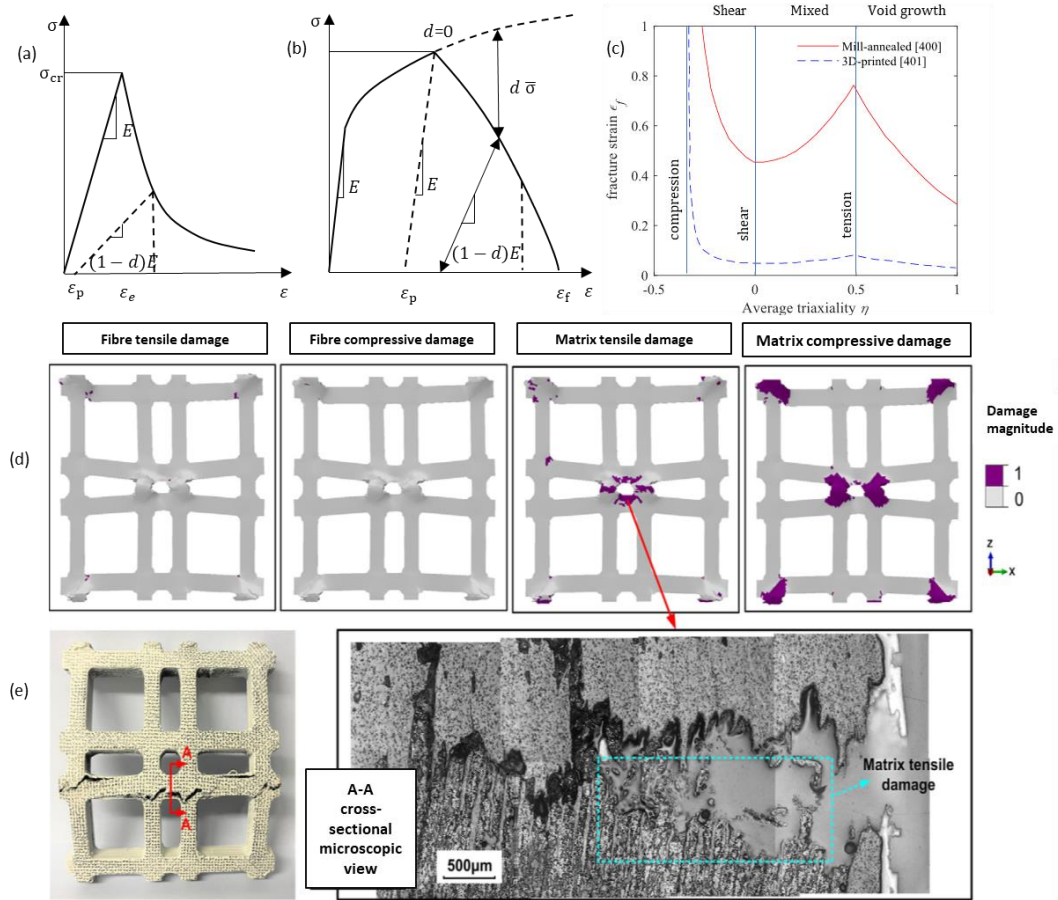
Figure 30. Failure criteria used for AM materials. (a-b) Schematic stress-strain curve with a brittle and ductile damage model, respectively; (c) failure model for Ti6Al4V with reduced ductility (red solid line: mill-annealed Ti6Al4V [436]; blue dashed line: 3D-printed Ti6Al4V) [437]; (d) numerical analysis of failure mechanisms (fiber tensile and compressive damage, matrix tensile, and compression damage); (e) experimental microscopic analysis. Matrix damage is predominant for 3D-printed CCF-PA composites under tension and compression loading [265].

Kao et al. [371] investigated the bending behaviors of a bi-material structure consisting of a stiff plaster frame and soft silicone elastomer filler using a brittle cracking material model. While it allowed for explaining the bending behaviors properly, the authors also pointed out the limitations of this model: (a) compression damage was not incorporated; (b) the hyperelastic model did not consider fracture, leading to an overly strong and tough structure prediction; and (c) mesh dependence may result in numerical inaccuracy. Yao et al. [438] adopted the maximum stretching strain criteria to predict the failure of bio-inspired structures, showing good agreement with the experimental results.

Fiber-reinforced composites typically feature brittle and anisotropic fractures. Hashin [439, 440] introduced fiber damage, matrix damage, and shear damage to simulate fiber buckling and kinking in compression and matrix cracking under transverse tension and shearing. Chen et al. [265] used the Hashin criterion and continuum damage mechanics to capture the responses and failure of the CCF/PA SCF/PA composites. They revealed that matrix rather than fiber damage is predominant for the composites that they fabricated (**Figure 30 (e-f)**) [265].

5.1.2.2 Ductile fracture

A ductile fracture can occur when plastic deformation exceeds a threshold [435]. Experimental observation suggests that ductile fracture is caused by nucleation, growth, and coalescence of voids [441]. Schematically, the ductile fracture may be illustrated in **Figure 30 (b)**. The stress - strain curves typically contain an initial elastic stage, a plastic hardening stage, and finally, a damage evolution stage. σ_{cr} and ε_p are the critical flow stress and effective plastic strain at the onset of damage. Due to damage, the curve presents a softening branch, and the corresponding elastic modulus reduces to $(1 - d)E$. The material is assumed to be fully damaged when fracture strain is reached.

(1) Constant strain criteria

Constant strain criteria assume that material would fail if a strain quantity, e.g., effective

plastic strain or maximum plastic strain, reaches a threshold. Such criteria are convenient to implement in commercial programs but may only provide a rough estimation to fracture behaviors. In this regard, Tallon et al. [51] employed a total plastic strain failure criterion to study the crush performance of micro-lattice reinforced plates made of maraging steel. Kucewicz et al. [442] applied effective plastic strain as an erosion criterion to simulate the deformation of cellular structures under quasi-static and dynamic conditions. Tkac et al. [443] provided an easy-to-implement approach to assess lattice/porous material deterioration using macroscopic damage initiation and evolution. Mahbod and Asgari [339] adopted a constant volumetric strain to determine the failure location for a double hexagonal pyramid lattice structure.

(2) Stress state-dependent ductile damage criteria

Stress state-dependent ductile damage criteria assume that fracture strain highly depends on the stress state. For example, the damage initiation has been formulated to rely on stress triaxiality η, i.e., $\varepsilon_f = \varepsilon_f(\eta)$ [444-451]. The damage will initiate when the following condition is satisfied:

$$D(\varepsilon_{\mathrm{p}}) = \int_0^{\varepsilon_{\mathrm{p}}} \frac{d\varepsilon_{\mathrm{p}}}{\varepsilon_{\mathrm{f}}(\eta)} = 1 \tag{7}$$

where D is a state variable that increases with plastic deformation monotonically.

The stress state-dependent ductile damage model is a built-in module in commercial FE code ABAQUS, which supports tabulated data input, thereby providing a flexible approach for numerical implementation. For example, the Bao-Wierzbicki model [452], a typical stress-state dependent ductile damage criterion, was calibrated in **Eq. (8)**, which was implemented for SLM Ti6Al4V auxetic 3D anti-tetrachiral metamaterials [437].

$$\varepsilon_f = \begin{cases} \dfrac{0.0176}{1 + 3\eta} + 0.0313, & -\dfrac{1}{3} < \eta \le 0 \\ 0.147\eta^2 - 0.0056\eta + 0.0494, & 0 < \eta \le 0.49 \\ 0.199e^{-1.89\eta}, & 0.49 \le \eta \end{cases} \tag{8}$$

in which the $-\dfrac{1}{3} < \eta \le 0$ region is associated with shear fracture, and the $\eta \ge 0.49$ region

1315 is related to void growth due to tensile stresses, while the intermediate region corresponds to a mixture of both shear and tensile failure mechanisms (see **Figure 30 (c)**). Compared with mill-annealed Ti6Al4V, the fracture strain of the 3D-printed part was one-tenth smaller than what was reported by Giglio et al. [436, 437]. Evidently, the ductility was reduced due to the SLM process.

1320 Xiao et al. [329] used a stress-state dependent ductile damage criterion to simulate the cell-wall fracture through a tabulated fracture strain and stress triaxiality with linear softening, which allowed analyzing damage dissipation. They further employed this model to characterize the compressive behavior of the reentrant honeycomb [453]. This model was originally designed for metallic materials but has been extended to non-metallic materials. For example,

1325 Airoldi et al. [225] adopted a ductile damage initiation criterion for polymeric materials to investigate the auxetic behavior under localized impacts.

(3) Strain-rate and/or temperature-dependent ductile fracture criteria

This subset of ductile fracture criteria assumes that fracture strain depends on not only stress state but also strain rate or working temperature. It would be necessary to apply those

1330 models when the material is subjected to impact loading or temperature change. The most commonly used model is the Johnson-Cook (J-C) damage criterion, defined as [454]:

$$\varepsilon_f = [D_1 + D_2 e^{D_3 \eta}][1 + D_4 \ln(\dot{\varepsilon}^*)][1 + D_5 T^*] \tag{9}$$

where ε_f is the fracture strain; $\dot{\varepsilon}^* = \dot{\varepsilon}_p/\dot{\varepsilon}_0$ in which $\dot{\varepsilon}_0$ is the reference strain rate and $\dot{\varepsilon}_p$ is the effective plastic strain rate; $T^* = (T - T_{room})/(T_{melt} - T_{room})$ in which T_{room} is room temperature, T_{melt} is melting temperature, and T is the current working

1335 temperature; D_1, D_2 and D_3 are the material constants related to the effects of stress triaxiality, and D_4 and D_5 are the constants related to strain rate and temperature effects, respectively. The material constants $D_1 \sim D_5$ can be identified experimentally.

Zhou et al. [332] used the J-C plastic and damage models to simulate the plastic deformation and layer-by-layer failure of network and sheet-based functionally graded

1340 structures. Xiao et al. [74] simulated the Ti-6Al-4V lattice structures at different velocities, and

the results were partly consistent with the experimental observations. Zhao et al. [333] showed that deformation behaviors, yield stress, and energy absorption of functionally graded sheet structures could be well predicted by the J-C model. Bai et al. [455] applied the J-C model to simulate the stress distribution of the failed lattice node, providing an effective way to reduce the stress concentration effect. Kadkhodapour et al. [187] applied the J-C damage model to evaluate the reliability of computational models in predicting mechanical properties. Li et al. [456] applied the J-C damage model to analyze the complex state of deformation, including compression, tension, and bending of metallic micro-lattice and epoxy interpenetrating phase composites. Parametric analysis of the J-C model was conducted for the BCC and FCC titanium lattice materials. It was revealed that the ductility of the base materials had more influence on the energy absorption capability of BCC than FCC [410].

GISSMO (Generalized Incremental Stress State MOdel) is another failure criterion used to model fracture behaviors of AM materials and structures [246, 457]. Compared with the J-C damage model, GISSMO has superior capability in predicting instability behaviors and non-proportional damage evolution [458]. It also includes the numerical techniques to reduce spurious mesh dependence, which often leads to unacceptable errors when damage occurs [459]. It is noted that while GISSMO was developed for metallic materials, Tabacu and Ducu [457] calibrated the GISSMO model for the ABS materials, which can then be applied to the lattice, honeycomb, and rectangular structures with high modeling accuracy. Novak et al. [246] also used GISSMO as the constitutive model for the base material (Ti6Al4V) in the parametric study of chiral auxetic cellular specimens.

A summary of the applications of fracture modeling for AM materials and structures is provided in **Table 10.** From the literature studies, energy absorption of additively manufactured ductile materials can be better predicted if the following fracture mechanisms are considered:

(1) Non-local damage models. The abovementioned studies have focused mainly on damage initiation. As for damage evolution, localized damage models are often used, where a damage variable is introduced to quantify the state of damage [460]. The disadvantage of local

damage models lies in spurious mesh dependence. Briefly, there is no uniqueness of solution as strain localization arises [461]. Therefore, non-local damage models, for example, gradient

1370 damage model [462], phase field method [463-468], and peridynamics [469] have been becoming prevalent recently, which include non-local counterpart of damage indicator in terms of weighted average or its gradient over a spatial neighborhood around each point [470, 471].

(2) Mesh dependence. Apart from non-local damage models, *ad hoc* numerical approaches have been developed to reduce mesh dependence. For example, Andrade et al. [459] introduced

1375 a function of mesh size for regularization numerically such that mesh dependence for damage modeling could be reduced significantly.

(3) Lode parameter. For the stress triaxiality-dependent ductile fracture model, another important parameter, namely the Lode parameter, which is related to the normalized third deviatoric stress invariant [472], was neglected in most of the existing studies. However,

1380 numerous experimental studies revealed that the Lode parameter is significant in determining the damage initiation for metallic materials [472, 473]. Therefore, the accuracy of ductile damage initiation should be enhanced by including the Lode parameter.

(4) Shear-dominated failure. A shear stress ratio may be introduced to consider shear band localization. Representative works in [474, 475] can be some further references.

1385

Table 10. A summary of the application of fracture modeling for AM materials and structures

Fracture category	Materials	Structures	Fracture criteria	Software platforms	AM techniques	Refs
Brittle damage	Plaster and silicone	bi-material structures	Yield function	Abaqus/Explicit	MJF	[371]
	Nylon	bio‐inspired protective structures	Maximum stretching strain	LS-DYNA	MJF	[438]
	carbon fibre (CF) reinforced polyamide	CF/PA metamaterials	Hashin criterion	Abaqus/Explicit	FDM	[265]
Ductile damage	maraging steel	steel lattice structures	Total plastic strain	LS-DYNA	PBF	[51]
	ABSplus	cellular structures	Effective plastic strain	LS-DYNA	FDM	[442]
	ABSplus-P430	lattice structures	Ultimate stress and strain	Abaqus	FDM	[443]
	polymer	functionally graded porous lattice structures	Effective plastic strain	LS-DYNA	SLA	[339]

Material	Structure	Model	Software	Process	Ref
AlSi10Mg	graded auxetic reentrant honeycomb, metallic auxetic reentrant honeycombs	Triaxiality-dependent fracture strain	Abaqus	SLM	[329, 453]
Ti6Al4V	3D anti-tetrarchical lattices	Bao- Wierzbicki model	Abaqus	SLM	[437]
polymer and polyurethane	cellular structures	Triaxiality-dependent fracture strain	Abaqus/Explicit	SLS	[225]
TC4	TPMS lattice structures	J-C model	Abaqus/Explicit	SLM	[332]
Ti-6Al-4V	lattice structures	J-C model	LS-DYNA	SEBM	[74]
Ti-6A-l4V	TPMS	J-C model	Abaqus /Standard	SLM	[333]
Ti6Al4V	Graded strut of BCC Lattices	J-C model	Abaqus/Explicit	SLM	[455]
Ti6Al4V	TPMS	J-C model	Abaqus/Explicit	SLM	[187]
Steel and epoxy	micro lattice and epoxy IPC	J-C model	Ansys Explicit Dynamics	SLM	[456]

Ti-6Al-4V	BCC and FCC lattices	J-C model	LS‑DYNA	SLM	[410]
Ti-6Al-4V	Chiral auxetic cellular structures	GISSMO	LS-DYNA	SEBM	[246]
ABS	lattice, honeycomb, and rectangular structures	GISSMO	LS-DYNA	FFF	[457]

5.1.3 Element types

In finite element (FE) analysis, 1D beam elements, 2D shell elements, and 3D solid elements can be used to model the energy-absorbing structures fabricated by additive manufacturing techniques [2, 18, 418, 476]. To improve computational efficiency, most of the studies used the 1D beam elements to construct the FE models of the strut-lattice structures [29, 32]. For instance, Li et al. [121] built the FE models by the two-node linear beam element (B31 in ABAQUS) to investigate the crushing behavior of multi-layer lattice panels. It was found that the beam elements can effectively predict the mechanical responses of the struct-lattices.

For plate/shell lattices and other structures with complex topology, shell elements [163] and solid elements [130, 159, 333] have been used to capture sophisticated geometric features. For instance, Wang et al. [477] studied the compressive behavior of TPMS lattice-based cylindrical shells using the shell elements. Zhou et al. [332] investigated the mechanical properties of TPMS sheet-network lattices using solid hexahedron elements. Kadkhodapour et al. [161, 187, 478] investigated the deformation mechanisms and mechanical properties of porous biomaterials using voxel meshes.

5.2 Modeling with defects

As stated in Section 4, various defects and imperfections resulted from the additive manufacturing processes can significantly affect the deformation modes and mechanical behavior of printed parts, implying that an idealized and defect-free model cannot predict mechanical responses accurately [12]. For example, Zhang et al. [159] adjusted the shell thicknesses of the FE models to replicate surface roughness. They found that a total thickness reduction of 60μm in the FE model is able to achieve a good agreement with experimental responses.

To simulate the manufacturing defects in the FE model realistically, the most commonly used method is X-ray computed tomography (CT), which enables the reconstruction of as-manufactured models nondestructively and precisely [33, 61, 127, 479-486]. For example, Lu

et al. [32] used X-ray computed tomography to develop as-manufactured models for predicting the elastic and failure responses of the strut lattices computationally, as shown in **Figure 31(a)**. It was found that the results of the as-manufactured models are closer to the experimental results than those of as-designed defect-free models. Lei et al. [33] employed X-ray micro-computed tomography (μ-CT) to capture the geometric imperfection of the BCC and BCCZ lattices, as shown in **Figure 31(b)**, which also showed that the reconstructed FE models can better predict the mechanical properties than their as-designed counterparts.

It is computationally expensive to obtain realistic mechanical properties and energy absorption characteristics for AM parts because the imperfections can be randomly distributed on them. The statistical approach has been used to construct probability distributions of the defects in literature [487, 488]. Based on the defect distributions, the numerical models can be built to more realistically obtain the mechanical responses of printed parts.

The FE model considering the statistical characteristics of defects was established using 1D beam elements to explore the resultant mechanical performance and energy absorption capability of the lattices, as shown in **Figure 31(c)**. It was found that the reconstructed models derived from the μ-CT images can improve the prediction accuracy compared with the as-designed and statistically-averaged models. To consider the geometric imperfections in printed structures, a first-order perturbation-based stochastic homogenization method was used to study the compressive responses of the AM lattices [30], as shown in **Figure 31(d)**. It was found that the simulated compressive stiffness of the lattice structures agrees well with the experimental results.

For pore defects in AM parts, Amani et al. [489] used a "double detector" tomography technique to capture the architecture and internal defects of the samples. Then, the Gurson-Tvergaard-Needleman (GTN) model was used to simulate void nucleation and growth. They revealed that the FE models incorporating the detailed microporosity had a better prediction accuracy of the fracture location and higher stress concentration than the homogenous models.
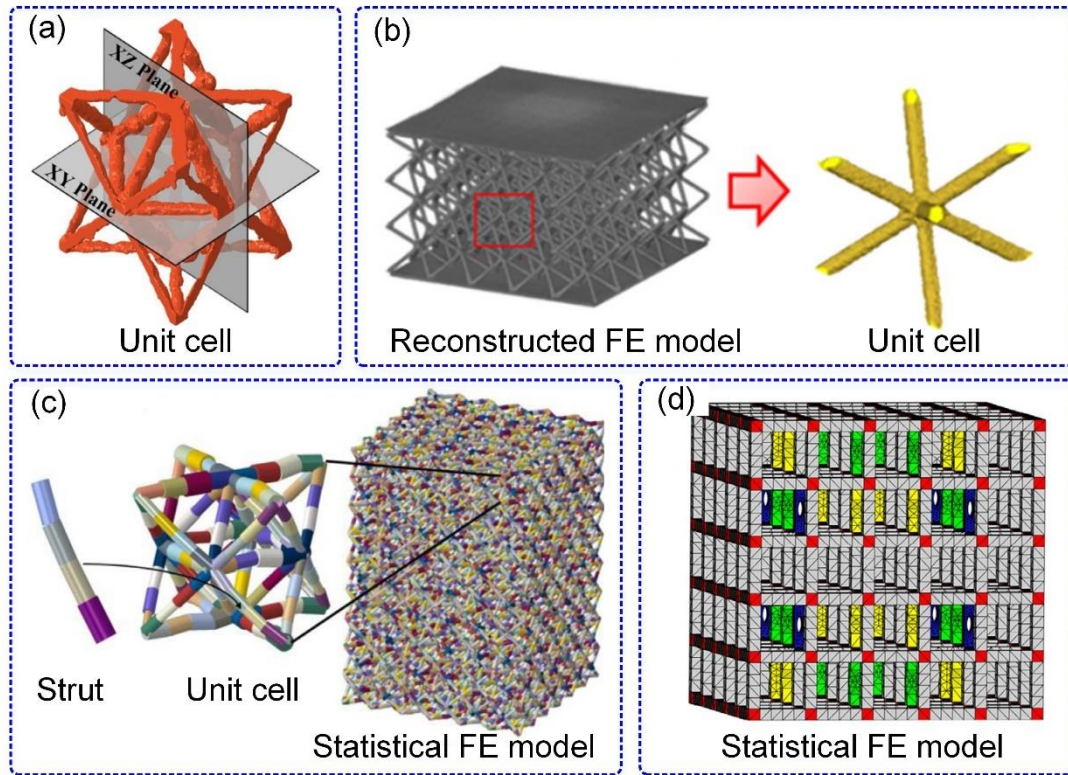
Figure 31. (a) Reconstructed unit cell for the as-manufactured structures [32]; (b) reconstructed FE models for the as-manufactured structures [33]; (c) FE models for the as-manufactured structures [32]; (d) FE model built used the first-order perturbation based stochastic homogenization method [30].

5.3 AM process simulation

Modeling and simulation of a specific AM process is a promising way to quantify the influence of process parameters on the resultant AM part properties [490-492]. Through AM process simulation, one can better understand AM's physical/chemical processes quantitatively, thereby improving the design for reducing the defects of the AM parts [493]. Due to different AM processes involving different physical/chemical reactions, the simulation of AM process needs to be realized in line with a specific AM process [494-496].

For PBF or DED, three subjects for AM process simulation are categorized as thermal fields, residual stresses, and melt pool characteristics [415]. For instance, Lee and Prabhu [497]

proposed a metamodel of heat transfer beneath the laser beam to optimize the additive

1455   manufacturing process. The results showed that the proposed optimizer could be used to control

temperature by tweaking the scan speed. Song et al. [498] used the ABAQUS AM module to

simulate the AM process of complex 3D parts. The simulated residual stresses and distortion

were validated with experimental results. Sahoo and Chou [499] developed a phase-field model

to predict the microstructural evolution of Ti6Al4V powder in the SEBM process. The

1460   simulation results were in good agreement with experimental and analytical counterparts.

For the filament-based material extrusion AM process, Serdeczny et al. [428] presented a

novel computational fluid dynamics (CFD) based model to predict the recirculation region,

stagnation point, and melt zone. Moreover, the pressure and temperature distributions inside

the channel were obtained by numerical simulation. The proposed numerical model was

1465   validated with the experimental results, which can be used to develop control strategies for

liquefier heaters. For the vat photopolymerization process, Classens et al. [500] developed a

modular control-oriented model to describe the multiphysical vat photopolymerization process.

Moreover, a tracking control strategy based on the proposed model was used to optimize the

material properties produced through vat photopolymerization.

1470   The imperfections and residual stress distributions of the AM parts can be modeled by the

AM process simulation, which may have a significant influence on the mechanical properties

and energy absorption of the AM parts [12, 380, 490, 501]. These simulated AM process results

can be used as the initial conditions of the large deformation simulation to improve the

computational efficiency and accuracy of the numerical modeling with defects.

1475   **6. Design Optimization**

Energy-absorbing structures with lightweight and high performances normally have

intricate geometries, thus limiting the applications of conventional manufacturing technologies.

In this regard, AM has exhibited a compelling capacity to take engineers a step closer to

achieving ideally desired performances of energy-absorbing structures [237, 319, 334, 502-504]. Compared with conventional manufacturing approaches, AM techniques have tremendous potential to produce geometrically complex components [2, 5, 13, 15, 505-507]. Such high flexibility thus makes AM a promising technology for generative design in multi-scale, multi-materials, and custom-made energy-absorbing structures [351, 508-510]. On the one hand, the manufacturability of novel structures is no longer a critical issue by using AM; on the other hand, new possibilities offered by AM call for more elegant and efficient design methodologies. While various novel materials and structures have been proposed, as reviewed in Section 3, it is possible to automatically generate the design with desirable mechanical properties and energy-absorbing capacity. For this purpose, growing research has focused on computational optimization for design of energy-absorbing structures in literature [34, 163, 225, 322, 511].

While various optimization approaches are significantly promising to provide structure-aware solutions, challenges remain when integrating them with AM. One of the key issues associated with AM is its manufacturing uncertainties. Due to geometric imperfection, material uncertainty, and defects induced in the manufacturing process, as-fabricated parts may considerably deviate from as-designed models. In some worst-case scenarios, the critical deviations can even drastically impair desired performances of as-built parts [33, 127, 380, 512]. In particular, the deformation behavior of energy-absorbing structures is highly sensitive to geometry, which can further affect energy absorption performances [33]. Uncertainty in physical, chemical, and mechanical properties is also a critical issue, which may play an key role in the energy absorption performances of as-built parts [55]. Therefore, this section reviews the state-of-the-art optimization studies on the design of energy-absorbing structures considering various AM factors.

6.1 Parametric optimization

In contrast to trial-and-error-based approaches, parametric optimization provides a more

efficient and effective means, which has drawn substantial attention from academia and industry [513-516]. In parametric optimization, desired performances are typically classified as objectives or constraints, then treated as explicit functions with respect to design parameters [316, 419, 517]. The design parameters are often related to the size and shape of the structural profile [518-524]. Parametric optimization aims to seek an optimum solution for structural and material parameters such that the best performance of objective functions can be achieved while satisfying the design and manufacturing constraints.

In the past decades, substantial research efforts have been devoted to parametric optimization for a range of energy-absorbing structures [163, 225, 322, 517, 525-527], including strut-based lattices [129, 298, 525], TPMS-based lattices [528], bio-inspired lattices [166, 222, 331], auxetic structures [517], honeycombs [55], and origami-inspired structures [529] etc. as reviewed in Section 3. For example, Mahbod et al. [322] investigated a strut-based lattice, namely a double pyramid dodecahedron, in which the ratios between the lengths of horizontal and inclined struts were defined as design parameters to tailor mechanical properties. Yin et al. [163] explored the design of sheet-based TPMS structures, where the level-set constant and thickness were parametrized as design variables to generate different geometries. Fernandes et al. [207] studied the thickness and location of diagonal struts in a lattice structure inspired by deep-sea glass sponges. Airoldi et al. [225] investigated an auxetic structure composed of chiral units in which the length and thickness of ligaments were used to describe the geometry. Once energy-absorbing materials and structures are parameterized, computational modeling techniques such as FEA can be used to calculate the responses of objectives and constraints with respect to design parameters. Following this, the performances of energy-absorbing structures can be tailored by optimizing these design parameters [13, 524, 530-532].

Computational modeling of energy-absorbing structures under large deformation typically involves material and geometrical nonlinearities. Direct coupling computational modeling with optimization algorithms can be fairly expensive when iteratively evaluating many designs [22].

To address the issue, surrogate modeling, which represents some approximate functions of objectives and constraints with respect to design parameters, has often been developed to replace FEA in an offline fashion [22]. The first step of surrogate-based optimization is to generate sample points in the design space by Design of Experiments (DoE) [533]. Then, the mechanical responses at these sample points are calculated using FEA or other numerical simulation techniques, and the surrogate models are constructed based on these sampling data. Various surrogate models have been adopted to design energy-absorbing structures and materials, and interested readers can refer to a previous review article [22, 534].

Substantial works have been carried out with surrogate-based AM structural parametric optimization. For example, Ye et al. [518] presented a Kriging-based parametric optimization for enhancing the gradually stiffer property of a 3D periodic structure. Wang and Rai [535] proposed a surrogate model-based optimization scheme to design lightweight and high-strength functional components with spatially varying conformal cubic periodic cellular structures. Gorguluarslan [523] proposed a surrogate-based multiobjective size optimization for lattice structures by considering the AM constraints, such as the minimum printable size. Doan et al. [536] presented a new approach for optimizing buckling loads of lattice structures by coupling a Reduced Order Model (ROM) based on the Homotopy Perturbation Method (HPM) and a Kriging model with the AM constraints.

6.2 Topology optimization

Topology optimization, as an advanced and powerful tool, aims to optimize the material distribution in a given design domain for achieving the desirable goal, which typically enables better use of material. Topology optimization starts with an initial design and evolves the material distribution into a new configuration that can significantly differ from the initial counterpart. The manufacturability issue of intricate parts generated by topology optimization used to be a critical bottleneck in realization. Fortunately, the advances in additive manufacturing have largely changed this situation and made it possible to fabricate almost any

sophisticated configuration [537]. Therefore, AM has been gaining significant interest and popularity in the topology optimization of energy-absorbing structures [353, 504, 520, 538-540].

6.2.1 Density-based topology optimization methods

As one of the most popular methods, density-based topology optimization has demonstrated significant success. For example, Xiao et al. [128] employed a solid isotropic material with the penalization (SIMP) technique [541] to optimize structural topology for a single lattice, which was manufactured by SLM for energy absorption. Song et al. [34] also used the SIMP model to optimize the lattice structures for fabrication with SLA, in which the experimental tests on the fabricated parts also showed an enhanced energy absorption efficiency. Zhang and Yanagimoto [504] optimized a strut-based lattice by the SIMP approach and experimentally tested the energy absorption capability of the lattice structures made by 3D-printed polylactic acid [76]. Duan et al. [511] performed topology optimization on a single lattice by using the bidirectional evolutionary structural optimization (BESO) approach [542]; they prototyped the design using SLA for testing mechanical performances, including energy absorption efficiency.

In the density-based approaches [543, 544], a pseudo density ρ is commonly assigned to each element as a design variable which is used to interpolate material properties. Penalization schemes such as a power-law model are usually applied on the pseudo density ρ to push it to be either 0 (void) or 1 (solid material). As such, sensitivity analyses of objectives and constraints are deduced with respect to the pseudo density ρ, which are then used to drive topological evolution during optimization processes. In a typical SIMP procedure, the analytical sensitivities provide mathematical algorithms (such as the method of moving asymptotes (MMA) [545]) with gradient information to determine the iterative update of the pseudo density ρ. In the BESO algorithm, a heuristic scheme is adopted to directly add or remove elements partially or entirely according to the relative rank of the analytical sensitivities [546, 547].

6.2.2 Boundary-based topology optimization methods

In literature, boundary-based topology optimization methods have gained considerable popularity in the design of additively manufactured energy-absorbing structures. Unlike the density-based approach, the boundary-based method employs an explicit function to describe structural interfaces between different material phases, in which topological change is achieved by evolving such an explicit function during the optimization process. The level-set function [548, 549] and the phase-field function [550] are typical functions employed in the boundary-based methods. For example, Zhang et al. [551] adopted the level-set method to design lattice structures. The optimized part was fabricated by SLM to show a notably high energy absorption efficiency. Takezawa et al. [552] designed a lattice structure using the phase-field approach. The experimental tests were conducted to investigate the mechanical properties of the selective electron-beam melting (SEBM) based as-built parts. A more recently proposed moving morphable components (MMC) method [553] was also employed for the design of additively manufactured graded lattice structures [554]. The MMC method uses an explicit function to directly describe the shape and spatial position of each component for achieving better performance by optimizing topological configuration.

6.2.3 Nonlinear sensitivity analysis

One of the key steps in topology optimization is to obtain sufficiently accurate gradient information for driving the evolution of structural configuration. In dynamic energy absorption analysis, challenges remain in the sensitivity analysis attributed to the associated high material, geometry, and even contact nonlinearities presented in the FEA. In order to consider all these nonlinear behaviors accurately, path/time-dependent sensitivity analysis needs to be carried out if the computational cost in deriving sensitivities is at an acceptable level [555-559].

6.2.4 Topology optimization methods for energy absorbing structures

Several approaches have been proposed for the topology optimization of energy-absorbing structures to solve such a highly complex yet important topic in an efficient and effective way [22]. In general, these related studies could be classified into several main methodological

categories, namely the nonlinear programming-based algorithms [559-561], the BESO-based methods [555, 562, 563], the hybrid cellular automaton (HCA) approaches [561, 564-567], evolutionary heuristic algorithms [539], and the equivalent static loads (ESLs) approach [568-572].

In the BESO-based design of energy-absorbing structures, maximizing total external work is typically considered an objective function subject to a displacement-controlled load for numerical stability [555, 562, 563]. To calculate the sensitivity involved in the nonlinear FEA, the external work is approximately expressed by the sum of the external work through many small loading steps and assuming a linear force-displacement relationship within each small-time step. By using the adjoint equations corresponding to each time step, the sensitivity can be obtained, which equals the total strain energy of each element in its final deformed state. Such a path-dependent sensitivity has been demonstrated to be simple yet effective for enhancing the energy absorption efficiency of the optimized structure.

In the HCA approach, a so-called cellular automaton (CA) is combined with nonlinear FEA. A CA cell can be defined as a single element or a group of elements in the design domain. Similar to the density-based approach, a pseudo density between 0 and 1 is associated with each CA cell. In addition, field variables such as stress, strain energy, and internal energy of each CA can be obtained from the nonlinear FEA. Then, the field variables of each CA cell are averaged by using its neighboring CA cells during the optimization process. Since the goal of the HCA approach is to redistribute the structural mass for a homogenous distribution of the desired field variables, a heuristic scheme is adopted to update the density of each CA cell. Typically, the error between the field variable and its ideal target value forming a uniform distribution is employed as the clue to update the density; e.g., if the field variable of one CA cell is lower than its target value, its density is then reduced, and vice versa. It should be noted that HCA characterizes a heuristic approach without gradient information, thereby bypassing the complicated sensitivity analyses in a nonlinear FEA.

The ESLs approach was first proposed by Lee and Park for dynamic topology optimization

[568]. The idea is to calculate sequential linear static loads generating the same response field as the nonlinear dynamic analysis at each time step. Under the equivalent linear static loads, the sensitivity information can be easily derived, and then the well-developed density-based or boundary-based approaches can be applied, substantially reducing the computational cost.

6.2.5 Additive manufacturing constraints in topology optimization

AM process could also raise new manufacturing constraints for topology optimization of energy-absorbing structures [573-584]. In the powder-based AM process, a powder-removing hole is essential for cleaning sintered parts with residual metal powder, meaning no enclosed void is allowed in the optimized architecture. For example, Takezawa et al. [552] employed a phase-field-based method to generate the lattices with isotropic stiffness. In their study, a fixed powder-removing hole with different layouts was manually embedded in the design space to investigate the effects on optimized parts. More recently, Xiong et al. [585] proposed a BESO-based topology optimization approach to automatically avoid enclosed voids in the optimized structures. **Table 11** summarizes the studies considering typical AM constraints using different topology optimization methods.

Table 11 Examples of additive manufacturing constraints used in topology optimization for the design of energy-absorbing materials and structures

AM constraints	Optimization methods	Refs
Overhang/self-support	Level-set with single domain integral	[586]
	SIMP with an edge detection algorithm	[587]
	SIMP with projection operations	[588]
	SIMP with maximum density function	[584]
	SIMP with multiple filtering methods	[589]
	MMC and Moving Morphable Voids (MMV)	[590]
Building direction	BESO	[574]
	Multiresolution SIMP	[581]
Building	SIMP with component partitioning vector field	[583]

volume/partition		
Enclosed voids	Level-set with a side constraint scheme	[589]
	SIMP with Poisson method	[591]
	SIMP with virtual scalar field method	[592]
Thermal residual stress/distortion	Level-set with thermo-elastic evolution model	[593]
	SIMP with a transient heat transfer model	[594]
	SIMP with element birth technique and inherent strain technique	[579]
	SIMP with Inherent strain method	[595, 596]
	SIMP with Inherent strain method and homogenization	[103]
	Level set with Inherent strain method	[597]

6.3 Design optimization considering fabrication-induced uncertainties

While AM facilitates the fabrication of structures and materials with rather complex geometry, manufacturing-induced uncertainties and defects arise in material property and structural geometry, which are fairly different from traditional manufacturing technologies [33, 598-604]. On the one hand, much effort has been made to minimize the defects by imposing proper constraints, optimizing process parameters [598], and introducing post-processing, as reviewed in Section 4.3. It would also be beneficial for enhancing the optimization effectiveness if the AM process and resultant mechanical behavior are considered simultaneously in the stage of computational design. In other words, both the AM process parameters and the material/structural features can be treated as design variables for achieving desirable mechanical properties and energy absorption characteristics under loading [605-610].

On the other hand, it would be possible to develop uncertainty-based optimization approaches to accommodate fabrication-induced imperfections without eliminating the source of uncertain variability [22, 611-613]. In this regard, topology optimization considering material and geometry uncertainties has become an active research topic with the advent of various AM technologies [607, 614-620]. For example, Liu et al. [605] studied a non-

probabilistic reliability-based topology optimization by considering local material uncertainty in AM, in which a multi-dimensional ellipsoid model was correlated with the uncertainties in several subdomains. Alacoque et al. [621] investigated a robust topology optimization for periodic lattice structures composed of thermoelastic multi-materials, in which material and geometry uncertainties were considered simultaneously by assuming uniform distributions of manufacturing uncertainties. **Table 12** summarizes the literature studies on AM uncertainties with different materials and the corresponding optimization schemes. Note that while recent attention has been paid to the manufacturing uncertainties, further studies on nondeterministic topology optimization are still expected to explore more effective algorithms by considering various effects of AM processes on design of novel energy-absorbing materials and structures.

Table 12 Design optimization involving AM-induced uncertainties

Refs	Materials	Uncertainties	Optimization schemes
[621]	Multi-materials	Density/composition	Robust topology optimization
[103]	VDI - AlSi10Mg	Material property	worst-case topology optimization
[605]	Metal		non-probabilistic reliability-based topology optimization
[614]	Metal		Reliability-based topology optimization
[617]	Metal		Topology optimization with random fields of material parameters
[618]	Metal		Robust BESO topology optimization
[539]	Metal	Load	Evolutionary level set method
[619]	Metal	geometric uncertainty	Monte Carlo-based topology optimization
[622]	Metal	Material & load	Non-probabilistic reliability-based topology optimization
[607]	Metal		Robust topology optimization
[611]	Metal	Mechanical properties	Robust BESO topology optimization
[612]	Metal		Robust multiphase topology optimization
[620]	Metal		Reliability-based and robust topology optimization
[615]	Metal	Material &	SIMP topology optimization with

		geometrical	stochastic collocation methods
[616]	Metal		SIMP-based topology optimization with stochastic collocation methods

1685

7. Data-driven and machine learning in additive manufacturing

Machine learning (ML) signifies an artificial intelligence approach that automatically deals with a large amount of data observed in nature, bespoken by humans, or generated by other methods. ML techniques have exhibited compelling outcomes in many fields such as

1690 image analysis [623], neural language processing [624], data mining, and health sciences [625]. Recently, the unprecedented success of ML techniques has inspired researchers to explore their applications in fields of engineering, aiming to improve the material properties of fabricated parts. A growing number of studies have investigated the synergy of ML techniques in computational mechanics [533, 626, 627] and material and structural design [628, 629]. In the

1695 recent years, AM has undoubtfully become one of the fast-growing areas drawing substantial attention for ML research and applications [630-639]. This section thus aims to review the recent studies on ML in AM from three aspects: (1) ML in design for additive manufacturing (DAM); (2) ML in AM process parameters; (3) ML for the in-situ monitoring of AM process.

7.1 Overview of data-driven and machine learning approach

1700 From a perspective of learning types, ML algorithms could be briefly categorized into supervised learning, unsupervised learning, semi-supervised learning, reinforcement learning, etc.; while from a view of ML tasks, the applications of ML algorithms could be generally classified into regression, classification, and clustering. **Figure 32** summarizes the commonly used ML techniques in AM. For regression tasks, ML techniques can be applied in several

1705 different AM fields, including DAM, design of process parameters, prediction of mechanical/physical properties, and prediction of dimension/geometry deviations [640]. Logistic & linear regression [489, 641, 642], Gaussian processing (GP) [643], random forest

(RF) [644], support vector machine (SVM) [645], artificial neural network (ANN) [646] and convolutional neural network (CNN) [623] are some typical ML techniques, which have been widely employed for various regression analyses. Classification is commonly used for defect detection, microstructure prediction, and melt pool monitor in AM, which includes decision tree (DT) [647], K-Nearest Neighbors (KNN) [648], RF, SVM, ANN, and CNN. Clustering is normally used for data mining and analysis, such as material data and processing data, to determine some clues on how different materials and AM processing parameters would affect the mechanical properties and energy absorption characteristics of as-built parts [649, 650]. Commonly used clustering approaches include principal component analysis (PCA), self-organizing map (SOM), etc [651-654].

ANN and CNN are the most widely employed ML models in AM studies [655-660]. Both ANN and CNN contain a number of nodes (neurons) and are usually composed of an input layer, one or more hidden layers, and an output layer. In ANN, neurons in one layer are fully connected with neurons in the next layer by weight factors that are trained with ground truth data using a backpropagation scheme. Different from ANN, CNN is a representative deep learning algorithm using a convolutional operator between each layer where neurons between different layers are not fully connected. CNN exhibits good performance in feature recognition with high efficiency [661-663].
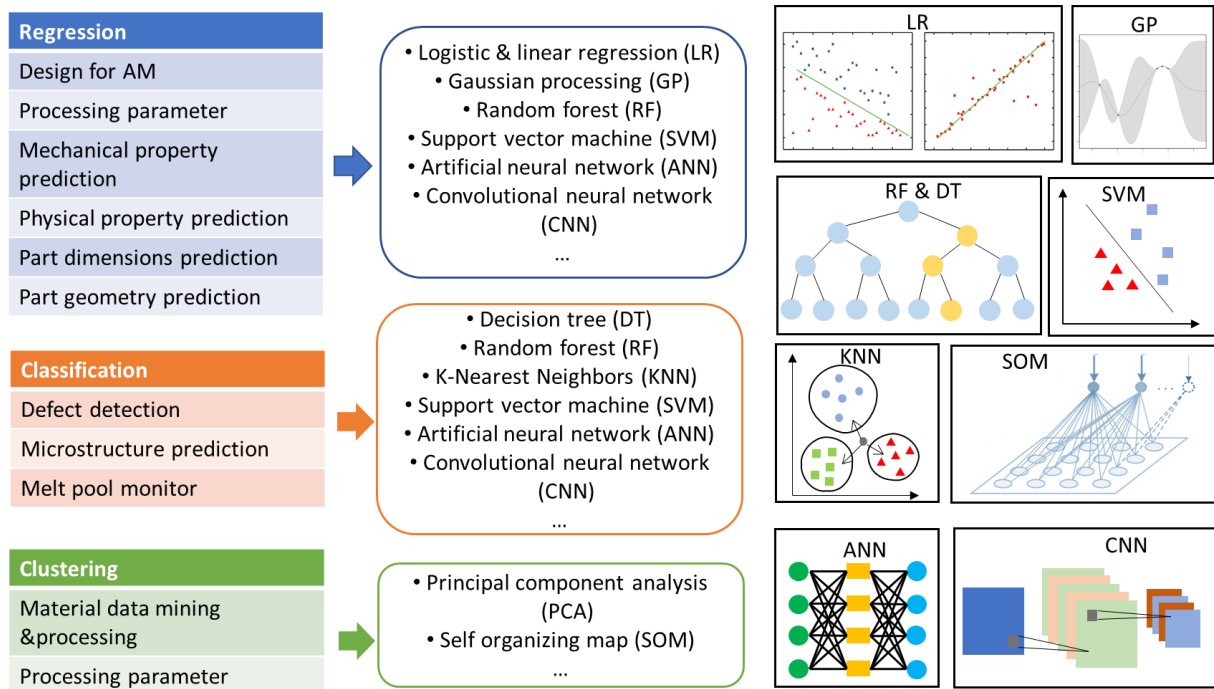
Figure 32 A summary of commonly used machine learning techniques in additive manufacturing.

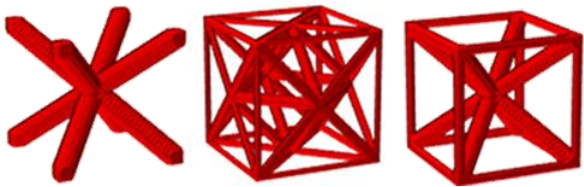## 7.2 Design for additive manufacturing

Concerning the design optimization of energy-absorbing materials and structures, surrogate modeling introduced in Section 6.1 may be regarded as one class of ML algorithms. Looking forward, more advanced ML algorithms could be developed for the AM-oriented analysis and design of energy-absorbing materials and structures [664-666].

In literature, there have been some research attempts in data-driven and machine learning-based design for additively manufactured materials and structures [667, 668]. For example, Guo et al. [669] proposed three-dimensional convolutional neural networks (3D-CNN) to model the effective elasticity tensor and its gradients for general AM voxel-based nonparametric microstructures. Xiong et al. [670] developed a two-step surrogate-based design framework using the Bayesian network classifier as the reasoning approach, allowing to explore the design space in the embodiment design stage and the Gaussian process regression
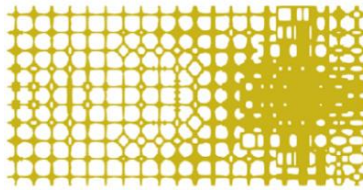
model to exploit the design space in detailed design stage. Garland et al. [665] proposed a machine-learning approach for discovering new unit cells in the Pareto frontier for optimizing multiple competing objectives. Singh and Kapania [671] developed Deep Neural Networks (DNNs) to optimize curvilinear stiffeners for additive manufacturing. Nasiri and Khosravani [668] employed a machine learning (ML) approach to predict the structural performance and fracture of additively manufactured components. Gu et al. [672] proposed a machine learning-based approach to optimize hierarchical materials, which was trained with a database of hundreds of thousands of candidate shapes from FEA and a self-learning algorithm for discovering high-performing materials for additive manufacturing.

Data-driven/ML approaches have also been recently used to design lattice structures in literature. **Table 13** summarizes some representative studies on data-driven/machine-learning techniques for the design optimization of lattice structures. Unlike ML algorithms, data-driven methods directly employ ground truth data and a stochastic process such as the Gaussian process [673] to develop a design by following physical laws or optimization criteria, while machine learning techniques are essentially data-driven. Data-driven/ML approaches normally play two roles in the design of lattice structures: (1) generative models for automatically generating new structures, and (2) surrogate models for establishing the structure for desirable mechanical properties [674, 675].
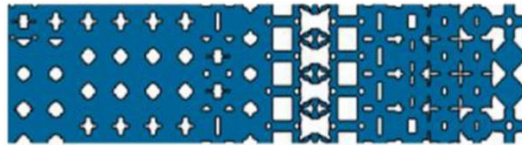
Table 13 A summary of data-driven/machine learning approaches in the design of lattice structures

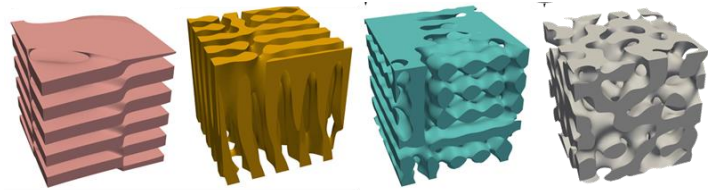| Refs	Optimization schemes	Lattice structures
[676, 677]	Data-driven/Latent-variable Gaussian process	

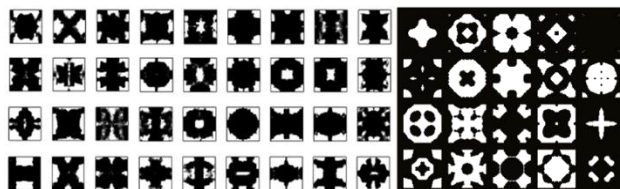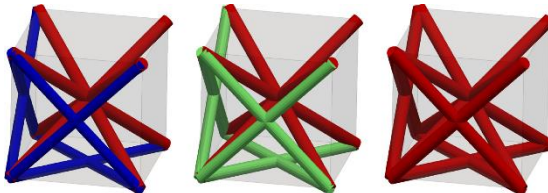| [678] | Data-driven/dual decomposition Markov random field (DD-MRF) | |
[679]	Data-driven/Laplace-Beltrami (LB) spectrum with Markov random field	
[680]	Deep neural network and Gaussian random field	
[681]	CNN	
[665]	CNN	
[682, 683]	ML/variational autoencoder	
[684]	ANN	
[685]	Scalable variational Gaussian process classification	

| [686] | ML/generative adversarial networks | |
| [687] | ANN | |
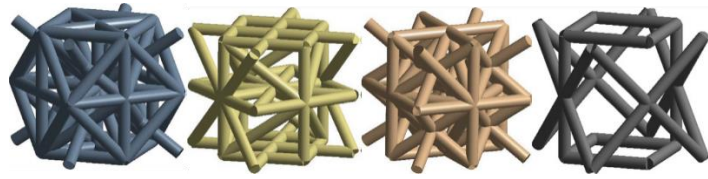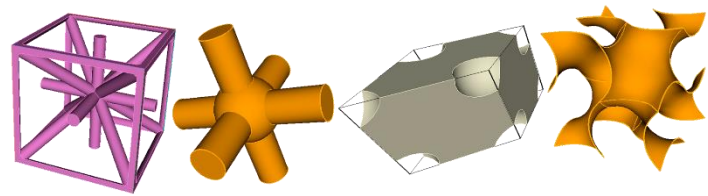
7.3 Process parameters

Process parameters in AM can have significant effects on material/structural characteristics of resultant parts. Adoption of different processing parameters can lead to different mechanical properties with varying defects/imperfections. For example, in laser-based AM processes such as SLS, SLM, and SEBM, laser power, scan speed, scan spacing, layer thickness, and processing temperature may influence the density, dimensions, and tensile strength of fabricated parts [688-690]. In the FDM process, layer thickness; air gap; raster angle; build orientation; road width; the number of contours can lead to different creep and recovery behavior, tensile/compressive strength, etc. [691-695]. For this reason, significant effort has been devoted to developing the relationship between process parameters and various materials/structural properties of as-built parts by using conventional modeling techniques, as discussed in section 5.3.

Table 14 A summary of ML techniques for predicting mechanical/physical/geometrical properties of AM parts with various process parameters.

Refs	AM	Materials	ML methods	Process parameters	Characteristics
[696]	PBF	Polymer	ANN	Laser power; scan speed; scan spacing; layer thickness	Density
[697]		Polymer	ANN	Laser power, scan speed, scan spacing, layer thickness	Dimensions
[698]		Polymer	ANN	Z-height, part volume, and bounding-box volume	Building-time
[699]		Polystyrene	ANN	Laser power, scan speed, hatch spacing, layer thickness, scan mode, temperature, interval time	Shrinkage ratio
[700]		Polystyrene	ANN	Laser power, scan speed, hatch spacing, layer thickness, scan mode, temperature, interval time	Density
[701]		316L Stainless steel	ANN	Laser power, scan speed, and layer thickness; annealing and hot isostatic pressing	High cycle fatigue
[702]		316L Stainless steel	Gaussian process	Laser power, scan speed, and laser beam size	Melt pool depth
[703]		Ti6Al4V	ANN, RF	Laser power, scan speed, hatch space, powder layer thickness	Fatigue life
[704]		Stainless steel	GP	Laser power, laser scanning speed	Porosity
[705]		Steel	GP; SVR	Laser radiation, pressure intensity, laser energy density	Porosity
[706]		316L Stainless steel	ANN, RF, SVM	Laser power, scan speed, hatch space, powder layer thickness	Fatigue life
[707]		Ti-6Al-4V	ANN	Spreader diameter, length, spreader translational/rotational speed	Surface roughness
[708]	SLA	Polymer	ANN	Layer thickness, Illuminating time, waiting time	Shape deviation
[709]		Polymer	ANN	Layer thickness, border overcure, hatch overcure, fill cure depth, fill spacing, hatch spacing	Dimensions
[710]		Polymer	CNN	print orientation, Slice layer	Stress distribution
[711]	FDM	ABS polymer	ANN	Layer thickness, air gap, raster angle, build orientation, road width, the number of contours	Creep and recovery behavior

Ref	Process	Material	Method	Input parameters	Output
[712]		ABS polymer	ANN	Layer thickness, orientation, raster angle, raster width, air gap	Compressive strength
[713]		Polymer	ANN	Layer thickness, orientation, raster angle, raster width, air gap	Wear strength
[714]		ABSP400	ANN	Layer thickness, orientation, raster angle, raster width, air gap	Dimensions
[715]		ABSP400	ANN	Layer thickness, orientation, raster angle, raster width, air gap	Dimensions
[716]		Polymer	ANN	Orientation, slice thickness	Building time
[717]		Polymer	RF	Build plate and extruder temperature, vibrations	surface roughness
[718]	DED	316L stainless steel	SVM	Laser power, scan spacing	Depositing height
[719]		Copper	ANN	Wire feed rate, welding speed, arc voltage, nozzle to plate distance	Bead geometry
[720]		316L Stainless steel	CNN	Micro morphological and crystallographic	Yield strength
[40]		2024 Al Alloy	ANN	Laser power, scanning speed, powder feeding rate	Dimensions
[721]		316L Stainless steel	RNN	Geometry, build dimensions, toolpath strategy, laser power, scan speed	Thermal history in melt pool
[722]		Cobalt alloy	KNN	Power, feed rate, travel speed	Surface roughness
[723]	MJ	Stainless steel	ANN	Layer thickness, printing saturation, heater power ratio, drying time	Dimensions and surface roughness
[724]		Co-Cr-Mo alloy	ANN	Roller translational speed, roller rotational speed, drying time, binder level, layer thickness	Dimensions
[725]	DED	Carbon steel	ANN	Welding speed, wire feed speed, overlap ratio, measured roughness	Surface roughness
[726]		Steel	RF	Travel speed, wire feed speed, weaving wavelength, weaving amplitude	surface roughness
[727]		Stainless steel	ANN	Welding current, voltage, contact-to-workpiece distance, travel speed	deposited shape

Note that conventional modeling techniques heavily rely on physical/chemical rules for investigating process parameters, which are not always available and/or accurate enough due to the intrinsic complexity of different AM processes. Therefore, ML techniques have drawn growing attention to establishing process-properties relationships for various AM processes and certain materials, which makes physical/chemical rules unnecessary for such highly nonlinear and complex modeling problems. **Table 14** summarizes the studies on various ML techniques for predicting the characteristics of as-built parts with respect to different process parameters with different materials in different AM processes. In literature, ANN appears to be the most popular ML technique for linking material/structural properties to the process parameters as shown in **Table 14**. For example, Sood et al. [712] employed ANN to investigate the effects of layer thickness, printing orientation, raster angle, raster width, and air gap in an FDM process on the compressive strength of fabricated parts. In their study, the five factors are first sampled by a face-centered composite design; and then the experimental tests were performed in line with the sampled factors to collect different compressive strengths that were used as ground truth data to train the ANN model. Zheng et al. [701] employed ANN to study the high cycle fatigue life of stainless steel manufactured by PBF with respect to different laser powers, scan speeds, layer thicknesses (processing parameters), annealing and hot isostatic pressing (post-processing) conditions.

Once the process-property relationship is established by ML techniques, optimizing the process parameters to achieve desired part properties can be performed at a fairly low cost. In this case, ML models can be regarded as functional surrogates similar to those reviewed in Section 6.1 for parametric optimization, in which either conventional heuristic algorithms such as genetic algorithm (GA), particle swarm optimization (PSO), or machine learning-based methods such as Bayesian optimization can be applied for the process parametric optimization [724, 728-737]. For example, Park et al. [738] used ANN to optimize four process parameters (laser power, laser scanning speed, layer thickness, and hatch distance) in the SLM process to achieve a desirable density ratio and roughness. Their study first carried out experimental tests

to obtain the ground truth data for containing the implicit relationship between these four process parameters and two anticipated mechanical properties. Then, an ANN model was trained by the experiment data to establish their relationship explicitly. Since ANN can almost predict the desired properties with respect to different input parameters instantly, it is possible to even apply the simplest brute-force algorithm to optimize the process parameters for desired properties with acceptable efficiency.

7.4 In-situ monitoring

In-situ monitoring of AM enables to assure product quality and reliability, which provides a means to automatically control the printing process in a close loop without human intervention. The real-time data in the printing process requires a deep understanding of materials and AM mechanisms, as discussed in Section 5.2, which can notably restrict the spectrum of applications when using new materials and different AM machines. Besides, defects detection and other in-process factors such as melt-pool temperature rely on computer vision [739, 740]. A large amount of collected data could hinder in-situ monitoring by human operators.

To address these issues, ML techniques have drawn significant attention due to their excellent real-time processing ability and remarkable performances in image analyses [741, 742]. ML applications for the in-situ monitoring of AM process have two main active areas. The first is the real-time detection of defects such as cracks, surface deviation, and roughness, where ML techniques are employed to analyze image data collected from a camera or sensor. In this regard, Duman et al. [743] proposed a deep learning based approach for defect detection in the PBF process, in which layer images were collected during laser sintering processes in situ and were then transferred to a pre-trained CNN on ImageNet to predict micro cracks.

The second active area is to monitor the melt pool temperature during the manufacturing process, which can reduce microstructural defects (cracks, porosity) and thermal residual stress. In this aspect, Kumar et al. [744] employed CNN and Long Short-term Memory neural network (LSTM) to monitor the melt pool temperature in the WAAM process, in which the melt pool

temperature was observed using a thermal imaging camera and then analyzed by the trained CNN-LSTM.

1835   **Table 15** summarizes more studies that used ML techniques for the in-situ monitoring of various AM processes with different purposes.

Table 15 A summary of in-situ monitoring of AM process using machine learning techniques.

Refs	AM process	Monitor objectives	Machine learning methods	Data monitor/collection approaches
[745]	PBF	Surface topographies	Autoencoder neural network	Scattered light captured by a screen and recorded by a camera
[746]		Laser track welds	CNN	Camera/video clips
[747]		hot-spot defects	k-means, SVM, ANN	Camera: video-imaging data
[748]		microscopic pores	Autoencoders, PCA, k-means	Optical emission spectra signals
[749]		Porosity	Graph Fourier coefficients	X-ray Computed Tomography
[750]		Melt pools	Bag of Words	High-speed camera
[751]		Anomaly detection	CNN	Camera
[752]			k-means, CNN/filter bank	Camera
[753]			Variational autoencoder	High-speed camera
[754]		Part defects	XGBoost	Sensor
[755]			Reinforce learning algorithm	Fiber Bragg grating: acoustic emission
[756]			CNN	Fiber Bragg grating: acoustic emission
[757]			CNN	Fiber Bragg grating: acoustic emission
[758]			SVM	High-resolution digital camera
[759]			CNN	Camera
[760]			CNN	Multi-modal sensor fusion
[761]			PCA, Gaussian Mixture Model, variational auto-encoder [517]	Acoustic emission sensor
[762]			CNN	Camera
[763]			K-Means, KNN	Optical tomography monitoring
[764]			CNN	Camera
[765]		Porosity	ANN. SVM	High-speed camera
[766]	DED	Surface quality	KNN, SVM, GP, ANN	Robot joint data from the robot controller
[767]		Part defects	LSTM-Autoencoder, k-means	Emission spectroscopy

[768]			CNN	Acoustic emission
[769]	FDM	Surface roughness	RF	Sensor: temperature of the build plate, extruder, deposited material; ambient temperature, vibration of the build plate, the extruder
[770]			PCA	Illumination and microscope module
[717]			RF	Sensor: thermocouples, infrared temperature sensors, and accelerometers
[754]		Interlayer imperfections	CNN	Camera images
[771]		Layer inspection	SVM, CNN	Camera
[748]		Part defects	SOM	Acoustic emission sensor
[772]			Clustering by fast search and find of density peaks (CFSFDP)	Sensor: acoustic emission
[773]			ANN, CNN	Vibration sensor
[774]			SVM	Camera

8. Applications

8.1 Automotive Engineering

It is essential to use suitable energy-absorbing structures for protecting lives and goods from impact/blast loading. In engineering practice, many attempts have been made to improve the energy absorption capacity of lightweight structures [20, 199, 775]. Compared with conventional techniques, additive manufacturing can fabricate more sophisticated components, thereby enhancing the energy absorption capacity and efficiency [237]. Aiming to increase energy absorption capacity and decrease the weight of materials/structures, researchers have applied additively manufactured parts in automotive engineering as energy absorber components [776-779]. For instance, the brackets printed by SLM were used in BMW i8 Roadster in a series of vehicle production [36], in which a 44% weight reduction was achieved compared to its preceding design, as shown in **Figure 33(a)**. The rear uprights of the suspension assembly were designed by a topology optimization method and fabricated by SEBM [37], as shown in **Figure 33(b)**. In literature, Lee et al. [780] proposed an auxetic-core infilled tube, which was fabricated by the SLM method with stainless steel 316L, for the crash box of a cart. It is noteworthy that the auxetic tube not only possesses a higher energy absorption performance but also exhibits better damping characteristics under a low-speed impact condition than the honeycomb counterpart. Tan et al. [35] presented a novel auxetic hierarchical crash box comprising an outer square tube shell and an auxetic hierarchical filling core, in which multiobjective optimization was conducted to obtain the Pareto sets by using the non-dominated sorting genetic algorithm (NSGA-II), and archive-based micro genetic algorithm (AMGA). The auxetic hierarchical crash box was found to be of the highest SEA compared with the foam-filled crash box and traditional crash box.

8.2 Aerospace Engineering

The lightweight structures are widely used in aerospace to absorb acoustic, shock, and vibration energy [26, 781-784]. The optimally-designed aircraft fuselages and wing structures

can be fabricated using additive manufacturing. For example, Fasel et al. [781] demonstrated the applicability of composite AM to morphing aerospace structures, in which the drone body was fabricated and flight-tested successfully, evaluating the great potential of AM for improving lightweight and flight performance. Opgenoord and Willcox [785] proposed a lightweight design approach for an aircraft bracket using additively manufactured cellular structures. The aero-brackets were designed using the topology optimization method and manufactured by SLM [38], as shown in **Figure 33(c)**. Al-Ketan et al. [367] proposed the interpenetrating phase composites (IPC) based on the TPMS. They also explored the design features for an AM jet engine bracket based on the IPCs, as shown in **Figure 33(d)**.

Bühring et al. [786] investigated the potential of applying additively manufactured sandwich structures with pyramidal lattice cores for a small aircraft wing. Antony et al. [308] demonstrated the applicability of the AM natural fiber reinforced composites in the structural frame of the unmanned aerial vehicle (UAV). Li et al. [787] presented a topology optimization strategy for the design of AM-based functionally-graded cellular structures. An illustrative design example of a quadcopter arm was fabricated by FDM, as shown in **Figure 33(e)**. Palomba et al. [788] designed the drone frame structures using cellular structures and fabricated them using the FDM technology with PLA materials. Feng et al. [789] developed a sandwich panel for the aircraft wing, which consists of freeform T-spline surfaces with skin faces and TPMS cores. The designed sandwich panel for the aircraft wing was fabricated using the SLA technique. To protect the core parts of the UAVs from impact and collision during flight, a dual-phase OCT-BCC micro-lattice meta-material was used for airframe parts of the UAV, which was fabricated using PμSL [790]. Xiong et al. [39] reported the application of architected materials with shape recoverability in the legs of space landers.

8.3 Load-bearing tissue scaffolds and implants

A notable application area of AM cellular materials can be tissue engineering for load-bearing orthopedic treatments. The controllable porosity and biomechanical properties enable them to act as a natural bone, withstanding mechanical loading and absorbing impacting energy

[177]. Typically, the scaffolds can be of fairly sophisticated architecture, and it is difficult to fabricate using conventional methods. The development of 3D printing technology has vastly changed this situation and enabled the fabrication of various tissue scaffolds successfully.

For load-bearing applications, there have been tremendous studies on additively manufactured implants reported in the open literature. For example, Zhu et al. [791] presented a porous polycarbonate urethane (PCU) meniscal implant with deformed TPMS-P units. In their study, implant samples were fabricated by FDM; and the biomechanical properties of the porous implants with different volume fractions or functional periodicities were evaluated using a realistic total-knee FE model. It was found that the stress peak, stress concentration area, and meniscal extrusion were lessened by replacing the solid implant with the porous implant under loading. Zhang et al. [204] proposed a novel porous architecture with a diamond lattice pore structure and fabricated a sample using SLM for femoral-head repair implants. The biocompatibility and repair effects have been studied using *in-vivo* experiments. The clinical results indicated that the damaged bones were well reconstructed, and the implants exhibited superior load-bearing capability and biocompatibility. Tang et al. [792] demonstrated an application of the cervical vertebral fusion cages fabricated SEBM, as shown in **Figure 33(f)**. Thompson [701] designed a hemi-pelvic implant using a lattice structure fabricated by SEBM with Ti6Al4V, as shown in **Figure 33(g)**.

To develop a biomimetic scaffold, Vijayavenkataraman et al. [528] proposed a parametric optimization method for designing the TPMS sheet scaffolds. Three different applications, namely, tissue-specific scaffolds, scaffolds for stem cell differentiation, and functionally graded scaffolds with biomimetic gradients, were presented to illustrate the versatility of the proposed design method. Feng et al. [793] attempted to design porous scaffolds for tissue engineering with TPMS based on T-splines, and the designed porous scaffolds were manufactured by SLA. Tan et al proposed some mandibular prosthetic scaffolds which were fabricated by SEBM with Ti6Al4V material [41]. Aranda et al. [43] reported a case of sternocostal reconstruction using additive manufacturing technology with titanium alloy. Cronskär et al. [42] reconstructed the clavicle fixation plates using a computed tomography and fabricated the plates by SEBM with

1920 titanium alloy. Entezari et al. [794] developed different ceramic tissue scaffolds for skull reconstruction and obtained an optimal configuration *in-vivo*. They also proposed to optimize the parametric design for additive manufacturing (DAM) for ceramic scaffolds [795]. More recently, they developed a robust optimization method for ceramic scaffolds by taking account into the AM-induced uncertainties [796]. Wu et al. [626] proposed a machine learning method

1925 to predict tissue ingrowth in ceramic scaffolds through a sheep model. In summary, these studies demonstrated that AM has been playing a growing role in such a significant healthcare area and generating remarkable socioeconomic benefits.

8.4 Other applications

Additively manufactured energy-absorbing structures have been also applied in many other

1930 areas. For example, Mueller and Shea [44] studied the effects of buckling, build-orientation, and scaling on the mechanical properties of the printed lattice structures fabricated by Ployjet, which can be used as bicycle helmets, as shown in **Figure 33(h)**. Inspired by the luffa sponge, Xie et al. [222] proposed a bionic structure based on the fractal theory and prototyped it using FDM with TPU material. The luffa sponge bionic structures can be applied to the transport

1935 pallet by replacing the traditional solid wood pad. Weeger et al. [45] suggested a computational design tool for soft lattices where the lattice members were modeled as a 3D curved rod for nonlinear analysis using a spline-based isogeometric method. A lattice shoe sole prototype was presented to verify the effectiveness of the design tool, as shown in **Figure 33(i)**. Calle et al. [46] used the additively-manufactured samples for investigating the structural response of

1940 large-scale thin-walled marine structures in line with the scaling laws. Muhammad et al. [797, 798] proposed a wave spring with better load bearing capacity, stiffness, and energy absorption efficiency. A multifunctional shoe midsole was designed with functional gradient wave springs at the critical areas of foot pressure (heel, forefoot and toe).

Figure 33. Examples of applications. Automotive engineering: (a) roof brackets for BMW i8 Roadster [36], (b) rear upright of car suspension [37]. Aerospace engineering: (c) metal aero bracket [38], (d) jet engine bracket with interpenetrating phase composite [367], (e) quadcopter's arm [787]. Load-bearing tissue scaffolds and implants: (f) cervical vertebral fusion cage [792], (g) hemi-pelvic [799]. Other applications: (h) bicycle helmets [44]; (i) shoe sole [45].

9. Concluding remarks and outlooks

This review provides a comprehensive overview of recent advances in the development of additively manufactured materials and structures for energy absorption applications. A range of additive manufacturing (AM) technologies has been available to fabricate various energy-absorbing devices made of a range of materials such as polymers, metals, ceramics, and composites. A variety of additively manufactured materials and structures with excellent mechanical properties and energy absorption characteristics have been evaluated in the literature. The AM-induced defects differ from those yielded from traditional manufacturing processes, which significantly influence mechanical properties and energy absorption. Design constraints, optimal processing parameters, and post-processing techniques have been evaluated for minimizing AM-induced defects. Defect-free, modeling with defects, and AM process simulation methods were proposed and validated with experimental tests in literature. A range of design optimization approaches, such as parametric, topology, and machine learning-based optimization, were used to optimize the mechanical properties and energy absorption of the AM materials and structures. Although great effort has been made in additively manufactured energy-absorbing structures for different applications, some challenges remain for future research.

The advances in AM have made it possible to produce complex functional parts that may not have been able to fabricate using traditional manufacturing technologies. However, several significant limitations of AM technologies may need to be overcome, e.g., the AM processes are time-consuming and expensive in general, placing a challenge on mass production; and it is difficult and demanding to fabricate relatively large parts [16]. Besides, there are limited printable materials available which can be used for AM. Combine both advantages of AM process and traditional manufacturing technologies, in which hybrid manufacturing technologies could be an alternative to producing novel energy-absorbing structures.

A number of design strategies, such as bio-inspired design, functionally graded design, hierarchical design, and origami-inspired design, have been adopted for additively manufactured materials and structures. However, the reported energy-absorbing structures are

mainly produced using a single-phase material. It is well known that composites, e.g., multi-materials such as fiber-reinforced materials, exhibit better mechanical properties and energy absorption characteristics [260, 362]. More attention can be paid to the AM-based composite design for lightweight materials and structures [628, 800]]. The composite AM materials and structures could exhibit more desirable mechanical and energy absorbing properties.

In most of the existing studies, energy absorption of AM structures was mainly investigated under quasi-static loads, whereas the dynamic responses have been under-studied to date. However, energy-absorbing structures are used more often in a dynamic loading context such as vehicle collision and explosion protection. Dynamic and strain-rate effects can significantly influence the mechanical properties and energy-absorbing characteristics of AM materials and structures [801]; thus more experimental and modeling studies are still required to characterize the rate-dependent properties and energy absorption behavior [802].

AM-induced defects can greatly influence the performance of fabricated materials and structures [380]. The manufacturing defects are extensively investigated in the literature using the CT-based reconstruction and statistical analysis methods [803-806]. However, such methods are expensive and may not be suitable for mass production. It is recommended to couple the simulations of the manufacturing process and the subsequent mechanical loading process involving large deformation [807]. Further, the design optimization of AM materials and structures, incorporated with the simulations of the manufacturing processes and mechanical responses, could improve the efficiency of the product design and development.

A variety of failure criteria have been implemented in numerical simulations to predict the complex damage/crack initiation behaviors of lightweight AM materials and structures. However, the failure mechanisms of AM-based materials have not yet been well explored, and it remains unclear if the existing failure criteria developed for conventional materials are suitable for AM materials. Furthermore, damage evolution after initiation needs further study to better capture the crack propagation in additively manufactured materials and structures under large deformation.

While attempts have been made to minimize the fabrication-induced imperfections and

uncertainties, it is also recommended to develop advanced nondeterministic optimization algorithms for the design of AM materials and structures with superior mechanical properties and energy absorption characteristics. Advanced data science and artificial intelligence algorithms such as machine learning have exhibited a compelling capacity for prediction and optimization of novel additively manufactured materials and structures. In addition, artificial intelligence has great potential for studying how AM processing parameters affect the performances of as-built structures and in-situ monitoring of the manufacturing process.

Acknowledgments

References

[1] L.J. Gibson, M.F. Ashby, Cellular solids: structure and properties, Cambridge university press1999.

[2] A. Nazir, K.M. Abate, A. Kumar, J.-Y. Jeng, A state-of-the-art review on types, design, optimization, and additive manufacturing of cellular structures, Int J Adv Manuf Tech 104(9-12) (2019) 3489-3510, https://doi.org/10.1007/s00170-019-04085-3.

[3] M. Rashed, M. Ashraf, R. Mines, P.J. Hazell, Metallic microlattice materials: A current state of the art on manufacturing, mechanical properties and applications, Mater Design 95 (2016) 518-533.

[4] X. Yu, J. Zhou, H. Liang, Z. Jiang, L. Wu, Mechanical metamaterials associated with stiffness, rigidity and compressibility: A brief review, Prog Mater Sci 94 (2018) 114-173.

[5] T.A. Schaedler, W.B. Carter, Architected cellular materials, Ann Rev Mater Res 46 (2016) 187-210.

[6] D.-N. Fang, Y.-L. Li, H. Zhao, On the behaviour characterization of metallic cellular materials under impact loading, Acta Mech Sinica 26(6) (2010) 837-846.

[7] Y. Wu, J. Fang, Z. Cheng, Y. He, W. Li, Crashworthiness of tailored-property multi-cell tubular structures under axial crushing and lateral bending, Thin Wall Struct 149 (2020) 106640, 10.1016/j.tws.2020.106640.

[8] A. Baroutaji, A. Arjunan, J. Robinson, M. Ramadan, M. Abdelkareem, A.-G. Olabi, Metamaterial for crashworthiness applications, (2021).

[9] A. Baroutaji, A. Arjunan, A. Niknejad, T. Tran, A.G. Olabi, Application of cellular material in crashworthiness applications: an overview, (2019).

[10] A. Baroutaji, A. Arjunan, G. Singh, J. Robinson, Crushing and energy absorption properties

of additively manufactured concave thin-walled tubes, Results in Engineering 14 (2022) 100424.

[11] A.A. Zadpoor, Mechanical performance of additively manufactured meta-biomaterials, Acta biomaterialia 85 (2019) 41-59.

[12] T. Maconachie, M. Leary, B. Lozanovski, X. Zhang, M. Qian, O. Faruque, M. Brandt, SLM lattice structures: Properties, performance, applications and challenges, Mater Design 183 (2019) 108137, 10.1016/j.matdes.2019.108137.

[13] J. Plocher, A. Panesar, Review on design and structural optimisation in additive manufacturing: Towards next-generation lightweight structures, Mater Design 183 (2019) 108164.

[14] J. Fan, L. Zhang, S. Wei, Z. Zhang, S.-K. Choi, B. Song, Y. Shi, A review of additive manufacturing of metamaterials and developing trends, Materials Today (2021).

[15] T.D. Ngo, A. Kashani, G. Imbalzano, K.T. Nguyen, D. Hui, Additive manufacturing (3D printing): A review of materials, methods, applications and challenges, Composites Part B: Engineering 143 (2018) 172-196.

[16] X. Wang, M. Jiang, Z. Zhou, J. Gou, D. Hui, 3D printing of polymer matrix composites: A review and prospective, Composites Part B: Engineering 110 (2017) 442-458.

[17] F.S.L. Bobbert, K. Lietaert, A. Eftekhari, B. Pouran, S.M.A. Ahmadi, H.H. Weinans, A.A. Zadpoor, Additively manufactured metallic porous biomaterials based on minimal surfaces: A unique combination of topological, mechanical, and mass transport properties, Acta biomaterialia 53 (2017) 572-584.

[18] B. Hanks, J. Berthel, M. Frecker, T.W. Simpson, Mechanical properties of additively manufactured metal lattice structures: data review and design interface, Addit Manuf 35 (2020) 101301.

[19] H. Chen, Q. Han, C. Wang, Y. Liu, B. Chen, J. Wang, Porous scaffold design for additive manufacturing in orthopedics: A review, Frontiers in Bioengineering and Biotechnology 8 (2020) 609.

[20] N. San Ha, G. Lu, Thin-walled corrugated structures: A review of crashworthiness designs and energy absorption characteristics, Thin Wall Struct 157 (2020) 106995.

[21] A. Baroutaji, M. Sajjia, A.-G. Olabi, On the crashworthiness performance of thin-walled energy absorbers: recent advances and future developments, Thin Wall Struct 118 (2017) 137-163.

[22] J. Fang, G. Sun, N. Qiu, N.H. Kim, Q. Li, On design optimization for structural crashworthiness and its state of the art, Struct Multidiscip O 55(3) (2017) 1091-1119.

[23] G. Gao, S. Wang, Crashworthiness of passenger rail vehicles: a review, International journal of crashworthiness (2019).

[24] O. Duncan, T. Shepherd, C. Moroney, L. Foster, P.D. Venkatraman, K. Winwood, T. Allen, A. Alderson, Review of auxetic materials for sports applications: Expanding options in comfort and protection, Applied Sciences 8(6) (2018) 941.

[25] S.G. Kulkarni, X.-L. Gao, S. Horner, J.Q. Zheng, N. David, Ballistic helmets–their design, materials, and performance against traumatic brain injury, Compos Struct 101 (2013) 313-331.

[26] M. Pant, P. Pidge, L. Nagdeve, H. Kumar, A Review of Additive Manufacturing in Aerospace Application, Revue des Composites et des Matériaux Avancés 31(2) (2021).

[27] S.C. Altıparmak, B. Xiao, A market assessment of additive manufacturing potential for the aerospace industry, Journal of Manufacturing Processes 68 (2021) 728-738.

[28] O. Al-Ketan, R. Rowshan, R.K.A. Al-Rub, Topology-mechanical property relationship of 3D printed strut, skeletal, and sheet based periodic metallic cellular materials, Addit Manuf 19 (2018) 167-183.

[29] C. Li, H. Lei, Z. Zhang, X. Zhang, H. Zhou, P. Wang, D. Fang, Architecture design of periodic truss-lattice cells for additive manufacturing, Addit Manuf 34 (2020) 101172.

[30] N. Takano, H. Takizawa, P. Wen, K. Odaka, S. Matsunaga, S. Abe, Stochastic prediction of apparent compressive stiffness of selective laser sintered lattice structure with geometrical imperfection and uncertainty in material property, Int J Mech Sci 134 (2017) 347-356, 10.1016/j.ijmecsci.2017.08.060.

[31] A. Alghamdi, T. Maconachie, D. Downing, M. Brandt, M. Qian, M. Leary, Effect of additive manufactured lattice defects on mechanical properties: an automated method for the enhancement of lattice geometry, The International Journal of Advanced Manufacturing Technology 108 (2020) 957-971.

[32] L. Liu, P. Kamm, F. García-Moreno, J. Banhart, D. Pasini, Elastic and failure response of imperfect three-dimensional metallic lattices: the role of geometric defects induced by Selective Laser Melting, J. Mech. Phys. Solids 107 (2017) 160-184, 10.1016/j.jmps.2017.07.003.

[33] H. Lei, C. Li, J. Meng, H. Zhou, Y. Liu, X. Zhang, P. Wang, D. Fang, Evaluation of compressive properties of SLM-fabricated multi-layer lattice structures by experimental test and μ-CT-based finite element analysis, Mater Design 169 (2019) 107685, 10.1016/j.matdes.2019.107685.

[34] J. Song, Y. Wang, W. Zhou, R. Fan, B. Yu, Y. Lu, L. Li, Topology optimization-guided lattice composites and their mechanical characterizations, Composites Part B: Engineering (2019).

[35] H. Tan, Z. He, E. Li, A. Cheng, T. Chen, X. Tan, Q. Li, B. Xu, Crashworthiness design and multi-objective optimization of a novel auxetic hierarchical honeycomb crash box, Struct Multidiscip O (2021) 1-16.

[36] T. Luniya, G. Chimata, Extending the Life of Classic Cars, the Additive Manufacturing Way, ASME International Mechanical Engineering Congress and Exposition, American Society of Mechanical Engineers, 2021, p. V02AT02A008.

[37] D. Walton, H. Moztarzadeh, Design and development of an additive manufactured component by topology optimisation, Procedia Cirp 60 (2017) 205-210.

[38] L. Cheng, J. Bai, A.C. To, Functionally graded lattice structure topology optimization for the design of additive manufactured components with stress constraints, Comput Method Appl M (2019).

[39] Z. Xiong, M. Li, S. Hao, Y. Liu, L. Cui, H. Yang, C. Cui, D. Jiang, Y. Yang, H. Lei, 3D-Printing Damage-Tolerant Architected Metallic Materials with Shape Recoverability via Special Deformation Design of Constituent Material, ACS Applied Materials & Interfaces 13(33) (2021) 39915-39924.

[40] F. Caiazzo, A. Caggiano, Laser Direct Metal Deposition of 2024 Al Alloy: Trace Geometry Prediction via Machine Learning, Materials (Basel) 11(3) (2018), 10.3390/ma11030444.

[41] R. Yan, D. Luo, H. Huang, R. Li, N. Yu, C. Liu, M. Hu, Q. Rong, Electron beam melting

in the fabrication of three-dimensional mesh titanium mandibular prosthesis scaffold, Scientific Reports 8(1) (2018) 1-10.

[42] M. Cronskär, L.-E. Rännar, M. Bäckström, K.G. Nilsson, B. Samuelsson, Patient-specific clavicle reconstruction using digital design and additive manufacturing, J Mech Design 137(11) (2015).

[43] J.L. Aranda, M.F. Jiménez, M. Rodríguez, G. Varela, Tridimensional titanium-printed custom-made prosthesis for sternocostal reconstruction, Eur J Cardio-thorac 48(4) (2015) e92-e94.

[44] J. Mueller, K. Shea, Buckling, build orientation, and scaling effects in 3D printed lattices, Materials Today Communications 17 (2018) 69-75, 10.1016/j.mtcomm.2018.08.013.

[45] O. Weeger, N. Boddeti, S.-K. Yeung, S. Kaijima, M.L. Dunn, Digital design and nonlinear simulation for additive manufacturing of soft lattice structures, Addit Manuf 25 (2019) 39-49.

[46] M.A. Calle, M. Salmi, L.M. Mazzariol, M. Alves, P. Kujala, Additive manufacturing of miniature marine structures for crashworthiness verification: Scaling technique and experimental tests, Marine Structures 72 (2020) 102764.

[47] O. Al-Ketan, R.K. Abu Al-Rub, Multifunctional Mechanical Metamaterials Based on Triply Periodic Minimal Surface Lattices, Adv Eng Mater 21(10) (2019) 1900524.

[48] A. Velasco‐Hogan, J. Xu, M.A. Meyers, Additive manufacturing as a method to design and optimize bioinspired structures, Adv Mater 30(52) (2018) 1800940.

[49] C. Balletti, M. Ballarin, F. Guerra, 3D printing: State of the art and future perspectives, Journal of Cultural Heritage 26 (2017) 172-182.

[50] L. Riva, P.S. Ginestra, E. Ceretti, Mechanical characterization and properties of laser-based powder bed–fused lattice structures: a review, The International Journal of Advanced Manufacturing Technology (3) (2021) 1-23.

[51] J. Tallon, E. Cyr, A. Lloyd, M. Mohammadi, Crush performance of additively manufactured maraging steel microlattice reinforced plates, Eng Fail Anal 108 (2020) 104231.

[52] S. McKown, Y. Shen, W. Brookes, C. Sutcliffe, W. Cantwell, G. Langdon, G. Nurick, M. Theobald, The quasi-static and blast loading response of lattice structures, Int J Impact Eng 35(8) (2008) 795-810.

[53] L. Yang, M. Ferrucci, R. Mertens, W. Dewulf, C. Yan, Y. Shi, S. Yang, An investigation into the effect of gradients on the manufacturing fidelity of triply periodic minimal surface structures with graded density fabricated by selective laser melting, J Mater Process Tech 275 (2020) 116367.

[54] X. Cao, D. Xiao, Y. Li, W. Wen, T. Zhao, Z. Chen, Y. Jiang, D. Fang, Dynamic compressive behavior of a modified additively manufactured rhombic dodecahedron 316L stainless steel lattice structure, Thin Wall Struct 148 (2020) 106586.

[55] J. Harris, R.E. Winter, G.J. McShane, Impact response of additively manufactured metallic hybrid lattice materials, Int J Impact Eng 104 (2017) 177-191.

[56] H. Zhu, P. Wang, D. Wei, J. Si, Y. Wu, Energy absorption of diamond lattice cylindrical shells under axial compression loading, Thin Wall Struct 181 (2022) 110131.

[57] I. Maskery, N.T. Aboulkhair, A. Aremu, C. Tuck, I. Ashcroft, Compressive failure modes and energy absorption in additively manufactured double gyroid lattices, Addit Manuf 16 (2017) 24-29.

2170   [58] J. Yang, D. Gu, K. Lin, C. Ma, R. Wang, H. Zhang, M. Guo, Laser 3D printed bio-inspired impact resistant structure: failure mechanism under compressive loading, Virtual and Physical Prototyping 15(1) (2020) 75-86.

[59] Y. Zhang, Y. Lin, Y. Li, X. Li, 3D printed self-similar AlSi10Mg alloy hierarchical honeycomb architectures under in-plane large deformation, Thin Wall Struct 164 (2021) 107795,

2175   10.1016/j.tws.2021.107795.

[60] C. Neff, N. Hopkinson, N.B. Crane, Experimental and analytical investigation of mechanical behavior of laser-sintered diamond-lattice structures, Addit Manuf 22 (2018) 807-816, https://doi.org/10.1016/j.addma.2018.07.005.

[61] A.M. Abou-Ali, O. Al-Ketan, D.-W. Lee, R. Rowshan, R.K.A. Al-Rub, Mechanical

2180   behavior of polymeric selective laser sintered ligament and sheet based lattices of triply periodic minimal surface architectures, Mater Design 196 (2020) 109100.

[62] L. Bai, C. Gong, X. Chen, Y. Sun, L. Xin, H. Pu, Y. Peng, J. Luo, Mechanical properties and energy absorption capabilities of functionally graded lattice structures: Experiments and simulations, Int J Mech Sci 182 (2020) 105735.

2185   [63] J. Sun, Y. Yang, D. Wang, Mechanical properties of a Ti6Al4V porous structure produced by selective laser melting, Mater Design 49 (2013) 545-552.

[64] A. Cuadrado, A. Yánez, O. Martel, S. Deviaene, D. Monopoli, Influence of load orientation and of types of loads on the mechanical properties of porous Ti6Al4V biomaterials, Mater Design 135 (2017) 309-318.

2190   [65] A. Ataee, Y. Li, D. Fraser, G. Song, C. Wen, Anisotropic Ti-6Al-4V gyroid scaffolds manufactured by electron beam melting (EBM) for bone implant applications, Mater Design 137 (2018) 345-354.

[66] Z. Sun, Y. Guo, V. Shim, Static and dynamic crushing of polymeric lattices fabricated by fused deposition modelling and selective laser sintering–an experimental investigation, Int J

2195   Impact Eng 160 (2022) 104059.

[67] D.I. Stoia, E. Linul, L. Marsavina, Influence of manufacturing parameters on mechanical properties of porous materials by selective laser sintering, Materials 12(6) (2019) 871.

[68] L. Yuan, S. Ding, C. Wen, Additive manufacturing technology for porous metal implant applications and triple minimal surface structures: A review, Bioactive Materials 4 (2019) 56-

2200   70.

[69] H. Wu, W. Fahy, S. Kim, H. Kim, N. Zhao, L. Pilato, A. Kafi, S. Bateman, J. Koo, Recent developments in polymers/polymer nanocomposites for additive manufacturing, Prog Mater Sci 111 (2020) 100638.

[70] A. Awad, F. Fina, A. Goyanes, S. Gaisford, A.W. Basit, Advances in powder bed fusion 3D

2205   printing in drug delivery and healthcare, Adv Drug Deliver Rev 174 (2021) 406-424.

[71] M. Wiese, S. Thiede, C. Herrmann, Rapid manufacturing of automotive polymer series parts: A systematic review of processes, materials and challenges, Addit Manuf 36 (2020) 101582.

[72] Z. Snow, A.R. Nassar, E.W. Reutzel, Invited Review Article: Review of the formation and

2210   impact of flaws in powder bed fusion additive manufacturing, Addit Manuf 36 (2020) 101457.

[73] S. Yuan, C.K. Chua, K. Zhou, 3D‑printed mechanical metamaterials with high energy absorption, Advanced Materials Technologies 4(3) (2019) 1800419.

[74] L. Xiao, W. Song, C. Wang, H. Tang, Q. Fan, N. Liu, J. Wang, Mechanical properties of open-cell rhombic dodecahedron titanium alloy lattice structure manufactured using electron beam melting under dynamic loading, Int J Impact Eng 100 (2017) 75-89.

[75] Y.M. Hailu, A. Nazir, S.-C. Lin, J.-Y. Jeng, The Effect of Functional Gradient Material Distribution and Patterning on Torsional Properties of Lattice Structures Manufactured Using MultiJet Fusion Technology, Materials 14(21) (2021) 6521.

[76] P. Baranowski, P. Platek, A. Antolak-Dudka, M. Sarzynski, M. Kucewicz, T. Durejko, J. Malachowski, J. Janiszewski, T. Czujko, Deformation of honeycomb cellular structures manufactured with Laser Engineered Net Shaping (LENS) technology under quasi-static loading: Experimental testing and simulation, Addit Manuf 25 (2019) 307-316, 10.1016/j.addma.2018.11.018.

[77] S. Wickramasinghe, T. Do, P. Tran, FDM-based 3D printing of polymer and associated composite: A review on mechanical properties, defects and treatments, Polymers 12(7) (2020) 1529.

[78] O.A. Mohamed, S.H. Masood, J.L. Bhowmik, Optimization of fused deposition modeling process parameters: a review of current research and future prospects, Advances in Manufacturing 3(1) (2015) 42-53.

[79] N. Van de Werken, H. Tekinalp, P. Khanbolouki, S. Ozcan, A. Williams, M. Tehrani, Additively manufactured carbon fiber-reinforced composites: State of the art and perspective, Addit Manuf 31 (2020) 100962.

[80] Z. Sun, Y. Guo, V. Shim, Characterisation and modeling of additively-manufactured polymeric hybrid lattice structures for energy absorption, Int J Mech Sci 191 (2021) 106101.

[81] J. Plocher, A. Panesar, Effect of density and unit cell size grading on the stiffness and energy absorption of short fibre-reinforced functionally graded lattice structures, Addit Manuf 33 (2020) 101171.

[82] C. Quan, B. Han, Z. Hou, Q. Zhang, X. Tian, T.J. Lu, 3D printed continuous fiber reinforced composite auxetic honeycomb structures, Composites Part B: Engineering 187 (2020) 107858.

[83] H. Bikas, P. Stavropoulos, G. Chryssolouris, Additive manufacturing methods and modelling approaches: a critical review, The International Journal of Advanced Manufacturing Technology 83(1-4) (2016) 389-405.

[84] N.N.M. Mustafa, A.Z.A. Kadir, N.A. Ngadiman, A. Ma'aram, K. Zakaria, Comparison of different additive manufacturing patterns on the performance of rapid vacuum casting for mating parts via the Taguchi method, Journal of Mechanical Engineering and Sciences 14(1) (2020) 6417-6429.

[85] M. Pagac, J. Hajnys, Q.-P. Ma, L. Jancar, J. Jansa, P. Stefek, J. Mesicek, A review of vat photopolymerization technology: Materials, applications, challenges, and future trends of 3d printing, Polymers 13(4) (2021) 598.

[86] D.W. Abueidda, M. Elhebeary, C.-S.A. Shiang, R.K.A. Al-Rub, I.M. Jasiuk, Compression and buckling of microarchitectured Neovius-lattice, Extreme Mechanics Letters 37 (2020) 100688.

[87] J.J. Andrew, J. Schneider, J. Ubaid, R. Velmurugan, N.K. Gupta, S. Kumar, Energy absorption characteristics of additively manufactured plate-lattices under low- velocity impact

loading, Int J Impact Eng 149 (2021) 103768.

[88] M. Wang, J. Zhang, W. Wang, L. Gao, Compression behaviors of the bio-inspired hierarchical lattice structure with improved mechanical properties and energy absorption capacity, Journal of Materials Research and Technology 17 (2022) 2755-2771.

2260   [89] X. Zhang, Y. Wang, B. Ding, X. Li, Design, fabrication, and mechanics of 3D micro‑/nanolattices, Small 16(15) (2020) 1902842.

[90] J. Bauer, L.R. Meza, T.A. Schaedler, R. Schwaiger, X. Zheng, L. Valdevit, Nanolattices: an emerging class of mechanical metamaterials, Adv Mater 29(40) (2017) 1701850.

[91] V. Harinarayana, Y. Shin, Two-photon lithography for three-dimensional fabrication in

2265   micro/nanoscale regime: A comprehensive review, Optics & Laser Technology 142 (2021) 107180.

[92] K. Ben Othmen, N. Haddar, A. Jegat, P.-Y. Manach, K. Elleuch, Ductile fracture of AISI 304L stainless steel sheet in stretching, International Journal of Mechanical Sciences 172 (2020), 10.1016/j.ijmecsci.2019.105404.

2270   [93] B. Farkas, I. Romano, L. Ceseracciu, A. Diaspro, F. Brandi, S. Beke, Four-order stiffness variation of laser-fabricated photopolymer biodegradable scaffolds by laser parameter modulation, Materials Science and Engineering: C 55 (2015) 14-21.

[94] A. Alibeigloo, Thermoelastic analysis of functionally graded carbon nanotube reinforced composite cylindrical panel embedded in piezoelectric sensor and actuator layers, Composites

2275   Part B: Engineering 98 (2016) 225-243.

[95] T.A. Schaedler, A.J. Jacobsen, A. Torrents, A.E. Sorensen, J. Lian, J.R. Greer, L. Valdevit, W.B. Carter, Ultralight metallic microlattices, Science 334(6058) (2011) 962-965.

[96] S. Yin, A.J. Jacobsen, L. Wu, S.R. Nutt, Inertial stabilization of flexible polymer micro-lattice materials, J Mater Sci 48(19) (2013) 6558-6566.

2280   [97] O. Al‑Ketan, R. Rezgui, R. Rowshan, H. Du, N.X. Fang, R.K. Abu Al‑Rub, Microarchitected stretching‑dominated mechanical metamaterials with minimal surface topologies, Adv Eng Mater 20(9) (2018) 1800029.

[98] Z. Xu, C.S. Ha, R. Kadam, J. Lindahl, S. Kim, H.F. Wu, V. Kunc, X. Zheng, Additive manufacturing of two-phase lightweight, stiff and high damping carbon fiber reinforced

2285   polymer microlattices, Addit Manuf 32 (2020) 101106, 10.1016/j.addma.2020.101106.

[99] C. Groth, N.D. Kravitz, P.E. Jones, J.W. Graham, W.R. Redmond, Three-dimensional printing technology, J Clin Orthod 48(8) (2014) 475-85.

[100] W. Liu, H. Song, C. Huang, Maximizing mechanical properties and minimizing support material of PolyJet fabricated 3D lattice structures, Addit Manuf 35 (2020) 101257.

2290   [101] A.S. Babu, K. Binish, M. Jaivignesh, M. Sugavaneswaran, Modelling of Functional Gradient Porous Structure and its Fabrication using Additive Manufacturing Process, Materials Today: Proceedings 5(11) (2018) 24558-24567.

[102] N. Shahrubudin, T.C. Lee, R. Ramlan, An overview on 3D printing technology: Technological, materials, and applications, Procedia Manufacturing 35 (2019) 1286-1296.

2295   [103] J. Pellens, G. Lombaert, M. Michiels, T. Craeghs, M. Schevenels, Topology optimization of support structure layout in metal-based additive manufacturing accounting for thermal deformations, Struct Multidiscip O 61(6) (2020) 2291-2303.

[104] I. Gibson, D. Rosen, B. Stucker, Directed energy deposition processes, Additive

manufacturing technologies, Springer2015, pp. 245-268.

[105] F. Habib, P. Iovenitti, S. Masood, M. Nikzad, Fabrication of polymeric lattice structures for optimum energy absorption using Multi Jet Fusion technology, Mater Design 155 (2018) 86-98.

[106] H. Jiang, L. Le Barbenchon, B.A. Bednarcyk, F. Scarpa, Y. Chen, Bioinspired multilayered cellular composites with enhanced energy absorption and shape recovery, Addit Manuf 36 (2020) 101430.

[107] Y. Balit, P. Margerit, E. Charkaluk, A. Constantinescu, Crushing of additively manufactured thin-walled metallic lattices: Two-scale strain localization analysis, Mech Mater (2021) 103915.

[108] V. Carneiro, S. Rawson, H. Puga, J. Meireles, P. Withers, Additive manufacturing assisted investment casting: a low-cost method to fabricate periodic metallic cellular lattices, Addit Manuf 33 (2020) 101085.

[109] V. Carneiro, H. Puga, J. Meireles, Heat treatment as a route to tailor the yield-damping properties in A356 alloys, Materials Science and Engineering: A 729 (2018) 1-8.

[110] Y. Xue, W. Wang, F. Han, Enhanced compressive mechanical properties of aluminum based auxetic lattice structures filled with polymers, Composites Part B: Engineering 171 (2019) 183-191.

[111] A. Druschitz, C. Williams, D. Snelling, M. Seals, Additive manufacturing supports the production of complex castings, Shape Casting: 5th International Symposium 2014, Springer, 2014, pp. 51-57.

[112] V.H. Carneiro, S. Rawson, H. Puga, P. Withers, Macro-, meso-and microstructural characterization of metallic lattice structures manufactured by additive manufacturing assisted investment casting, Scientific Reports 11(1) (2021) 1-12.

[113] Y. Xue, X. Wang, W. Wang, X. Zhong, F. Han, Compressive property of Al-based auxetic lattice structures fabricated by 3-D printing combined with investment casting, Materials Science and Engineering: A 722 (2018) 255-262.

[114] Y. Xue, F. Han, Compressive mechanical property of a new three-dimensional aluminum based double-V lattice structure, Mater Lett 254 (2019) 99-102.

[115] Y. Huang, Y. Xue, X. Wang, F. Han, Mechanical behavior of three-dimensional pyramidal aluminum lattice materials, Materials ence & Engineering A 696(JUN.1) (2017) 520-528.

[116] S.C. Han, J.W. Lee, K. Kang, A new type of low density material: Shellular, Adv Mater 27(37) (2015) 5506-5511.

[117] X. Zheng, H. Lee, T.H. Weisgraber, M. Shusteff, J. DeOtte, E.B. Duoss, J.D. Kuntz, M.M. Biener, Q. Ge, J.A. Jackson, Ultralight, ultrastiff mechanical metamaterials, Science 344(6190) (2014) 1373-1377.

[118] L.R. Meza, S. Das, J.R. Greer, Strong, lightweight, and recoverable three-dimensional ceramic nanolattices, Science 345(6202) (2014) 1322-1326.

[119] T. Tancogne-Dejean, D. Mohr, Stiffness and specific energy absorption of additively-manufactured metallic BCC metamaterials composed of tapered beams, Int J Mech Sci 141 (2018) 101-116, 10.1016/j.ijmecsci.2018.03.027.

[120] M. Smith, Z. Guan, W. Cantwell, Finite element modelling of the compressive response of lattice structures manufactured using the selective laser melting technique, Int J Mech Sci 67

(2013) 28-41.

[121] C. Li, H. Lei, Y. Liu, X. Zhang, J. Xiong, H. Zhou, D. Fang, Crushing behavior of multi-layer metal lattice panel fabricated by selective laser melting, Int J Mech Sci 145 (2018) 389-399.

[122] R. Gümrük, R. Mines, S. Karadeniz, Static mechanical behaviours of stainless steel micro-lattice structures under different loading conditions, Materials Science and Engineering: A 586 (2013) 392-406.

[123] M. Al Rifaie, A. Mian, R. Srinivasan, Compression behavior of three-dimensional printed polymer lattice structures, Proceedings of the Institution of Mechanical Engineers, Part L: Journal of Materials: Design and Applications 233(8) (2019) 1574-1584.

[124] J.-H. Park, K. Park, Compressive behavior of soft lattice structures and their application to functional compliance control, Addit Manuf 33 (2020) 101148.

[125] A. Großmann, J. Gosmann, C. Mittelstedt, Lightweight lattice structures in selective laser melting: Design, fabrication and mechanical properties, Materials Science and Engineering: A 766 (2019) 138356, 10.1016/j.msea.2019.138356.

[126] P. Koehnen, C. Haase, J. Bueltmann, S. Ziegler, J.H. Schleifenbaum, W. Bleck, Mechanical properties and deformation behavior of additively manufactured lattice structures of stainless steel, Mater Design 145 (2018) 205-217.

[127] X. Cao, Y. Jiang, T. Zhao, P. Wang, Y. Wang, Z. Chen, Y. Li, D. Xiao, D. Fang, Compression experiment and numerical evaluation on mechanical responses of the lattice structures with stochastic geometric defects originated from additive-manufacturing, Composites Part B: Engineering 194 (2020) 108030.

[128] Z. Xiao, Y. Yang, R. Xiao, Y. Bai, C. Song, D. Wang, Evaluation of topology-optimized lattice structures manufactured via selective laser melting, Mater Design 143 (2018) 27-37.

[129] J. Song, W. Zhou, Y. Wang, R. Fan, Y. Wang, J. Chen, Y. Lu, L. Li, Octet-truss cellular materials for improved mechanical properties and specific energy absorption, Mater Design 173 (2019) 107773.

[130] T. Tancogne-Dejean, A.B. Spierings, D. Mohr, Additively-manufactured metallic micro-lattice materials for high specific energy absorption under static and dynamic loading, Acta Mater 116 (2016) 14-28, 10.1016/j.actamat.2016.05.054.

[131] X. Cao, S. Duan, J. Liang, W. Wen, D. Fang, Mechanical properties of an improved 3D-printed rhombic dodecahedron stainless steel lattice structure of variable cross section, Int J Mech Sci 145 (2018) 53-63.

[132] X. Liu, T. Wada, A. Suzuki, N. Takata, M. Kobashi, M. Kato, Understanding and suppressing shear band formation in strut-based lattice structures manufactured by laser powder bed fusion, Mater Design 199 (2021) 109416.

[133] B.C. White, A.P. Garland, R. Alberdi, B.L. Boyce, Interpenetrating lattices with enhanced mechanical functionality, Addit Manuf   (2020) 101741.

[134] D.T. Queheillalt, H.N. Wadley, Cellular metal lattices with hollow trusses, Acta Mater 53(2) (2005) 303-313.

[135] T. Tancogne-Dejean, D. Mohr, Elastically-isotropic elementary cubic lattices composed of tailored hollow beams, Extreme Mechanics Letters 22 (2018) 13-18.

[136] C. Bonatti, D. Mohr, Large deformation response of additively-manufactured FCC

metamaterials: From octet truss lattices towards continuous shell mesostructures, Int J Plasticity 92 (2017) 122-147, 10.1016/j.ijplas.2017.02.003.

[137] J. Xu, Y. Gao, H. Huang, Q. Yang, L. Guo, L. Jiang, Diamond-structured hollow-tube lattice Ni materials via 3D printing, Science China Chemistry 59(12) (2016) 1632-1637.

[138] Z. Hashin, S. Shtrikman, A variational approach to the theory of the elastic behaviour of multiphase materials, J. Mech. Phys. Solids 11(2) (1963) 127-140.

[139] S.C. Kapfer, S.T. Hyde, K. Mecke, C.H. Arns, G.E. Schröder-Turk, Minimal surface scaffold designs for tissue engineering, Biomaterials 32 29 (2011) 6875-82.

[140] J. Berger, H. Wadley, R. McMeeking, Mechanical metamaterials at the theoretical limit of isotropic elastic stiffness, Nature 543(7646) (2017) 533-537.

[141] T. Tancogne-Dejean, M. Diamantopoulou, M.B. Gorji, C. Bonatti, D. Mohr, 3D Plate-Lattices: An Emerging Class of Low-Density Metamaterial Exhibiting Optimal Isotropic Stiffness, Adv Mater 30(45) (2018) e1803334, 10.1002/adma.201803334.

[142] T. Tancogne-Dejean, X. Li, M. Diamantopoulou, C.C. Roth, D. Mohr, High Strain Rate Response of Additively-Manufactured Plate-Lattices: Experiments and Modeling, Journal of Dynamic Behavior of Materials 5(3) (2019) 361-375, 10.1007/s40870-019-00219-6.

[143] J.J. Andrew, P. Verma, S. Kumar, Impact behavior of nanoengineered, 3D printed plate-lattices, Mater Design 202 (2021) 109516.

[144] R. Xue, X. Cui, P. Zhang, K. Liu, Y. Li, W. Wu, H. Liao, Mechanical design and energy absorption performances of novel dual scale hybrid plate-lattice mechanical metamaterials, Extreme Mechanics Letters 40 (2020) 100918.

[145] S. Duan, W. Wen, D. Fang, Additively-manufactured anisotropic and isotropic 3D plate-lattice materials for enhanced mechanical performance: Simulations & experiments, Acta Mater 199 (2020) 397-412.

[146] T. Li, F. Jarrar, R.K.A. Al-Rub, W.J. Cantwell, Additive manufactured semi-plate lattice materials with high stiffness, strength and toughness, Int J Solids Struct (2021) 111153.

[147] Y.-j. Wang, Z.-j. Zhang, X.-w. Xue, J. Zhou, Z.-x. Song, Axial and lateral crushing performance of plate-lattice filled square sandwich tubes, Compos Struct 274 (2021) 114404.

[148] M. Dai, H. Jiang, X. Dai, G. Chen, F. Yang, X. He, Investigations of the compressive mechanical properties of open-cell hollow-sphere structures, Mech Mater 148 (2020) 103517.

[149] X. Chen, Q. Ji, J. Wei, H. Tan, J. Yu, P. Zhang, V. Laude, M. Kadic, Light-weight shell-lattice metamaterials for mechanical shock absorption, Int J Mech Sci 169 (2020) 105288.

[150] H. Jiang, H. Ziegler, Z. Zhang, H. Meng, D. Chronopoulos, Y. Chen, Mechanical properties of 3D printed architected polymer foams under large deformation, Mater Design 194 (2020) 108946.

[151] C. Bonatti, D. Mohr, Smooth-shell metamaterials of cubic symmetry: Anisotropic elasticity, yield strength and specific energy absorption, Acta Mater 164 (2019) 301-321, 10.1016/j.actamat.2018.10.034.

[152] X. Li, C.C. Roth, T. Tancogne-Dejean, D. Mohr, Rate-and temperature-dependent plasticity of additively manufactured stainless steel 316L: Characterization, modeling and application to crushing of shell-lattices, Int J Impact Eng 145 (2020) 103671.

[153] C. Bonatti, D. Mohr, Mechanical performance of additively-manufactured anisotropic and isotropic smooth shell-lattice materials: Simulations & experiments, J. Mech. Phys. Solids

122 (2019) 1-26, 10.1016/j.jmps.2018.08.022.

[154] C. Bhat, A. Kumar, J.-Y. Jeng, Effect of atomic tessellations on structural and functional properties of additive manufactured lattice structures, Addit Manuf 47 (2021) 102326.

[155] T. Yang, Z. Wu, H. Chen, Y. Zhu, L. Li, Quantitative 3D structural analysis of the cellular microstructure of sea urchin spines (I): Methodology, Acta biomaterialia 107 (2020) 204-217.

[156] R.W. Corkery, E.C. Tyrode, On the colour of wing scales in butterflies: iridescence and preferred orientation of single gyroid photonic crystals, Interface focus 7(4) (2017) 20160154.

[157] B. Deng, G.J. Cheng, Soap film inspired mechanical metamaterials approaching theoretical bound of stiffness across full density range, Materials Horizons 8(3) (2021) 987-996.

[158] P.J. Gandy, S. Bardhan, A.L. Mackay, J. Klinowski, Nodal surface approximations to the P, G, D and I-WP triply periodic minimal surfaces, Chem. Phys. Lett. 336(3-4) (2001) 187-195.

[159] L. Zhang, S. Feih, S. Daynes, S. Chang, M.Y. Wang, J. Wei, W.F. Lu, Energy absorption characteristics of metallic triply periodic minimal surface sheet structures under compressive loading, Addit Manuf 23 (2018) 505-515, 10.1016/j.addma.2018.08.007.

[160] Al-Ketan, Oraib, Abu, Al-Rub, Rashid, K., The effect of architecture on the mechanical properties of cellular structures based on the IWP minimal surface, J. Mater. Res. (2018).

[161] H. Montazerian, E. Davoodi, M. Asadi-Eydivand, J. Kadkhodapour, M. Solati-Hashjin, Porous scaffold internal architecture design based on minimal surfaces: A compromise between permeability and elastic properties, Mater Design 126 (2017) 98-114.

[162] H. Jia, H. Lei, P. Wang, J. Meng, C. Li, H. Zhou, X. Zhang, D. Fang, An experimental and numerical investigation of compressive response of designed Schwarz Primitive triply periodic minimal surface with non-uniform shell thickness, Extreme Mechanics Letters 37 (2020) 100671.

[163] H. Yin, Z. Liu, J. Dai, G. Wen, C. Zhang, Crushing behavior and optimization of sheet-based 3D periodic cellular structures, Composites Part B: Engineering 182 (2020) 107565, 10.1016/j.compositesb.2019.107565.

[164] D.W. Abueidda, M. Bakir, R.K. Abu Al-Rub, J.S. Bergström, N.A. Sobh, I. Jasiuk, Mechanical properties of 3D printed polymeric cellular materials with triply periodic minimal surface architectures, Mater Design 122(MAY15) (2017) 255-267, 10.1016/j.matdes.2017.03.018.

[165] O. Al-Ketan, R. Rowshan, A.N. Palazotto, R.K. Abu Al-Rub, On Mechanical Properties of Cellular Steel Solids with Shell-Like Periodic Architectures Fabricated by Selective Laser Sintering, Journal of Engineering Materials and Technology (2018).

[166] H. Yin, X. Zheng, G. Wen, C. Zhang, Z. Wu, Design optimization of a novel bio-inspired 3D porous structure for crashworthiness, Compos Struct 255 (2021) 112897.

[167] X. Cao, Z. Huang, C. He, W. Wu, L. Xi, Y. Li, D. Fang, In-situ synchrotron X-ray tomography investigation of the imperfect smooth-shell cylinder structure, Compos Struct (2021).

[168] N. Kladovasilakis, K. Tsongas, D. Tzetzis, Mechanical and FEA-Assisted Characterization of Fused Filament Fabricated Triply Periodic Minimal Surface Structures, 2021.

[169] M. Shen, W. Qin, B. Xing, W. Zhao, S. Gao, Y. Sun, T. Jiao, Z.Q. Zhao, Mechanical properties of 3D printed ceramic cellular materials with triply periodic minimal surface

architectures, J Eur Ceram Soc 41 (2021) 1481-1489.

[170] Y. Liang, W. Zhou, Y. Liu, Z. Li, Y. Yang, H. Xi, Z. Wu, Energy Absorption and Deformation Behavior of 3D Printed Triply Periodic Minimal Surface Stainless Steel Cellular Structures under Compression, Steel Research International (2020) 2000411.

[171] M.M. Sychov, L.A. Lebedev, S.V. Dyachenko, L.A. Nefedova, Mechanical properties of energy-absorbing structures with triply periodic minimal surface topology, Acta Astronaut (2018).

[172] X. Li, L. Xiao, W. Song, Compressive behavior of selective laser melting printed Gyroid structures under dynamic loading, Addit Manuf 46 (2021) 102054, 10.1016/j.addma.2021.102054.

[173] D.W. Abueidda, M. Elhebeary, C.S. Shiang, S. Pang, I.M. Jasiuk, Mechanical properties of 3D printed polymeric Gyroid cellular structures: Experimental and finite element study, Mater Design 165 (2019) 107597.

[174] A. Alhammadi, O. Al-Ketan, K.A. Khan, M. Ali, R. Rowshan, R.K.A. Al-Rub, Microstructural characterization and thermomechanical behavior of additively manufactured AlSi10Mg sheet cellular materials, Materials Science and Engineering: A 791 (2020) 139714.

[175] L. Chen, J. Zhang, B. Du, H. Zhou, H. Liu, Y. Guo, W. Li, D. Fang, Dynamic crushing behavior and energy absorption of graded lattice cylindrical structure under axial impact load, Thin Wall Struct 127 (2018) 333-343.

[176] J. Kadkhodapour, H. Montazerian, S. Raeisi, Investigating internal architecture effect in plastic deformation and failure for TPMS-based scaffolds using simulation methods and experimental procedure, Materials science & engineering. C, Materials for biological applications 43 (2014) 587-97, 10.1016/j.msec.2014.07.047.

[177] I. Maskery, L. Sturm, A.O. Aremu, A. Panesar, C.B. Williams, C.J. Tuck, R.D. Wildman, I.A. Ashcroft, R.J.M. Hague, Insights into the mechanical properties of several triply periodic minimal surface lattice structures made by polymer additive manufacturing, Polymer 152 (2018) 62-71, 10.1016/j.polymer.2017.11.049.

[178] A.M. Abou-Ali, O. Al-Ketan, R. Rowshan, R.A. Al-Rub, Mechanical response of 3D printed bending-dominated ligament-based triply periodic cellular polymeric solids, J Mater Eng Perform 28(4) (2019) 2316-2326.

[179] C. Yan, L. Hao, A. Hussein, P. Young, Ti–6Al–4V triply periodic minimal surface structures for bone implants fabricated via selective laser melting, Journal of the mechanical behavior of biomedical materials 51 (2015) 61-73.

[180] L. Yang, C. Yan, C. Han, P. Chen, Y. Shi, Mechanical response of a triply periodic minimal surface cellular structures manufactured by selective laser melting, Int J Mech Sci 148 (2018).

[181] F.P.W. Melchels, K. Bertoldi, R. Gabbrielli, A.H. Velders, J. Feijen, D.W. Grijpma, Mathematically defined tissue engineering scaffold architectures prepared by stereolithography, Biomaterials 31 27 (2010) 6909-16.

[182] A. Ataee, Y. Li, M. Brandt, C. Wen, Ultrahigh-strength titanium gyroid scaffolds manufactured by selective laser melting (SLM) for bone implant applications, Acta Mater (2018).

[183] Chunze, Yan, and, Liang, Hao, and, Ahmed, Hussein, and, David, Evaluations of cellular lattice structures manufactured using selective laser melting, Int J Mach Tool Manu (2012).

[184] C. Yan, H. Liang, A. Hussein, P. Young, D. Raymont, Advanced lightweight 316L stainless steel cellular lattice structures fabricated via selective laser melting, Mater Design 55(mar.) (2014) 533-541.

[185] M. Zhao, F. Liu, G. Fu, D.Z. Zhang, T. Zhang, H. Zhou, Improved mechanical properties and energy absorption of BCC lattice structures with triply periodic minimal surfaces fabricated by SLM, Materials 11(12) (2018) 2411.

[186] S.Z. Khan, S.H. Masood, E.M.A. Ibrahim, Z. Ahmad, Compressive behaviour of Neovius Triply Periodic Minimal Surface cellular structure manufactured by fused deposition modelling, Virtual and Physical Prototyping 14 (2019) 360 - 370.

[187] J. Kadkhodapour, H. Montazerian, A.C. Darabi, A. Zargarian, S. Schmauder, The relationships between deformation mechanisms and mechanical properties of additively manufactured porous biomaterials, Journal of the mechanical behavior of biomedical materials 70 (2017) 28-42.

[188] A.G. Evans, J.W. Hutchinson, N.A. Fleck, M.F. Ashby, H.N.G. Wadley, The topological design of multifunctional cellular metals, Prog Mater Sci 46(3-4) (2001) 309-327, 10.1016/s0079-6425(00)00016-5.

[189] Z. Chen, Y.M. Xie, X. Wu, Z. Wang, Q. Li, S. Zhou, On hybrid cellular materials based on triply periodic minimal surfaces with extreme mechanical properties, Mater Design 183 (2019) 108109.

[190] A.M. Abou-Ali, D.-W. Lee, R.K. Abu Al-Rub, On the Effect of Lattice Topology on Mechanical Properties of SLS Additively Manufactured Sheet-, Ligament-, and Strut-Based Polymeric Metamaterials, Polymers 14(21) (2022) 4583.

[191] I. Maskery, I. Ashcroft, The deformation and elastic anisotropy of a new gyroid-based honeycomb made by laser sintering, Addit Manuf 36 (2020) 101548.

[192] M. Saleh, S. Anwar, A.M. Al-Ahmari, A. Alfaify, Compression Performance and Failure Analysis of 3D-Printed Carbon Fiber/PLA Composite TPMS Lattice Structures, Polymers 14(21) (2022) 4595.

[193] J. Fang, G. Sun, N. Qiu, T. Pang, S. Li, Q. Li, On hierarchical honeycombs under out-of-plane crushing, Int J Solids Struct 135 (2018) 1-13.

[194] P. Wang, Y. Bian, F. Yang, H. Fan, B. Zheng, Mechanical properties and energy absorption of FCC lattice structures with different orientation angles, Acta Mech 231 (2020) 3129-3144.

[195] J. Fu, Q. Liu, K. Liufu, Y. Deng, J. Fang, Q. Li, Design of bionic-bamboo thin-walled structures for energy absorption, Thin Wall Struct 135 (2019) 400-413.

[196] Y. Wu, Q. Liu, J. Fu, Q. Li, D. Hui, Dynamic crash responses of bio-inspired aluminum honeycomb sandwich structures with CFRP panels, Composites Part B: Engineering 121 (2017) 122-133.

[197] R. Yao, T. Pang, S. He, Q. Li, B. Zhang, G. Sun, A bio-inspired foam-filled multi-cell structural configuration for energy absorption, Composites Part B: Engineering 238 (2022) 109801.

[198] Z. Wang, Q. Luo, Q. Li, G. Sun, Design optimization of bioinspired helicoidal CFRPP/GFRPP hybrid composites for multiple low-velocity impact loads, Int J Mech Sci 219 (2022) 107064.

[199] N.S. Ha, G. Lu, A review of recent research on bio-inspired structures and materials for

energy absorption applications, Composites Part B: Engineering 181 (2020) 107496, 10.1016/j.compositesb.2019.107496.

[200] T. Van Le, A. Ghazlan, T. Ngo, T. Nguyen, A. Remennikov, A comprehensive review of selected biological armor systems–from structure-function to bio-mimetic techniques, Compos Struct 225 (2019) 111172.

[201] G.X. Gu, M. Takaffoli, A.J. Hsieh, M.J. Buehler, Biomimetic additive manufactured polymer composites for improved impact resistance, Extreme Mechanics Letters 9 (2016) 317-323.

[202] J. Chen, N. Hao, L. Pan, L. Hu, S. Du, Y. Fu, Characteristics of compressive mechanical properties and strengthening mechanism of 3D-printed grid beetle elytron plates, J Mater Sci 55(20) (2020) 8541-8552.

[203] A. Ghazlan, T. Nguyen, T. Ngo, S. Linforth, Performance of a 3D printed cellular structure inspired by bone, Thin Wall Struct 151 (2020) 106713.

[204] B. Zhang, X. Pei, C. Zhou, Y. Fan, Q. Jiang, A. Ronca, U. D'Amora, Y. Chen, H. Li, Y. Sun, The biomimetic design and 3D printing of customized mechanical properties porous Ti6Al4V scaffold for load-bearing bone reconstruction, Mater Design 152 (2018) 30-39.

[205] X. Song, H. Tetik, T. Jirakittsonthon, P. Parandoush, G. Yang, D. Lee, S. Ryu, S. Lei, M.L. Weiss, D. Lin, Biomimetic 3D printing of hierarchical and interconnected porous hydroxyapatite structures with high mechanical strength for bone cell culture, Adv Eng Mater 21(1) (2019) 1800678.

[206] A. Arjunan, M. Demetriou, A. Baroutaji, C. Wang, Mechanical performance of highly permeable laser melted Ti6Al4V bone scaffolds, Journal of the mechanical behavior of biomedical materials 102 (2020) 103517.

[207] M.C. Fernandes, J. Aizenberg, J.C. Weaver, K. Bertoldi, Mechanically robust lattices inspired by deep-sea glass sponges, Nature Materials 20(2) (2021) 237-241.

[208] J. Cadman, C.-C. Chang, J. Chen, Y. Chen, S. Zhou, W. Li, Q. Li, Bioinspired lightweight cellular materials-Understanding effects of natural variation on mechanical properties, Materials Science and Engineering: C 33(6) (2013) 3146-3152.

[209] J. Cadman, S. Zhou, Y. Chen, Q. Li, Cuttlebone: characterisation, application and development of biomimetic materials, Journal of Bionic Engineering 9(3) (2012) 367-376.

[210] J. Cadman, S. Zhou, Y. Chen, W. Li, R. Appleyard, Q. Li, Characterization of cuttlebone for a biomimetic design of cellular structures, Acta Mech Sinica 26(1) (2010) 27-35.

[211] S. Hou, C. Shu, S. Zhao, T. Liu, X. Han, Q. Li, Experimental and numerical studies on multi-layered corrugated sandwich panels under crushing loading, Compos Struct 126 (2015) 371-385.

[212] C. Yang, Q. Li, Advanced lattice material with high energy absorption based on topology optimisation, Mech Mater 148 (2020) 103536.

[213] C. Yang, Q. Li, Y. Wang, Compressive properties of cuttlebone-like lattice (CLL) materials with functionally graded density, European Journal of Mechanics-A/Solids 87 (2021) 104215.

[214] T. Yang, Z. Jia, H. Chen, Z. Deng, W. Liu, L. Chen, L. Li, Mechanical design of the highly porous cuttlebone: A bioceramic hard buoyancy tank for cuttlefish, Proceedings of the National Academy of Sciences 117(38) (2020) 23450-23459.

2600   [215] K. Ko, S. Jin, S.E. Lee, I. Lee, J.-W. Hong, Bio-inspired bimaterial composites patterned using three-dimensional printing, Composites Part B: Engineering 165 (2019) 594-603.

[216] P. Tran, T.D. Ngo, A. Ghazlan, D. Hui, Bimaterial 3D printing and numerical analysis of bio-inspired composite structures under in-plane and transverse loadings, Compos Part B-eng 108 (2017) 210-223.

2605   [217] Z. Wei, X. Xu, Gradient design of bio-inspired nacre-like composites for improved impact resistance, Composites Part B: Engineering 215 (2021) 108830, https://doi.org/10.1016/j.compositesb.2021.108830.

[218] Y. Du, D. Gu, L. Xi, D. Dai, T. Gao, J. Zhu, C. Ma, Laser additive manufacturing of bio-inspired lattice structure: forming quality, microstructure and energy absorption behavior, 2610   Materials Science and Engineering: A 773 (2020) 138857.

[219] X. Yu, X. Zhang, J. Chen, L. Pan, Y. Xu, Y. Fu, Experimental verification and optimization research on the energy absorption abilities of beetle elytron plate crash boxes, Materials Research Express 6(11) (2019) 1165e2.

[220] X. Yu, L. Pan, J. Chen, X. Zhang, P. Wei, Experimental and numerical study on the energy 2615   absorption abilities of trabecular–honeycomb biomimetic structures inspired by beetle elytra, J Mater Sci 54(3) (2019) 2193-2204.

[221] H. Tsang, K. Tse, K. Chan, G. Lu, A.K. Lau, Energy absorption of muscle-inspired hierarchical structure: Experimental investigation, Compos Struct 226 (2019) 111250.

[222] Y. Xie, H. Bai, Z. Liu, N. Chen, A novel bionic structure inspired by luffa sponge and its 2620   cushion properties, Applied Sciences 10(7) (2020) 2584.

[223] H. Yang, B. Wang, L. Ma, Mechanical properties of 3D double-U auxetic structures, Int J Solids Struct 180 (2019) 13-29.

[224] J. Simpson, Z. Kazancı, Crushing investigation of crash boxes filled with honeycomb and re-entrant (auxetic) lattices, Thin Wall Struct 150 (2020) 106676.

2625   [225] A. Airoldi, N. Novak, F. Sgobba, A. Gilardelli, M. Borovinšek, Foam-filled energy absorbers with auxetic behaviour for localized impacts, Materials Science and Engineering: A 788 (2020) 139500.

[226] S. Hou, T. Liu, Z. Zhang, X. Han, Q. Li, How does negative Poisson's ratio of foam filler affect crashworthiness?, Mater Design 82 (2015) 247-259.

2630   [227] J. Choi, R. Lakes, Fracture toughness of re-entrant foam materials with a negative Poisson's ratio: experiment and analysis, Int J Fracture 80(1) (1996) 73-83.

[228] I.I. Argatov, R. Guinovart-Díaz, F.J. Sabina, On local indentation and impact compliance of isotropic auxetic materials from the continuum mechanics viewpoint, Int J Eng Sci 54 (2012) 42-57.

2635   [229] V. Coenen, K. Alderson, Mechanisms of failure in the static indentation resistance of auxetic carbon fibre laminates, physica status solidi (b) 248(1) (2011) 66-72.

[230] F. Scarpa, P.J. Tomlin, On the transverse shear modulus of negative Poisson's ratio honeycomb structures, Fatigue Fract Eng M 23(8) (2010) 717-720.

[231] J. Choi, R. Lakes, Non-linear properties of metallic cellular materials with a negative 2640   Poisson's ratio, J Mater Sci 27(19) (1992) 5375-5381.

[232] L. Hu, Z. Luo, Z. Zhang, M. Lian, L. Huang, Mechanical property of re-entrant anti-trichiral honeycombs under large deformation, Composites Part B: Engineering 163 (2019)

107-120.

[233] A. Alomarah, D. Ruan, S. Masood, Z. Gao, Compressive properties of a novel additively manufactured 3D auxetic structure, Smart Materials and Structures 28(8) (2019) 085019.

[234] A. Alomarah, S.H. Masood, I. Sbarski, B. Faisal, Z. Gao, D. Ruan, Compressive properties of 3D printed auxetic structures: experimental and numerical studies, Virtual and Physical Prototyping 15(1) (2020) 1-21.

[235] K.P. Logakannan, V. Ramachandran, J. Rengaswamy, D. Ruan, Dynamic performance of a 3D re-entrant structure, Mech Mater 148 (2020) 103503.

[236] K. Meena, S. Singamneni, Novel hybrid auxetic structures for improved in-plane mechanical properties via additive manufacturing, Mech Mater 158 (2021) 103890.

[237] J. Zhang, G. Lu, Z. You, Large deformation and energy absorption of additively manufactured auxetic materials and structures: A review, Composites Part B: Engineering (2020) 108340.

[238] C. Luo, C.Z. Han, X.Y. Zhang, X.G. Zhang, X. Ren, Y.M. Xie, Design, manufacturing and applications of auxetic tubular structures: A review, Thin Wall Struct 163 (2021) 107682.

[239] X. Ren, R. Das, P. Tran, T.D. Ngo, Y.M. Xie, Auxetic metamaterials and structures: a review, Smart materials and structures 27(2) (2018) 023001.

[240] A. Joseph, V. Mahesh, D. Harursampath, On the application of additive manufacturing methods for auxetic structures: a review, Advances in Manufacturing 9(3) (2021) 342-368.

[241] Y. Wu, L. Yang, Elastic and failure characteristics of additive manufactured thin wall lattice structures with defects, Thin Wall Struct 161 (2021) 107493.

[242] C. Hu, J. Dong, J. Luo, Q.-H. Qin, G. Sun, 3D printing of chiral carbon fiber reinforced polylactic acid composites with negative Poisson's ratios, Composites Part B: Engineering 201 (2020) 108400.

[243] C. Yang, H.D. Vora, Y. Chang, Behavior of auxetic structures under compression and impact forces, Smart Materials and Structures 27(2) (2018) 025012.

[244] L. Wei, X. Zhao, Q. Yu, G. Zhu, Quasi-static axial compressive properties and energy absorption of star-triangular auxetic honeycomb, Compos Struct (2021).

[245] R. Hamzehei, J. Kadkhodapour, A.P. Anaraki, S. Rezaei, S. Dariushi, A.M. Rezadoust, Octagonal auxetic metamaterials with hyperelastic properties for large compressive deformation, Int J Mech Sci 145 (2018) 96-105.

[246] N. Novak, L. Starčevič, M. Vesenjak, Z. Ren, Blast response study of the sandwich composite panels with 3D chiral auxetic core, Compos Struct 210 (2019) 167-178.

[247] M.-F. Guo, H. Yang, L. Ma, Design and characterization of 3D AuxHex lattice structures, Int J Mech Sci 181 (2020) 105700.

[248] Y. Xiang, Y. Xin, R.A. Xin, M. Yi, W.A. Yao, Y. Yi, L. Shi, A. Czh, A novel type of tubular structure with auxeticity both in radial direction and wall thickness, Thin Wall Struct 163.

[249] Y. Wu, L. Sun, P. Yang, J. Fang, W. Li, Energy absorption of additively manufactured functionally bi-graded thickness honeycombs subjected to axial loads, Thin Wall Struct 164 (2021) 107810, https://doi.org/10.1016/j.tws.2021.107810.

[250] S.R. Bates, I.R. Farrow, R.S. Trask, 3D printed polyurethane honeycombs for repeated tailored energy absorption, Mater Design 112 (2016) 172-183.

[251] J. Banhart, Manufacture, characterisation and application of cellular metals and metal

foams, Prog Mater Sci 46(6) (2001) 559-632.

[252] J. Jiang, H. Oguzlu, F. Jiang, 3D printing of lightweight, super-strong yet flexible all-cellulose structure, Chem Eng J 405 (2021) 126668.

[253] A. Antolak-Dudka, P. Płatek, T. Durejko, P. Baranowski, J. Małachowski, M. Sarzyński, T. Czujko, Static and dynamic loading behavior of Ti6Al4V honeycomb structures manufactured by Laser Engineered Net Shaping (LENSTM) technology, Materials 12(8) (2019) 1225.

[254] S. Wang, Y. Ding, F. Yu, Z. Zheng, Y. Wang, Crushing behavior and deformation mechanism of additively manufactured Voronoi-based random open-cell polymer foams, Materials Today Communications 25 (2020) 101406.

[255] Y. Duan, X. Zhao, Z. Liu, N. Hou, H. Liu, B. Du, B. Hou, Y. Li, Dynamic response of additively manufactured graded foams, Composites Part B: Engineering 183 (2020) 107630.

[256] Y. Duan, X. Zhao, B. Du, X. Shi, H. Zhao, B. Hou, Y. Li, Quasi-static compressive behavior and constitutive model of graded foams, Int J Mech Sci 177 (2020) 105603.

[257] B. Liu, H. Chen, W. Cao, A novel method for tailoring elasticity distributions of functionally graded porous materials, Int J Mech Sci 157 (2019) 457-470.

[258] S. Wang, Z. Zheng, C. Zhu, Y. Ding, J. Yu, Crushing and densification of rapid prototyping polylactide foam: Meso-structural effect and a statistical constitutive model, Mech Mater 127 (2018) 65-76.

[259] P. Pinto, N. Peixinho, F. Silva, D. Soares, Compressive properties and energy absorption of aluminum foams with modified cellular geometry, J Mater Process Tech 214(3) (2014) 571-577.

[260] P. Parandoush, D. Lin, A review on additive manufacturing of polymer-fiber composites, Compos Struct 182 (2017) 36-53.

[261] S.F. Kabir, K. Mathur, A.-F.M. Seyam, A critical review on 3D printed continuous fiber-reinforced composites: History, mechanism, materials and properties, Compos Struct 232 (2020) 111476.

[262] Y. Chen, Q. He, 3D-printed short carbon fibre reinforced perforated structures with negative Poisson's ratios: Mechanisms and design, Compos Struct 236 (2020) 111859.

[263] C. Zeng, L. Liu, W. Bian, J. Leng, Y. Liu, Compression behavior and energy absorption of 3D printed continuous fiber reinforced composite honeycomb structures with shape memory effects, Addit Manuf 38(6) (2021) 101842.

[264] D.R. Hetrick, S.H.R. Sanei, O. Ashour, C.E. Bakis, Charpy impact energy absorption of 3D printed continuous Kevlar reinforced composites, J Compos Mater 55 (2021) 1705 - 1713.

[265] Y. Chen, L. Ye, Y. Zhang, K. Fu, Compression behaviours of 3D-printed CF/PA metamaterials: Experiment and modelling, Int J Mech Sci 206 (2021) 106634.

[266] G. Sun, Z. Wang, H. Yu, Z. Gong, Q. Li, Experimental and numerical investigation into the crashworthiness of metal-foam-composite hybrid structures, Compos Struct 209 (2019) 535-547.

[267] G. Sun, D. Chen, X. Huo, G. Zheng, Q. Li, Experimental and numerical studies on indentation and perforation characteristics of honeycomb sandwich panels, Compos Struct 184 (2018) 110-124.

[268] G. Sun, X. Huo, H. Wang, P.J. Hazell, Q. Li, On the structural parameters of honeycomb-

core sandwich panels against low-velocity impact, Composites Part B: Engineering 216 (2021) 108881.

[269] E. Wang, Q. Li, G. Sun, Computational analysis and optimization of sandwich panels with homogeneous and graded foam cores for blast resistance, Thin Wall Struct 147 (2020) 106494.

[270] G. Sun, E. Wang, J. Zhang, S. Li, Y. Zhang, Q. Li, Experimental study on the dynamic responses of foam sandwich panels with different facesheets and core gradients subjected to blast impulse, Int J Impact Eng 135 (2020) 103327.

[271] A.J. Turner, M. Al Rifaie, A. Mian, R. Srinivasan, Low-velocity impact behavior of sandwich structures with additively manufactured polymer lattice cores, J Mater Eng Perform 27(5) (2018) 2505-2512.

[272] B.D. de Castro, F. de Castro Magalhães, T.H. Panzera, J.C.C. Rubio, An Assessment of Fully Integrated Polymer Sandwich Structures Designed by Additive Manufacturing, J Mater Eng Perform (2021) 1-8.

[273] A. Beharic, R.R. Egui, L. Yang, Drop-weight impact characteristics of additively manufactured sandwich structures with different cellular designs, Mater Design 145 (2018) 122-134.

[274] S. Abrate, G. Epasto, E. Kara, V. Crupi, E. Guglielmino, H. Aykul, Computed tomography analysis of impact response of lightweight sandwich panels with micro lattice core, Proceedings of the Institution of Mechanical Engineers, Part C: Journal of Mechanical Engineering Science 232(8) (2018) 1348-1362.

[275] J.J. Andrew, J. Ubaid, F. Hafeez, A. Schiffer, S. Kumar, Impact performance enhancement of honeycombs through additive manufacturing-enabled geometrical tailoring, Int J Impact Eng 134 (2019) 103360.

[276] O. Fashanu, M. Rangapuram, A. Abutunis, J. Newkirk, K. Chandrashekhara, H. Misak, D. Klenosky, Mechanical performance of sandwich composites with additively manufactured triply periodic minimal surface cellular structured core, Journal of Sandwich Structures & Materials (2021) 10996362211037012.

[277] A.C. Pinho, A.P. Piedade, Sandwich Multi-Material 3D-Printed Polymers: Influence of Aging on the Impact and Flexure Resistances, Polymers 13(22) (2021) 4030.

[278] G. Qi, B. Ji, L. Ma, Mechanical response of pyramidal lattice truss core sandwich structures by additive manufacturing, Mechanics of Advanced Materials and Structures 26(15) (2019) 1298-1306.

[279] K. Sugiyama, R. Matsuzaki, M. Ueda, A. Todoroki, Y. Hirano, 3D printing of composite sandwich structures using continuous carbon fiber and fiber tension, Composites Part A: Applied Science and Manufacturing 113 (2018) 114-121.

[280] Z. Liu, H. Chen, S. Xing, Mechanical performances of metal-polymer sandwich structures with 3D-printed lattice cores subjected to bending load, Archives of Civil and Mechanical Engineering 20(3) (2020) 1-17.

[281] C. Peng, K. Fox, M. Qian, H. Nguyen-Xuan, P. Tran, 3D printed sandwich beams with bioinspired cores: Mechanical performance and modelling, Thin Wall Struct 161 (2021) 107471.

[282] K. Wei, Q. Yang, X. Yang, Y. Tao, H. Xie, Z. Qu, D. Fang, Mechanical analysis and modeling of metallic lattice sandwich additively fabricated by selective laser melting, Thin Wall

Struct 146 (2020) 106189.

[283] J. Zhang, J. Yanagimoto, Density-based topology optimization integrated with genetic algorithm for optimizing formability and bending stiffness of 3D printed CFRP core sandwich sheets, Composites Part B: Engineering 225 (2021) 109248.

[284] S. Gao, C. Wang, B. Xing, M. Shen, W. Zhao, Z. Zhao, Experimental investigation on bending behaviour of ZrO2 honeycomb sandwich structures prepared by DLP stereolithography, Thin Wall Struct 157 (2020) 107099.

[285] N. Kladovasilakis, P. Charalampous, K. Tsongas, I. Kostavelis, D. Tzetzis, D. Tzovaras, Experimental and Computational Investigation of Lattice Sandwich Structures Constructed by Additive Manufacturing Technologies, Journal of Manufacturing and Materials Processing 5(3) (2021) 95.

[286] M.R. Khosravani, A. Zolfagharian, M. Jennings, T. Reinicke, Structural performance of 3D-printed composites under various loads and environmental conditions, Polym Test 91 (2020) 106770.

[287] D. Kotzem, D. Tazerout, T. Arold, T. Niendorf, F. Walther, Failure mode map for E-PBF manufactured Ti6Al4V sandwich panels, Eng Fail Anal 121 (2021) 105159.

[288] D. Lee, H.-J. Kwon, S. Yang, M.-S. Kim, Fabrication, testing, and analysis of sandwich structure with composite skin and additive manufactured core, J Reinf Plast Comp 40(17-18) (2021) 654-664.

[289] D. Marschall, H. Rippl, F. Ehrhart, M. Schagerl, Boundary conformal design of laser sintered sandwich cores and simulation of graded lattice cells using a forward homogenization approach, Mater Design 190 (2020) 108539.

[290] F. Brenne, T. Niendorf, H. Maier, Additively manufactured cellular structures: Impact of microstructure and local strains on the monotonic and cyclic behavior under uniaxial and bending load, J Mater Process Tech 213(9) (2013) 1558-1564.

[291] R. Mines, S. Tsopanos, Y. Shen, R. Hasan, S. McKown, Drop weight impact behaviour of sandwich panels with metallic micro lattice cores, Int J Impact Eng 60 (2013) 120-132.

[292] H.Y. Sarvestani, A. Akbarzadeh, H. Niknam, K. Hermenean, 3D printed architected polymeric sandwich panels: Energy absorption and structural performance, Compos Struct 200 (2018) 886-909.

[293] H.Y. Sarvestani, A. Akbarzadeh, A. Mirbolghasemi, K. Hermenean, 3D printed meta-sandwich structures: Failure mechanism, energy absorption and multi-hit capability, Mater Design 160 (2018) 179-193.

[294] İ. Özen, K. Çava, H. Gedikli, Ü. Alver, M. Aslan, Low-energy impact response of composite sandwich panels with thermoplastic honeycomb and reentrant cores, Thin Wall Struct 156 (2020) 106989.

[295] J.A. Harris, G.J. McShane, Impact response of metallic stacked origami cellular materials, Int J Impact Eng 147 (2021) 103730.

[296] R. Critchley, R. Hazael, K. Bhatti, D. Wood, A. Peare, S. Johnson, T. Temple, Blast mitigation using polymeric 3D printed auxetic re-entrant honeycomb structures: A preliminary study, International Journal of Protective Structures (2021) 20414196211052062.

[297] G. Ye, H. Bi, L. Chen, Y. Hu, Compression and Energy Absorption Performances of 3D Printed Polylactic Acid Lattice Core Sandwich Structures, 3D Printing and Additive

Manufacturing 6(6) (2019) 333-343.

[298] M. Tafazoli, M.D. Nouri, Experimental and numerical study and multi-objective optimisation of quasi-static compressive test on three-dimensional printed lattice-core sandwich structures, International Journal of Crashworthiness (2020) 1-11.

[299] T. Li, L. Wang, Bending behavior of sandwich composite structures with tunable 3D-printed core materials, Compos Struct 175 (2017) 46-57.

[300] D.H. Choi, Y.C. Jeong, K. Kang, A monolithic sandwich panel with microlattice core, Acta Mater (2017) 822-834.

[301] A. Haldar, V. Managuli, R. Munshi, R. Agarwal, Z. Guan, Compressive behaviour of 3D printed sandwich structures based on corrugated core design, Materials today communications 26 (2021) 101725.

[302] H. Bharath, D. Bonthu, S. Gururaja, P. Prabhakar, M. Doddamani, Flexural response of 3D printed sandwich composite, Compos Struct 263 (2021) 113732.

[303] S.M. Zaharia, L.A. Enescu, M.A. Pop, Mechanical performances of lightweight sandwich structures produced by material extrusion-based additive manufacturing, Polymers 12(8) (2020) 1740.

[304] J. Monteiro, M. Sardinha, F. Alves, A. Ribeiro, L. Reis, A. Deus, M. Leite, M.F. Vaz, Evaluation of the effect of core lattice topology on the properties of sandwich panels produced by additive manufacturing, Proceedings of the Institution of Mechanical Engineers, Part L: Journal of Materials: Design and Applications 235(6) (2021) 1312-1324.

[305] D.L. Edelen III, H.A. Bruck, Predicting failure modes of 3D-printed multi-material polymer sandwich structures from process parameters, Journal of Sandwich Structures & Materials 24(2) (2022) 1049-1075.

[306] B. Ji, H. Han, R. Lin, H. Li, Failure modes of lattice sandwich plate by additive-manufacturing and its imperfection sensitivity, Acta Mech Sinica 36(2) (2020) 430-447.

[307] Z. Zhao, J. Ren, S. Du, X. Wang, Z. Wei, Q. Zhang, Y. Zhou, Z. Yang, T.J. Lu, Bending response of 3D-printed titanium alloy sandwich panels with corrugated channel cores, Materials 14(3) (2021) 556.

[308] S. Antony, A. Cherouat, G. Montay, Fabrication and characterization of hemp fibre based 3D printed honeycomb sandwich structure by FDM process, Appl Compos Mater 27(6) (2020) 935-953.

[309] S. Ghannadpour, M. Mahmoudi, K.H. Nedjad, Structural behavior of 3D-printed sandwich beams with strut-based lattice core: Experimental and numerical study, Compos Struct 281 (2022) 115113.

[310] X. Zhou, C. Qu, Y. Luo, R. Heise, G. Bao, Compression Behavior and Impact Energy Absorption Characteristics of 3D Printed Polymer Lattices and Their Hybrid Sandwich Structures, J Mater Eng Perform 30(12) (2021) 8763-8770.

[311] S.-Y. Jhou, C.-C. Hsu, J.-C. Yeh, The Dynamic Impact Response of 3D-Printed Polymeric Sandwich Structures with Lattice Cores: Numerical and Experimental Investigation, Polymers 13(22) (2021) 4032.

[312] C. Zeng, L. Liu, W. Bian, J. Leng, Y. Liu, Bending performance and failure behavior of 3D printed continuous fiber reinforced composite corrugated sandwich structures with shape memory capability, Compos Struct 262 (2021) 113626.

[313] S. Pirouzfar, A. Zeinedini, Effect of geometrical parameters on the flexural properties of sandwich structures with 3D-printed honeycomb core and E-glass/epoxy Face-sheets, Structures, Elsevier, 2021, pp. 2724-2738.

[314] A.W. Alshaer, D.J. Harland, An investigation of the strength and stiffness of weight-saving sandwich beams with CFRP face sheets and seven 3D printed cores, Compos Struct 257 (2021) 113391.

[315] F. Xu, X. Zhang, H. Zhang, A review on functionally graded structures and materials for energy absorption, Eng Struct 171 (2018) 309-325.

[316] A. Baroutaji, A. Arjunan, M. Stanford, J. Robinson, A.G. Olabi, Deformation and energy absorption of additively manufactured functionally graded thickness thin-walled circular tubes under lateral crushing, Eng Struct 226 (2021) 111324.

[317] J. Fang, Y. Gao, G. Sun, G. Zheng, Q. Li, Dynamic crashing behavior of new extrudable multi-cell tubes with a functionally graded thickness, Int J Mech Sci 103 (2015) 63-73, 10.1016/j.ijmecsci.2015.08.029.

[318] O. Rahman, K.Z. Uddin, J. Muthulingam, G. Youssef, C. Shen, B. Koohbor, Density‐Graded Cellular Solids: Mechanics, Fabrication, and Applications, Adv Eng Mater (2021) 2100646.

[319] S.Y. Choy, C.-N. Sun, W.J. Sin, K.F. Leong, P.-C. Su, J. Wei, P. Wang, Superior energy absorption of continuously graded microlattices by electron beam additive manufacturing, Virtual and Physical Prototyping 16(1) (2021) 14-28.

[320] R. Duraibabu, R. Prithvirajan, M. Sugavaneswaran, G. Arumaikkannu, Compression behavior of Functionally Graded Cellular Materials fabricated with FDM, Materials Today: Proceedings 24 (2020) 1035-1041.

[321] S. Daynes, S. Feih, W.F. Lu, J. Wei, Design concepts for generating optimised lattice structures aligned with strain trajectories, Comput Method Appl M 354 (2019) 689-705.

[322] M. Mahbod, M. Asgari, C. Mittelstedt, Architected functionally graded porous lattice structures for optimized elastic-plastic behavior, Proceedings of the Institution of Mechanical Engineers, Part L: Journal of Materials: Design and Applications 234(8) (2020) 1099-1116.

[323] I. Maskery, A. Aremu, M. Simonelli, C. Tuck, R. Wildman, I. Ashcroft, R. Hague, Mechanical properties of Ti-6Al-4V selectively laser melted parts with body-centred-cubic lattices of varying cell size, Exp Mech 55(7) (2015) 1261-1272.

[324] J. Plocher, A. Panesar, Mechanical Performance of Additively Manufactured Fiber-Reinforced Functionally Graded Lattices, JOM 72(3) (2020) 1292-1298.

[325] X. Fan, Q. Tang, Q. Feng, S. Ma, J. Song, M. Jin, F. Guo, P. Jin, Design, mechanical properties and energy absorption capability of graded-thickness triply periodic minimal surface structures fabricated by selective laser melting, Int J Mech Sci 204 (2021) 106586.

[326] O. Al-Ketan, D.W. Lee, R. Rowshan, R.K. Abu Al-Rub, Functionally graded and multi-morphology sheet TPMS lattices: Design, manufacturing, and mechanical properties, Journal of the mechanical behavior of biomedical materials 102 (2020) 103520, 10.1016/j.jmbbm.2019.103520.

[327] M. Teimouri, M. Asgari, Mechanical performance of additively manufactured uniform and graded porous structures based on topology-optimized unit cells, Proceedings of the Institution of Mechanical Engineers, Part C: Journal of Mechanical Engineering Science 235(9)

(2021) 1593-1618.

[328] C. Bhat, A. Kumar, S.-C. Lin, J.-Y. Jeng, A novel bioinspired architectured materials with interlocking designs based on tessellation, Addit Manuf 58 (2022) 103052.

[329] D. Xiao, Z. Dong, Y. Li, W. Wu, D. Fang, Compression behavior of the graded metallic auxetic reentrant honeycomb: experiment and finite element analysis, Materials Science and Engineering: A 758 (2019) 163-171.

[330] R. Alberdi, R. Dingreville, J. Robbins, T. Walsh, B.C. White, B. Jared, B.L. Boyce, Multi-morphology lattices lead to improved plastic energy absorption, Mater Design 194 (2020) 108883.

[331] Y. Nian, S. Wan, X. Li, Q. Su, M. Li, How does bio-inspired graded honeycomb filler affect energy absorption characteristics?, Thin Wall Struct 144 (2019) 106269.

[332] H. Zhou, M. Zhao, Z. Ma, D.Z. Zhang, G. Fu, Sheet and network based functionally graded lattice structures manufactured by selective laser melting: Design, mechanical properties, and simulation, Int J Mech Sci 175 (2020) 105480, 10.1016/j.ijmecsci.2020.105480.

[333] M. Zhao, D.Z. Zhang, F. Liu, Z. Li, Z. Ma, Z. Ren, Mechanical and energy absorption characteristics of additively manufactured functionally graded sheet lattice structures with minimal surfaces, Int J Mech Sci 167 (2020) 105262, 10.1016/j.ijmecsci.2019.105262.

[334] S. Kumar, J. Ubaid, R. Abishera, A. Schiffer, V. Deshpande, Tunable energy absorption characteristics of architected honeycombs enabled via additive manufacturing, ACS applied materials & interfaces 11(45) (2019) 42549-42560.

[335] X. Wu, Y. Su, J. Shi, In-plane impact resistance enhancement with a graded cell-wall angle design for auxetic metamaterials, Compos Struct 247 (2020) 112451.

[336] I. Maskery, A. Hussey, A. Panesar, A. Aremu, C. Tuck, I. Ashcroft, R. Hague, An investigation into reinforced and functionally graded lattice structures, J Cell Plast 53(2) (2017) 151-165.

[337] R. Gautam, S. Idapalapati, Compressive properties of additively manufactured functionally graded Kagome lattice structure, Metals 9(5) (2019) 517.

[338] J. Sienkiewicz, P. Płatek, F. Jiang, X. Sun, A. Rusinek, Investigations on the mechanical response of gradient lattice structures manufactured via SLM, Metals 10(2) (2020) 213.

[339] M. Mahbod, M. Asgari, Elastic and plastic characterization of a new developed additively manufactured functionally graded porous lattice structure: Analytical and numerical models, Int J Mech Sci 155 (2019) 248-266.

[340] F. Liu, Z. Mao, P. Zhang, D.Z. Zhang, J. Jiang, Z. Ma, Functionally graded porous scaffolds in multiple patterns: New design method, physical and mechanical properties, Mater Design 160 (2018) 849-860, 10.1016/j.matdes.2018.09.053.

[341] X.-Y. Zhang, G. Fang, S. Leeflang, A.A. Zadpoor, J. Zhou, Topological design, permeability and mechanical behavior of additively manufactured functionally graded porous metallic biomaterials, Acta biomaterialia 84 (2019) 437-452.

[342] M. Afshar, A.P. Anaraki, H. Montazerian, Compressive characteristics of radially graded porosity scaffolds architectured with minimal surfaces, Materials Science and Engineering: C 92 (2018) 254-267.

[343] L. Xiao, W. Song, Additively-manufactured functionally graded Ti-6Al-4V lattice structures with high strength under static and dynamic loading: Experiments, Int J Impact Eng

111(jan.) (2017) 255-272.

[344] H. Rahman, E. Yarali, A. Zolfagharian, A. Serjouei, M. Bodaghi, Energy Absorption and Mechanical Performance of Functionally Graded Soft-Hard Lattice Structures, Materials (Basel) 14(6) (2021), 10.3390/ma14061366.

[345] A. Ajdari, B.H. Jahromi, J. Papadopoulos, H. Nayeb-Hashemi, A. Vaziri, Hierarchical honeycombs with tailorable properties, Int J Solids Struct 49(11-12) (2012) 1413-1419.

[346] Y. Wu, J. Fang, Y. He, W. Li, Crashworthiness of hierarchical circular-joint quadrangular honeycombs, Thin Wall Struct 133 (2018) 180-191, 10.1016/j.tws.2018.09.044.

[347] G. Sun, J. Zhang, S. Li, J. Fang, E. Wang, Q. Li, Dynamic response of sandwich panel with hierarchical honeycomb cores subject to blast loading, Thin Wall Struct 142 (2019) 499-515.

[348] G. Sun, H. Jiang, J. Fang, G. Li, Q. Li, Crashworthiness of vertex based hierarchical honeycombs in out-of-plane impact, Mater Design 110 (2016) 705-719.

[349] P. Wang, J. Xuan, R. Zhang, H. Zhang, Q. Wang, H. Wang, H. Liu, L. Zhang, Hierarchically Structured Components: Design, Additive Manufacture, and Their Energy Applications, Advanced Materials Technologies (2021) 2100672.

[350] K.M. Lichade, Y. Jiang, Y. Pan, Hierarchical Nano/Micro-structured Surfaces With High Surface Area/Volume Ratios, Journal of Manufacturing Science and Engineering 143(8) (2021) 081002.

[351] A. Ingrole, T.G. Aguirre, L. Fuller, S.W. Donahue, Bioinspired energy absorbing material designs using additive manufacturing, Journal of the mechanical behavior of biomedical materials 119 (2021) 104518.

[352] P. Wang, F. Yang, D. Ru, B. Zheng, H. Fan, Additive-manufactured hierarchical multi-circular lattice structures for energy absorption application, Mater Design 210 (2021) 110116.

[353] J. Zhang, J. Yanagimoto, Topology optimization of CFRP hierarchical pyramidal structures fabricated by additive manufacturing, Composites Part B: Engineering 224 (2021) 109241.

[354] Y. Sha, L. Jiani, C. Haoyu, R.O. Ritchie, X. Jun, Design and strengthening mechanisms in hierarchical architected materials processed using additive manufacturing, Int J Mech Sci 149 (2018) 150-163.

[355] C. Tan, J. Zou, S. Li, P. Jamshidi, A. Abena, A. Forsey, R.J. Moat, K. Essa, M. Wang, K. Zhou, Additive manufacturing of bio-inspired multi-scale hierarchically strengthened lattice structures, International Journal of Machine Tools and Manufacture 167 (2021) 103764.

[356] Y. Zhang, T. Liu, H. Ren, I. Maskery, I. Ashcroft, Dynamic compressive response of additively manufactured AlSi10Mg alloy hierarchical honeycomb structures, Compos Struct 195 (2018) 45-59.

[357] Y. Tao, W. Li, K. Wei, S. Duan, W. Wen, L. Chen, Y. Pei, D. Fang, Mechanical properties and energy absorption of 3D printed square hierarchical honeycombs under in-plane axial compression, Composites Part B: Engineering (2019).

[358] L.R. Meza, A.J. Zelhofer, N. Clarke, A.J. Mateos, D.M. Kochmann, J.R. Greer, Resilient 3D hierarchical architected metamaterials, Proceedings of the National Academy of Sciences 112 (2015) 11502 - 11507.

[359] A.K. Mishra, A. Kumar, In-plane compression behavior of FDM-manufactured

hierarchical and hybrid hierarchical hexagonal honeycombs for infrastructural safety applications, Journal of Micromanufacturing (2021) 25165984211015412.

[360] H.U. Hong, M.-l. Hu, L. Dai, Dynamic Mechanical Behavior of Hierarchical Resin Honeycomb by 3D Printing, Polymers 13 (2020).

[361] S. Li, Z. Liu, V. Shim, Y. Guo, Z. Sun, X. Li, Z. Wang, In-plane compression of 3D-printed self-similar hierarchical honeycombs–Static and dynamic analysis, Thin Wall Struct 157 (2020) 106990.

[362] L. Wang, J. Lau, E.L. Thomas, M.C. Boyce, Co‐continuous composite materials for stiffness, strength, and energy dissipation, Adv Mater 23(13) (2011) 1524-1529.

[363] R. Johnston, Z. Kazancı, Analysis of additively manufactured (3D printed) dual-material auxetic structures under compression, Addit Manuf 38 (2021) 101783.

[364] C. Wei, H. Gu, Q. Li, Z. Sun, Y.-h. Chueh, Z. Liu, L. Li, Understanding of process and material behaviours in additive manufacturing of Invar36/Cu10Sn multiple material components via laser-based powder bed fusion, Addit Manuf 37 (2021) 101683.

[365] O. Al-Ketan, R.K. Abu Al-Rub, R. Rowshan, Mechanical Properties of a New Type of Architected Interpenetrating Phase Composite Materials, Advanced Materials Technologies 2(2) (2017) 1600235, 10.1002/Admt.201600235.

[366] O. Al‐Ketan, A. Soliman, A.M. AlQubaisi, R.K. Abu Al‐Rub, Nature‐Inspired Lightweight Cellular Co‐Continuous Composites with Architected Periodic Gyroidal Structures, Adv Eng Mater 20(2) (2018) 1700549.

[367] O. Al-Ketan, M. Adel Assad, R.K. Abu Al-Rub, Mechanical properties of periodic interpenetrating phase composites with novel architected microstructures, Compos Struct 176 (2017) 9-19, 10.1016/j.compstruct.2017.05.026.

[368] M.J. Prajapati, A. Kumar, S.-C. Lin, J.-Y. Jeng, Multi-material additive manufacturing with lightweight closed-cell foam-filled lattice structures for enhanced mechanical and functional properties, Addit Manuf 54 (2022) 102766.

[369] M.J. Prajapati, C. Bhat, A. Kumar, S. Verma, S.-C. Lin, J.-Y. Jeng, Supportless Lattice Structure for Additive Manufacturing of Functional Products and the Evaluation of Its Mechanical Property at Variable Strain Rates, Materials 15(22) (2022) 7954.

[370] V.R. Boopathy, A. Sriraman, G. Arumaikkannu, Energy absorbing capability of additive manufactured multi-material honeycomb structure, Rapid Prototyping Journal (2019).

[371] Y.-T. Kao, Y. Zhang, J. Wang, B.L. Tai, Bending behaviors of 3D-printed Bi-material structure: Experimental study and finite element analysis, Addit Manuf 16 (2017) 197-205.

[372] M.M. Osman, M. Shazly, E.A. El-Danaf, P. Jamshidi, M.M. Attallah, Compressive behavior of stretched and composite microlattice metamaterial for energy absorption applications, Composites Part B: Engineering 184 (2020) 107715.

[373] E.D. Demaine, J. O'Rourke, Geometric folding algorithms: linkages, origami, polyhedra, Cambridge university press2007.

[374] X. Xiang, G. Lu, Z. You, Energy absorption of origami inspired structures and materials, Thin Wall Struct 157 (2020) 107130.

[375] K. Yang, S. Xu, J. Shen, S. Zhou, Y.M. Xie, Energy absorption of thin-walled tubes with pre-folded origami patterns: Numerical simulation and experimental verification, Thin Wall Struct 103 (2016) 33-44.

3030   [376] Z. Chen, T. Wu, G. Nian, Y. Shan, X. Liang, H. Jiang, S. Qu, Ron Resch origami pattern inspired energy absorption structures, Journal of Applied Mechanics 86(1) (2019) 011005.

[377] S. Townsend, R. Adams, M.R. Robinson, B. Hanna, P.S. Theobald, 3D printed origami honeycombs with tailored out-of-plane energy absorption behavior, Mater Design 195 (2020) 108930.

3035   [378] J. Qi, C. Li, Y. Tie, Z. Yanping, D. Yuechen, Energy absorption characteristics of origami-inspired honeycomb sandwich structures under low-velocity impact loading, Mater Design 207 (2021) 109837.

[379] A. Wickeler, H.E. Naguib, Novel origami-inspired metamaterials: Design, mechanical testing and finite element modelling, Mater Design 186 (2020) 108242.

3040   [380] I. Echeta, X.B. Feng, B. Dutton, R. Leach, S. Piano, Review of defects in lattice structures manufactured by powder bed fusion, Int J Adv Manuf Tech 106(5-6) (2020) 2649-2668, 10.1007/s00170-019-04753-4.

[381] E. Maleki, S. Bagherifard, M. Bandini, M. Guagliano, Surface post-treatments for metal additive manufacturing: Progress, challenges, and opportunities, Addit Manuf 37 (2021)

3045   101619.

[382] D. Li, R. Qin, B. Chen, J. Zhou, Analysis of mechanical properties of lattice structures with stochastic geometric defects in additive manufacturing, Materials Science and Engineering: A 822 (2021) 141666, 10.1016/j.msea.2021.141666.

[383] M. Kumar, G.J. Gibbons, A. Das, I. Manna, D. Tanner, H.R. Kotadia, Additive

3050   manufacturing of aluminium alloy 2024 by laser powder bed fusion: Microstructural evolution, defects and mechanical properties, Rapid Prototyping Journal   (2021).

[384] H.-y. Chen, D.-d. Gu, Q. Ge, X.-y. Shi, H.-m. Zhang, R. Wang, H. Zhang, K. Kosiba, Role of laser scan strategies in defect control, microstructural evolution and mechanical properties of steel matrix composites prepared by laser additive manufacturing, International

3055   Journal of Minerals, Metallurgy and Materials 28(3) (2021) 462-474.

[385] A. Du Plessis, I. Yadroitsava, I. Yadroitsev, Effects of defects on mechanical properties in metal additive manufacturing: A review focusing on X-ray tomography insights, Mater Design 187 (2020) 108385.

[386] P. Wang, H. Lei, X. Zhu, H.-C. Chen, D. Fang, Influence of manufacturing geometric

3060   defects on the mechanical properties of AlSi10Mg alloy fabricated by selective laser melting, J Alloy Compd   (2019).

[387] J. Robinson, M. Stanford, A. Arjunan, Correlation between selective laser melting parameters, pore defects and tensile properties of 99.9% silver, Materials Today Communications 25 (2020) 101550.

3065   [388] J. Fu, H. Li, X. Song, M. Fu, Multi-scale defects in powder-based additively manufactured metals and alloys, J Mater Sci Technol   (2022).

[389] L. Xiao, S. Li, W. Song, X. Xu, S. Gao, Process-induced geometric defect sensitivity of Ti-6Al-4V lattice structures with different mesoscopic topologies fabricated by electron beam melting, Materials Science and Engineering 778(Mar.19) (2020) 139092.1-139092.16.

3070   [390] M. Dallago, F. Zanini, S. Carmignato, D. Pasini, M. Benedetti, Effect of the geometrical defectiveness on the mechanical properties of SLM biomedical Ti6Al4V lattices, Procedia structural integrity 13 (2018) 161-167.

[391] M. Dallago, B. Winiarski, F. Zanini, S. Carmignato, M. Benedetti, On the effect of geometrical imperfections and defects on the fatigue strength of cellular lattice structures additively manufactured via Selective Laser Melting, Int J Fatigue 124 (2019) 348-360, 10.1016/j.ijfatigue.2019.03.019.

[392] B. ISO, 4287: 2000,"Geometrical product specification–surface texture: profile method–terms, definitions and surface texture parameters", British Standards Institution (2000).

[393] A. Hs, B. Lnc, B. Mma, C. Hgs, Influence of processing parameters on internal porosity and types of defects formed in Ti6Al4V lattice structure fabricated by selective laser melting, Materials Science and Engineering: A 767.

[394] P. Jiang, C. Edward, S. Basu, The influence of defects on the elastic response of lattice structures resulting from additive manufacturing, Comp Mater Sci 199 (2021) 110716.

[395] A. Sombatmai, V. Uthaisangsuk, S. Wongwises, P. Promoppatum, Multiscale investigation of the influence of geometrical imperfections, porosity, and size-dependent features on mechanical behavior of additively manufactured Ti-6Al-4V lattice struts, Mater Design 209 (2021) 109985.

[396] R.S. Mishra, S. Thapliyal, Design approaches for printability-performance synergy in Al alloys for laser-powder bed additive manufacturing, Mater Design 204 (2021) 109640.

[397] S. Cao, H. Wang, X. Lu, J. Tong, Z. Sheng, Topology Optimization Considering Porosity Defects in Metal Additive Manufacturing, Applied Sciences 11(12) (2021) 5578.

[398] D.K. Pattanayak, A. Fukuda, T. Matsushita, M. Takemoto, S. Fujibayashi, K. Sasaki, N. Nishida, T. Nakamura, T. Kokubo, Bioactive Ti metal analogous to human cancellous bone: Fabrication by selective laser melting and chemical treatments, Acta biomaterialia 7(3) (2011) 1398-1406.

[399] D. Melancon, Z.S. Bagheri, R.B. Johnston, L. Liu, M. Tanzer, D. Pasini, Mechanical characterization of structurally porous biomaterials built via additive manufacturing: experiments, predictive models, and design maps for load-bearing bone replacement implants, Acta biomaterialia 63 (2017) 350-368, 10.1016/j.actbio.2017.09.013.

[400] A. Moussa, D. Melancon, A. El Elmi, D. Pasini, Topology optimization of imperfect lattice materials built with process-induced defects via Powder Bed Fusion, Addit Manuf (2020) 101608.

[401] J. Gockel, L. Sheridan, B. Koerper, B. Whip, The influence of additive manufacturing processing parameters on surface roughness and fatigue life, Int J Fatigue 124 (2019) 380-388.

[402] D. Jafari, T.H. Vaneker, I. Gibson, Wire and arc additive manufacturing: Opportunities and challenges to control the quality and accuracy of manufactured parts, Mater Design (2021) 109471.

[403] K. Atli, H. Boon, R. Seede, B. Zhang, A. Elwany, R. Arroyave, I. Karaman, Laser-based additive manufacturing of a binary Ni-5 wt.% Nb alloy, Journal of Manufacturing Processes 62 (2021) 720-728.

[404] A. Jinoop, C. PAU, J. Denny, S. Nayak, V. Krishna, K. Bindra, Laser Additive Manufacturing (LAM) of Hastelloy-X Thin Walls Using Directed Energy Deposition (DED): Parametric Investigation and Multi-objective Analysis, Lasers in Engineering (Old City Publishing) 46 (2020).

[405] G. Papazetis, G.-C. Vosniakos, Mapping of deposition-stable and defect-free additive

manufacturing via material extrusion from minimal experiments, The International Journal of Advanced Manufacturing Technology 100(9) (2019) 2207-2219.

[406] X. Zhou, N. Dai, M. Chu, L. Wang, D. Li, L. Zhou, X. Cheng, X-ray CT analysis of the influence of process on defect in Ti-6Al-4V parts produced with Selective Laser Melting technology, The International Journal of Advanced Manufacturing Technology 106(1) (2020) 3-14.

[407] S. Ghouse, S. Babu, R.J. Van Arkel, K. Nai, P.A. Hooper, J.R.T. Jeffers, The influence of laser parameters and scanning strategies on the mechanical properties of a stochastic porous material, Mater Design 131(oct.) (2017) 498-508.

[408] D.S. Egan, D.P. Dowling, Influence of process parameters on the correlation between in-situ process monitoring data and the mechanical properties of Ti-6Al-4V non-stochastic cellular structures, Addit Manuf 30 (2019) 100890.

[409] C. de Formanoir, M. Suard, R. Dendievel, G. Martin, S. Godet, Improving the mechanical efficiency of electron beam melted titanium lattice structures by chemical etching, Addit Manuf 11 (2016) 71-76.

[410] N.-J. Jin, Z. Yan, Y. Wang, H. Cheng, H. Zhang, Effects of heat treatment on microstructure and mechanical properties of selective laser melted Ti-6Al-4V lattice materials, Int J Mech Sci 190 (2021) 106042.

[411] B. Gorny, T. Niendorf, J. Lackmann, M. Thoene, T. Troester, H. Maier, In situ characterization of the deformation and failure behavior of non-stochastic porous structures processed by selective laser melting, Materials Science and Engineering: A 528(27) (2011) 7962-7967.

[412] R. Wauthle, B. Vrancken, B. Beynaerts, K. Jorissen, J. Schrooten, J.-P. Kruth, J. Van Humbeeck, Effects of build orientation and heat treatment on the microstructure and mechanical properties of selective laser melted Ti6Al4V lattice structures, Addit Manuf 5 (2015) 77-84.

[413] X. Yan, S. Yue, J. Ge, C. Chen, R. Lupoi, S. Yin, Microstructural and mechanical optimization of selective laser melted Ti6Al4V lattices: Effect of hot isostatic pressing, Journal of Manufacturing Processes 77 (2022) 151-162.

[414] A. Suzuki, K. Sekizawa, M. Liu, N. Takata, M. Kobashi, Effects of Heat Treatments on Compressive Deformation Behaviors of Lattice‐Structured AlSi10Mg Alloy Fabricated by Selective Laser Melting, Adv Eng Mater 21(10) (2019) 1900571.

[415] B. Schoinochoritis, D. Chantzis, K. Salonitis, Simulation of metallic powder bed additive manufacturing processes with the finite element method: A critical review, Proceedings of the Institution of Mechanical Engineers, Part B: Journal of Engineering Manufacture 231(1) (2017) 96-117.

[416] K. Davami, M. Mohsenizadeh, M. Munther, T. Palma, A. Beheshti, K. Momeni, Dynamic energy absorption characteristics of additively-manufactured shape-recovering lattice structures, Materials Research Express 6(4) (2019) 045302.

[417] R. Saremian, M. Badrossamay, E. Foroozmehr, M. Kadkhodaei, F. Forooghi, Experimental and numerical investigation on lattice structures fabricated by selective laser melting process under quasi-static and dynamic loadings, The International Journal of Advanced Manufacturing Technology 112 (2021) 2815-2836.

[418] Z. Alomar, F. Concli, A review of the selective laser melting lattice structures and their numerical models, Adv Eng Mater 22(12) (2020) 2000611.

[419] F. Baertsch, A. Ameli, T. Mayer, Finite-Element Modeling and Optimization of 3D-Printed Auxetic Reentrant Structures with Stiffness Gradient under Low-Velocity Impact, Journal of Engineering Mechanics 147(7) (2021) 04021036.

[420] E. Cetin, C. Baykasoğlu, Energy absorption of thin-walled tubes enhanced by lattice structures, Int J Mech Sci 157 (2019) 471-484.

[421] N. Kladovasilakis, K. Tsongas, I. Kostavelis, D. Tzovaras, D. Tzetzis, Effective Mechanical Properties of Additive Manufactured Strut‐Lattice Structures: Experimental and Finite Element Study, Adv Eng Mater (2021) 2100879.

[422] T. Shepherd, K. Winwood, P. Venkatraman, A. Alderson, T. Allen, Validation of a finite element modeling process for auxetic structures under impact, physica status solidi (b) 257(10) (2020) 1900197.

[423] X. Wang, R. Qin, B. Chen, Laser-based additively manufactured bio-inspired crashworthy structure: Energy absorption and collapse behaviour under static and dynamic loadings, Mater Design 211 (2021) 110128.

[424] H. Zhang, X. Wang, Z. Shi, J. Xue, F. Han, Compressive and Energy Absorption Properties of Pyramidal Lattice Structures by Various Preparation Methods, Materials 14(21) (2021) 6484.

[425] D.W. Abueidda, A.S. Dalaq, R.K.A. Al-Rub, H. Younes, Finite element predictions of effective multifunctional properties of interpenetrating phase composites with novel triply periodic solid shell architectured reinforcements, Int J Mech Sci 92 (2015) 80-89.

[426] Z. Sun, Y.-H. Chueh, L. Li, Multiphase mesoscopic simulation of multiple and functionally gradient materials laser powder bed fusion additive manufacturing processes, Addit Manuf 35 (2020) 101448.

[427] B. Kumar, M. Manikandan, Assessment of process, parameters, residual stress mitigation, post treatments and finite element analysis simulations of wire arc additive manufacturing technique, Met Mater-int (2021) 1-58.

[428] M.P. Serdeczny, R. Comminal, M.T. Mollah, D.B. Pedersen, J. Spangenberg, Numerical modeling of the polymer flow through the hot-end in filament-based material extrusion additive manufacturing, Addit Manuf 36 (2020) 101454.

[429] L. Yang, C. Yan, C. Han, P. Chen, S. Yang, Y. Shi, Mechanical response of a triply periodic minimal surface cellular structures manufactured by selective laser melting, Int J Mech Sci 148 (2018) 149-157.

[430] D.W. Abueidda, M. Elhebeary, C.-S. Shiang, S. Pang, R.K. Abu Al-Rub, I.M. Jasiuk, Mechanical properties of 3D printed polymeric Gyroid cellular structures: Experimental and finite element study, Mater Design 165 (2019) 107597, 10.1016/j.matdes.2019.107597.

[431] J. Yan, C. Jiang, Z. Fan, Q. Xu, H. Du, W. Sun, G. Wang, B. Niu, Compression Experiment and Failure Analysis of Additive Manufactured Multi-Layer Lattice Sandwich Structure, International Journal of Applied Mechanics 13(07) (2021) 2150077.

[432] U. Zerbst, G. Bruno, J.-Y. Buffiere, T. Wegener, T. Niendorf, T. Wu, X. Zhang, N. Kashaev, G. Meneghetti, N. Hrabe, Damage tolerant design of additively manufactured metallic components subjected to cyclic loading: State of the art and challenges, Prog Mater Sci 121

(2021) 100786.

[433] T. Russell, D.A. Jack, Strength prediction in single beads of large area additive manufactured short‑fiber polymers, Polym Composite 42(12) (2021) 6534-6550.

[434] F. Abdi, H. Baid, N. Moazami, J. Batten, D. Huang, A. Eftekharian, R. Hajiha, K. Nikbin, Reactive Additive Manufacturing Simulation of Thermoset Nano Graphene Inclusion, Journal of Multiscale Modelling 11(03) (2020) 2050004.

[435] J. Lemaitre, A course on damage mechanics, Springer Science & Business Media2012.

[436] M. Giglio, A. Manes, F. Vigano, Ductile fracture locus of Ti–6Al–4V titanium alloy, Int J Mech Sci 54(1) (2012) 121-135.

[437] I.P. Seetoh, X. Liu, K. Markandan, L. Zhen, C.Q. Lai, Strength and energy absorption characteristics of Ti6Al4V auxetic 3D anti-tetrachiral metamaterials, Mech Mater 156 (2021) 103811.

[438] G.-f. Yao, R. Liu, Z. Xu, X. Renlong, L. Chen, Z. Yu, Z. Zhang, Study on quasi-static mechanical properties of four 3D-printed bio-inspired structures based on functional relationship, Compos Struct 274 (2021) 114304.

[439] Z. Hashin, A. Rotem, A fatigue failure criterion for fiber reinforced materials, J Compos Mater 7(4) (1973) 448-464.

[440] Z. Hashin, Failure criteria for unidirectional fiber composites,   (1980).

[441] V. Tvergaard, A. Needleman, Analysis of the cup-cone fracture in a round tensile bar, Acta Metall. 32(1) (1984) 157-169.

[442] M. Kucewicz, P. Baranowski, M. Stankiewicz, M. Konarzewski, P. Płatek, J. Małachowski, Modelling and testing of 3D printed cellular structures under quasi-static and dynamic conditions, Thin Wall Struct 145 (2019) 106385.

[443] J. Tkac, S. Samborski, K. Monkova, H. Debski, Analysis of mechanical properties of a lattice structure produced with the additive technology, Compos Struct 242 (2020) 112138.

[444] S.L. Kramer, A. Jones, A. Mostafa, B. Ravaji, T. Tancogne-Dejean, C.C. Roth, M.G. Bandpay, K. Pack, J.T. Foster, M. Behzadinasab, The third Sandia Fracture Challenge: predictions of ductile fracture in additively manufactured metal, Int J Fracture 218(1) (2019) 5-61.

[445] D.P. Naragani, J.-S. Park, P. Kenesei, M.D. Sangid, Void coalescence and ductile failure in IN718 investigated via high-energy synchrotron X-ray tomography and diffraction, J. Mech. Phys. Solids 145 (2020) 104155.

[446] A.E. Wilson-Heid, A.M. Beese, Fracture of laser powder bed fusion additively manufactured Ti–6Al–4V under multiaxial loading: Calibration and comparison of fracture models, Materials Science and Engineering: A 761 (2019) 137967.

[447] A.E. Wilson-Heid, A.M. Beese, Combined effects of porosity and stress state on the failure behavior of laser powder bed fusion stainless steel 316L, Addit Manuf 39 (2021) 101862.

[448] A.E. Wilson-Heid, E.T. Furton, A.M. Beese, Contrasting the Role of Pores on the Stress State Dependent Fracture Behavior of Additively Manufactured Low and High Ductility Metals, Materials 14(13) (2021) 3657.

[449] A.E. Wilson-Heid, S. Qin, A.M. Beese, Multiaxial plasticity and fracture behavior of stainless steel 316L by laser powder bed fusion: Experiments and computational modeling, Acta Mater 199 (2020) 578-592.

[450] X. Yang, Y. Li, M.-g. Duan, W. Jiang, D. Chen, B. Li, An investigation of ductile fracture behavior of Ti6Al4V alloy fabricated by selective laser melting, J Alloy Compd 890 (2022) 161926.

[451] X. Yang, Y. Li, W. Jiang, M.-g. Duan, D. Chen, B. Li, Ductile fracture prediction of additive manufactured Ti6Al4V alloy based on an extended GTN damage model, Eng Fract Mech 256 (2021) 107989.

[452] Y. Bao, T. Wierzbicki, On fracture locus in the equivalent strain and stress triaxiality space, Int J Mech Sci 46(1) (2004) 81-98.

[453] Z. Dong, Y. Li, T. Zhao, W. Wu, D. Xiao, J. Liang, Experimental and numerical studies on the compressive mechanical properties of the metallic auxetic reentrant honeycomb, Mater Design 182 (2019) 108036.

[454] G.R. Johnson, W.H. Cook, Fracture characteristics of three metals subjected to various strains, strain rates, temperatures and pressures, Eng Fract Mech 21(1) (1985) 31-48.

[455] L. Bai, C. Yi, X. Chen, Y. Sun, J. Zhang, Effective design of the graded strut of BCC lattice structure for improving mechanical properties, Materials 12(13) (2019) 2192.

[456] X. Li, Y.H. Tan, P. Wang, X. Su, J. Ding, Metallic microlattice and epoxy interpenetrating phase composites: Experimental and simulation studies on superior mechanical properties and their mechanisms, Composites Part A Applied Science and Manufacturing 135 (2020) 105934.

[457] S. Tabacu, C. Ducu, Numerical investigations of 3D printed structures under compressive loads using damage and fracture criterion: Experiments, parameter identification, and validation, Extreme Mechanics Letters 39 (2020) 100775.

[458] F.X.C. Andrade, M. Feucht, A. Haufe, F. Neukamm, An incremental stress state dependent damage model for ductile failure prediction, International Journal of Fracture 200(1-2) (2016) 127-150, 10.1007/s10704-016-0081-2.

[459] F. Andrade, M. Feucht, A. Haufe, F. Neukamm, An incremental stress state dependent damage model for ductile failure prediction, Int J Fracture 200(1) (2016) 127-150.

[460] V. Keim, A. Cerrone, A. Nonn, Using local damage models to predict fracture in additively manufactured specimens, Int J Fracture 218(1) (2019) 135-147.

[461] M. Jirásek, Nonlocal damage mechanics, Revue européenne de génie civil 11(7-8) (2007) 993-1021.

[462] R. Alessi, J.-J. Marigo, S. Vidoli, Gradient damage models coupled with plasticity and nucleation of cohesive cracks, Arch Ration Mech An 214(2) (2014) 575-615.

[463] G. Molnár, A. Gravouil, 2D and 3D Abaqus implementation of a robust staggered phase-field solution for modeling brittle fracture, Finite Elem Anal Des 130 (2017) 27-38.

[464] J. Fang, C. Wu, T. Rabczuk, C. Wu, C. Ma, G. Sun, Q. Li, Phase field fracture in elasto-plastic solids: Abaqus implementation and case studies, Theor Appl Fract Mec 103 (2019) 102252.

[465] A. Dean, J. Reinoso, N. Jha, E. Mahdi, R. Rolfes, A phase field approach for ductile fracture of short fibre reinforced composites, Theor Appl Fract Mec 106 (2020) 102495.

[466] C. Li, J. Fang, C. Wu, G. Sun, G. Steven, Q. Li, Phase field fracture in elasto-plastic solids: Incorporating phenomenological failure criteria for ductile materials, Comput Method Appl M 391 (2022) 114580.

[467] J. Fang, C. Wu, T. Rabczuk, C. Wu, G. Sun, Q. Li, Phase field fracture in elasto-plastic

solids: a length-scale insensitive model for quasi-brittle materials, Comput Mech 66(4) (2020) 931-961.

[468] J. Fang, C. Wu, J. Li, Q. Liu, C. Wu, G. Sun, Q. Li, Phase field fracture in elasto-plastic solids: Variational formulation for multi-surface plasticity and effects of plastic yield surfaces and hardening, Int J Mech Sci 156 (2019) 382-396.

[469] S.A. Silling, R.B. Lehoucq, Peridynamic theory of solid mechanics, Adv. Appl. Mech. 44 (2010) 73-168.

[470] M. Jirásek, S. Marfia, Non‐local damage model based on displacement averaging, Int J Numer Meth Eng 63(1) (2005) 77-102.

[471] J. Lemaitre, Handbook of Materials Behavior Models, Three-Volume Set: Nonlinear Models and Properties, Elsevier2001.

[472] Y. Bai, T. Wierzbicki, A new model of metal plasticity and fracture with pressure and Lode dependence, Int J Plasticity 24(6) (2008) 1071-1096.

[473] Y. Lou, L. Chen, T. Clausmeyer, A.E. Tekkaya, J.W. Yoon, Modeling of ductile fracture from shear to balanced biaxial tension for sheet metals, Int J Solids Struct 112 (2017) 169-184.

[474] H. Hooputra, H. Gese, H. Dell, H. Werner, A comprehensive failure model for crashworthiness simulation of aluminium extrusions, International Journal of Crashworthiness 9(5) (2004) 449-464.

[475] K. Nahshon, J. Hutchinson, Modification of the Gurson model for shear failure, European Journal of Mechanics-A/Solids 27(1) (2008) 1-17.

[476] M. Helou, S. Kara, Design, analysis and manufacturing of lattice structures: an overview, Int J Comp Integ M 31(3) (2018) 243-261.

[477] Y. Wang, X. Ren, Z. Chen, Y. Jiang, X. Cao, S. Fang, T. Zhao, Y. Li, D. Fang, Numerical and experimental studies on compressive behavior of Gyroid lattice cylindrical shells, Mater Design 186 (2020) 108340, 10.1016/j.matdes.2019.108340.

[478] M.K. Afshar, A.P. Anaraki, H. Montazerian, J. Kadkhodapour, Additive manufacturing and mechanical characterization of graded porosity scaffolds designed based on triply periodic minimal surface architectures, Journal of the mechanical behavior of biomedical materials 62 (2016) 481-494.

[479] N. Korshunova, G. Alaimo, S.B. Hosseini, M. Carraturo, A. Reali, J. Niiranen, F. Auricchio, E. Rank, S. Kollmannsberger, Image-based numerical characterization and experimental validation of tensile behavior of octet-truss lattice structures, Addit Manuf 41 (2021) 101949.

[480] L. Geng, W. Wu, L. Sun, D. Fang, Damage characterizations and simulation of selective laser melting fabricated 3D re-entrant lattices based on in-situ CT testing and geometric reconstruction, Int J Mech Sci 157-158 (2019) 231-242, 10.1016/j.ijmecsci.2019.04.054.

[481] B. Lozanovski, M. Leary, P. Tran, D. Shidid, M. Qian, P. Choong, M. Brandt, Computational modelling of strut defects in SLM manufactured lattice structures, Mater Design (2019).

[482] W. Hu, X. Cao, X. Zhang, Z. Huang, Z. Chen, W. Wu, L. Xi, Y. Li, D. Fang, Deformation mechanisms and mechanical performances of architected mechanical metamaterials with gyroid topologies: Synchrotron X-ray radiation in-situ compression experiments and 3D image based finite element analysis, Extreme Mechanics Letters 44 (2021) 101229.

[483] B. Lozanovski, D. Downing, R. Tino, A. du Plessis, P. Tran, J. Jakeman, D. Shidid, C. Emmelmann, M. Qian, P. Choong, Non-destructive simulation of node defects in additively manufactured lattice structures, Addit Manuf 36 (2020) 101593.

[484] B.M. Patterson, L. Kuettner, T. Shear, K. Henderson, M.J. Herman, A. Ionita, N. Chawla, J. Williams, T. Sun, K. Fezzaa, Synchrotron CT imaging of lattice structures with engineered defects, J Mater Sci 55 (2020) 11353-11366.

[485] J. Shi, L. Zhu, L. Li, Z. Li, J. Yang, X. Wang, A TPMS-based method for modeling porous scaffolds for bionic bone tissue engineering, Scientific reports 8(1) (2018) 1-10.

[486] Z. Xia, Z. He, Q. Wang, Y. Wang, A New Finite Element Model with Manufactured Error for Additive Manufacturing, Computer Modeling in Engineering & Sciences 124(2) (2020) 703-720.

[487] B. Lozanovski, D. Downing, P. Tran, D. Shidid, M. Qian, P. Choong, M. Brandt, M. Leary, A Monte Carlo simulation-based approach to realistic modelling of additively manufactured lattice structures, Addit Manuf 32 (2020) 101092, 10.1016/j.addma.2020.101092.

[488] L. Salari-Sharif, S. Godfrey, M. Tootkaboni, L. Valdevit, The effect of manufacturing defects on compressive strength of ultralight hollow microlattices: A data-driven study, Addit Manuf 19 (2018) 51-61.

[489] Y. Amani, S. Dancette, P. Delroisse, A. Simar, E. Maire, Compression behavior of lattice structures produced by selective laser melting: X-ray tomography based experimental and finite element approaches, Acta Mater 159 (2018) 395-407, 10.1016/j.actamat.2018.08.030.

[490] S.M. Hashemi, S. Parvizi, H. Baghbanijavid, A.T. Tan, M. Nematollahi, A. Ramazani, N.X. Fang, M. Elahinia, Computational modelling of process–structure–property–performance relationships in metal additive manufacturing: A review, Int Mater Rev 67(1) (2022) 1-46.

[491] P. Stavropoulos, P. Foteinopoulos, Modelling of additive manufacturing processes: a review and classification, Manufacturing Review 5 (2018) 2.

[492] B.N. Turner, R. Strong, S.A. Gold, A review of melt extrusion additive manufacturing processes: I. Process design and modeling, Rapid prototyping journal (2014).

[493] M.M. Francois, A. Sun, W.E. King, N.J. Henson, D. Tourret, C.A. Bronkhorst, N.N. Carlson, C.K. Newman, T. Haut, J. Bakosi, Modeling of additive manufacturing processes for metals: Challenges and opportunities, Current Opinion in Solid State and Materials Science 21(4) (2017) 198-206.

[494] J. Baiges, M. Chiumenti, C.A. Moreira, M. Cervera, R. Codina, An Adaptive Finite Element strategy for the numerical simulation of Additive Manufacturing processes, Addit Manuf 37 (2021) 101650.

[495] S. Jayanath, A. Achuthan, A computationally efficient finite element framework to simulate additive manufacturing processes, Journal of Manufacturing Science and Engineering 140(4) (2018).

[496] M.E. Stender, L.L. Beghini, J.D. Sugar, M.G. Veilleux, S.R. Subia, T.R. Smith, C.W. San Marchi, A.A. Brown, D.J. Dagel, A thermal-mechanical finite element workflow for directed energy deposition additive manufacturing process modeling, Addit Manuf 21 (2018) 556-566.

[497] J. Lee, V. Prabhu, Simulation modeling for optimal control of additive manufacturing processes, Addit Manuf 12 (2016) 197-203.

[498] X. Song, S. Feih, W. Zhai, C.-N. Sun, F. Li, R. Maiti, J. Wei, Y. Yang, V. Oancea, L.R.

Brandt, Advances in additive manufacturing process simulation: Residual stresses and distortion predictions in complex metallic components, Mater Design 193 (2020) 108779.

[499] S. Sahoo, K. Chou, Phase-field simulation of microstructure evolution of Ti–6Al–4V in electron beam additive manufacturing process, Addit Manuf 9 (2016) 14-24.

[500] K. Classens, T. Hafkamp, S. Westbeek, J.J. Remmers, S. Weiland, Multiphysical modeling and optimal control of material properties for photopolymerization processes, Addit Manuf 38 (2021) 101520.

[501] Z. Wang, W. Yang, Q. Liu, Y. Zhao, P. Liu, D. Wu, M. Banu, L. Chen, Data-driven modeling of process, structure and property in additive manufacturing: A review and future directions, Journal of Manufacturing Processes 77 (2022) 13-31.

[502] A. Seharing, A.H. Azman, S. Abdullah, A review on integration of lightweight gradient lattice structures in additive manufacturing parts, Advances in Mechanical Engineering 12(6) (2020) 1687814020916951.

[503] S. Wang, J. Wang, Y. Xu, W. Zhang, J. Zhu, Compressive behavior and energy absorption of polymeric lattice structures made by additive manufacturing, Frontiers of Mechanical Engineering 15(2) (2020) 319-327.

[504] J. Zhang, J. Yanagimoto, Topology optimization of microlattice dome with enhanced stiffness and energy absorption for additive manufacturing, Compos Struct 255 (2021) 112889.

[505] S. Budholiya, A. Bhat, S.A. Raj, M.T. Hameed Sultan, A.U. Md Shah, A. A Basri, State of the Art Review about Bio-Inspired Design and Applications: An Aerospace Perspective, Applied Sciences 11(11) (2021) 5054.

[506] C. Han, Q. Fang, Y. Shi, S.B. Tor, C.K. Chua, K. Zhou, Recent advances on high‐entropy alloys for 3D printing, Adv Mater 32(26) (2020) 1903855.

[507] J. Noronha, M. Qian, M. Leary, E. Kyriakou, M. Brandt, Hollow-walled lattice materials by additive manufacturing: Design, manufacture, properties, applications and challenges, Current Opinion in Solid State and Materials Science 25(5) (2021) 100940.

[508] H. Zhang, H. Zhou, Z. Zhou, Z. Huizhong, X. Zhang, J. Yang, H. Lei, F. Han, Energy absorption diagram characteristic of metallic self-supporting 3D lattices fabricated by additive manufacturing and design method of energy absorption structure, Int J Solids Struct (2021) 111082.

[509] S. Peng, S. Mooraj, R. Feng, L. Liu, J. Ren, Y. Liu, F. Kong, Z. Xiao, C. Zhu, P.K. Liaw, Additive manufacturing of three-dimensional (3D)-architected CoCrFeNiMn high-entropy alloy with great energy absorption, Scripta Mater 190 (2021) 46-51.

[510] P. Wang, F. Yang, P. Li, B. Zheng, H. Fan, Design and additive manufacturing of a modified face-centered cubic lattice with enhanced energy absorption capability, Extreme Mechanics Letters 47 (2021) 101358.

[511] S. Duan, L. Xi, W. Wen, D. Fang, Mechanical performance of topology-optimized 3D lattice materials manufactured via selective laser sintering, Compos Struct 238 (2020) 111985.

[512] J. Liu, A.T. Gaynor, S. Chen, Z. Kang, K. Suresh, A. Takezawa, L. Li, J. Kato, J. Tang, C.C.L. Wang, L. Cheng, X. Liang, A.C. To, Current and future trends in topology optimization for additive manufacturing, Struct Multidiscip O 57 (2018) 2457-2483.

[513] M. Al Khalil, N. Lebaal, F. Demoly, S. Roth, A design and optimization framework of variable-density lattice structures for additive manufacturing, Mechanics of Advanced

Materials and Structures   (2021) 1-15.

[514] E. Boesch, A. Siadat, M. Rivette, A.A. Baqai, Impact of fused deposition modeling (FDM) process parameters on strength of built parts using Taguchi's design of experiments, The international journal of Advanced Manufacturing technology 101(5) (2019) 1215-1226.

[515] H. Klippstein, A. Diaz De Cerio Sanchez, H. Hassanin, Y. Zweiri, L. Seneviratne, Fused deposition modeling for unmanned aerial vehicles (UAVs): a review, Adv Eng Mater 20(2) (2018) 1700552.

[516] M. Spoerk, F. Arbeiter, H. Cajner, J. Sapkota, C. Holzer, Parametric optimization of intra‑ and inter‑layer strengths in parts produced by extrusion‑based additive manufacturing of poly (lactic acid), J Appl Polym Sci 134(41) (2017) 45401.

[517] S.R. Bronder, M. Adorna, T. Fíla, P. Koudelka, J. Falta, O. Jirovaek, A. Jung, Hybrid Auxetic Structures: Structural Optimization and Mechanical Characterization, Adv Eng Mater (2021) 2001393.

[518] M. Ye, H. Li, X. Cai, L. Gao, A. Zhang, Z. Zhao, Progressive design of gradually stiffer metamaterial using surrogate model, Compos Struct 264 (2021) 113715.

[519] U. Simsek, M. Ozdemir, P. Sendur, An efficient design methodology for graded surface-based lattice structures using free-size optimization and enhanced mapping method, Mater Design 210 (2021) 110039.

[520] B. Aslan, A.R. Yıldız, Optimum design of automobile components using lattice structures for additive manufacturing, Materials testing 62(6) (2020) 633-639.

[521] P. Dal Fabbro, S. Rosso, A. Ceruti, D. Boscolo Bozza, R. Meneghello, G. Concheri, G. Savio, Analysis of a Preliminary Design Approach for Conformal Lattice Structures, Applied Sciences 11(23) (2021) 11449.

[522] W. Chen, X. Zheng, S. Liu, Finite-element-mesh based method for modeling and optimization of lattice structures for additive manufacturing, Materials 11(11) (2018) 2073.

[523] R.M. Gorguluarslan, Multi-objective design optimization of additively manufactured lattice structures for improved energy absorption performance, Proceedings of the Institution of Mechanical Engineers, Part C: Journal of Mechanical Engineering Science 236(1) (2022) 3-15.

[524] S. Rosso, F. Uriati, L. Grigolato, R. Meneghello, G. Concheri, G. Savio, An optimization workflow in design for additive manufacturing, Applied Sciences 11(6) (2021) 2572.

[525] A. Baykaso lu, C. Baykasoglu, E. Çetin, Multi-objective crashworthiness optimization of lattice structure filled thin-walled tubes, Thin Wall Struct 149 (2020) 106630.

[526] H. Yin, C. Chen, T. Hu, G. Wen, Optimisation for bending crashworthiness of functionally graded foam-filled cellular structure, International Journal of Crashworthiness 23 (2018) 446 - 460.

[527] G. Sun, T. Pang, J. Fang, G. Li, Q. Li, Parameterization of criss-cross configurations for multiobjective crashworthiness optimization, Int J Mech Sci 124 (2017) 145-157.

[528] S. Vijayavenkataraman, L. Zhang, S. Zhang, J.Y. Hsi Fuh, W.F. Lu, Triply periodic minimal surfaces sheet scaffolds for tissue engineering applications: An optimization approach toward biomimetic scaffold design, ACS Applied Bio Materials 1(2) (2018) 259-269.

[529] Y. Feng, K. Li, Y. Gao, H. Qiu, J. Liu, Design and optimization of origami-inspired orthopyramid-like core panel for load damping, Applied Sciences 9(21) (2019) 4619.

3460 [530] C. Imediegwu, R. Murphy, R. Hewson, M. Santer, Multiscale structural optimization towards three-dimensional printable structures, Struct Multidiscip O 60(2) (2019) 513-525.

[531] C.H.P. Nguyen, Y. Kim, Q.T. Do, Y. Choi, Implicit-based computer-aided design for additively manufactured functionally graded cellular structures, Journal of Computational Design and Engineering 8(3) (2021) 813-823.

3465 [532] C. Imediegwu, R. Murphy, R. Hewson, M. Santer, Multiscale thermal and thermo-structural optimization of three-dimensional lattice structures, Struct Multidiscip O 65(1) (2022) 1-21.

[533] T. Kirchdoerfer, M. Ortiz, Data-driven computational mechanics, Comput Method Appl M 304 (2016) 81-101.

3470 [534] J. Kudela, R. Matousek, Recent advances and applications of surrogate models for finite element method computations: a review, Soft Computing   (2022) 1-25.

[535] J. Wang, R. Rai, Generative design of conformal cubic periodic cellular structures using a surrogate model-based optimisation scheme, Int J Prod Res   (2020) 1-20.

[536] V. Doan, F. Massa, T. Tison, H. Naceur, Coupling of Homotopy Perturbation Method and 3475 Kriging surrogate model for an efficient fuzzy linear buckling analysis: Application to additively manufactured lattice structures, Appl Math Model 97 (2021) 602-618.

[537] D. Gu, X. Shi, R. Poprawe, D.L. Bourell, R. Setchi, J. Zhu, Material-structure-performance integrated laser-metal additive manufacturing, Science 372(6545) (2021) eabg1487.

3480 [538] J. Zhang, Y. Sato, J. Yanagimoto, Homogenization-based topology optimization integrated with elastically isotropic lattices for additive manufacturing of ultralight and ultrastiff structures, CIRP Annals 70(1) (2021) 111-114.

[539] M. Bujny, M. Olhofer, N. Aulig, F. Duddeck, Topology Optimization of 3D-printed joints under crash loads using Evolutionary Algorithms, Struct Multidiscip O 64(6) (2021) 4181-4206.

3485 [540] A.I.H. Nasrullah, S.P. Santosa, T. Dirgantara, Design and optimization of crashworthy components based on lattice structure configuration, Structures, Elsevier, 2020, pp. 969-981.

[541] M.P. Bendsøe, O. Sigmund, Material interpolation schemes in topology optimization, Arch Appl Mech 69 (1999) 635-654.

[542] X. Huang, Y.M. Xie, Bi-directional evolutionary topology optimization of continuum 3490 structures with one or multiple materials, Comput Mech 43 (2008) 393-401.

[543] K. Maute, O. Sigmund, Topology optimization approaches: A comparative review, Struct Multidiscip O 6 (2013).

[544] L. Xia, Q. Xia, X. Huang, Y.M. Xie, Bi-directional evolutionary structural optimization on advanced structures and materials: a comprehensive review, Arch Comput Method E 25(2) 3495 (2018) 437-478.

[545] K. Svanberg, The method of moving asymptote- a new method for structural optimization, Int J Numer Meth Eng 24 (1987) 359-373.

[546] M. Bi, P. Tran, Y.M. Xie, Topology optimization of 3D continuum structures under geometric self-supporting constraint, Addit Manuf 36 (2020) 101422.

3500 [547] R. Picelli, R. Sivapuram, Y.M. Xie, A 101-line MATLAB code for topology optimization using binary variables and integer programming, Struct Multidiscip O 63(2) (2021) 935-954.

[548] G. Allaire, F. Jouve, A.-M. Toader, A level-set method for shape optimization, Comptes

Rendus Mathematique 334 (2002) 1125-1130.

[549] M.Y. Wang, X. Wang, D.-m. Guo, A level set method for structural topology optimization, Comput Method Appl M 192 (2003) 227-246.

[550] M.Y. Wang, S. Zhou, Phase Field: A Variational Method for Structural Topology Optimization, Cmes-comp Model Eng 6 (2004) 547-566.

[551] L. Zhang, B. Song, J.J. Fu, S.S. Wei, L. Yang, C.Z. Yan, H. Li, L. Gao, Y.S. Shi, Topology-optimized lattice structures with simultaneously high stiffness and light weight fabricated by selective laser melting: Design, manufacturing and characterization, Journal of Manufacturing Processes 56 (2020) 1166-1177.

[552] T. Akihiro, Y. Kazuo, K. Yuichiro, X. Zhang, K. Mitsuru, Isotropic Ti–6Al–4V Lattice via Topology Optimization and Electron-Beam Melting, Addit Manuf (2018) S2214860418300629-.

[553] X. Guo, W. Zhang, W. Zhong, Doing Topology Optimization Explicitly and Geometrically A New Moving Morphable Components Based Framework, Journal of Applied Mechanics 81 (2014) 081009.

[554] E. Raponi, M. Bujny, M. Olhofer, N. Aulig, S. Boria, F. Duddeck, Kriging-assisted topology optimization of crash structures, Comput Method Appl M (2019).

[555] X. Huang, Y.M. Xie, G. Lu, Topology optimization of energy-absorbing structures, International Journal of Crashworthiness 12 (2007) 663 - 675.

[556] C. Wu, K. Zheng, J. Fang, G.P. Steven, Q. Li, Time-dependent topology optimization of bone plates considering bone remodeling, Comput Method Appl M 359 (2020) 112702.

[557] C. Wu, J. Fang, A. Entezari, G. Sun, M.V. Swain, Y. Xu, G.P. Steven, Q. Li, A time-dependent mechanobiology-based topology optimization to enhance bone growth in tissue scaffolds, J Biomech 117 (2021) 110233.

[558] C. Wu, J. Fang, S. Zhou, Z. Zhang, G. Sun, G.P. Steven, Q. Li, A path-dependent level set topology optimization with fracture criterion, Comput Struct 249 (2021) 106515.

[559] F. Fernandez, M.A. Puso, J. Solberg, D.A. Tortorelli, Topology optimization of multiple deformable bodies in contact with large deformations, Comput Method Appl M 371 (2020) 113288.

[560] C.B. Pedersen, Topology optimization design of crushed 2D-frames for desired energy absorption history, Struct Multidiscip O 25(5) (2003) 368-382.

[561] J. Jia, D. Da, J. Hu, S. Yin, Crashworthiness design of periodic cellular structures using topology optimization, Compos Struct 271 (2021) 114164.

[562] N. Bahramian, A. Khalkhali, Crashworthiness topology optimization of thin-walled square tubes, using modified Bidirectional Evolutionary Structural Optimization approach, Thin Wall Struct 147 (2020) 106524.

[563] X. Huang, Y.M. Xie, Topology optimization of nonlinear structures under displacement loading, Eng Struct 30 (2008) 2057-2068.

[564] C. Yang, Q.M. Li, Advanced lattice material with high energy absorption based on topology optimisation, Mech Mater 148 (2020) 103536.

[565] N. Gan, S. Yao, Y. Xiong, X. Hong, A hybrid cellular automaton–bi-directional evolutionary optimization algorithm for topological optimization of crashworthiness, Eng Optimiz 50(12) (2018) 2054-2070.

[566] D. Zeng, F. Duddeck, Improved hybrid cellular automata for crashworthiness optimization of thin-walled structures, Struct Multidiscip O 56 (2017) 101-115.

[567] H. Wang, H. Xie, Multi-objective optimization of crashworthiness of vehicle front longitudinal beam, Struct Multidiscip O 61 (2019) 2111-2123.

[568] H.-A. Lee, G.-J. Park, Nonlinear dynamic response topology optimization using the equivalent static loads method, Comput Method Appl M 283 (2015) 956-970.

[569] Z. Ahmad, T. Sultan, M. Zoppi, M. Abid, G. Jin Park, Nonlinear response topology optimization using equivalent static loads—case studies, Eng Optimiz (2016) 1-17.

[570] M. Li, W. Tang, M. Yuan, Structural dynamic topology optimization based on dynamic reliability using equivalent static loads, Struct Multidiscip O 49 (2014) 121-129.

[571] H.-A. Lee, G.-J. Park, Topology Optimization for Structures With Nonlinear Behavior Using the Equivalent Static Loads Method, J Mech Design 134 (2012) 031004.

[572] Y. Bai, H.S. Zhou, F. Lei, H. Lei, An improved numerically-stable equivalent static loads (ESLs) algorithm based on energy-scaling ratio for stiffness topology optimization under crash loads, Struct Multidiscip O 59 (2018) 117-130.

[573] M. Ebeling-Rump, D. Hömberg, R. Lasarzik, T. Petzold, Topology optimization subject to additive manufacturing constraints, Journal of Mathematics in Industry 11(1) (2021) 1-19.

[574] G. Fiuk, M. Mrzygłód, Topology optimization of structures with stress and additive manufacturing constraints, Journal of Theoretical and Applied Mechanics 58 (2020).

[575] A. Garaigordobil, R. Ansola, E. Veguería, I. Fernandez, Overhang constraint for topology optimization of self-supported compliant mechanisms considering additive manufacturing, Comput Aided Design 109 (2019) 33-48.

[576] J. Liu, A.C. To, Deposition path planning-integrated structural topology optimization for 3D additive manufacturing subject to self-support constraint, Comput Aided Design 91 (2017) 27-45.

[577] S. Mantovani, G.A. Campo, A. Ferrari, Additive manufacturing and topology optimization: A design strategy for a steering column mounting bracket considering overhang constraints, Proceedings of the Institution of Mechanical Engineers, Part C: Journal of Mechanical Engineering Science 235(10) (2021) 1703-1723.

[578] K. Mhapsekar, M. McConaha, S. Anand, Additive manufacturing constraints in topology optimization for improved manufacturability, Journal of Manufacturing Science and Engineering 140(5) (2018).

[579] G. Misiun, E. van de Ven, M. Langelaar, H. Geijselaers, F. van Keulen, T. van den Boogaard, C. Ayas, Topology Optimization for additive manufacturing with distortion constraints, Comput Method Appl M 386 (2021) 114095.

[580] E. van de Ven, C. Ayas, M. Langelaar, R. Maas, F. van Keulen, Accessibility of support structures in topology optimization for additive manufacturing, Int J Numer Meth Eng 122(8) (2021) 2038-2056.

[581] K. Zhang, G. Cheng, Three-dimensional high resolution topology optimization considering additive manufacturing constraints, Addit Manuf 35 (2020) 101224.

[582] K. Zhang, G. Cheng, L. Xu, Topology optimization considering overhang constraint in additive manufacturing, Comput Struct 212 (2019) 86-100.

[583] Y. Zhou, T. Nomura, K. Saitou, Multicomponent topology optimization for additive

manufacturing with build volume and cavity free constraints, Journal of Computing and Information Science in Engineering 19(2) (2019).

[584] J. Zou, Y. Zhang, Z. Feng, Topology optimization for additive manufacturing with self-supporting constraint, Struct Multidiscip O 63(5) (2021) 2341-2353.

[585] Y. Xiong, S. Yao, Z.-l. Zhao, Y.M. Xie, A new approach to eliminating enclosed voids in topology optimization for additive manufacturing, Addit Manuf 32 (2020) 101006.

[586] Y. Wang, J. Gao, Z. Kang, Level set-based topology optimization with overhang constraint: Towards support-free additive manufacturing, Comput Method Appl M 339 (2018) 591-614.

[587] A. Garaigordobil, R. Ansola, J. Santamaría, I. Fernández de Bustos, A new overhang constraint for topology optimization of self-supporting structures in additive manufacturing, Struct Multidiscip O 58(5) (2018) 2003-2017.

[588] A.T. Gaynor, J.K. Guest, Topology optimization considering overhang constraints: Eliminating sacrificial support material in additive manufacturing through design, Struct Multidiscip O 54(5) (2016) 1157-1172.

[589] L. Zhou, W. Zhang, Topology optimization method with elimination of enclosed voids, Struct Multidiscip O 60(1) (2019) 117-136.

[590] X. Guo, J. Zhou, W. Zhang, Z. Du, C. Liu, Y. Liu, Self-supporting structure design in additive manufacturing through explicit topology optimization, Comput Method Appl M 323 (2017) 27-63.

[591] C. Wang, B. Xu, Q. Meng, J. Rong, Y. Zhao, Numerical performance of Poisson method for restricting enclosed voids in topology optimization, Comput Struct 239 (2020) 106337.

[592] Q. Li, W. Chen, S. Liu, L. Tong, Structural topology optimization considering connectivity constraint, Struct Multidiscip O 54(4) (2016) 971-984.

[593] G. Allaire, L. Jakabčin, Taking into account thermal residual stresses in topology optimization of structures built by additive manufacturing, Mathematical Models and Methods in Applied Sciences 28(12) (2018) 2313-2366.

[594] M. Zhou, Y. Liu, Z. Lin, Topology optimization of thermal conductive support structures for laser additive manufacturing, Comput Method Appl M 353 (2019) 24-43.

[595] L. Cheng, X. Liang, J. Bai, Q. Chen, J. Lemon, A. To, On utilizing topology optimization to design support structure to prevent residual stress induced build failure in laser powder bed metal additive manufacturing, Addit Manuf 27 (2019) 290-304.

[596] S. Xu, J. Liu, Y. Ma, Residual stress constrained self-support topology optimization for metal additive manufacturing, Comput Method Appl M 389 (2022) 114380.

[597] T. Miki, T. Yamada, Topology optimization considering the distortion in additive manufacturing, Finite Elem Anal Des 193 (2021) 103558.

[598] X. Wang, W. Xiong, Uncertainty quantification and composition optimization for alloy additive manufacturing through a CALPHAD-based ICME framework, npj Computational Materials 6(1) (2020) 1-11.

[599] C. Dordlofva, P. Törlind, Evaluating design uncertainties in additive manufacturing using design artefacts: examples from space industry, Design Science 6 (2020).

[600] D. Garcia, Z. Wu, J.Y. Kim, Z.Y. Hang, Y. Zhu, Heterogeneous materials design in additive manufacturing: Model calibration and uncertainty-guided model selection, Addit

Manuf 27 (2019) 61-71.

[601] Z. Hu, S. Mahadevan, Uncertainty quantification and management in additive manufacturing: current status, needs, and opportunities, The International Journal of Advanced Manufacturing Technology 93(5) (2017) 2855-2874.

[602] S. Korneev, Z. Wang, V. Thiagarajan, S. Nelaturi, Fabricated shape estimation for additive manufacturing processes with uncertainty, Comput Aided Design 127 (2020) 102852.

[603] F. Lopez, P. Witherell, B. Lane, Identifying uncertainty in laser powder bed fusion additive manufacturing models, J Mech Design 138(11) (2016).

[604] H. Zhang, J. Guilleminot, L.J. Gomez, Stochastic modeling of geometrical uncertainties on complex domains, with application to additive manufacturing and brain interface geometries, Comput Method Appl M 385 (2021) 114014.

[605] B. Liu, C. Jiang, G. Li, X. Huang, Topology optimization of structures considering local material uncertainties in additive manufacturing, Comput Method Appl M 360 (2020) 112786.

[606] P. Nath, J.D. Olson, S. Mahadevan, Y.-T.T. Lee, Optimization of fused filament fabrication process parameters under uncertainty to maximize part geometry accuracy, Addit Manuf 35 (2020).

[607] Y.-C. Chan, K. Shintani, W. Chen, Robust topology optimization of multi-material lattice structures under material and load uncertainties, Frontiers of Mechanical Engineering 14(2) (2019) 141-152, 10.1007/s11465-019-0531-4.

[608] J. Greifenstein, M. Stingl, Topology optimization with worst-case handling of material uncertainties, Struct Multidiscip O 61(4) (2020) 1377-1397.

[609] J. Liu, J. Yan, H. Yu, Stress-constrained topology optimization for material extrusion polymer additive manufacturing, Journal of Computational Design and Engineering 8(3) (2021) 979-993.

[610] D. Popov, Y. Kuzminova, E. Maltsev, S. Evlashin, A. Safonov, I. Akhatov, A. Pasko, CAD/CAM System for Additive Manufacturing with a Robust and Efficient Topology Optimization Algorithm Based on the Function Representation, Applied Sciences 11(16) (2021) 7409.

[611] T. Chatterjee, S. Chakraborty, S. Goswami, S. Adhikari, M.I. Friswell, Robust topological designs for extreme metamaterial micro-structures, Scientific Reports 11(1) (2021) 1-14.

[612] V. Keshavarzzadeh, K.A. James, Robust multiphase topology optimization accounting for manufacturing uncertainty via stochastic collocation, Struct Multidiscip O 60(6) (2019) 2461-2476.

[613] L. Wang, T.T. Allen, M.A. Groeber, Tabu efficient global optimization with applications in additive manufacturing, Struct Multidiscip O 63(6) (2021) 2811-2833.

[614] M. Jalalpour, M.P. Tootkaboni, An efficient approach to reliability-based topology optimization for continua under material uncertainty, Struct Multidiscip O 53 (2016) 759-772.

[615] B.S. Lazarov, M. Schevenels, O. Sigmund, Topology optimization considering material and geometric uncertainties using stochastic collocation methods, Struct Multidiscip O 46 (2012) 597-612.

[616] S.A.L. Rostami, A. Ghoddosian, Topology optimization of continuum structures under hybrid uncertainties, Struct Multidiscip O 57 (2018) 2399-2409.

[617] J. Guilleminot, A. Asadpoure, M.P. Tootkaboni, Topology optimization under

3675   topologically dependent material uncertainties, Struct Multidiscip O (2019) 1-5.

[618] Y. Zheng, Y. Wang, X. Lu, J. Zheng, J. Qu, Topology optimisation for isotropic mechanical metamaterials considering material uncertainties, Mech Mater 155 (2021) 103742.

[619] N. Changizi, H. Kaboodanian, M. Jalalpour, Stress-based topology optimization of frame structures under geometric uncertainty, Comput Method Appl M 315 (2017) 121-140.

3680   [620] V. Keshavarzzadeh, F. Fernandez, D. Tortorelli, Topology optimization under uncertainty via non-intrusive polynomial chaos expansion, Comput Method Appl M 318 (2017) 120-147.

[621] L. Alacoque, R.T. Watkins, A.Y. Tamijani, Stress-based and robust topology optimization for thermoelastic multi-material periodic microstructures, Comput Method Appl M (2021).

[622] L. Wang, H. Xia, Y. Yang, Y. Cai, Z. Qiu, A novel approach of reliability-based topology

3685   optimization for continuum structures under interval uncertainties, Rapid Prototyping Journal (2019).

[623] Y. LeCun, Y. Bengio, G. Hinton, Deep learning, Nature 521(7553) (2015) 436-444.

[624] T. Young, D. Hazarika, S. Poria, E. Cambria, Recent Trends in Deep Learning Based Natural Language Processing [Review Article], IEEE Computational Intelligence Magazine

3690   13(3) (2018) 55-75, 10.1109/mci.2018.2840738.

[625] I. Kavakiotis, O. Tsave, A. Salifoglou, N. Maglaveras, I.P. Vlahavas, I. Chouvarda, Machine Learning and Data Mining Methods in Diabetes Research, Computational and Structural Biotechnology Journal 15 (2017) 104 - 116.

[626] C. Wu, A.R. Entezari, K. Zheng, J. Fang, H. Zreiqat, G.P. Steven, M.V. Swain, Q. Li, A

3695   machine learning-based multiscale model to predict bone formation in scaffolds, Nature Computational Science (2021).

[627] A. Oishi, G. Yagawa, Computational mechanics enhanced by deep learning, Comput Method Appl M 327 (2017) 327-351.

[628] Y. Xu, Y. Gao, C. Wu, J. Fang, G. Sun, G.P. Steven, Q. Li, Machine learning based

3700   topology optimization of fiber orientation for variable stiffness composite structures, Int J Numer Meth Eng (2021).

[629] K.T. Butler, D.W. Davies, H.M. Cartwright, O. Isayev, A. Walsh, Machine learning for molecular and materials science, Nature 559 (2018) 547-555.

[630] C. Wang, X.P. Tan, S.B. Tor, C.S. Lim, Machine learning in additive manufacturing: State-

3705   of-the-art and perspectives, Addit Manuf 36 (2020) 101538.

[631] G.D. Goh, S.L. Sing, W.Y. Yeong, A review on machine learning in 3D printing: applications, potential, and challenges, Artif Intell Rev 54(1) (2021) 63-94.

[632] S. Guo, M. Agarwal, C. Cooper, Q. Tian, R.X. Gao, W.G. Grace, Y. Guo, Machine learning for metal additive manufacturing: Towards a physics-informed data-driven paradigm,

3710   J Manuf Syst 62 (2022) 145-163.

[633] J. Jiang, Y. Xiong, Z. Zhang, D.W. Rosen, Machine learning integrated design for additive manufacturing, J Intell Manuf (2020) 1-14.

[634] N. Johnson, P. Vulimiri, A. To, X. Zhang, C. Brice, B. Kappes, A. Stebner, Invited review: Machine learning for materials developments in metals additive manufacturing, Addit Manuf

3715   36 (2020) 101641.

[635] L.J. Ladani, Applications of artificial intelligence and machine learning in metal additive manufacturing, Journal of Physics: Materials 4(4) (2021) 042009.

[636] L. Meng, B. McWilliams, W. Jarosinski, H.-Y. Park, Y.-G. Jung, J. Lee, J. Zhang, Machine Learning in Additive Manufacturing: A Review, Jom 72(6) (2020) 2363-2377, 10.1007/s11837-020-04155-y.

[637] X. Qi, G. Chen, Y. Li, X. Cheng, C. Li, Applying Neural-Network-Based Machine Learning to Additive Manufacturing: Current Applications, Challenges, and Future Perspectives, Engineering 5(4) (2019) 721-729, 10.1016/j.eng.2019.04.012.

[638] S.S. Razvi, S. Feng, A. Narayanan, Y.-T.T. Lee, P. Witherell, A review of machine learning applications in additive manufacturing, International Design Engineering Technical Conferences and Computers and Information in Engineering Conference, American Society of Mechanical Engineers, 2019, p. V001T02A040.

[639] S. Sing, C. Kuo, C. Shih, C. Ho, C. Chua, Perspectives of using machine learning in laser powder bed fusion for metal additive manufacturing, Virtual and Physical Prototyping 16(3) (2021) 372-386.

[640] J. Qin, F. Hu, Y. Liu, P. Witherell, C.C. Wang, D.W. Rosen, T. Simpson, Y. Lu, Q. Tang, Research and application of machine learning for additive manufacturing, Addit Manuf (2022) 102691.

[641] S. Menard, Applied logistic regression analysis, Sage2002.

[642] S. Weisberg, Applied linear regression, John Wiley & Sons2005.

[643] C.E. Rasmussen, Gaussian processes in machine learning, Summer school on machine learning, Springer, 2003, pp. 63-71.

[644] T.K. Ho, Random decision forests, Proceedings of 3rd international conference on document analysis and recognition, IEEE, 1995, pp. 278-282.

[645] C. Cortes, V. Vapnik, Support-vector networks, Mach Learn 20(3) (1995) 273-297.

[646] A.K. Jain, J. Mao, K.M. Mohiuddin, Artificial neural networks: A tutorial, Computer 29(3) (1996) 31-44.

[647] Y.-Y. Song, L. Ying, Decision tree methods: applications for classification and prediction, Shanghai archives of psychiatry 27(2) (2015) 130.

[648] J.M. Keller, M.R. Gray, J.A. Givens, A fuzzy k-nearest neighbor algorithm, IEEE transactions on systems, man, and cybernetics (4) (1985) 580-585.

[649] H. Wang, B. Li, F.-Z. Xuan, A dimensionally augmented and physics-informed machine learning for quality prediction of additively manufactured high-entropy alloy, J Mater Process Tech (2022) 117637.

[650] Y. Gui, K. Aoyagi, H. Bian, A. Chiba, Detection, classification and prediction of internal defects from surface morphology data of metal parts fabricated by powder bed fusion type additive manufacturing using an electron beam, Addit Manuf 54 (2022) 102736.

[651] Y. Zhu, Z. Wu, W.D. Hartley, J.M. Sietins, C.B. Williams, Z.Y. Hang, Unraveling pore evolution in post-processing of binder jetting materials: X-ray computed tomography, computer vision, and machine learning, Addit Manuf 34 (2020) 101183.

[652] M. Hiles, M. Grossutti, J.R. Dutcher, Classifying formulations of crosslinked polyethylene pipe by applying machine‐learning concepts to infrared spectra, Journal of Polymer Science Part B: Polymer Physics 57(18) (2019) 1255-1262.

[653] M. Khanzadeh, P. Rao, R. Jafari-Marandi, B.K. Smith, M.A. Tschopp, L. Bian, Quantifying geometric accuracy with unsupervised machine learning: Using self-organizing

map on fused filament fabrication additive manufacturing parts, Journal of Manufacturing Science and Engineering 140(3) (2018).

[654] K. Taherkhani, C. Eischer, E. Toyserkani, An unsupervised machine learning algorithm for in-situ defect-detection in laser powder-bed fusion, Journal of Manufacturing Processes 81 (2022) 476-489.

[655] M.A. Ansari, A. Crampton, R. Garrard, B. Cai, M. Attallah, A Convolutional Neural Network (CNN) classification to identify the presence of pores in powder bed fusion images, The International Journal of Advanced Manufacturing Technology 120(7) (2022) 5133-5150.

[656] B.P. Croom, M. Berkson, R.K. Mueller, M. Presley, S. Storck, Deep learning prediction of stress fields in additively manufactured metals with intricate defect networks, Mech Mater 165 (2022) 104191.

[657] A.P. Garland, B.C. White, B.H. Jared, M. Heiden, E. Donahue, B.L. Boyce, Deep convolutional neural networks as a rapid screening tool for complex additively manufactured structures, Addit Manuf 35 (2020) 101217.

[658] C. Herriott, A.D. Spear, Predicting microstructure-dependent mechanical properties in additively manufactured metals with machine-and deep-learning methods, Comp Mater Sci 175 (2020) 109599.

[659] R. Teharia, R.M. Singari, H. Kumar, Optimization of process variables for additive manufactured PLA based tensile specimen using taguchi design and artificial neural network (ANN) technique, Materials Today: Proceedings 56 (2022) 3426-3432.

[660] X. Xiao, C. Waddell, C. Hamilton, H. Xiao, Quality Prediction and Control in Wire Arc Additive Manufacturing via Novel Machine Learning Framework, Micromachines 13(1) (2022) 137.

[661] Y. Shi, Y. Zhang, R. Harik, Manufacturing feature recognition with a 2D convolutional neural network, CIRP Journal of Manufacturing Science and Technology 30 (2020) 36-57.

[662] N. Satterlee, E. Torresani, E. Olevsky, J.S. Kang, Comparison of machine learning methods for automatic classification of porosities in powder-based additive manufactured metal parts, The International Journal of Advanced Manufacturing Technology 120(9) (2022) 6761-6776.

[663] X. Fu, D. Peddireddy, V. Aggarwal, M.B.-G. Jun, Improved Dexel Representation: A 3D CNN Geometry Descriptor for Manufacturing CAD, IEEE Transactions on Industrial Informatics (2021).

[664] M. Ali, U. Sajjad, I. Hussain, N. Abbas, H.M. Ali, W.-M. Yan, C.-C. Wang, On the assessment of the mechanical properties of additively manufactured lattice structures, Eng Anal Bound Elem 142 (2022) 93-116.

[665] A.P. Garland, B.C. White, S.C. Jensen, B.L. Boyce, Pragmatic generative optimization of novel structural lattice metamaterials with machine learning, Mater Design 203 (2021) 109632, 10.1016/j.matdes.2021.109632.

[666] S. Lee, Z. Zhang, G.X. Gu, Generative machine learning algorithm for lattice structures with superior mechanical properties, Materials Horizons 9(3) (2022) 952-960.

[667] Y.D. Boon, S.C. Joshi, S.K. Bhudolia, G. Gohel, Recent advances on the design automation for performance-optimized fiber reinforced polymer composite components, Journal of Composites Science 4(2) (2020) 61.

[668] S. Nasiri, M.R. Khosravani, Machine learning in predicting mechanical behavior of additively manufactured parts, Journal of Materials Research and Technology 14 (2021) 1137-1153, 10.1016/j.jmrt.2021.07.004.

[669] G. Yilin, J. Fuh Ying Hsi, L. Wen Feng, Multiscale topology optimisation with nonparametric microstructures using three-dimensional convolutional neural network (3D-CNN) models, Virtual and Physical Prototyping 16(3) (2021) 306-317.

[670] Y. Xiong, P.L.T. Duong, D. Wang, S.-I. Park, Q. Ge, N. Raghavan, D.W. Rosen, Data-driven design space exploration and exploitation for design for additive manufacturing, J Mech Design 141(10) (2019).

[671] K. Singh, R.K. Kapania, Accelerated optimization of curvilinearly stiffened panels using deep learning, Thin Wall Struct 161 (2021) 107418, 10.1016/j.tws.2020.107418.

[672] G.X. Gu, C.-T. Chen, D.J. Richmond, M.J. Buehler, Bioinspired hierarchical composite design using machine learning: simulation, additive manufacturing, and experiment, Materials Horizons 5(5) (2018) 939-945, 10.1039/c8mh00653a.

[673] R.M. Dudley, Sample functions of the Gaussian process, Selected works of RM Dudley, Springer2010, pp. 187-224.

[674] R.M. Gorguluarslan, G.C. Ates, O. Utku Gungor, Y. Yamaner, Strut Diameter Uncertainty Prediction by Deep Neural Network for Additively Manufactured Lattice Structures, Journal of Computing and Information Science in Engineering 22(3) (2022).

[675] F. Veloso, J. Gomes-Fonseca, P. Morais, J. Correia-Pinto, A.C. Pinho, J.L. Vilaça, Overview of Methods and Software for the Design of Functionally Graded Lattice Structures, Adv Eng Mater 24(11) (2022) 2200483.

[676] L. Wang, S. Tao, P. Zhu, W. Chen, Data-Driven Topology Optimization With Multiclass Microstructures Using Latent Variable Gaussian Process, J Mech Design 143(3) (2021), 10.1115/1.4048628.

[677] L. Wang, A. van Beek, D. Da, Y.-C. Chan, P. Zhu, W. Chen, Data-driven multiscale design of cellular composites with multiclass microstructures for natural frequency maximization, Compos Struct 280 (2022) 114949, 10.1016/j.compstruct.2021.114949.

[678] D. Da, Y.-C. Chan, L. Wang, W. Chen, Data-driven and topological design of structural metamaterials for fracture resistance, Extreme Mechanics Letters 50 (2022) 101528, 10.1016/j.eml.2021.101528.

[679] L. Wang, Y.-C. Chan, Z. Liu, P. Zhu, W. Chen, Data-driven metamaterial design with Laplace-Beltrami spectrum as "shape-DNA", Struct Multidiscip O 61(6) (2020) 2613-2628, 10.1007/s00158-020-02523-5.

[680] L. Zheng, S. Kumar, D.M. Kochmann, Data-driven topology optimization of spinodoid metamaterials with seamlessly tunable anisotropy, Comput Method Appl M 383 (2021) 113894, 10.1016/j.cma.2021.113894.

[681] H.T. Kollmann, D.W. Abueidda, S. Koric, E. Guleryuz, N.A. Sobh, Deep learning for topology optimization of 2D metamaterials, Mater Design 196 (2020) 109098.

[682] L. Wang, Y.-C. Chan, F. Ahmed, Z. Liu, P. Zhu, W. Chen, Deep generative modeling for mechanistic-based learning and design of metamaterial systems, Comput Method Appl M 372 (2020) 113377, 10.1016/j.cma.2020.113377.

[683] T. Xue, T.J. Wallin, Y. Menguc, S. Adriaenssens, M. Chiaramonte, Machine learning

generative models for automatic design of multi-material 3D printed composite solids, Extreme Mechanics Letters 41 (2020) 100992, 10.1016/j.eml.2020.100992.

[684] M. Fernández, F. Fritzen, O. Weeger, Material modeling for parametric, anisotropic finite strain hyperelasticity based on machine learning with application in optimization of metamaterials, Int J Numer Meth Eng 123(2) (2021) 577-609, 10.1002/nme.6869.

[685] M.A. Bessa, P. Glowacki, M. Houlder, Bayesian Machine Learning in Metamaterial Design: Fragile Becomes Supercompressible, Adv Mater 31(48) (2019) e1904845, 10.1002/adma.201904845.

[686] A. Challapalli, D. Patel, G. Li, Inverse machine learning framework for optimizing lightweight metamaterials, Mater Design 208 (2021) 109937, 10.1016/j.matdes.2021.109937.

[687] D.A. White, W.J. Arrighi, J. Kudo, S.E. Watts, Multiscale topology optimization using neural network surrogate models, Comput Method Appl M 346 (2019) 1118-1135, 10.1016/j.cma.2018.09.007.

[688] S. Sanchez, P. Smith, Z. Xu, G. Gaspard, C.J. Hyde, W.W. Wits, I.A. Ashcroft, H. Chen, A.T. Clare, Powder Bed Fusion of nickel-based superalloys: A review, International Journal of Machine Tools and Manufacture 165 (2021) 103729.

[689] H. Soni, M. Gor, G.S. Rajput, P. Sahlot, A comprehensive review on effect of process parameters and heat treatment on tensile strength of additively manufactured Inconel-625, Materials Today: Proceedings 47 (2021) 4866-4871.

[690] D. Vogiatzief, A. Evirgen, M. Pedersen, U. Hecht, Laser powder bed fusion of an Al-Cr-Fe-Ni high-entropy alloy produced by blending of prealloyed and elemental powder: process parameters, microstructures and mechanical properties, J Alloy Compd (2022) 165658.

[691] T.Q. Tran, F.L. Ng, J.T.Y. Kai, S. Feih, M.L.S. Nai, Tensile Strength Enhancement of Fused Filament Fabrication Printed Parts: A Review of Process Improvement Approaches and Respective Impact, Addit Manuf (2022) 102724.

[692] G. Gao, F. Xu, J. Xu, G. Tang, Z. Liu, A Survey of the Influence of Process Parameters on Mechanical Properties of Fused Deposition Modeling Parts, Micromachines 13(4) (2022) 553.

[693] R.V. Pazhamannil, A. Edacherian, Property enhancement approaches of fused filament fabrication technology: A review, Polymer Engineering & Science 62(5) (2022) 1356-1376.

[694] V. Cojocaru, D. Frunzaverde, C.-O. Miclosina, G. Marginean, The influence of the process parameters on the mechanical properties of PLA specimens produced by fused filament fabrication—A review, Polymers 14(5) (2022) 886.

[695] C. Palanisamy, R. Raman, Additive manufacturing: a review on mechanical properties of polyjet and FDM printed parts, Polym Bull (2021) 1-52.

[696] X. Shen, J. Yao, Y. Wang, J. Yang, Density Prediction of Selective Laser Sintering Parts Based on Artificial Neural Network, 3174 (2004) 832-840, 10.1007/978-3-540-28648-6_133.

[697] X.-f. Li, J.-h. Dong, Y.-z. Zhang, Modeling and Applying of RBF Neural Network Based on Fuzzy Clustering and Pseudo-Inverse Method, (2009) 1-4, 10.1109/iciecs.2009.5362683.

[698] J. Munguía, J. Ciurana, C. Riba, Neural-network-based model for build-time estimation in selective laser sintering, Proceedings of the Institution of Mechanical Engineers, Part B: Journal of Engineering Manufacture 223(8) (2009) 995-1003, 10.1243/09544054jem1324.

[699] W. Rong-Ji, L. Xin-hua, W. Qing-ding, W. Lingling, Optimizing process parameters for

selective laser sintering based on neural network and genetic algorithm, The International Journal of Advanced Manufacturing Technology 42(11-12) (2008) 1035-1042, 10.1007/s00170-008-1669-0.

[700] R.-J. Wang, J. Li, F. Wang, X. Li, Q. Wu, ANN model for the prediction of density in selective laser sintering, International Journal of Manufacturing Research 4(3) (2009) 362-373.

[701] M. Zhang, C.-N. Sun, X. Zhang, P.C. Goh, J. Wei, D. Hardacre, H. Li, High cycle fatigue life prediction of laser additive manufactured stainless steel: A machine learning approach, Int J Fatigue 128 (2019) 105194, 10.1016/j.ijfatigue.2019.105194.

[702] G. Tapia, S. Khairallah, M. Matthews, W.E. King, A. Elwany, Gaussian process-based surrogate modeling framework for process planning in laser powder-bed fusion additive manufacturing of 316L stainless steel, The International Journal of Advanced Manufacturing Technology 94(9-12) (2017) 3591-3603, 10.1007/s00170-017-1045-z.

[703] Z. Zhan, H. Li, A novel approach based on the elastoplastic fatigue damage and machine learning models for life prediction of aerospace alloy parts fabricated by additive manufacturing, Int J Fatigue 145 (2021) 106089, 10.1016/j.ijfatigue.2020.106089.

[704] G. Tapia, A.H. Elwany, H. Sang, Prediction of porosity in metal-based additive manufacturing using spatial Gaussian process models, Addit Manuf 12 (2016) 282-290, 10.1016/j.addma.2016.05.009.

[705] R. Liu, S. Liu, X. Zhang, A physics-informed machine learning model for porosity analysis in laser powder bed fusion additive manufacturing, The International Journal of Advanced Manufacturing Technology 113(7-8) (2021) 1943-1958, 10.1007/s00170-021-06640-3.

[706] Z. Zhan, H. Li, Machine learning based fatigue life prediction with effects of additive manufacturing process parameters for printed SS 316L, Int J Fatigue 142 (2021) 105941, 10.1016/j.ijfatigue.2020.105941.

[707] W. Zhang, A. Mehta, P.S. Desai, C.F. Higgs III, Machine learning enabled powder spreading process map for metal additive manufacturing (AM), 2017 International Solid Freeform Fabrication Symposium, University of Texas at Austin, 2017.

[708] R. de Souza Borges Ferreira, A. Sabbaghi, Q. Huang, Automated Geometric Shape Deviation Modeling for Additive Manufacturing Systems via Bayesian Neural Networks, IEEE Transactions on Automation Science and Engineering 17(2) (2020) 584-598, 10.1109/tase.2019.2936821.

[709] S.H. Lee, W.S. Park, H.S. Cho, W. Zhang, M.C. Leu, A neural network approach to the modelling and analysis of stereolithography processes, Proceedings of the Institution of Mechanical Engineers, Part B: Journal of Engineering Manufacture 215(12) (2016) 1719-1733, 10.1177/095440540121501206.

[710] A. Khadilkar, J. Wang, R. Rai, Deep learning–based stress prediction for bottom-up SLA 3D printing process, The International Journal of Advanced Manufacturing Technology 102(5-8) (2019) 2555-2569, 10.1007/s00170-019-03363-4.

[711] O.A. Mohamed, S.H. Masood, J.L. Bhowmik, Influence of processing parameters on creep and recovery behavior of FDM manufactured part using definitive screening design and ANN, Rapid Prototyping Journal 23(6) (2017) 998-1010, 10.1108/rpj-12-2015-0198.

[712] A.K. Sood, R.K. Ohdar, S.S. Mahapatra, Experimental investigation and empirical

modelling of FDM process for compressive strength improvement, Journal of Advanced Research 3(1) (2012) 81-90, 10.1016/j.jare.2011.05.001.

[713] A.K. Sood, A. Equbal, V. Toppo, R.K. Ohdar, S.S. Mahapatra, An investigation on sliding wear of FDM built parts, CIRP Journal of Manufacturing Science and Technology 5(1) (2012) 48-54, 10.1016/j.cirpj.2011.08.003.

[714] A. Equbal, A.K. Sood, S. Mahapatra, Prediction of dimensional accuracy in fused deposition modelling: a fuzzy logic approach, International Journal of Productivity and Quality Management 7(1) (2011) 22-43.

[715] R.M. Gorguluarslan, R.V. Grandhi, H.-J. Choi, S.-K. Choi, Prediction assessment and validation of multiscale models for additively manufactured lattice structures under uncertainty, Journal of Mechanical Science and Technology 33 (2019) 1365-1379.

[716] G.C. Vosniakos, T. Maroulis, D. Pantelis, A method for optimizing process parameters in layer-based rapid prototyping, Proceedings of the Institution of Mechanical Engineers, Part B: Journal of Engineering Manufacture 221(8) (2007) 1329-1340, 10.1243/09544054jem815.

[717] Z. Li, Z. Zhang, J. Shi, D. Wu, Prediction of surface roughness in extrusion-based additive manufacturing with machine learning, Robot Cim-int Manuf 57 (2019) 488-495, 10.1016/j.rcim.2019.01.004.

[718] Z.L. Lu, D.C. Li, B.H. Lu, A.F. Zhang, G.X. Zhu, G. Pi, The prediction of the building precision in the Laser Engineered Net Shaping process using advanced networks, Opt Laser Eng 48(5) (2010) 519-525, 10.1016/j.optlaseng.2010.01.002.

[719] J. Xiong, G. Zhang, J. Hu, L. Wu, Bead geometry prediction for robotic GMAW-based rapid manufacturing through a neural network and a second-order regression analysis, J Intell Manuf 25(1) (2012) 157-163, 10.1007/s10845-012-0682-1.

[720] C. Herriott, A.D. Spear, Predicting microstructure-dependent mechanical properties in additively manufactured metals with machine- and deep-learning methods, Comp Mater Sci 175 (2020) 109599, 10.1016/j.commatsci.2020.109599.

[721] M. Mozaffar, A. Paul, R. Al-Bahrani, S. Wolff, A. Choudhary, A. Agrawal, K. Ehmann, J. Cao, Data-driven prediction of the high-dimensional thermal history in directed energy deposition processes via recurrent neural networks, Manufacturing Letters 18 (2018) 35-39, 10.1016/j.mfglet.2018.10.002.

[722] P. Kumar, N.K. Jain, Surface roughness prediction in micro-plasma transferred arc metal additive manufacturing process using K-nearest neighbors algorithm, The International Journal of Advanced Manufacturing Technology 119(5-6) (2022) 2985-2997, 10.1007/s00170-021-08639-2.

[723] H. Chen, Y.F. Zhao, Learning Algorithm Based Modeling and Process Parameters Recommendation System for Binder Jetting Additive Manufacturing Process, International Design Engineering Technical Conferences and Computers and Information in Engineering Conference, 2015.

[724] R. Onler, A.S. Koca, B. Kirim, E. Soylemez, Multi-objective optimization of binder jet additive manufacturing of Co-Cr-Mo using machine learning, The International Journal of Advanced Manufacturing Technology 119(1-2) (2021) 1091-1108, 10.1007/s00170-021-08183-z.

[725] C. Xia, Z. Pan, J. Polden, H. Li, Y. Xu, S. Chen, Modelling and prediction of surface

roughness in wire arc additive manufacturing using machine learning, J Intell Manuf (2021), 10.1007/s10845-020-01725-4.

[726] A. Yaseer, H. Chen, Machine learning based layer roughness modeling in robotic additive manufacturing, Journal of Manufacturing Processes 70 (2021) 543-552, 10.1016/j.jmapro.2021.08.056.

[727] X. Xiao, C. Waddell, C. Hamilton, H. Xiao, Quality Prediction and Control in Wire Arc Additive Manufacturing via Novel Machine Learning Framework, Micromachines 13(1) (2022), 10.3390/mi13010137.

[728] C. Silbernagel, A. Aremu, I. Ashcroft, Using machine learning to aid in the parameter optimisation process for metal-based additive manufacturing, Rapid Prototyping Journal 26(4) (2019) 625-637, 10.1108/rpj-08-2019-0213.

[729] I. Baturynska, O. Semeniuta, K. Martinsen, Optimization of Process Parameters for Powder Bed Fusion Additive Manufacturing by Combination of Machine Learning and Finite Element Method: A Conceptual Framework, Procedia CIRP 67 (2018) 227-232, 10.1016/j.procir.2017.12.204.

[730] J. Jiang, C. Yu, X. Xu, Y. Ma, J. Liu, Achieving better connections between deposited lines in additive manufacturing via machine learning, Math. Biosci. Eng 17(4) (2020).

[731] L. Cao, J. Li, J. Hu, H. Liu, Y. Wu, Q. Zhou, Optimization of surface roughness and dimensional accuracy in LPBF additive manufacturing, Optics & Laser Technology 142 (2021) 107246, 10.1016/j.optlastec.2021.107246.

[732] P.V. Osswald, S.K. Mustafa, C. Kaa, P. Obst, M. Friedrich, M. Pfeil, D. Rietzel, G. Witt, Optimization of the production processes of powder-based additive manufacturing technologies by means of a machine learning model for the temporal prognosis of the build and cooling phase, Production Engineering 14(5-6) (2020) 677-691, 10.1007/s11740-020-00987-4.

[733] S. Srinivasan, B. Swick, M.A. Groeber, Laser Powder Bed Fusion Parameter Selection via Machine-Learning-Augmented Process Modeling, Jom 72(12) (2020) 4393-4403, 10.1007/s11837-020-04383-2.

[734] S. Mondal, D. Gwynn, A. Ray, A. Basak, Investigation of Melt Pool Geometry Control in Additive Manufacturing Using Hybrid Modeling, Metals 10(5) (2020) 683, 10.3390/met10050683.

[735] A. Menon, B. Póczos, A.W. Feinberg, N.R. Washburn, Optimization of silicone 3D printing with hierarchical machine learning, 3D Printing and Additive Manufacturing 6(4) (2019) 181-189.

[736] J.R. Deneault, J. Chang, J. Myung, D. Hooper, A. Armstrong, M. Pitt, B. Maruyama, Toward autonomous additive manufacturing: Bayesian optimization on a 3D printer, Mrs Bull (2021) 1-10.

[737] A.R. Dhar, D. Gupta, S.S. Roy, A.K. Lohar, Forward and backward modeling of direct metal deposition using metaheuristic algorithms tuned artificial neural network and extreme gradient boost, Progress in Additive Manufacturing (2022), 10.1007/s40964-021-00251-w.

[738] H.S. Park, D.S. Nguyen, T. Le-Hong, X. Van Tran, Machine learning-based optimization of process parameters in selective laser melting for biomedical applications, J Intell Manuf (2021), 10.1007/s10845-021-01773-4.

[739] B.L. DeCost, E.A. Holm, Characterizing powder materials using keypoint-based

computer vision methods, Comp Mater Sci 126 (2017) 438-445.

[740] B.L. DeCost, H. Jain, A.D. Rollett, E.A. Holm, Computer vision and machine learning for autonomous characterization of am powder feedstocks, Jom 69(3) (2017) 456-465.

[741] D. Cannizzaro, A.G. Varrella, S. Paradiso, R. Sampieri, Y. Chen, A. Macii, E. Patti, S. Di Cataldo, In-situ defect detection of metal Additive Manufacturing: an integrated framework, IEEE Transactions on Emerging Topics in Computing 10(1) (2021) 74-86.

[742] B. Wu, X.-y. Ji, J.-x. Zhou, H.-q. Yang, D.-j. Peng, Z.-m. Wang, Y.-j. Wu, Y.-j. Yin, In situ monitoring methods for selective laser melting additive manufacturing process based on images—A review, China Foundry 18(4) (2021) 265-285.

[743] B. Duman, K. Özsoy, A deep learning-based approach for defect detection in powder bed fusion additive manufacturing using transfer learning, Journal of the Faculty of Engineering and Architecture of Gazi University 37(1) (2022) 361-375.

[744] P.K. Nalajam, R. Varadarajan, A Hybrid Deep Learning Model for Layer-Wise Melt Pool Temperature Forecasting in Wire-Arc Additive Manufacturing Process, IEEE Access 9 (2021) 100652-100664, 10.1109/access.2021.3097177.

[745] M. Liu, N. Senin, R. Leach, P. Lehmann, W. Osten, A. Albertazzi Gonçalves, Intelligent quality monitoring for additive manufactured surfaces by machine learning and light scattering, (2021) 2, 10.1117/12.2592554.

[746] B. Yuan, G.M. Guss, A.C. Wilson, S.P. Hau‐Riege, P.J. DePond, S. McMains, M.J. Matthews, B. Giera, Machine‐Learning‐Based Monitoring of Laser Powder Bed Fusion, Advanced Materials Technologies 3(12) (2018) 1800136, 10.1002/admt.201800136.

[747] M. Bugatti, B.M. Colosimo, Towards real-time in-situ monitoring of hot-spot defects in L-PBF: a new classification-based method for fast video-imaging data analysis, J Intell Manuf 33(1) (2021) 293-309, 10.1007/s10845-021-01787-y.

[748] W. Sun, Z. Zhang, W. Ren, J. Mazumder, J. Jin, In Situ Monitoring of Optical Emission Spectra for Microscopic Pores in Metal Additive Manufacturing, Journal of Manufacturing Science and Engineering 144(1) (2022), 10.1115/1.4051532.

[749] M. Montazeri, A.R. Nassar, A.J. Dunbar, P. Rao, In-process monitoring of porosity in additive manufacturing using optical emission spectroscopy, IISE Transactions 52(5) (2019) 500-515, 10.1080/24725854.2019.1659525.

[750] L. Scime, J. Beuth, Using machine learning to identify in-situ melt pool signatures indicative of flaw formation in a laser powder bed fusion additive manufacturing process, Addit Manuf 25 (2019) 151-165, 10.1016/j.addma.2018.11.010.

[751] L. Scime, J. Beuth, A multi-scale convolutional neural network for autonomous anomaly detection and classification in a laser powder bed fusion additive manufacturing process, Addit Manuf 24 (2018) 273-286, 10.1016/j.addma.2018.09.034.

[752] L. Scime, J. Beuth, Anomaly detection and classification in a laser powder bed additive manufacturing process using a trained computer vision algorithm, Addit Manuf 19 (2018) 114-126, 10.1016/j.addma.2017.11.009.

[753] S. Larsen, P.A. Hooper, Deep semi-supervised learning of dynamics for anomaly detection in laser powder bed fusion, J Intell Manuf 33(2) (2021) 457-471, 10.1007/s10845-021-01842-8.

[754] W. Halsey, D. Rose, L. Scime, R. Dehoff, V. Paquit, Localized defect detection from

spatially mapped, in-situ process data with machine learning, Frontiers in Mechanical Engineering 7 (2021).

[755] K. Wasmer, T. Le-Quang, B. Meylan, S.A. Shevchik, In Situ Quality Monitoring in AM Using Acoustic Emission: A Reinforcement Learning Approach, J Mater Eng Perform 28(2) (2018) 666-672, 10.1007/s11665-018-3690-2.

[756] S.A. Shevchik, G. Masinelli, C. Kenel, C. Leinenbach, K. Wasmer, Deep Learning for In Situ and Real-Time Quality Monitoring in Additive Manufacturing Using Acoustic Emission, IEEE Transactions on Industrial Informatics 15(9) (2019) 5194-5203, 10.1109/tii.2019.2910524.

[757] S.A. Shevchik, C. Kenel, C. Leinenbach, K. Wasmer, Acoustic emission for in situ quality monitoring in additive manufacturing using spectral convolutional neural networks, Addit Manuf 21 (2018) 598-604.

[758] C. Gobert, E.W. Reutzel, J. Petrich, A.R. Nassar, S. Phoha, Application of supervised machine learning for defect detection during metallic powder bed fusion additive manufacturing using high resolution imaging, Addit Manuf 21 (2018) 517-528, 10.1016/j.addma.2018.04.005.

[759] Z. Snow, B. Diehl, E.W. Reutzel, A. Nassar, Toward in-situ flaw detection in laser powder bed fusion additive manufacturing through layerwise imagery and machine learning, J Manuf Syst 59 (2021) 12-26, 10.1016/j.jmsy.2021.01.008.

[760] J. Petrich, Z. Snow, D. Corbin, E.W. Reutzel, Multi-modal sensor fusion with machine learning for data-driven process monitoring for additive manufacturing, Addit Manuf 48 (2021) 102364, 10.1016/j.addma.2021.102364.

[761] M. Ghayoomi Mohammadi, D. Mahmoud, M. Elbestawi, On the application of machine learning for defect detection in L-PBF additive manufacturing, Optics & Laser Technology 143 (2021) 107338, 10.1016/j.optlastec.2021.107338.

[762] E. Westphal, H. Seitz, A machine learning method for defect detection and visualization in selective laser sintering based on convolutional neural networks, Addit Manuf 41 (2021) 101965, 10.1016/j.addma.2021.101965.

[763] P. Yadav, V.K. Singh, T. Joffre, O. Rigo, C. Arvieu, E. Le Guen, E. Lacoste, Inline Drift Detection Using Monitoring Systems and Machine Learning in Selective Laser Melting, Adv Eng Mater 22(12) (2020) 2000660, 10.1002/adem.202000660.

[764] J. Li, Q. Zhou, X. Huang, M. Li, L. Cao, In situ quality inspection with layer-wise visual images based on deep transfer learning during selective laser melting, J Intell Manuf (2021), 10.1007/s10845-021-01829-5.

[765] J. Li, L. Cao, J. Xu, S. Wang, Q. Zhou, In situ porosity intelligent classification of selective laser melting based on coaxial monitoring and image processing, Measurement 187 (2022) 110232, 10.1016/j.measurement.2021.110232.

[766] L. Chen, X. Yao, P. Xu, S.K. Moon, G. Bi, Rapid surface defect identification for additive manufacturing with in-situ point cloud processing and machine learning, Virtual and Physical Prototyping 16(1) (2020) 50-67, 10.1080/17452759.2020.1832695.

[767] W. Ren, G. Wen, Z. Zhang, J. Mazumder, Quality monitoring in additive manufacturing using emission spectroscopy and unsupervised deep learning, Mater Manuf Process (2021) 1-8, 10.1080/10426914.2021.1906891.

4105   [768] M.S. Hossain, H. Taheri, In-situ process monitoring for metal additive manufacturing through acoustic techniques using wavelet and convolutional neural network (CNN), The International Journal of Advanced Manufacturing Technology 116(11-12) (2021) 3473-3488, 10.1007/s00170-021-07721-z.

[769] D. Wu, Y. Wei, J. Terpenny, Surface Roughness Prediction in Additive Manufacturing
4110   Using Machine Learning,   (2018), 10.1115/msec2018-6501.

[770] W.P. Syam, R. Leach, K. Rybalcenko, A. Gaio, J. Crabtree, In-process measurement of the surface quality for a novel finishing process for polymer additive manufacturing, Procedia CIRP 75 (2018) 108-113, 10.1016/j.procir.2018.04.088.

[771] A. Rossi, M. Moretti, N. Senin, Layer inspection via digital imaging and machine learning
4115   for in-process monitoring of fused filament fabrication, Journal of Manufacturing Processes 70 (2021) 438-451, 10.1016/j.jmapro.2021.08.057.

[772] J. Liu, Y. Hu, B. Wu, Y. Wang, An improved fault diagnosis approach for FDM process with acoustic emission, Journal of Manufacturing Processes 35 (2018) 570-579, 10.1016/j.jmapro.2018.08.038.

4120   [773] R.M. Scheffel, A.A. Fröhlich, M. Silvestri, Automated fault detection for additive manufacturing using vibration sensors, Int J Comp Integ M 34(5) (2021) 500-514, 10.1080/0951192x.2021.1901316.

[774] U. Delli, S. Chang, Automated Process Monitoring in 3D Printing Using Supervised Machine Learning, Procedia Manufacturing 26 (2018) 865-870, 10.1016/j.promfg.2018.07.111.

4125   [775] F. Tarlochan, Sandwich structures for energy absorption applications: A review, Materials 14(16) (2021) 4731.

[776] A. Borrelli, G. D'Errico, C. Borrelli, R. Citarella, Assessment of crash performance of an automotive component made through additive manufacturing, Applied Sciences 10(24) (2020) 9106.

4130   [777] G.-W. Kim, Y.-I. Park, K. Park, Topology Optimization and Additive Manufacturing of Automotive Component by Coupling Kinetic and Structural Analyses, International Journal of Automotive Technology 21(6) (2020) 1455-1463.

[778] F. Marin, J.R. de Miranda, A.F. de Souza, Study of the design of cooling channels for polymers injection molds, Polymer Engineering & Science 58(4) (2018) 552-559.

4135   [779] S. Vinodh, Parametric optimization of fused deposition modelling process using Grey based Taguchi and TOPSIS methods for an automotive component, Rapid Prototyping Journal (2020).

[780] W. Lee, Y. Jeong, J. Yoo, H. Huh, S.-J. Park, S.H. Park, J. Yoon, Effect of auxetic structures on crash behavior of cylindrical tube, Compos Struct 208 (2019) 836-846.

4140   [781] U. Fasel, D. Keidel, L. Baumann, G. Cavolina, M. Eichenhofer, P. Ermanni, Composite additive manufacturing of morphing aerospace structures, Manufacturing Letters 23 (2020) 85-88.

[782] A. Chintala, M. Tejaswi Kumar, M. Sathishkumar, N. Arivazhagan, M. Manikandan, Technology development for producing Inconel 625 in aerospace application using wire arc
4145   additive manufacturing process, J Mater Eng Perform 30(7) (2021) 5333-5341.

[783] P. Gradl, D.C. Tinker, A. Park, O.R. Mireles, M. Garcia, R. Wilkerson, C. Mckinney, Robust Metal Additive Manufacturing Process Selection and Development for Aerospace

Components, J Mater Eng Perform (2022) 1-32.

[784] A. Katz-Demyanetz, V.V. Popov Jr, A. Kovalevsky, D. Safranchik, A. Koptioug, Powder-bed additive manufacturing for aerospace application: Techniques, metallic and metal/ceramic composite materials and trends, Manufacturing review 6 (2019).

[785] M.M. Opgenoord, K.E. Willcox, Design for additive manufacturing: cellular structures in early-stage aerospace design, Struct Multidiscip O 60(2) (2019) 411-428.

[786] J. Bühring, M. Nuño, K.-U. Schröder, Additive manufactured sandwich structures: Mechanical characterization and usage potential in small aircraft, Aerosp Sci Technol 111 (2021) 106548.

[787] D. Li, W. Liao, N. Dai, G. Dong, Y. Tang, Y.M. Xie, Optimal design and modeling of gyroid-based functionally graded cellular structures for additive manufacturing, Comput. Aided Des. 104 (2018) 87-99.

[788] G. Palomba, V. Crupi, G. Epasto, Additively manufactured lightweight monitoring drones: Design and experimental investigation, Polymer (2022) 124557.

[789] J. Feng, J. Fu, C. Shang, Z. Lin, B. Li, Sandwich panel design and performance optimization based on triply periodic minimal surfaces, Comput. Aided Des. 115 (2019) 307-322.

[790] R. Xiao, X. Li, H. Jia, J.U. Surjadi, J. Li, W. Lin, L. Gao, P. Chirarattananon, Y. Lu, 3D printing of dual phase-strengthened microlattices for lightweight micro aerial vehicles, Mater Design 206 (2021) 109767.

[791] L.-y. Zhu, M. Cheng, W.-c. Sun, J.-q. Yang, L. Li, Q. Jiang, Influence of deformed primitive architecture on mechanical behavior of artificial porous meniscus, Mater Design 186 (2020) 108303.

[792] H. Tang, P. Zhao, C. Xiang, N. Liu, L. Jia, Ti-6Al-4V orthopedic implants made by selective electron beam melting, Titanium in medical and dental applications, Elsevier2018, pp. 239-249.

[793] J. Feng, J. Fu, C. Shang, Z. Lin, B. Li, Porous scaffold design by solid T-splines and triply periodic minimal surfaces, Comput Method Appl M (2018).

[794] A. Entezari, I. Roohani, G. Li, C.R. Dunstan, P. Rognon, Q. Li, X. Jiang, H. Zreiqat, Architectural design of 3D printed scaffolds controls the volume and functionality of newly formed bone, Advanced healthcare materials 8(1) (2019) 1801353.

[795] A. Entezari, N.C. Liu, I. Roohani, Z. Zhang, J. Chen, B. Sarrafpour, H. Zoellner, M. Behi, H. Zreiqat, Q. Li, On design for additive manufacturing (DAM) parameter and its effects on biomechanical properties of 3D printed ceramic scaffolds, Materials Today Communications 23 (2020) 101065.

[796] A. Entezari, N.-C. Liu, Z. Zhang, J. Fang, C. Wu, B. Wan, M. Swain, Q. Li, Nondeterministic multiobjective optimization of 3D printed ceramic tissue scaffolds, Journal of the mechanical behavior of biomedical materials (2022) 105580.

[797] M.R. ul Haq, A. Nazir, S.-C. Lin, J.-Y. Jeng, Design and performance evaluation of multifunctional midsole using functionally gradient wave springs produced using multijet fusion additive manufacturing process, Materials Today Communications 31 (2022) 103505.

[798] M.R. ul Haq, A. Nazir, J.-Y. Jeng, Design for additive manufacturing of variable dimension wave springs analyzed using experimental and finite element methods, Addit Manuf

44 (2021) 102032.

[799] R. Thompson, Anatomics 3D-printed titanium implants from head to heel, Titanium in Medical and Dental Applications, Elsevier2018, pp. 225-237.

[800] Y. Xu, Y. Gao, C. Wu, J. Fang, G. Sun, G.P. Steven, Q. Li, Concurrent optimization of topological configuration and continuous fiber path for composite structures—A unified level set approach, Comput Method Appl M 399 (2022) 115350.

[801] Y. Sun, Q.M. Li, Dynamic compressive behaviour of cellular materials: A review of phenomenon, mechanism and modelling, Int J Impact Eng 112 (2018) 74-115, 10.1016/j.ijimpeng.2017.10.006.

[802] J. Luo, Q. Luo, G. Zhang, Q. Li, G. Sun, On strain rate and temperature dependent mechanical properties and constitutive models for additively manufactured polylactic acid (PLA) materials, Thin Wall Struct 179 (2022) 109624.

[803] A. Entezari, S.-I. Roohani-Esfahani, Z. Zhang, H. Zreiqat, C.R. Dunstan, Q. Li, Fracture behaviors of ceramic tissue scaffolds for load bearing applications, Scientific reports 6(1) (2016) 1-10.

[804] N. Korshunova, I. Papaioannou, S. Kollmannsberger, D. Straub, E. Rank, Uncertainty quantification of microstructure variability and mechanical behavior of additively manufactured lattice structures, Comput Method Appl M 385 (2021) 114049.

[805] F. Liu, T. Zhou, T. Zhang, H. Xie, Y. Tang, P. Zhang, Shell offset enhances mechanical and energy absorption properties of SLM-made lattices with controllable separated voids, Mater Design 217 (2022) 110630.

[806] K. Zhang, Q. Meng, X. Zhang, Z. Qu, R. He, Quantitative characterization of defects in stereolithographic additive manufactured ceramic using X-ray computed tomography, J Mater Sci Technol 118 (2022) 144-157.

[807] G. Sun, H. Zhang, R. Wang, X. Lv, Q. Li, Multiobjective reliability-based optimization for crashworthy structures coupled with metal forming process, Struct Multidiscip O 56(6) (2017) 1571-1587.